AD-A065 567 NAVAL OCEANOGRAPHIC OFFICE NSTL STATION MS F/G 8/10
STRATIGRAPHY AND ABSOLUTE AGE OF DEEP-SEA SEDIMENTS IN THE WEST--ETC(U)
1979 E A ROMANKEVICH, P L BEZRUKOV
UNCLASSIFIED N00-T-32(532) NL

OF 2
AD
A065567

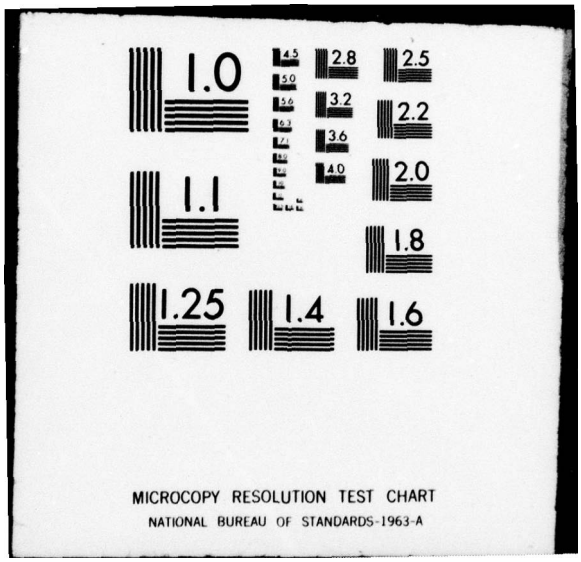
1.0
1.1
1.25
1.4
1.6
1.8
2.0
2.2
2.5
2.8
3.2
3.6
4.0
4.5
5.0
5.6
MICROCOPY RESOLUTION TEST CHART
NATIONAL BUREAU OF STANDARDS-1963-A

LEVEL I

8

NAVAL OCEANOGRAPHIC OFFICE TRANSLATION NOO T-32(532)

STRATIGRAFIYA I ABSOLYUTNYY VOZRAST GLUBOKOVODNYKH OSADKOV ZAPADNOY CHASTI TIKHOGO OKEANA

(Stratigraphy and Absolute Age of Deep-Sea Sediments in the Western Pacific Ocean)

E. A. ROMANKEVICH
P. L. BEZRUKOV
V. I. BARANOV
L. A. KRISTIANOVA

OCEANOLOGY, n. 14, Results of Research on International Geophysical Projects, publ. NAUKA, Moscow, 1966.

1979
TRANSLATION

Translator: M. Slessers
Editor: J. Duncan
Typist: K. Dunn

NAVAL OCEANOGRAPHIC OFFICE
NSTL Station, Bay St. Louis, MS 39522

1

(14) NAVAL OCEANOGRAPHIC OFFICE TRANSLATION NOO-T-32(532)

(STRATIGRAFIYA I ABSOLYUTNYY VOZRAST GLUBOKOVODNYKH OSADKOV ZAPADNOY CHASTI TIKHOGO OKEANA)

(6) # Stratigraphy and Absolute Age of Deep-Sea Sediments in the Western Pacific Ocean

(10) E. A. ROMANKEVICH,
P. L. BEZRUKOV,
V. I. BARANOV
L. A. KRISTIANOVA

(21) Trans. of OCEANOLOGY, [redacted] Results of Research on International Geophysical Projects, [redacted] 1966 (USSR) n14, n.p., 1966, by M. Slessers.

(11) 1979
TRANSLATION

(12) 192 p.

Translator: M. Slessers
Editor: J. Duncan
Typist: K. Dunn

NAVAL OCEANOGRAPHIC OFFICE
NSTL Station, Bay St. Louis, MS 39522

250 450

UNCLASSIFIED

SECURITY CLASSIFICATION OF THIS PAGE (When Data Entered)

REPORT DOCUMENTATION PAGE		READ INSTRUCTIONS BEFORE COMPLETING FORM
1. REPORT NUMBER T-32 (532)	2. GOVT ACCESSION NO.	3. RECIPIENT'S CATALOG NUMBER
4. TITLE (and Subtitle) Stratigraphy and Absolute Age of Deep-Sea Sediments in the Western Pacific Ocean (STRATIGRAFIYA I ABSOLYUTNYY VOZRAST GLUBOKOV-ODNYKH OSADKOV ZAPADNOY CHASTI TIKHOGO OKEANA)		5. TYPE OF REPORT & PERIOD COVERED 6. PERFORMING ORG. REPORT NUMBER
7. AUTHOR(s) E.A. Romankevich, P.L. Bezrukov, V.I. Baranov, L.A. Kristianova		8. CONTRACT OR GRANT NUMBER(s)
9. PERFORMING ORGANIZATION NAME AND ADDRESS U.S. Naval Oceanographic Office NSTL Station, Bay St. Louis, MS 39522		10. PROGRAM ELEMENT, PROJECT, TASK AREA & WORK UNIT NUMBERS
11. CONTROLLING OFFICE NAME AND ADDRESS U.S. Naval Oceanographic Office NSTL Station, Bay St. Louis, MS 39522		12. REPORT DATE 1979 13. NUMBER OF PAGES 190
14. MONITORING AGENCY NAME & ADDRESS(if different from Controlling Office)		15. SECURITY CLASS. (of this report) UNCLASSIFIED 15a. DECLASSIFICATION/DOWNGRADING SCHEDULE

16. DISTRIBUTION STATEMENT (of this Report)

Approved for public release; distribution unlimited.

17. DISTRIBUTION STATEMENT (of the abstract entered in Block 20, if different from Report)

18. SUPPLEMENTARY NOTES Translation of OKEANOLOGIYA, no. 14, Results of Research on International Geophysical Projects, Published by Academy of Sciences, USSR, Soviet, Geophysical Committee, NAUKA, MOSCOW, 1966.

19. KEY WORDS (Continue on reverse side if necessary and identify by block number)

OCEANOGRAPHY	GEOCHRONOLOGY	GEOCHEMISTY
BOTTOM SEDIMENTS	RADIO-ISOTOPES	PLEISTROCENE CLIMATES
PACIFIC OCEAN	SEDIMENT CORES	
STRATIGRAPHY	PLANKTON	

20. ABSTRACT (Continue on reverse side if necessary and identify by block number)

Seventeen deepsea sediment cores from the Pacific Ocean collected by Soviet expeditions were analyzed for chemical and grain-size composition, isotopes of radium, uranium, and thorium and plankton composition. Analysis methods are described in detail. Periods of deposition of various layers were determined to establish the stratigraphic sequence of Quaternary deposits. Eight horizons are correlated with glacial and interglacial stages and correlated with continental glaciation of the Würm, Riss, Mindel and Gunz stages of Western Europe.

DD FORM 1 JAN 73 1473 EDITION OF 1 NOV 65 IS OBSOLETE S/N 0102-014-6601 |

UNCLASSIFIED

SECURITY CLASSIFICATION OF THIS PAGE (When Data Entered)

CONTENTS

Introduction ---------- 1

Chapter I. History of the stratigraphic study of Quaternary deeps-sea deposits ---------- 5

Chapter II. Radioactive elements in seawater and bottom sediments -- 14
1. The content of natural radioactive elements in the ocean---------- 14
2. The distribution of radioelements in bottom sediments -- 16
3. The ionium method of determining the deposition rate of marine silts (oozes) ---------- 19

Chapter III. Laboratory analysis methods ---------- 26
1. Methods of determining the graulometric and basic chemical composition of sediments ---------- 26
2. Methods of determining radium, uranium and thorium isotopes in bottom sediments ---------- 27

Chapter IV. Main features of contemporary sedimentation in the western Pacific ---------- 38

Chapter V. The distribution of radioactive elements in the surface sediment layer ---------- 49

Chapter VI. Lithology, absolute age, and stratigraphy of deep-sea sediments ---------- 57
1. The principles of stratigraphic classification of Quaternary deep-sea deposits ---------- 57
2. Core at station 3163 ---------- 59
3. Core at station 4068 ---------- 72
4. Core samples at stations 3378, 3325, 3342, and 3359-- 79
5. Core at station 3451 ---------- 88
6. Core at station 3625 ---------- 93
7. Core sample at station 3495 ---------- 97
8. Core at station 3520 ---------- 102
9. Core at station 3532 ---------- 108
10. Core at station 3530 ---------- 115
11. Core at station 3481 ---------- 116
12. Core at station 3873 ---------- 118
13. Core at station 3746 ---------- 120
14. Core at station 3797 ---------- 122
15. Core at station 3995 ---------- 127
16. Sedimentary stratigraphy of the equatorial zone ----- 130

Chapter VII. The history of deep-water sedimentation of the Quaternary period in the western Pacific ---------- 133

Literature ---------- 146

Appendixes ---------- 159

FIGURES

1. Station chart ---------- 3
2. The scheme for analyzing sediments to determine the content of the isotopes of thorium, uranium and radium ---------- 31
3. The α spectra of ionium separated from bottom sediments -------- 32
4. Water types (masses) of the western Pacific Ocean ---------- 39
5. Drainage basin and bottom relief chart of the western Pacific Ocean ---------- 40
6. Schematic chart of ionium distribution in the surface sediment layer ---------- 51
7. Schematic chart of thorium distribution in the surface sediment layer ---------- 52
8. Schematic chart of radium distribution in the surface sediment layer ---------- 53
9. Relationship between the content of ionium and manganese, radium and manganese, and thorium and manganese in the sediments ------- 55
10. Paleotemperature curve, absolute age of Atlantic Ocean sediments, and correlation with the Quaternary stratigraphy of Western Europe and North America ---------- 58
11. Bottom relief in the region of station 3163 ---------- 59
12. Core at station 3163 ---------- 61
13. Relationship between the content of amorphous silica and calcuim carbonate ---------- 64
14. Bottom relief in the region of station 4068 ---------- 72
15. Core sample at station 4068 ---------- 73
16. Relationship between the content of $SiO_{2\ amorph}$ and Mn in the core at station 4068 ---------- 74
17. Relationship between the content of $SiO_{2amorph}$ and Fe in the core at station 4068 ---------- 74

18. Bottom relief in the area of station 3378 ---------- 80
19. Bottom relief in the area of station 3325 ---------- 80
20. Bottom relief in the area of station 3342 ---------- 80
21. Bottom relief in the area of station 3359 ---------- 80
22. Core at station 3378---------- 81
23. Core at station 3325 ---------- 81
24. Core at station 3342 ---------- 82
25. Core at station 3359 ---------- 82
26. Relationship between the percentage of $SiO_{2\ amorph}$ and $CaCO_3$ at station 3378 ---------- 83
27. Relationship between the percentage of $SiO_{2\ amorph}$ and C_{org} at station 3378 ---------- 83
28. Bottom relief in the area of station 3451 ---------- 88
29. Core sample at station 3451 ---------- 90
30. Relationship between the content of $SiO_{2\ amorph}$ and $CaCO_3$ at station 3451 ---------- 90
31. Relationship between the content of $SiO_{2\ amorph}$ and Fe at station 3451 ---------- 90
32. Relationship between the content of $CaCO_3$ and C_{org} at station 3451 ---------- 90
33. Relationship between the content of $SiO_{2\ amorph}$ and C_{org} at station 3451 ---------- 90

FIGURES (con)

34. Bottom relief in the region of station 3625 ---------- 93
35. The relationship between SiO_2 amorph and Mn content in the core at station 3625 ---------- 95
36. The core sample at station 3625 ---------- 96
37. Bottom relief near station 3495 ---------- 99
38. The core at station 3495 ---------- 100
39. Relationship between SiO_2 amorph and Mn content at station 3495 -- 101
40. Bottom relief in the region of station 3520 ---------- 104
41. Core at station 3520 ---------- 105
42. Relationship between SiO_2 amorph and C org content at station 3520 ---------- 106
43. Relationship between $CaCO_3$ and C org content at station 3520 ----- 106
44. Relationship between Io and Th content at station 3520 ---------- 108
45. Bottom relief in the region of station 3532 ---------- 109
46. Core at station 3532 ---------- 111
47. Relationship between SiO_2 amorph and $CaCO_3$ content at station 3532 ---------- 112
48. Relationship between SiO2 amorph and C org content at station 3532 ---------- 112
49. Bottom relief in the region of station 3530 ---------- 115
50. The core at station 3530 ---------- 116
51. Bottom relief in the region of station 3481 ---------- 116
52. The core at station 3481 ---------- 117
53. Bottom relief in the region of station 3873 ---------- 118
54. Core at station 3873 ---------- 118
55 ottom relief in the region of station 3746 ---------- 120
56. The core at station 3746 ---------- 123
57. Bottom relief in the region of station 3797 ---------- 124
58. The core at station 3797 ---------- 126
59. Bottom relief in the region of station 3995 ---------- 127
60. The core at station 3995 ---------- 128
61. Relationship between the Fe and Th content in the core at station 3995 ---------- 129
62. The core at station 3921 ---------- 130
63. The core at station 3993 ---------- 131
64. The core at station 3989 ---------- 132
65. The core at station 3650 ---------- 132
66. Comparison of the thickness of horizons of identical age in the western Pacific Ocean ---------- 143
67. Comparison of the thickness of horizons of identical age in the western Pacific ---------- 145

TABLES

1. The content of radioactive isotopes in seawater ---------- 15
2. The content of thorium, ionium and radium in marine and oceanoc sediments ---------- 18
3. The content and activity of radioelements in pelagic sediments ---- 19
4. Sediment deposition rates determined from the radium content of sediments by scientists of the American school ---------- 22
5. Sediment deposition rates determined by scientists of the Swedish school ---------- 22
6. Quantity of radium separated by various analysis methods ---------- 37
7. Thermohaline characteristics of the water masses of the western Pacific Ocean ---------- 43
8. The content of various radioelements in various tyoes of sediments in the western Pacific Ocean ---------- 50
9. Sedimentary stratigraphy of the core at station 3163 ---------- 67
10. The stratigraphy of sediments at core station 4068 ---------- 78
11. Depths within cores of layers having relatively large or small amounts of amorphous silica ---------- 84
12. Depth from the sediment surface of layers of warm and cold water diatoms ---------- 86
13. The stratigraphy of the sediments of cores from stations 3378, 3325, 3342, and 3359 ---------- 87
14. Stratigraphy of the sediment core at station 3451 ---------- 94
15. Stratigraphy of the sediment core at station 3625 ---------- 98
16. Stratigraphy of the sediment core at station 3495 ---------- 103
17. Stratigraphy of the sediment core at station 3520 ---------- 110
18. Stratigraphy of the sediment of the core at station 3532 ---------- 114
19. Stratigraphy of the sediment of the core at station 3873 ---------- 121
20. Comparison of the thickness and absolute age of stratigraphic horizons in cores from the temperate and tropical regions of the Pacific Ocean ---------- 134
21. The absolute age of sediments of the glacial and interglacial epochs of the western Pacific Ocean ---------- 138
22. Comparison of the absolute age of glacial and inter-glacial deposits in the Pacific and Atlantic Oceans ---------- 139
23. Sedimentation rates and sediment thickness in the northwest Pacific Ocean ---------- 144

Appendix Tables

I. Characteristics of the surface sediment layer of the western Pacific Ocean and the radio-isotope content of the sediments ---------- 160
II. Characteristics of the sediment core at station 3163 ---------- 162
III. Characteristics of the sediment core at station 4068 ---------- 164
IV. Characteristics of the sediment core at station 3378 ---------- 165
V. Characteristics of the sediment core at station 3325 ---------- 166
VI. Characteristics of the sediment core at station 3342 ---------- 167
VII. Characteristics of the sediment core at station 3359 ---------- 168
VIII. Characteristics of the sediment core at station 3451 ---------- 169
IX. Characteristics of the sediment core at station 3625 ---------- 170
X. Characteristics of the sediment core at station 3495 ---------- 170A

TABLES (con)

XI. Characteristics of the sediment core at station 3520 ---------- 171
XII. Characteristics of the sediment core at station 3532 ---------- 172
XIII. Characteristics of the sediment core at station 3530 ---------- 173
XIV. Characteristics of the sediment core at station 3481 ---------- 174
XV. Characteristics of the sediment core at station 3873 ---------- 175
XVI. Characteristics of the sediment core at station 3746 ---------- 176
XVII. Characteristics of the sediment core at station 3797 ---------- 177
XVIII. Characteristics of the sediment core at station 3595 ---------- 179
XIX. Characteristics of the sediment core at station 3921 ---------- 180
XX. Characteristics of the sediment core at station 3993 ---------- 180
XXI. Characteristics of the sediment core at station 3989 ---------- 181
XXII. Characteristics of the sediment core at station 3650 ---------- 182
XXIII. Depths and coordinates of stations ---------- 183

INTRODUCTION

The study of the stratigraphy of deep-sea sediments to recreate 5
the geological history of the seas and oceans began about forty years ago. However, the most significant results were attained only during the postwar years (1945 - 1965), when core sampling technology attained significant development and methods of relative sediment chronology were expanded and reinforced by radiochemical methods of absolute sediment-age determination.

Hundreds of core samples of deep-sea sediments from the Pacific, Atlantic, Indian, and Arctic oceans have been studied in the Soviet Union and abroad during this period. The lithologic composition of sediments was studied in most of the core samples and the quantitative and qualitative characteristics of the vertical variation of microfauna and microflora were determined in many of them. The absolute age of and sediments was determined using ionium, radio-carbon, and protactinium-ionium metods. Paleotemperatures of the ocean basins were also determined, based on the correlation of oxygen O^{18} and O^{16} within the carbonates and shells of foraminifera in some core samples.

The core samples, taken from the bottom of deep ocean basins, contain detailed records of past epochs and are the most valuable data on earth from which to reconstruct the history of the Quaternary period. It should be noted that the development of a single-scale of the Anthropogen(ic) based on study of material from continental deposits often encounter considerable and sometimes unsurmoutable difficulties as a result of numberous regional hiatuses at different ages, local climatic fluctuations, and migrations of terrestrial fauna. An exception are the events of the last 10 to 20 thousand years, which are difficult to decode in deep-sea sediments. The difficulty results from the small thickness of pelagic sediments (from a fraction of a millimeter to 10 to 20 cm, and very seldom more than 20 cm) deposited during that short period of time and, partly, from the mixing of the uppermost sediment layer by (burrowing) organisms that inhabit the bottom. Even though the probability of alteration of deep-sea sediment texture by benthic animals is slight, because of their insignificant biomass (less than 0.05 g/m^2 far from the coast), it should not be completely excluded, especially, if one remembers that underwater photographs usually show traces of the activity of organisms on the bottom in the form of small mounds and tunnels of mud-eaters, probably formed at different times.

The main purpose of this work was to determine the straitigraphy of bottom sediments and to reconstruct the history of deep-sea sedimentation in the western Pacific Ocean based on comparison of data from lithologic and micropaleontologic study of the sediment cores and determination of their absolute age by the ionium method. In most

foreign works, the application of relative chronology in the stratigraphy of deep-sea sediments is based, first of all, on study of the distribution of calcium carbonate ($CaCO_3$) and the composition of the planktonic foraminifera in the sediments. The present study is based on the patterns of vertical variation, in core samples, of the content, not only of calcium carbonate, but also other components, and especially variations in the content of biogenic amorphous silica (SiO_2 amorph) and the composition of aquatic diatom flora. In the environment of deep parts of the Pacific Ocean, this has certain advantages, due to the extremely low solubility of biogenic silica in the water column compared to carbonate materials. Calcium carbonate nearly always dissolves completely in the cold bottom waters at depths of 4.5 to 5 km or more that are typical of the deep oceans. The amorphous silica that forms the valves of diatom plants is deposited at all depths up to 11 km, and its distribution in deep-sea sediments does not depend on the temperature and pressure of water at the bottom of the ocean.

The other goal was to study the pattern of distribution of the uranium family of radioactive elements (U^{238}, TH^{232}, TH^{230}, Ra) in sediments of the western Pacific Ocean. Such a study is very interesting, not only to determine the deposition rate and the absolute age of the sediments and their stratigraphy, but also the geo-chemical reaction of the radioactive elements in the ocean.

The data used in this study consist of core samples of deep-sea bottom sediments collected by the ship VITYAZ' on expeditions of the Institute of Oceanology, USSR Academy of Sciences in the western Pacific Ocean from 1953 to 1958. From more than 200 core samples, 65 cores from 2 to 12 m long were selected for this study. Twenty-three core samples were subjected to an especially thorough study. In addition grab (or scoopfish?) samples of the surface sediment layer were analyzed to determine the content of radioactive elements and other components (fig. 1) .

It should be noted that from 1949 to 1951, a VITYAZ' cruise in the Far Eastern seas took much longer core samples (up to 34m), but they were analyzed only for micropaleontology and lithology. The 1961 to 1962 VITYAZ' expedition in the Pacific and Indian oceans collected a number of long core samples using a heavy large-diameter (190 mm) bottom corer. These large cores are especially valuable in studying the absolute age of the sediments, but, because their analysis has just begun, data from them could not be used in this work.

Most of the analyzed core samples were taken from the bottom of deep basins with an undulating or hilly relief. Sediments from the temperate, tropical, and equatorial regions of the western Pacific Ocean of the most diverse lithologic type (terrigenous clays, siliceous diatom, and calcareous foraminiferal oozes, and deep-sea red clays) were studied. Core samples were selected through visual and microscopic study of the sediments. Most of the core samples showed slight changes

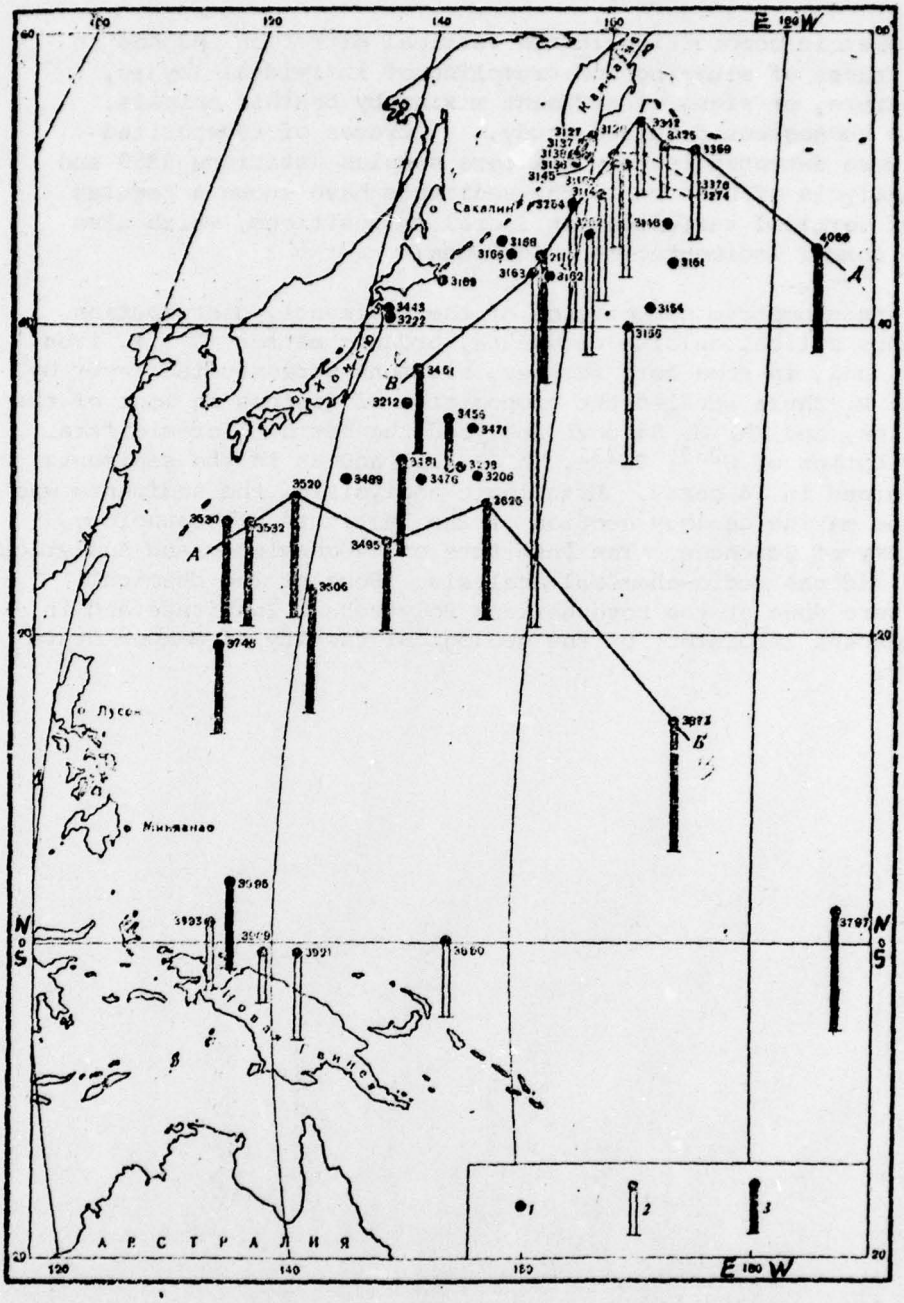

Figure 1. Station chart. 1. bottom grab samples; 2. bottom sediment cores; 3. core in which the absolute age of the sediments has been determined; AB and CDE are section lines (see figures 66 and 67). Here and farther on the stations are denoted by numbers.

7

in granulometric composition in the vertical direction and had no apparent traces of slumping and crumpling of individual layers, graded texture, or signs of sediment mixing by benthic animals. During the subsequent detailed study, traces of redeposited material were detected in only two core samples (stations 3359 and 3495). Analysis of diatoms in the sediments have shown a regular pattern of vertical variations in floral compositions, which also points to normal sedimentation conditions.

The granulometric composition of the sediments, distribution of amorphous silica, calcium carbonate, organic matter (C_{org}), iron, manganese, and, in some core samples, bitumens were studied layer by layer. A. P. Zhuze studied the composition of diatoms in most of the core samples, and Kh. M. Saidova analysed the benthic foraminifera. The distribution of U^{238}, Th^{232}, Th^{230} (Io) and Ra in the sediments was determined in 14 cores. Lithologic analysis of the sediments was done in the marine geology section of the Institute of Oceanology, USSR Academy of Sciences. The Institute of Geochemistry and Analytical Chemistry did the radio-chemical analysis. Some of the chemical analyses were done at the Novocherkask Polytechnic Institute and in the luminescent laboratory of the geological faculty of Moscow State University.

Chapter I

HISTORY OF THE STRATIGRAPHIC STUDY OF QUATERNARY DEEP-SEA DEPOSITS

9

The authors do not intend to give a detailed history of the accumulation of knowledge of the stratigraphy of Quaternary deep-sea deposits, but to offer only brief glimpses of the main stages of development of this branch of geology, mention the most important works of each stage, and express some opinions of the validity of the stratigraphic construction in specific studies.

Until the 1920's, very short coring tubes were used on oceanographic expeditions. Only a few of these showed vertical variations in sediment compositions [143] and they provided very little stratigraphic information. Among the earliest studies, in which stratigraphic and paleographic conclusions were based on longer (up to 3 to 4 m) core samples of deep-sea sediments, are classic works by A. D. Arkhangel'skiiy and N.M. Strakhov on the geologic structure and history of the Black Sea [1, 2]. Lithologic studies of sediments were used for the first time in these reports to determine the stratigraphy of deep-sea sediments.

In 1925 to 1927, the German expedition on the ship METEOR collected extensive data on the bottom sediments of the Atlantic Ocean, but the core samples obtained by the expedition did not exceed 98 cm in length. In analyzing this material, planktonic foraminifera (156) were used for the first time, along with lithologic methods (97), to subdivide the sediments biostratigraphically. W. Schott has shown that in the central Atlantic, sediments that are quite poor in $CaCO_3$ and contain a colder-water type of fauna lie beneath globigerina silts (oozes) containing warm-water species of globigerina. The deposition of these low $CaCO_3$ sediments, in Schott's opinion, corresponded to the last continental glaciation and was accompanied by a sharp drop in the production of planktonic foraminifera in the ocean. During the same period M. Bramlette and W. Bradley studied the stratigraphy of sediments in cores up to 3 m long that were taken in the North Atlantic Ocean using a Piggot corer. The works of I. Cushman and L. Henbest continued Schott's investigations [93,98,99].

In 1947, B. Kullenberg constructed a piston corer that could obtain deep-sea core samples up to 15 to 16 m long [131]. This corer was first used successfully by the Swedish deep-sea oceanographic expedition on the ship ALBATROSS and then was adopted by many expeditions of the USA and some other countries. As a consequence, many reports on the Quaternary stratigraphy of deep-sea oceanic sediments and paleoclimatology of the oceans appeared. 10

Most of the initial studies dealt with the vertical distribution

of calcareous material - $CaCO_3$ content in the fractions larger than 0.062 and larger than 0.074 mm (often reflecting the $CaCO_3$ content within pelagic sediments) - as well as the content and correlation of the warm-water and temperate cold-water planktonic foraminifera and the correlation of Globorotalia truncatulinoides with right-hand and left-hand spiral shells [106, 107, 138, 144, 145, 157, 158].

It is necessary to emphasize the ambiguity of a paleoclimatic synthesis that is based only on quantitative and qualitative vertical variations, in core samples, of the biogenic carbonate material formed in surface waters. Repeated fluctuations of oceanic water temperatures during the Quaternary period were reflected not only in the production and species composition of planktonic foraminifera (the main source of $CaCO_3$ in sediments), but also in the solubility of their shells on the bottom during the changing reactivity of the bottom waters. In addition, shells of different species of foraminifera dissolve at different speeds and, as a result, their correlation in sediments can vary somewhat from their correlation in plankton. If, however, it is assumed that during the Quaternary period changes occurred not only in the ocean water temperature, but also in the depth of the ocean (to which the solubility of carbonate material on the bottom is related), then the paleogeographic conclusions based on present studies of planktonic foraminifera in core samples can be no less definite.

Nevertheless, palectemperatures of ocean surface waters, determined, in recent years, from the oxygen in the shells of planktonic foraminifera, have shown a distinct relationship between paleotemperatures on the one hand, and the $CaCO_3$ content and correlation of cold-water and warm-water foraminifera in sediments on the other. And as a result there was a growing confidence that paleogeographic determinations based on the distribution of planktonic foraminifera and $CaCO_3$ in sediments reflects real climatic changes of the Quaternary period [100,102]. Conclusions based on all of the other lithologic data and on methods of absolute geochronology [96,106,107,109,137] coincide well with this contention.

During the 1940's, the radium method of dating pelagic deposits was devised and used to determine the absolute age of silts (oozes) in a series of core samples from the Atlantic and the Pacific Oceans [148,149,164,165]. At the present time it has been determined that the radium method does not produce dependable results in most cases, because of the redistribution of radium within the sediment layer and its transfer through lixiviation into the bottom waters [42]. Exceptions are individual core samples of deep-sea red clays, within which no radium redistribution has taken place and the calculated ionium curve seems to be satisfactory [165,168]. Unfortunately, the data from two red-clay core samples from the Pacific Ocean could not be chronologically correlated with events of the Quaternary period. At the same time, one should note that the absolute age of the last cool period (which can be seen in most core samples of globigerina silts (oozes) from the Atlantic Ocean and is characterized by a decrease in the proportion of grains less than 0.074 mm, calcium carbonate, and warm-water species of foraminifera) was determined by the radium method to be 15,000 to 65,000 years [129]. This was later confirmed by a direct determination of age from the Pa/Io ratio and by extrapolation of C^{14} data [103,153].

In 1953, there was an unsuccessful, from our point of view, attempt to determine the detailed stratigraphy of sediments of the equatorial Pacific Ocean in the South American region based on determination of the absolute age of the sediments in one core by the radium method [121]. This work was based on the premise that dark brown clayey silts (red clays) were deposited under conditions of ocean surface water cooling, whereas the accumulation of highly calcareous, nearly white, globigerina silts (oozes) occurred under conditions of warming climate. Based on this, a large number of substages were combined, according to the absolute age data, into a series of glacial and interglacial horizons that were represented by repeated alternations of calcareous sediments and red clays, and were identified in the core column. Comparison of the above horizons with the horizons of two cores from the North Atlantic and Ross Sea, also dated by the radium method [149, 165], and with similarly identified horizons of a series of cores from the equatorial Atlantic and Pacific Oceans [102, 120, 153], is quite difficult.

In 1952, G. Arrhenius published a large report in which a wide range of problems of sedimentation in the eastern equatorial Pacific Ocean was discussed [91]. Arrhenius's stratigraphic plan relied on data on the distribution of $CaCO_3$ within cores of globigerina silts (oozes), which (data) was supplemented by the individual C_{14} determination (86) of the absolute age of the sediments within a core (No. 61B) [86] and extrapolation of these data based on the distribution of titanium in the sediments. The "titanium" method, proposed by Arrhenius, is one of the methods of extrapolation of data from the direct determination of absolute age. It rests, first of all, on the firmly established fact that titanium is a "pure" terrigenous component and, secondly, on the assumption that its rate of accumulation remained constant through the entire period of time being dated. Consequently, the increase of TiO_2 content within some layer of the core, when recalculated on the basis of the lack of carbonate compared to a layer of equal thickness whose absolute age is known, proves that this layer was deposited over a longer period of time.

Among the 24 core samples studied, Arrhenius described two (No. 58,990 cm long, and No. 62, 1,475 cm long) which represented, according to his data, the entire column of Quaternary deposits and exposed the upper layers of the Pliocene. Arrhenius drew the lower boundary of Quaternary deposits at a depth of 395 cm in core No. 58 and at 1,050 in core No. 62 based on the noticeable change in the $CaCO_3$ accumulation rate. It should be noted, that below this depth the $CaCO_3$ content fluctuates in a number of layers (Pliocene), as significantly as in the Quaternary deposits. The criteria defining the Pliocene- Pleistocene boundary are vague and force one to view these depths as only two among many possible ones. Arrhenius identified 9 high carbonate and 9 low carbonate stages in the Pleistocene and compared them respectively to epochs of cooling and warming ocean surface waters in the equatorial Pacific Ocean.

In this comparison, lies the concept most closely related to it of intensification of atmospheric and oceanic circulation in the equatorial Pacific Ocean during the glacial period, As a result, the inflow of cold abyssal waters rich in biogenic elements increased during the glacial epochs. The increase in nutrients within the layer of photosynthesis led to an explosive development of phyto- and zooplankton and increased deposition of their sketal remains on the bottom. The author correlated the four most clearly defined upper high carbonate ("glacial") stages in the eastern equatorial Pacific Ocean, with the four glacial advances in high latitudes. 12

Since 1949, systematic geologic studies in the Pacific Ocean have been made by the research ship VITYAZ" of the Institute of Oceanology, USSR Academy of Sciences. Use of sediment corers of different designs developed by the institute (uniflow, piston, and hydrostatic) [83,84] resulted in collection of a large number of deep-sea sediment cores from 1 or 2 to 12 to 15 m long, and in some cases (in the Okhotsk and Bering Seas) as much as 27 to 34 m long, during the VITYAZ' cruises, first in the Far Eastern seas and then in the Pacific Ocean.

The Institute of Oceanology used analyses of lithology, diatoms, foraminifera, and spore-pollen to clarify the stratigraphy of bottom sediments and the paleogeographic environment of their deposition. Lithologic analysis showed that cores from the Okhotsk and Bering Seas and the northwest Pacific Ocean contain repeated vertical variations in the content of a series of biogenic components (SiO_2, amorph, $CaCO_3$, C_{org}, and plant pigments), as well as (but not everywhere) volcanic ashes and rudaceous (coarse-grained, i.e. larger than 2 mm) glacially transported material [9, 13, 16, 17, 56-58, 60]. This made it possible to subdivide the analyzed sediment layer into several horizons and relate them to changes in climate and volcanic activity in the North Pacific Ocean. One of the sediment horizons rich in SiO_2, amorph, $CaCO_3$, and C_{org}, which was assigned to the warm stage of the last glacial advance based on ionium dating, was identified from the Aleutian Islands to the Philippine Basin [13].

We used diatom analysis, which was well developed in A.P. Zuze's work, with data from the Pacific Ocean to study many bottom sediment cores and came to important conclusions on the biostratigraphy and variation of climatic conditions in the Far Eastern seas and in the northwest Pacific Ocean [30-32, 34, 68]. From analysis of the long sediment cores from the Okhotsk and Bering Seas, we found that neritic Arctic-boreal and Arctic diatom flora twice invaded the central and southern regions of these seas from the north, replacing warmth-loving oceanic flora similar in composition to the flora now being developed here. Parallel to this, redeposited Tertiary and sublittoral fresh water diatoms increased in the sediments. In the northwest Pacific Ocean, during the general predominance of oceanic diatoms and the negligible proportion of neritic and sublittoral flora in the sediments, the changes were reflected in the replacement of warm-water diatom complexes by cold-water plants.

These data were used to identify up to five biostratigraphic horizons in the longest cores from the Okhotskh, Bering, and Japanese Seas and the northwest Pacific Ocean. The sediments formed during the period of warm surface water (horizons, I,III, and V) were assigned by A.P. Zhuze to the postglacial and interglacial epochs, and the sediments deposited during the cool water periods (horizons II and IV) were assigned to epochs during which the glaciation of the Far-Eastern seas increased.

Spore-pollen analysis was used successfully by E.V. Koreneva to study the stratigraphy of the bottom deposits and the paleogeography of the Okhotsk and Japen Seas [40,41]. Here stratigraphic results were similar to those derived from diatom analysis. It was determined that during the cool water epochs in the southern Sea of Okhotsk, spore-pollen complexes typical of dark coniferous taiga and wide-leaved species were replaced by forest-tundra suites. The similarity of the boundaries of horizons defined by diatom and spore-pollen analyses (30) attests the similar conditions that caused the displacement of marine and dry-land floral complexes in the North Pacific Ocean. Such conditions, on the opinion of A.P. Zhuze and E.V. Koreneva, were climatic changes, as well as fluctuations of sea level.

Foraminiferal analysis attained a new dimension in the study of the material collected by VITYAZ'. In order to clarify the stratigraphy of the bottom sediments and to reestablish the paleogeographic environment of their deposition, Kh. M. Saidova used for the first time, benthic not planktonic, foraminifera-both calcareous (secretional) and arenaceous (agglutinative) [63,65,66]. As a result of study of the ecology and distribution of these foraminifera in the bottom surface layer and data showing their distribution in cores, Saidova also identified, in sediments of the Far-Eastern seas and northwest Pacific Ocean, up to five and in places, even more horizons and tried to correlate them with the main subdivisions of continental Quaternary of Europe and North America. At the same time, it was concluded that the replacement of benthic foraminifera complexes in Quaternary sediments was related to changes in the bottom paleorelief of the Far Eastern seas and northwest Pacific Ocean.

As noted by the above researchers, the stratigraphic horizons identified by diatoms, spores, pollen, and benthic foraminifera do not always coincide even within the same core. The 17-meter core taken at station 3602 in the Sea of Japan is an example [40,64,66,68]. Depths within this core and layer thicknesses determined by the three methods differ considerably. There are also discrepancies in paleogeographic interpretation of the results obtained by the three paleontologic methods. This is because diatom flora and terrestrial vegetation react much more quickly and sharply to climatic fluctuations on the earth's surface than do benthic and especially deep-sea microfauna. However, the latter can be an index of changes in depths and physico-chemical conditions of the bottom waters, which usually is completely excluded in the case of diatom plants.

Thus, the application of different micropaleontological methods,

which either significantly complement each other or produce initially almost incomparable results, must always be supplemented by detailed lithologic study of the bottom sediments. The lack or disregard of such studies can result in questionable and even incorrect results. For example, if one identifies lamination of the "graded bedding"type in cores, it may be that the diatoms or foraminifera in the sediments are redeposited, which must influence stratigraphic and paleogeographic interpretations. However, if the particle and material composition of the sediments in the core do not vary vertically and the bottom microfauna change significantly, one should look for the cause, not in sharp fluctations of depth, but in changes in the physicochemical properties of the bottom waters. Many such examples can be supplied. 14

Farther on in this book (chapters VI,VII) an attempt is made to compare and correlate the lithologic sediment data and the distribution of aqueous diatom plants and foraminifera in a series of cores taken in the northwest Pacific Ocean.

The development of new radiochemical and physical methods of analysis (ionium, protactinium, radio carbon, isotope-oxygen) marked the beginning of a qualitatively new stage in the paleogeography of the Quaternary period. The wide use of these methods along with the lithologic and micropaleontologic studies of bottom deposits permits a critical evaluation of stratigraphic data on sediments in various regions of the World Ocean, a more valid correlation of individual cores, and comparison of the Quaternary chronology of the oceans and continents.

At the present time, because of limitations of radiocarbon and isotope-oxygen methods, high carbonate globigerina silts are the principal subject of study. Most of the core and grab samples analyzed by these methods were taken in the tropical regions of the oceans [28,100-104, 106, 107, 109, 153-155]. The stratigraphy of noncarbonate terrigenous and siliceous sediments and deep-sea red clays, whose absolute age was determined by ionium and ionium-thorium methods [4, 6-8, 44, 75, 116-118, 135], were almost unstudied.

The stratigraphy and paleogeography of Quaternary deep-sea deposits were established by lithologic and micropaleontologic analysis of the sediments and determination of the temperatures and absolute age of globigerina silts (oozes) in cores. Isotope-oxygen analysis of plantonic foraminifera in globigerina silts of the Atlantic Ocean has shown that the surface water temperatures in tropical regions of the ocean apparently underwent repeated periodic fluctuations of up to 6°C during Quaternary times. Study of a series of cores indicates that there are sharp transitions from the low temperatures typical of glacial advances to temperatures that correspond to those of contemporary and interglacial stages [102,153].

In the equatorial Pacific Ocean climatic changes are less sharply defined than in the Atlantic. Temperature fluctuations here were only 2 to 4° [10]. In the equatorial region water temperatures were, according to Arrhenius, somewhat lower during most of the Quaternary period than in adjacent regions to the north and south. This resulted, it seems, from upwelling at the equator of cold abyssal waters, which was especially intensive during the continental glacial epochs [87,91]. During maximum cooling (as well as during maximum warming) the temperature of the surface water layers was approximately the same [102], which agrees with fossil flora data which also indicates that during the interglacial epochs the subaerial temperatures were similar [114].

The determination of paleotemperatures based on the O^{18}/O^{16} ratio confirmed previously obtained data [150] that indicate that there is a direct as well as an inverse relationship, and a lack of relationship as well between the $CaCO_3$ content of sediments and paleotemperature variation. The presence of one or the other relationship depends on the correlation between the production of carbonates and their solution, as well as on the correlation of the quantities of incoming biogenic $CaCO_3$ and terrigenous material [100,105].

It was also determined that most of the analyzed cores from the postglacial and interglacial deposits of the Atlantic Ocean, Caribbean Sea, Mediterranean Sea, northwest Pacific Ocean, and the Arctic Ocean contain more $CaCO_3$ [20, 21, 47, 56, 58, 61, 111, 112, 169-171]. 15
This was confirmed by direct measurements of paleotemperatures in a number of cores from the Atlantic Ocean [100]. It was shown that changes in the $CaCO_3$ content of the sediments, amounting to more than 3 percent, correspond to changes in paleotemperatures. This relationship between minor fluctuations of $CaCO_3$ content and paleotemperatures cannot be confirmed at the present time, because the corresponding temperature variations lie within the range of error (+1°C) of the isotope-oxygen method [100,169].

In addition, analyses of core samples of globigerina silts (oozes) from the tropical Atlantic Ocean has established: 1. a direct relationship between paleotemperature fluctuations on one hand, and the content of the greater than 0.062 mm (or greater than 0.074 mm) grain size fraction and the correlation of warm-water and moderately warm-water planktonic foraminifera, on the other, and 2. an inverse relationship between paleotemperature and the magnitude of the $MgCO_3/CaCO_3$ ratio and , in some cases, the content of the clay fraction [102, 104, 107, 109, 153].

Data on the isotope composition of oxygen have confirmed G. Arrhenius's [91] concept that high carbonate deposits in the equatorial Pacific Ocean accumulated during the epoch of surface water cooling and intensified vertical circulation, which caused the replenishment of nutrients and increased production of calcareous and siliceous organisms [87, 90, 102].

The temperature of bottom waters in the equatorial Pacific Ocean (determined from the isotope composition of calcareous bottom foraminifera) during the glacial and interglacial periods, hardly differed, according to Emiliani, from contemporary temperatures. In the equatorial Atlantic, bottom temperatures were approximately 2.1°C lower during the glacial periods than at the present time. Such a difference was caused by the lesser volume of the Atlantic Ocean and the large inflow of ice into it. During the interglacial periods, cold melt waters were distributed along the bottom of the Atlantic [102].

In one Pacific Ocean core of globigerina silt that penetrated the layer of Quaternary deposits, Emiliani counted approximately 15 complete temperature cycles (increasing and decreasing.). He estimated the duration of the Quaternary period, from this core and based on its orientation, to be 600,000 years [102]. The deposition rate was estimated at about 1 cm per 1,000 years.

The determination of the absolute age of sediments (based on C^{14} and the Pa/Io ratio) and paleotemperatures (based on the O^{18}/O^{16} ratio) made it possible to determine the following:

1. The postglacial temperature rise began an average of 11,000 years ago and continued up to 6,000 years ago. About 6,000 years ago the climatic (temperature) maximum corresponded to the climatic optimum [104,108,154,155].

2. The last temperature minimum coincided with the main stage of the last (Würm) glaciation.

3. The temperature rise during the last glaciation lasted a comparatively short time (about 10,000 years or less).

4. The last interglacial temperature maximum occurred about 95,000 years ago [153]. The dating of the beginning of the Holocene and the temperature maximum of the last interglacial period is very significant, because these events are also recorded on the continents in pollen spectra, in buried soil horizons, and in cave deposits.

Based on direct methods of absolute sediment age determination from C^{14} (up to 40 to 50 thousand years) and Pa/Io (up to 150 thousand years), the determination of paleotemperatures from the O^{18}/O^{16} ratio in two globigerina silt cores in the Carribbean Sea, and the comparison of horizons identified with continental events dated by the C^{14} method, the following Holocene and Pleistocene chronology has been established [153]: Holocene - 0 to 10 thousand years BP (Before Present), Late and Middle Würm (Wisconsin) period - 10 to 30 thousand years BP, last interglacial stage - 30 to 50 thousand years BP, Early Wurm (Iowa) period - 50 to 65 thousand years BP, Riss (Illinois) period - 100 to 130 thousand years BP, and 130 to 175 thousand years BP, Mindel-Riss (Yarmouth) period. Even though the comparison of the temperature

fluctuations that preceded the last interglacial period in these cores (100 thousand years ago and later) with continental events should be viewed as preliminary, it is of great interest.

No unanimous opinion exists in the literature on the differences in sediment accumulation rates during glacial and interglacial periods. According to W. Broecker, K. Turekian, and B. Heezen 's data [95], the sedimentation rate in the Atlantic and Pacific Oceans depended on surface water temperature. During the Holocene (0 to 11 thousand years BP) and interglacial time (from about 70 to 80 thousand up to 150 thousand years) it was 3.7 and 2.1 times smaller, for the clay and carbonate sediment fractions respectively compared to the last glacial period. According to other authors sedimentation rates of the fine (<0.062 mm) and coarse (>0.062mm) carbonate fraction, did not differ noticeably during the last glacial and interglacial periods, but were considerably lower during the postglacial period [153].

The question of the criteria for subdividing Pleistocene and Pliocene sediments is of great interest. Some authors have noted that near the Pliocene-Pleistocene boundary discoasters had almost died out, apparently the number of right-hand spiral shells of Globorotalia menardii decreased, the number of foraminifera with left-hand spiral valves increased, and, according to Arrhenius, the deposition rate of carbonate material increased [9, 110, 151]. Nevertheless, these data were obtained from only ten cores (seven from the Atlantic, one from the Indian, and two from the Pacific Ocean) need confirmation from a considerably larger body of data, and proof that the above mentioned changes in flora and fauna were caused by changes in climate.

Chapter II

RADIOACTIVE ELEMENTS IN SEA WATER AND BOTTOM SEDIMENTS 17

In 1902 P. Curie stated at the conference of the French Physics Society that radioactive fission is a "standard" of time, because our solar system contains no force that can influence its (fission) progress, or change its direction and form. This concept was not immediately understood; only after completion of the scientific works of Rutherford and Boltwood, who understood the geologic aspects of this phenomenon, was radioactivity used to determine geologic time.

First of all, the absolute age of various igneous and sedimentary rocks on land and of the main geochronology scale were established. Later, initial efforts were made to estimate sedimentation rates in the ocean. No direct measurements of the content of radioactive elements in the water, bottom sediments, and organisms existed at that time, and consequently, there was no data on their mutual correlation.

V.I. Vernadskiy in Geochemical Reviews wrote: "...the main question in the ocean is whether uranium exists in the seas in quantities of the order of radioactive equilibrium with radium, i.e., is 10^{-6} to 10^{-7} percent applicable here or not. " [26, p. 246]. Only the answer to this question will make it possible to approach the solution to the problem of geochronology in the ocean. In subsequent years, in studies by V. I. Vernadskiy and a number of foreign scientists, a painstaking effort was begun to accumulate precise analytical data on the content of the radioelements in oceanic and fresh waters. The first measurements were of radium. The high sensitivity radiation method of radium content determination was proposed by J. Joly [123], following which, radium content was measured in the waters of various seas and oceans [113]. A large number of radium measurements were made of different types of marine bottom deposits (terrigenous sediments, foraminiferal and radiolarian silts (oozes), and deep-sea red clays) as well as iron-manganese modules (concretions) [42, 119, 130, 141, 165].

The first dependable data on the thorium and ionium content of bottom sediments were obtained in 1953 to 1954 [3, 122], and for oceanic waters it was obtained in 1957 [125]. This is not surprising considering the extremely low content of thorium isotopes in sea water. Although the qualitative aspects of the distribution of radio-active elements in bottom deposits is comparatively well known at the present time, existent data are still inadequate to completely resolve the problem of radioisotope geochemistry in the ocean.

1. The Content of Natural Radioactive Elements in the Ocean. 18

At the present time we can accept as proven that practically all radioisotopes found in the Earth's crust also exist in the ocean, but in an extremely dispersed state. For example, if in different continental

rock formations there is about x times 10^{-4} percent of uranium, then in seawater there is only x times 10^{-7} percent, i.e. approximately one-thousandth as much. The difference in thorium content is even more striking: the mean content in rocks is x times 10^{-3} percent, and it is present in seawater in exceedingly small quantity -x times 10^{-9} percent. Even lower quantities of other natural radioisotopes were measured.

It is necessary to note that the radioactivity of seawater is determined mainly by K^{40} and the radioactivity level of other radioisotopes is infinitely small (table 1).

Table 1

The content of radioactive isotopes in seawater (E. Picciotto's data [146]).

a. Radioactive isotopes
b. Half-life period (in years)
c. Concentration, g/ml
d. Isotope occurence, %
e. Number of decompositions, min/l

a Радиоактивные изотопы	b Период полураспада, годы	c Концентрация, г/мл	d Изотопная распространенность, %	e Число распадов, мин/л
H^3	$1{,}2\cdot10^{1}$	$3{,}2\cdot10^{-18}$	$1{,}0\cdot10^{-16}$	$6{,}6\cdot10^{-2}$ β
C^{14}	$5{,}5\cdot10^{3}$	$3{,}1\cdot10^{-14}$	$1{,}3\cdot10^{-10}$	$31{,}2\cdot10^{-2}$ β
Be^{10}	$2{,}7\cdot10^{6}$	$1\cdot10^{-13}$		$42\cdot10^{-4}$ β
K^{40}	$1{,}3\cdot10^{9}$	$4{,}5\cdot10^{-5}$	$1{,}2\cdot10^{-2}$	$6{,}6\cdot10^{2}$ β + γ
Rb^{87}	$5{,}0\cdot10^{10}$	$3{,}4\cdot10^{-5}$	27,8	6,0 β
U^{238}	$4{,}5\cdot10^{9}$	$2\cdot10^{-6}$	99,3	$15\cdot10^{-1}$ α
Th^{230} (Io)	$8{,}0\cdot10^{4}$	$6\cdot10^{-13}$	$>3\cdot10^{-3}$	$24\cdot10^{-3}$ α
Ra^{226}	$1{,}6\cdot10^{3}$	$8\cdot10^{-14}$	~100	$17{,}4\cdot10^{-2}$ α
U^{235}	$7{,}1\cdot10^{8}$	$1{,}4\cdot10^{-8}$	~0,7	$6{,}6\cdot10^{-2}$ α
Pa^{231}	$3{,}4\cdot10^{4}$	$5\cdot10^{-14}$	~100	$48\cdot10^{-4}$ α
Th^{227} (RaAc)	—	$7\cdot10^{-20}$		$48\cdot10^{-4}$ α
Th^{232}	$1{,}4\cdot10^{10}$	$2\cdot10^{-8}$	~100	$48\cdot10^{-4}$ α
Th^{228} (RaTh)	1,9	$4\cdot10^{-18}$		$7{,}2\cdot10^{-3}$ α
Ra^{228} (MsTh)	6,7	$1{,}4\cdot10^{-17}$	$\sim1\cdot10^{-2}$	$7{,}2\cdot10^{-3}$ β

The last column of the table makes it possible to calculate the overall radioactivity of seawater measured by α and β emissions: 3×10^{-10} and 8×10^{-3} Cu/l respectively. At the same time, if β radioactivity is almost wholly determined by K^{40}, then α emission is almost wholly determined by the uranium isotopes and by radium. From table 1, one more peculiarity of the activity of radioelements in the ocean can be seen: the lack of radioactive equilibrium in uranium series, particularly, the sharp imbalance of ionium and radium compared to the existing uranium, and the insufficiency of ionium compared to the existing radium. This phenomenon indicates the predominant deposition of ionium compared to radium. The same phenomenon characterized the actinium-uranium family: the ocean

contains only 0.1 of the protactinium produced by the U^{235} in the water. The thorium family also shows a predominant lack of thorium compared to mesothorium. It is hard to explain these patterns without data on the form in which the radioelements exist in the ocean. One can only guess that either radium isotopes exist in a form which has a lower sorption compared to thorium isotopes and, consequently, are absorbed to a lesser degree into the sea bottom, or the supply of radium in the water is reinforced by radium dissolving out of the bottom sediments. The latter assumption has many adherents, such as F. Koczy, who uses this assumption in estimating the diffusion rate of bottom waters [126]. 19

One more peculiarity of radioelements in the ocean, particularly of uranium and thorium should be noted. The ratio of thorium to uranium and thorium should be noted. The ratio of thorium to uranium in seawater is 0.01, whereas in rock strata it is approximately 3. Consequently, there is a sharp separation of uranium and thorium in the ocean water layers, which, according to H. Pettersson, is a geochemical peculiarity of the ocean [140]. This peculiarity was noticed even earlier by V. I. Vernadskiy, who pointed out that "... thorium belongs to those chemical elements that stand outside the geochemistry of water or, to be more exact, of water solutions," "...it (Th) can be found in solution only in the form of dispersed atoms." The history of uranium is quite different: "...unlike thorium, uranium penetrates liquid masses, bottom waters, and exists in solution, it is thought, in any natural water, eventhough in a state of extreme dilution" [26]. Vernadskiy's prediction has been wholly confirmed by the entire body of information accumulated by science during the last 30 years.

As can be seen from table 1, two groups of radioisotopes are present in sea water: single radioelements- (tritium, radiocarbon, berillium -10), which are of cosmic origin, and radioelements that are members of the radioactive families of uranium, actinouranium, thorium, and potassium-40. This causes the diversity of the age determination variants. At the same time, such radioisotopes as tritium, radiocarbon, and berillium can be used to solve problems of the dynamics of water masses, because they enter the ocean mainly from the atmosphere, and to determine the absolute age of bottom sediments. In the first case, H^3 and C^{14} are especially promising and in the second case - C^{14} and Be^{10}. Among the radioelements of the uranium and thorium family, only the Ra^{226} can be used in problems of water mass dynamics, where the concentration of other derivative products (RaTh), MsTh) is exceedingly small.

2. The Distribution of Radioelements in Bottom Sediments.

All types of deep-sea sediments have some radioactivity and contain all the elements that have been found in rocks and in seawater.

This raises the natural question of the different ways radioelements reach the sea bottom. To answer this question, one must know the forms in which radioelements are found in seawater and the form of their transfer from the liquid to the solid phase. Unfortunately, we lack the necessary data to provide a single solution to the question of forms of movement of radioelements in the ocean. Knowledge of the chemical properties of the radioelements and the physico-chemical structure of the ocean yields several hypotheses, which at present have been partially confirmed by data obtained by Soviet scientists [73,74].

These hypotheses stem from the established fact that during Post-Cambrian times "...the main form of migration of Al, Fe, Mn, V, Cr, and other lesser elements were fine suspensions in which the elements existed either within the network of fine clayey particles or in an absorbed state on their micells (colloidal ions)" [81, p.17]. This material contains uranium and thorium within a complex of fairly stable minerals, such as zircon and monazite. The other source of radioelement entrance into the sea bottom is seawater, which contains in a dissolved state, such elements as uranium (in the form of a stable carbonate complex) and radium (in the form of a true solution). At the same time, the uranium is the source of radium and ionium. 20
A certain quantity of radium in the water column is formed by lixiviation from the bottom sediments. According to E. Goldberg and M. Koide, 75 percent of the ionium enters seawater from the uranium in seawater and 25 percent comes from terrigenous material [117]. At the same time, nearly all the ionium enters the sea bottom through joint precipitation with ferric and manganese hydroxide [27], as well as by means of the absorbed colloidal particles of the hydrated aluminum silicate minerals [88]. The third source of radioelements in marine silts (oozes) is their introduction with the biogenic part of the suspension. The precipitation of radioelements by these means and with volcanic material seems to be insignificant. It should be noted that in spite of the variable injection mechanisms of uranium, radium, and thorium isotopes into the bottom, their main carriers in all cases are terrigenous, hydrogenous, and, to a lesser degree, biogenic substances in suspension.

Although all sediments types have some radioactivity, the amount varies within a wide range. Deep-sea red clays are the most radioactive; sands, aleurites (silts) and diatomaceous silts (oozes) - the least. This pattern can be clearly seen in table 2, which we compiled in our previous radiochemical study of sediments.

Table 2

The content of thorium, ionium, uranium and radium in marine and oceanic sediments.

a. type of sediments	Th 10^{-6}g/g	Io		U 10^{-6}g/g	RA	
		10^{-10}g/g	10^{-6}g/g em. U.		10^{-12}g/g	10^{-6}g/g em.U
Sands	0,9	0,32	2,0	3,7	0,6	1,8
Aleurites (silts)	1,0	0,54	3,0	2,6	0,8	2,3
Daitomaceous silts (oozes)	0,5	0,4	2,2	0,2	0,1	0,3
Foraminiferal silts (oozes)	1,0-1,7	2,0-4,0	11-22	0,3	3,0	9
Clayey calcareous silts (oozes)	0,4	2,5	14	0,5	13,0	38
Fine clay silts (oozes)	6,0	5,5	30	6,5	7,0	18
Deep-sea red clays	6,0	20	111	2,4	20,0	60

The table shows that the disturbance in the radioactive equilibrium in the uranium series is typical of all types of deep-sea pelagic silts (oozes). This disturbance is especially well defined in deep-sea red clays, where the Ra/U ratio reaches 25, and the Io/U ratio is more than 50 (at equilibrium both ratios are one). This means that radium has 25 times, and ionium more than 50 times greater values than the equilibrium values of uranium. Unlike the deep-sea red clays, sands and silts are distinguished not only by a lower content of radioelements, but also by Ra/U and Io/U ratios that are close to the equilibrium values. Table 3 shows that the overall level of α radioactivity is determined primarily by ionium and radium, whose concentration in pelagic sediments is tens of times greater than the uranium concentration. This can be seen clearly from the data recently published by E. Picciotto [146] (table 3), which show that in bottom sediments there is a measureable quantity of protactinium and berillium-10, which are prospective elements for geochronology [139,153].

If one compares the distribution pattern of radioelements of the uranium family in sea water to that in sediments, the direction of the process will be clearly apparent. The derivative products of uranium and actinouranium (radium, ionium, and protactinium) decay, in particular, move from the water into the bottom sediments, which

disturbs radioactive equilibrium of the uranium family in the surface sediment layer, in the bottom deposits this equilibrium must gradually reestablish itself and make possible an estimate of the thickness of sediments accumulated during certain intervals of time.

Table 3

The content and activity of radioelements in pelagic sediments. (E. Picciotto's data).

Elements	Concentration of the dry sediment, g/g	Activity, dissoc/ min/year
K	$2,4 \times 10^{-2}$	6
U	$1,4 \times 10^{-6}$	1,2-7,2
Th	$6\text{-}15 \times 10^{-6}$	1,2-3,6
Io	$5\text{-}30 \times 10^{-10}$	18-120
Ra	$20\text{-}50 \times 10^{-10}$	18-120
Pa_{10}	$1\text{-}6 \times 10^{-11}$	0,6-4,8
Be	1.10^{-13}	6×10^{-3}

The real pattern of distribution of radioactive elements in sediments significantly deviates in many cores from the theoretical one. This applies more to the derivative products of uranium decay - radium and ionium, whereas uranium and thorium do not vary greatly in the thickness of deposits (several meters) studied. The pattern clearest and closest to the calculated one occurs in deep-sea red clays, and the most complex pattern is in the heterogenous (in type and granulometric composition) sediments on the ocean fringe. Uranium and thorium and radium and ionium concentrations change here in the transition from layer to layer, and the curve assumes a general sinusoidal appearance.

3. The Ionium Method of Determining the Deposition Rate of Marine Silts (cozes).

All the radioelements or combinations of several radioelements discussed theoretically can be used in marine chronology. At the present time, in spite of the methodological difficulties of carbon and berillium isotope determination, and in the lack of dependable concepts of the geochemical conduct of these radioisotopes in the hydrosphere, the radio-carbon method, which makes is possible to date within 50 to 100 and 50 to 70 thousand years intervals, and

the radiumberillium method, which can be used to date within the 500,000 to 10,000,000 years interval, find ever greater acceptance.

The radium-ionium, ionium, and ionium-thorium methods were quite widely applied in dating marine and oceanic sediments. The development of these methods is related to four stages of radiochemical studies of the ocean. The first stage was the work by Joly, who discovered the high content of radium in pelagic clays [123]. The second was L. M. Kurbatov's discovery of the high radium content in iron - manganese nodules, which he used to determine the age of these concretions [46]. The third stage was the extensive research of W. Urry and C. Piggot into methods of determining radium and uranium content in bottom sediments cores. Urry and Piggott developed the general theoretical bases of their geochronology [162, 167] from the large body of data on the content and distribution of these elements in sediments. The beginning of the fourth-contemporary-stage is tied to the name of H. Pettersson. He hypothecated the origin of radium in marine silts (oozes) based on the ionium content. This hypothesis stimulated marine geochronology in a new direction [140,53]. 22

Without dwelling in detail on Joly's early works, which are now only of historic interest, let us discuss the substance of the three subsequent stages of research. Kurbatov proposed and used the radio-active method of measuring the sedimentation rate in the sea to study ferro-manganese nodules from the Kara Sea [46,132]. The basis of this method is the established fact that radioactive equilibrium in the uranium series is disturbed as radioelements settle on the bottom. Kurbatov has determined that the radium content decreases from the surface of ferro-manganese nodules to the center, but the basic chemical compsition of the nodules does not change. He believed that this decrease in radium concentration was the result of radium decay. Kurbatov estimated the age of the concretion to be 5,300 to 5,500 years. He pointed out several possible ways for radium to reach the sea bottom; the precipitation of radium related to its absorption by mineral particles, and precipitation in connection with various chemical and biochemical processes. Thus, Kurbatov not only developed radioactive geochronology in its general form, but gave it a practical and theoretical basis.

Beginning in 1941, studies conducted under W. Urry's guidance appeared [148,149,152,162, 165 - 167]. The authors, in addition to the theoretical bases for the radioactive-equilibrium-disturbance method of determining marine sedimentation rates, dwell at length on such questions as the development of dependable and accurate instruments to measure radium, methods of obtaining precise radium standards, and methods and instruments to measure small amounts of uranium. Serious attention was paid to investigating causes and the degree of deformation of cores during extraction by different coring tubes and the influence of the distortion on measurement

precision. The authors used extensive lithologic data to interpret the results. The main object of these studies were silts of the Carribean Sea and the Atlantic and Pacific Oceans, Data on the deposition rate of different types of sediments resulting from these studies are presented in table 4, which shows that the sedimentation rate varies considerably depending on sediment composition and the location of the cores. The lowest deposition rates are for oceanic red clays; the rates are considerably higher in globigerina silts and are highest in terrigenous glacial marine deposits.

Parallel to Urry's and Piggot's works, extensive research into marine radioactivity was conducted by a school of researchers guided by Pettersson. Beginning in 1937 to 1939, thorium isotopes were included in the range of study along with radium and uranium. Pettersson suggested that the shortage of radium in seawater can be caused by a more complete settlement of ionium, which is the parent of radium [115, 140]. In 1949 F. Koczy's methodical work appeared [127], in which the degree of thorium isotope absorption in red clay, manganese dioxide powder, and iron-manganese nodule powder was demonstrated. This work attempted to resolve the problem of the mechanism of extraction of thorium isotopes from the seawater by experimentation. It also assumed that all thorium carried into the sea by rivers settles in the coastal zone of seas and oceans.

Pettersson also devoted great attention to the question of thorium isotope activity in seawater and bottom deposits [141, 142]. 23
In his later works Petersson, as well as Kroll and Koczy, discussed problems of marine chronology and tried to estimate the equilibrium of radioelements in the ocean [42, 128-130]. In the same report, the authors dwelt in detail on the premises of radioactive dating, particularly of the ionium method. They substantiate a number of assumptions, with which the ionium method can produce reliable age determinations. These assumptions are as follows: 1. the ionium deposition rate per unit of surface area must remain constant during the time interval under investigation; 2. ionium, like radium precipitated on the sea bottom, must not migrate within the sediment layer; 3. the quantity of uranium, ionium, and radium that reaches the sea bottom by different routes (not from seawater) must be minimal; 4. the analysis must be made on cores with an undisturbed top, because calculations assume the age of the surface sediments to be zero. Sediment deposition rates found by this group of scientists are given in table 5. It is seen that deep-sea red clays of the Pacific Ocean are deposited at a rate of 0.5 to 2 mm per 1,000 years. These data are close to the values obtained for red clays by American researchers [148,166].

Table 4

Sediment deposition rates determined from the radium content of sediments by scientists of the American school.

Region studied	Sediment type	Sedimentation rates mm/1,000 years	Bibliographic reference
Caribbean Sea	Globigerina silt (ooze)	5-10	[148]
		25	[166]
		17	[166]
Northern Atlantic	Globigerina silt (ooze)	17	[166]
	Glacial marine sediments	150	[166]
	Blue clay	337	[166]
Pacific Ocean	Deep-sea red clay	5-6	[149]
		6.8	[166]
		1-6	[166]
Southeast Pacific Ocean	Deep-sea red clay	18	[166]
Equatorial Pacific Ocean	Globigerina silt (ooze)	13	[166]
		59	[166]
		25	[166]
Antarctic	Glacial marine sediments		

Table 5

24

Sediment deposition rates determined by scientists of the Swedish school.

Region studied	Sediment type	Sedimentation rates (mm/1000 years)	Bibliographic reference
Pacific Ocean	Deep-sea red clay	0.5	[142]
		0.8	[147]
Central Pacific Ocean	Deep-sea red clay	1.0	[130]
		1-2	[129]
North Paicifc Ocean	Iron-manganese nodules (concretions)	0.7-5.9	[129]
Atlantic Ocean	Deep-sea red clays	10-20	[129]

It should be noted, that all the previously mentioned sediment deposition rates were calculated from the radium content of the sediments and subsequent recalculations assumed that during the last 10 thousand years radium was in radioactive equilibrium with ionium. As was demonstrated by the studies, radium can migrate within the sediment layer and the equilibrium between it and ionium is disturbed in this case [122]. Only the direct determination of ionium can correct this shortcoming of the ionium method and produce more dependable concepts of bottom sediment accumulation rates. 23

Research directed by E. Picciotto who, beginning in 1953 has made direct measurements of ionium in bottom sediments and in seawater is of 24
is of great interest in this matter [119,122,125,146,147]. These works are distinguished by their originality of execution of the experiment and the great dependability of the results. Picciotto's report, which contained a condensed but comprehensive discussion of the problems of the geochemistry of radioelements in the ocean and of methods of marine geochronology, appeared in 1961 [146].

Just as interesting is the research of Soviet scientists collectively directed by I.E. Starik [69, 72-74]. Along with the development of the ionium method of age determination of marine silts, these authors devoted some effort to the forms in which radioelements in the water and in the bottom deposits. This is one of the most complex problems of the geochemistry of radioelements in the ocean.

In recent years, two new variants of the ionium method have appeared. The first, the ionium-thorium method, was proposed and developed by E. Goldberg and M. Koide [117]. Its foundation is the concept that both isotopes settle on the ocean floor in the same ratio that they occur in seawater. The main objection to this variant is that ionium and thorium are present in seawater in different forms and reach the sea bottom by different routes. This can lead to a shift in the ratios of these isotopes in seawater, and in such a case the variation of the Io /Th ratio through the core will not reflect a uniform process of their arrival on the sea bottom.

The other variant of this method, ionium-protactinium, is being developed by J. Rosholt et al. [153]. It is based on the assumption that protactinium and ionium are found in seawater in a single form, because both of these radioisotopes are decay products of U^{238} and U^{235} isotopes. The objection to this variant is that, in spite of certain similarities of the chemical properties of ionium and protactinium, there are also some differences between them that can influence the absorption ability of these radioisotopes. This, in its turn, can cause a shift in the Io/Pa ratio in marine silts, Nevertheless, complete development of this method and accumulation of the necessary data, may prove its reliability.

As already mentioned, the initial variant of the ionium method of sediment age determination was developed by Piggot and Urry. It was based on a sharp (up to twentyfold) excess of ionium over uranium in the material that settles on the ocean bottom. The decrease in ionium content with depth results from radioactive decay law. For the central parts of the World Ocean, under conditions of constant rates of sediment deposition, the ionium method produces completely satisfactory results and makes it possible to date individual layers. Age determination of sediments deposited in the coastal regions of the ocean are complicated by the irregular deposition rate, variations in composition, and a large admixture of land-derived material in which the amount of radioelements can predominate over the quantity deposited directly from the water.

25

In all cases, evaluation of the lower limit of the sedimentation rate can be made by determining experimentally the thickness of the sediment layer in which radioactive equilibrium is attained. For different deposition rates, the following values will be obtained for Ra/Io and Io/U:

Deposition rate, mm/year	Layer thickness based on Ra/Io, cm	Equilibrium based on Io/U, m
0.03	3.2	1.6
0.1	110	60
1.0	1100	600

To determine the sedimentation rate under conditions of heterogenous sedimentation (precipitation), in most cases it is possible, not to date layer by layer, but only to estimate the mean deposition rate for the interval studied based on sediment thickness.

In using the ionium method of calculating sedimentation rate, the computations are made from a pair of radioelements, Ra - Io or Io-U, of which one has a long life span compared to the other, i.e. it does not decay noticeably during the period of time needed to establish equilibrium between them. Let the content of the short life span element in the upper layer be equal to N_o, and in the equilibrium layer N_{oo}. The content N in the intermediate layer will be equal to where h is the depth in

$$N = N_o e^{-\lambda \frac{h}{v}} + N_\infty (1 - e^{-\lambda \frac{h}{v}}),$$

cm, $\underline{v}$ is the average deposition rate in cm/year, and $\underline{\lambda}$ is the radioactive constant in units per year. From this equation it follows that log $(N-N_{oo})$ is the linear function of $\underline{h}$.

Having constructed the $(N-N_{oo}) = f(h)$ graph on semilogarithmic scale, let us draw a mean line through the experimental points and calculate the value of v for the interval studied. If N_{oo} or N_o are unknown, then it is possible to calculate the mean sediment deposition rate. For this purpose, determinations of radium or ionium content in the sediments are made at different depths. The results are plotted on a graph with rectangular coordinates, plotting the depth of the sample from the sea bottom surface along the horizontal axis, and the content of the radioelements along the vertical axis. A mean curve is drawn through the experimental points and then subdivided into sections equidistant along the depth axis. Corresponding ordinates will be equal to

$$N_0;\ N_1 = N_0 e^{-\lambda \frac{h_0}{v}} + N_\infty \left(1 - e^{-\lambda \frac{h_0}{v}}\right) = N_0 x + N_\infty (1 - x),$$

where $x = e^{-\lambda \frac{h_0}{v}}$;

$$N_2 = N_0 x^2 + N_\infty (1 - x^2);\ N_3 = N_0 x^3 + N_\infty (1 - x^3) \quad \text{etc.} \tag{26}$$

On the basis of this we find

$$x = \frac{N_1 - N_2}{N_0 - N_1} = \frac{N_2 - N_3}{N_1 - N_2} = \dots,$$

$$N_\infty = \frac{N_0 N_2 - N_1^2}{N_0 - 2N_1 + N_2} = \frac{N_1 N_3 - N_2^2}{N_2 - 2N_2 + N_3} = \dots,$$

$$N_0 = \frac{N_1 (N_1 - N_3) - N_2 (N_1 - N_2)}{N_2 - N_3} = \dots$$

From these equations, the average sedimentation rate v, the equilibrium concentration N_{oo}, and the initial concentration N_o can be calculated.

Chapter III

LABORATORY ANALYSIS METHODS

1. Methods of Determining the Granulometric and Basic Chemical Composition of Sediments.

The granulometric (grain-size) composition of bottom sediments was determined using the mechanical water analysis method developed in 1949 and 1950 at the Institute of Oceanology, USSR Academy of Sciences [50]. Only samples with a natural moisture content were used in the analysis of granulometric composition. They were elutriated using common tap water in greatly diluted suspensions, which improved settlement of the suspended particles and reduced flocculation. The separation of sediments into fractions was continuously controlled under a microscope during the process of particle separation into fractions larger than 0.1 mm, 0.1 to 0.05 mm, 0.05 to 0.01 mm, and less than 0.01 mm.

Beginning in 1960, the granulometric composition of sediments was analyzed in a number of cores based on a new variant of the mechanical water analysis (pipette?) method developed by V.P. Petelin [51]. It is based on the previous method [50], but a pipette is used, which makes it possible to separate from a single weighed portion the fractions larger than 0.1 mm; 0.1 to 0.05 mm; 0.05 to 0.01 mm; 0.01 to 0.005 mm; 0.005 to 0.001 mm; and less than 0.001 mm. This variant method has the advantage of determining all grain-size fractions of the sediments by weight; and the sum of all the fractions is compared to the (weight) of dry matter taken for the analysis. This permits quality control of each analysis without duplicating each. The new method also used experimentally selected deflocculants (dehydrated physphates) in varying quantities depending on the type of sediment. The addition of deflocculants completely eliminates secondary flocculation of fine dispersed material in th beakers and the clustering of clay material around the mineral particles.

Calcium carbonate and organic mater (C_{org}) were determined from one weighed portion of the dry sediment using the rapid combustion (Knopa-Fresenius) method. The quantity of $CaCO_3$ was determined by digesting the carbonate in a 10 percent solution of H_2SO_4 during heating. The gas products were purified and CO_2 was trapped on ascarite, weighed, and recalculated relative to $CaCO_3$. After this, the organic matter in the same sample was oxidized by a solution of $K_2Cr_2O_7$ in concentrated H_2SO_4 to CO_2, which was also absorbed to ascarite, weighed, and recalculated relative to C_{org}.

The amount of amorphous SiO_2 was determined by double processing 28
the weighed portion of finely ground dry sediment in a 5 percent solution of $NaCO_3$ during heating. The SiO_2 amorph was analyzed by the usual method double separation without using gelatin. The quantity of SiO_2 amorph

was determining by weighing [35].

The amount of iron, manganese, and titanium in the sediments was determined by the usually accepted method [54]. A weighed portion of finely ground, dry sediment was decomposed in hydrofluoric acid and fused with potassium pyrosulfate. The cooled alloy was completely dissolved in 5 percent H_2SO_4. The aliquot parts were removed from the solution obtained and divided ino its mineral components.

Iron was reduced by metallic bismuth in Johnson's reductor up to two valent one. The overall (bulk) content of the iron was calculated from the results of titration of the Fe^{2+} solution by potassium bichromate. Manganese content was measured by oxidation to permanganic acid by ammonium persulfate in a sulfuric acid solution in the presence of H_3PO_4. A $AgNO_3$ solution was used a catalyst. The amount of manganese was determined by colorimetric titration using a 0.05 N. solution K MnO_4 as a standard. The presence of titanium was determined by the appearance of a yellow tint while adding a 3 percent solution of H_2O_2 to the sulfuric acid solution of titanium; colorimetric titration was used to determine the quantity. Micropaleontologic analysis methods were described previously in reports [34,66] and are not given here.

2. Methods of Determining Radium, Uranium, and Thorium Isotopes in Bottom Sediments.

The analysis of radioactive elements in bottom deposits does not differ essentially from determination of these elements in sedimentary rock strata. The main problems are transfer of the sample into solution and separation of the coexisting elements that interfere with quantitative determination of the isotopes.

Current Methods of Analyzing Radium, Uranium, and Thorium Isotopes.

The first element that could be measured in marine sediments was radium, because the analysis method is relatively simple and is based on its radioactive properties. Radium is analyzed by current methods that relate it to radon and quantitative separation of the gas is necessary. At the present time, the entire analyzed weighed portion is transferred into a solution from which the radon is blown off [5]. This method is widely used, well conceived, and produces dependable results.

Small quantities of uranium are measured at the present time based mainly on ten fluorescence spectrum. This method was also well conceived and has been repeatedly described in the literature. If one carefully separates out interfering elements and uses highly sensitive fluorimeters, one can detect 10^{-11} g of uranium by this

method. However, the need to separate out exceptionally pure uranium considerably complicates the process, which depends to a great extent on the completeness and purity of separation of the accompanying elements.

Methods based on the radiochemical properties of uranium have been developed, i.e. on the measurement of α or β radiation of uranium, or of an equivalent product of uranium decay UX_1 [45]. The main requirements are the radiochemical degrees of purity of the preparations extracted for measurement, separation of the usual elements to intensify the specific activity, and the preparation of the material (compounds) in a thin layer to avoid absorption. Various methods are used to solve these problems. For example, W. Urry [163] separates the uranium isotopes by the carrier method. Iron is used to separate the isotopes of thorium, lead, bismuth, actinium, and radium. In order to obtain thin, even layers from the oxides of iron and uranium, an acetone suspension is prepared and is evaporated in a suitable apparatus. In the determination of uranium based on beta (β) radiation of an equivalent UX_1, the main requirement is the separation of other beta emitters. The requirement for thickness of the sample measurement layer is not very strict, but the comparison standards must be prepared with the same quantity of carrier. If the first method was not widely acceptable, the second method is convenient for simultaneous determination of thorium, ionium, and radium from the same weighed portion. However, where one has to measure only the uranium, Volkov's luminescence method is the most convenient one [48]. 29

The emanation method [127] was used in the first work devoted to measuring thorium in marine silts. However this method, which is essential in measuring radium, is not very useful for thorium, because it is considerably less sensitive (lower limit of 5×10^{-3} percent, and to obtain reliable results, large weighed portions (not less than 20 g of dry sediment) are needed. At the same time, determinations are made not of thorium itself, but of radiothorium, which is assumed to be equivalent to it. Most dependable are the direct colorimetric analysis methods based on the color reaction of thorium with one or another organic reagent, for example, with thoron or arsenazo III [43,62].

Ionium in marine silts was determined directly in 1953 and 1954 [147]. Thorium was measured simltaneously with ionium, because both radioelements being isotopes, come together during any chemical analysis. The method chosen by the authors is distinguished by its originality, but is quite complex. It consists of measuring the activity of thorium isotopes, separated in a radiochemically pure state, by the radiography method that was later used to measure thorium isotopes in seawater [125].

Other methods of ionium determination also use its radiochemical properties. The most dependable is based on measuring ionium from radium concentrated in the separated preparations of ionium. However, to accumulate measurable quantities of radium one needs about two years [71]. There are several methods of ionium measurement based on the specific α activity of ionium separated in a radiochemically pure state, which differs in the method of separation of ionium free from other α emitters. Best thought out is the method of separating and measuring ionium proposed by I. E. Starik et al [70], described as follows: After decomposition of the minerals, the thorium istopes are precipitated on to 3 mg of cerium, which is the carrier. It is purified from polonium, radium D, and radium E by electrolysis. The completeness of separation of the isotopes is controlled by UX_2 (Th^{234}). The most significant deficiency of this method is that it can be used only for minerals with a large uranium content.

Somewhat later, some scientists, with the help of I. E. Starik, developed a new variant of the same method applicable to marine silts. The shortcoming of their method is the large amount of work required. The separation operation alone requires continuous electrolysis for 10 hours and thorium is measured by the colorimetric method simultaneously with ionium [69].

In determining the age of oceanic sediments, one must obtain numerical data on the content of thorium and uranium. Nevertheless, the investigator usually does not have enough material, especially when analyzing silts from cores. Consequently, an important requirement of analysis methods is the measurement of all four radioelements from a single weighed sample. Such a variant method has been developed at the Institute of Geochemistry and Analytical Chemistry of the Academy of Sciences of the USSR and is described below. It should be noted, that to solve the problem at hand the method must fulfill the requirements of adequate precision, speed of analysis, and utility for serial analyses.

Because the concentration of ionium in marine silts (oozes) is of the order of 10^{-10} g/g, ionium can be measured from the count of its α activity. The quantitative determination of ionium requires the following: 1. separation of ionium in radiochemically pure form; 2. separated material of specific activity sufficient for measurement in the counting instrument used (in our case a DA with a 2π ionization chamber); 3. separated material in layers of such a thickness (~ 0.5 mg/cm^2) that absorption within the carrier layer can be disregarded.

In addition, since ionium is the isotope of thorium (Th^{232}) that is the same as radio thorium (Th^{228}), which is an α emitter and exists in silts in perceptible concentration that exceeds several fold the weight concentration of ionium, it is necessary to introduce a correction for its α emission. Consequently, one must also measure the thorium within the same weighed portion. In turn, it necessary to separate out most of the accompanying elements, which could distort the result of colorimeter

determination. Since the quantity of uranium is calculated from UX_1 (TH^{234}), one should separate extraneous emission sources from the sample. Finally, the method must provide for radium determination from radon in the same weighed sample.

Analysis Scheme

In the proposed method, ionium and uranium are determined radiochemically from the α and β radiation of ionium and th UX_1 equivalent to uranium, of which it is the first decay product. Thorium is determined colorimetrically with thoron which, in a mineral acid medium, turns pink with thorium. In developing this method we used the circumstance that all the three radioelements - ionium (TH^{230}), thorium (Th^{232}), and UX_1 (Th^{234}) - are isotopes. Consequently, the problem is reduced to the quantitative separation of the thorium isotope in a chemically and radiochemically pure state.

Because the analysis of ionium is made from α radiation, separation of the α emitting elements, uranium, polonium and radium is important to acquire dependable data. In analyzing uranium from the radiation of UX_1 the greatest danger is the active β emitters, RaD (Pb), RaE (Bi), and ThB(Pb), whereas other β emitters of all three radioactive families have a short half-life and will disintegrate completely toward the end of the analysis. The half-life periods (T) for RaB is 26.8 min (Bi); MsTHII - 6.13 hours (Ac); ThC-60.5 min (Bi); AcB - 36.0 min (Pb); and AcC - 2.16 min (Bi).

In analysing thorium with thoron one must separate large amounts 31
of other elements. This is because, in our case, the thorium content of marine silts is very small (about 2 to 3×10^{-6} g/g) and, in spite of the great sensitivity of the reagent (detectable minimum of 1 γ Th in 1 ml), large quantities of extraneous material can distort the result, slowing down the development of color. One should pay special attention to such elements as zirconium, titanium, and hafnium which, together with thoron, produce coloring similar to, but weaker than, the color of thorium. Elements that have colored ions must also be separated. Reliable results can be obtained on thorium only when it is practically pure.

An analysis method consisting of several stages was developed to resolve these problems. Radioactive admixtures are separated out in each stage and the usual chemical elements are removed (fig. 2). At the same time, the thorium isotopes are present in the precipitate (sediment) at all stages which, in spite of the large number of operations, excludes losses due to absorption.

First stage. The silt (ooze) is completely decomposed by mixing it with sodium peroxide. Leaching the solution with water and filtering separates the uranium, lead (RaD, ThB) and polonium, and removes most of the silicon, aluminum, etc. At this stage the carrier of the thorium isotopes is iron, which is always present in quantities sufficient for this purpose.

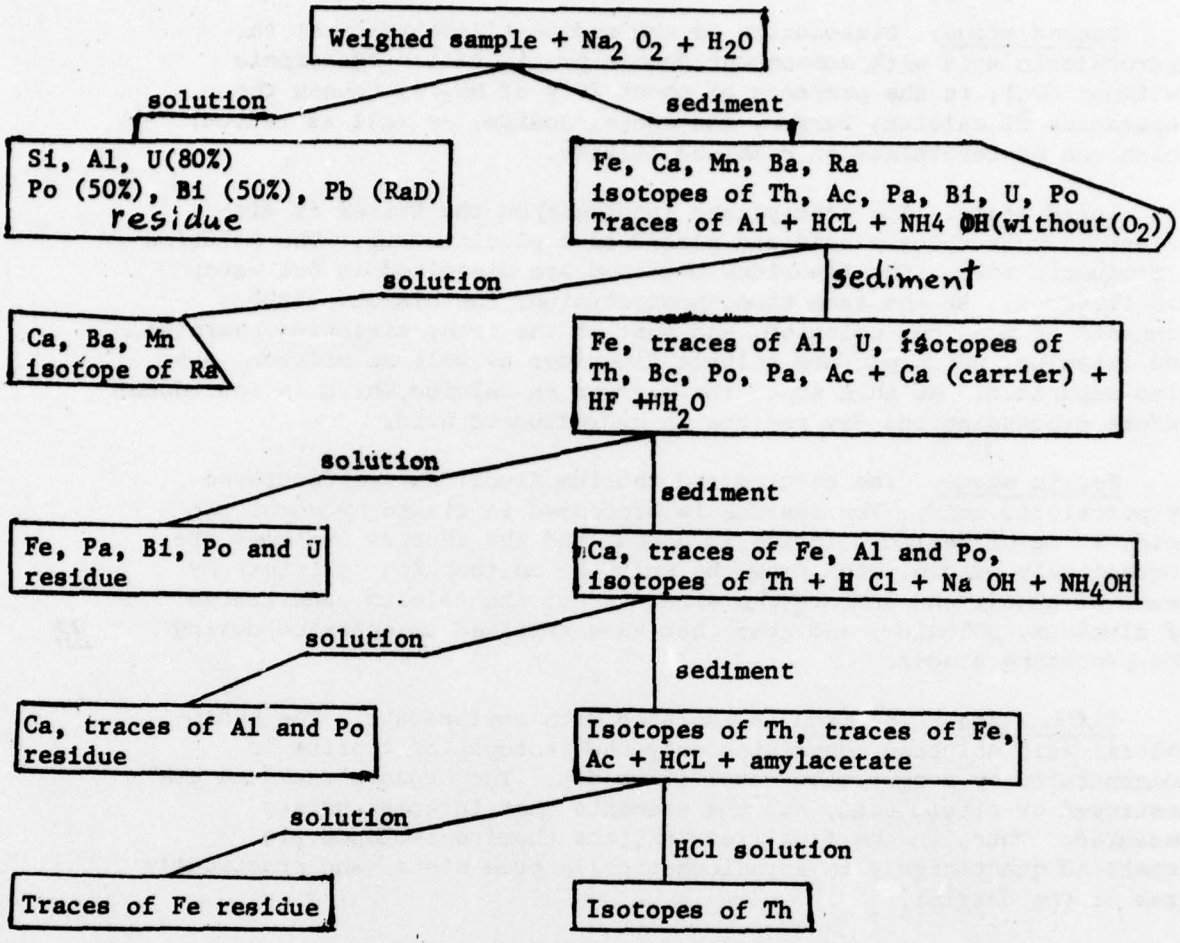

Figure 2. The scheme for analyzing sediments to determine the content of the isotopes of thorium, uranium, and radium.

Second stage. Dissolution of the sediment (precipitate) in hydrochloric acid with subsequent double precipitation by ammonia (without CO_2), in the presence of about 20 g of NH_4Cl, causes the separation of calcium, barium, manganese, sodium, as well as radium, which can be determined on combined filters.

Third stage. The precipitate (sediment) on the filter is dissolved in hydrochloric acid and placed on a platinum cup. The solution hydrofluoric acid. The fluorides obtained are dissolved in hot water and filtered. At the same time, protactinium, the bismuth (RaE) remnants of uranium, polonium, and most of the iron, zirconium, hafnium, and titanium, which produce soluble fluorides as well as silicon, are also separated. At this stage the carrier is calcium, which is introduced before processing the dry residue in hydrofluoric acid.

Fourth stage. The calcium and thorium fluorides are destroyed by perchloric acid. The residue is processed in dilute hydrochloric acid, 10 mg of ferric chloride is added, and the thorium isotopes are sequentially precipitated from the solution on the iron (carrier) by means of alkali and ammonia, to separate out the calcium and traces of aluminum, polonium, and lead that have remained unseparated during the preceding stages. 32

Fifth stage. The iron is isolated with amylacetate. The hydrochloric acid solution containing only the isotopes of thorium is concentrated by evaporation until it is dry. The organic residues are destroyed by nitric acid, and the elements that interest us are measured. Thus, in the final results, the thorium isotopes are separated quantitively in a radiochemically pure state, and practically free of the carrier.

Sixth stage. The ammonia filter formed during the second stage is acidified until a bright green color appears. Barium chloride is added to it and the barium-radium sulfates are precipitated. After they have settled, the sulfates are filtered out and dissolved in a soda solution by Trilon B. The solution obtained is transferred into a bubbler (diffuser), is blown out, and sealed (by fusing).

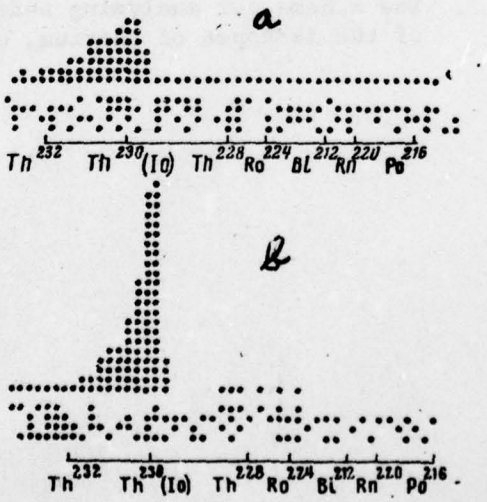

Figure 3. The α spectra of ionium separated from the bottom sediments (a) and from the bottom sediments contaminated by equilibrium pitchblende (b).

The proposed method of analysis has been verified for completeness and radiochemical and chemical purity of separation of the thorium and radium isotopes. Chemical, radiochemical, and physical control methods were used for verification. For example, to control the completeness of thorium isotope extraction, Th^{234} (UX_1) was added to the weighed portion of silt before analysis. The determination of thorium has shown that in the final stage of analysis the thorium isotope yield is about 95 percent. Then, in order to verify the completeness of RaD, RaE, and Po extraction, these radioelements were added to the weighed portion of the silt, and then they were measured in the final stage of the analysis. This experience showed that contamination of the thorium isotopes by radioactive lead, bismuth, and polonium does not exceed about 5 percent. The radiochemical purity of the thorium isotopes also was verified by long-term measurements of the separated preparations by α and β counters. Constancy of the α activity through time indicates the purity of the thorium isotope extraction, and decrease in β activity with T=24.5 days shows the purity of the separated UX_1. The most objective method, which permits a single value solution to the problem of how completely the radioactive mixtures are separated, is measurement of the separated preparations of ionium on a multichannel α analyzer that permits identification of the radioactive α emitters from the radiation energy. This was verified by an instrument designed by, Yu. A. Surkov of the Institute of Geochemistry and Analytical Chemistry. The α spectrum of the separated ionium in figure 3 shows that the ionium was obtained in a radiochemically pure state.

The influence of the chemical admixtures on thorium determination was analyzed using an addition method. Experience has shown that practically all the added thorium is retained and is quantitatively measured with thoron in the final residue. The completeness of radium separation was determined by adding radium of known concentration to the weighed portion. (All these control (verification) methods prove that the proposed method of analysis of thorium and radium isotopes from a single weighed portion can be used successfully to determine the content of uranium, ionium, thorium, and radium in marine silts (oozes). A detailed description of this method is given below. 33

Prescribed Method

Separation of Thorium Isotopes

A weighed 5-g sample of silt was heated and fused in a nickel crucible with 6 to 10 times as much Na_2O_2. After cooling, the fusion was washed in hot water (in a 1.5-l glass). After settling out for 10 to 15 minutes the residue was filtered through a folded filter, washed with hot water and dissolved HCL (1:1). The hydrochloric acid solution was diluted to one liter, and the sesquioxides were twice precipitated by NH_4OH. Thirty grams of NH_4Cl were added after each precipitation. After the second precipitation the residue was washed with hot water and dissolved in a small volume of HCl (1:1), 50 to 70 mg of $CaCl_2$ (in a solution) was added, and the solution placed in a platinum cup and evaporated until dry. The dry residue was processed by hydrofluoric acid and again concentrated by evaporation until dry. The fluorides were moistened with 0.5 to 1.0 ml of concentrated HCl, washed in hot water, and filtered through a folded "white ribbon" filter. The residue was washed into a platinum cup, concentrated by evaporation until dry, and processed by $HClO_4$ until there were no dense white vapors. The residue was again processed by HF, concentrated by evaporation, moistened with 0.5 to 1.0 ml of concentrated HCl, dissolved in hot water, filtered, washed with hot water into a platinum cup, concentrated by evaporation, and then the fluorides were destroyed by double processing with $HClO_4$. The residue was processed by concentrated HCl (5 ml), heated to dissolve it, transferred into a 100-ml glass, and dissolved with water up to 50 ml. Then 5 g of NH_4Cl was added to and it was precipitated by ammonia.[1]

The residue obtained was filtered, washed, dissolved in HCl (1:1), and twice reprecipitated by NaOH (25 percent), and once again by NH_4CH with an added 5 g of NH_4Cl. The final residue is dissolved in a small volume of HCl (1:1) and is concentrated by evaporation in a small glass until dry. The dry residue is dissolved in HCl (5:1), transferred into a separatory funnel, and the iron was separated by amylacetate previously saturated with HCl of the same concentration. The hydrochloric acid solution, now containing only the thorium isotopes and traces of associated elements, is concentrated by evaporation until dry, processed twice by concentrated HNO_3, and then by concentrated HCl (5 ml), and was concentrated by evaporation each time until dry. If the iron has not been removed completely, the separation by amylacetate was repeated. The final dry residue was dissolved in a 1 percent solution of HCl.

Thorium Determination

The 1 percent hydrochloric acid solution of thorium isotopes is

---

[1] If the iron is completely removed during the second processing (the dilute hydrochloric acid solution is almost colorless), 10 mg of $FeCl_3$ is added before precipitation by NH_4OH.

transferred to a colorimetric test tube, dissolved in 5 to 7 ml of water, and thoron (0.1 percent solution) is added until a pink color appears; then thoron is added again until the color of the solution will not change from rose to orange.

Into the other test tube, containing 1 percent hydrochloric acid, the same quantity of thoron is added and the thorium solution is titrated until the analyzed solution and the standard reach the same color density. When there is more thorium in the sample than 20 γ, the solution is diluted in a measured flask and its active part is titrated. 34

Uranium Determination

After the thorium analysis, the contents of the test tube is transferred to a small beaker and 1 ml of concentrated hydrochloric acid and 20 mg of ferric chloride (in solution) are added. After dilution to 50 ml, the contents of the beaker are heated and the iron and the thorium isotopes are precipitated by ammonia. The residue is filtered through a "white ribbon" filter, dried, calcinated, baked, and weighed. The β activity of the residue is measured on a terminal end counter with a mica window. The uranium content is measured from the activity found and the standard curve.

When the uranium content is equal to 1×10^{-4} percent, the weighed portions must be smaller than 10 to 15 g. At the same time, it is convenient to process simultaneously three portions of 5 g each, combining all three into one prior to uranium analysis. After the thorium analysis, the contents of all three test tubes are poured into one beaker and the thorium isotopes are precipitated on the iron in the usual manner.

Ionium Determination

The residue is measured on a β counter, then placed in an agate mortar and powdered under acetone. A fine suspension is concentrated by evaporation on a suspended disc under a lamp. The residue and the disc are weighed and its α activity is measured by the α counter. The ionium content is expressed in pulses/min or in uranium units by comparison with the uranium standard prepared in a thin layer. In order to avoid noticeable aborption of the ionium radiation in the carrier layer, the quantity of sediment on the disc must not exceed 0.5 to 0.7 mg/cm^2. The duration of the measurement is determined by the strength of the preparation and the required degree of precision.

Construction of the Standard Curve for the Analysis of Uranium using the UX_1 β Counter

100, 200, 300, 400, and 500 γ of radiochemically pure uranium together with UX_1-UX_{11} are precipitated by NH_4OH (without CO_2). 20 mg

of $FeCl_3$ is added to each standard as a carrier. The residue is dried, baked, and measured on the terminal end β counter. A graph of the dependence of the value of the measured β activity on the uranium content is constructed.

Preparation of Uranium Standards

A uranium standard prepared in a thin layer is required for continuous daily control of the DA installation operation, to determine its exploitation coefficient, and to express the results of the ionium analysis in uranium units. A series of such standards were prepared by elctrochemical precipitation of uranium from an alcoholic medium with pH = 5 or 6 radiochemically pure uranium[1]. The underlying platinum discs were thoroughly degreased,baked, and weighed. 34
Electrolysis was carried out in a special simple device, proposed by us, with a current density of 15 to 20 ma/cm^2 of the disc area. A platinum rod serves as the anode. Electrolysis duration was 1 min.

The residues on the discs from electrolysis are baked to a constant weight at a temperature of the order of 800 to 900° C. The weight of uranium and uranous oxides on the disc was then determined from the difference in weight of the disc before and after precipitation. Then all the standards were measured on the α counter and a graph of the dependence of the uranium weight on the pulses/min. value was constructed; the disparity between individual standards did not exceed 0.5 to 1 percent in all cases. The absolute number of particles emitted by the standard was calculated from the weight of uranium on the disc and the efficiency of the DA installation was calculated.

Radium Determination

From the analysis method it is seen that the radium is separated during precipitation of the sesquioxides by ammonia not containing CO_2; traces of radium remaining in the residue are separated at the end of the analysis during reprecipitation of the thorium isotopes on iron by ammonia (without CO_2). The radium on all these filters is determined by usual emanation method.

The experiment was conducted as follows: All the ammonia filters were collected into a 1.5-liter glass and concentrated by evaporation to 600 to 700 ml. The solution was acidified by hydrochloric acid until the blue coloring (ammonia copper complex) turned to bright green, 50 mg of barium chloride was added and the barium-uranium sulfates were precipitated from the hot solution by sulfuric acid. The solution was boiled about 30 minutes and left overnight. After settling, the solution was filtered through a "blue ribbon' filter, the filtrate was washed with 1 percent hydrochloric acid and transferred from the filter into a small 50-ml beaker by means of a thin stream of a soda solution of trilon B (5 percent solution of the trilon B in a 5% solution of Na_2CO_3). The

1 The radiochemically pure uranium was prepared by Urry's method of sequential precipitation of the radioactive admixtures on carriers.

Table 6

Quantity of radium separated by various analysis methods.

Sample Number	Radium Content (10^{-12} g/g) By the usual decomposition method	By the proposed method
1	4.6	5.0
2	3.5	3.7
3	1.08	1.08
4	0.37	0.4
5	0.38	0.40
6	0.57	0.60

barium-radium sulfates were dissolved by heating in this solution and poured into a bubbler (diffuser). The solution was blown through, the bubbler was sealed by fusion, and after some period of time the radium was analyzed by the method described above (a slight cloudiness of the trilon solutions is caused by the products of partial decomposition of Trilon B and has no influence on the radium determination).

Such an analysis procedure saves time because there is no need to additionally decompose the samples with soda and alkali and to separate the radium isotopes by the usual method [5]. The dissolution of barium-radium sulfates in Trilon B also saved considerable time compared with the transfer into solution by fusion with soda. With a limited quantity of material, the analysis of the four elements- uranium, thorium, ionium, and radium- from one weighed portion is also quite advantageous. In order to validate this scheme, radium in the silts was determined by the usual method, i.e. with special decomposition of the sample, as well as analysis of the radium parallel to the analysis of ionium and thorium. The data obtained are presented in table 5, which shows that quantitative determinations of radium made by both analysis schemes agree well.

Chapter IV

MAIN FEATURES OF CONTEMPORARY SEDIMENTATION IN THE WESTERN PACIFIC

The factors that influence contemporary sedimentation in the western Pacific Ocean were discussed previously [9,17,19]. The most important are: (1) climate; (2) orography and river flow from the drainage basin; (3) geologic structure and petrographic compostion of the continental rocks that fringe the ocean; (4) dynamics, physical-chemical properties, and biological productivity of the ocean waters, and (5) bottom relief.

The region discussed in this article is located in the temperate, subtropical, tropical, and equatorial zones of the Pacific Ocean. East-west climatic changes are reflected, not only in the hydrologic and biological processes of the ocean, but also determine the zones of contemporary sediment deposition

The influence of climate on sediment deposition becomes apparent even before the sedimentary material enters the sphere of hydrologic and biological action [77-81]. During the weathering of rocks and detrital movement on dry land, air temperature, the amount of precipitation, and the relief of the drainage basins influence the type of erosion and the relationship between various forms of sedimentary material carried into the ocean. On the northern periphery of the region (north of Hokkaido Island), where average annual temperatures fluctuate between - 1° and +10°C (fig. 4), the products of the mechanical weathering of rocks generally enter the ocean very slightly affected by chemical weathering. Chemical weathering is more active in the regions of contemporary volcanism (Aleutians, Kamchatka, Kuriles). Farther south, especially in the humid tropical region, where high annual average temperatures (20° to 26° C) coincide with abundant rainfall, continental rocks are subject to ever deeper chemical weathering, resulting in lateritic soils and a thick weathered layer.

A good example of this phenomenon is the north-to-south modification of a drainage basin's soil cover. Dern-podzol, mountain-forest, and moutain-taiga chestnut soils predominate in Kamchatka, the Kurile Islands, Hokkaido, and in the northern part of Honshu Island (up to 35°N). Yellow mountain and silica soils predominate in most of the Japanese Islands and the Nansei chain (approximately to the Tropic of Cancer). In the tropical and equatorial regions of the Pacific Ocean (Taiwan, the Philippines, New Guinea) they are replaced by moutain laterites and laterites. At the same time, as one moves from high latitudes to low latitudes, the proportion of montmorillonite and especially of kaolinite (in the laterites) in the clay fraction increases, and the content of illite and chlorite decreases. 38

Terrigenous material is brought into the ocean mainly by numerous rivers and, to a lesser extent, by coastal erosion. Figure 5, compiled from N. M. Strakhova's classification [78], provides some concept of

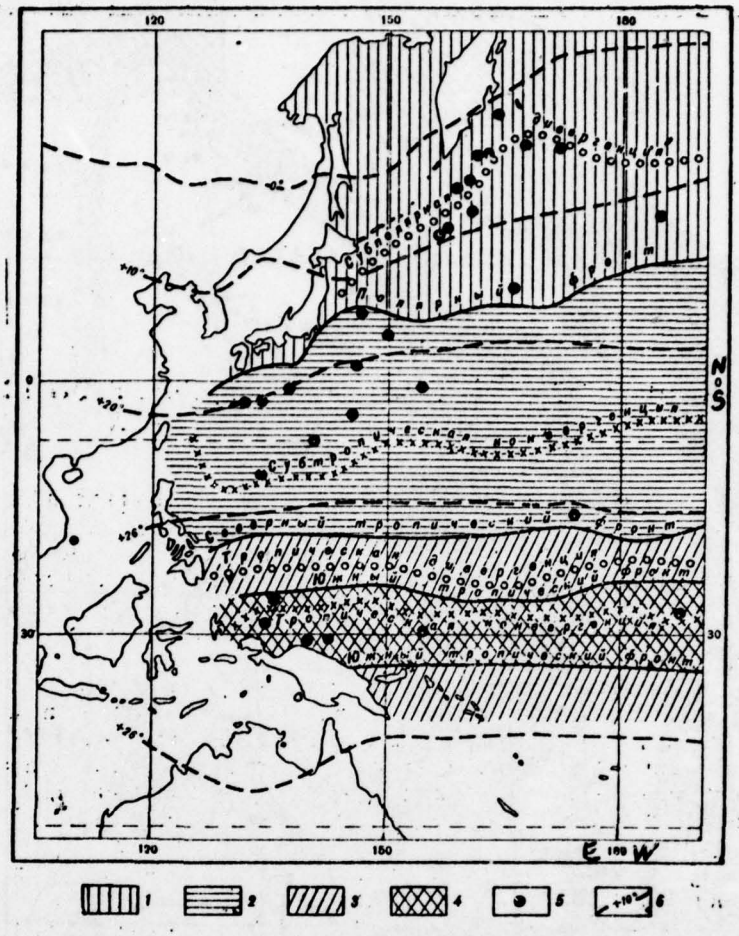

Figure 4. Water types (masses) of the western Pacific Ocean (according to V. A. Burkov) and mean annual air temperatures.

1. subarctic waters; 2. subtropical waters; 3. northern and southern tropical waters; 4. equatorial waters; 5. locations of core samples; 6. mean annual air temperature isotherms.

the quantity of clastic products that enter the ocean from every square kilometer of the drainage basin. Most of this material settles in the marginal seas and deep-oceanic trenches that girdle the Pacific Ocean in an almost continuous band along its northern and western margins. Thus, only the finest products of continental erosion are carried through the straits into the open ocean. This specific feature of the Pacific Ocean, most evident in this region and not typical of the Atlantic, 40

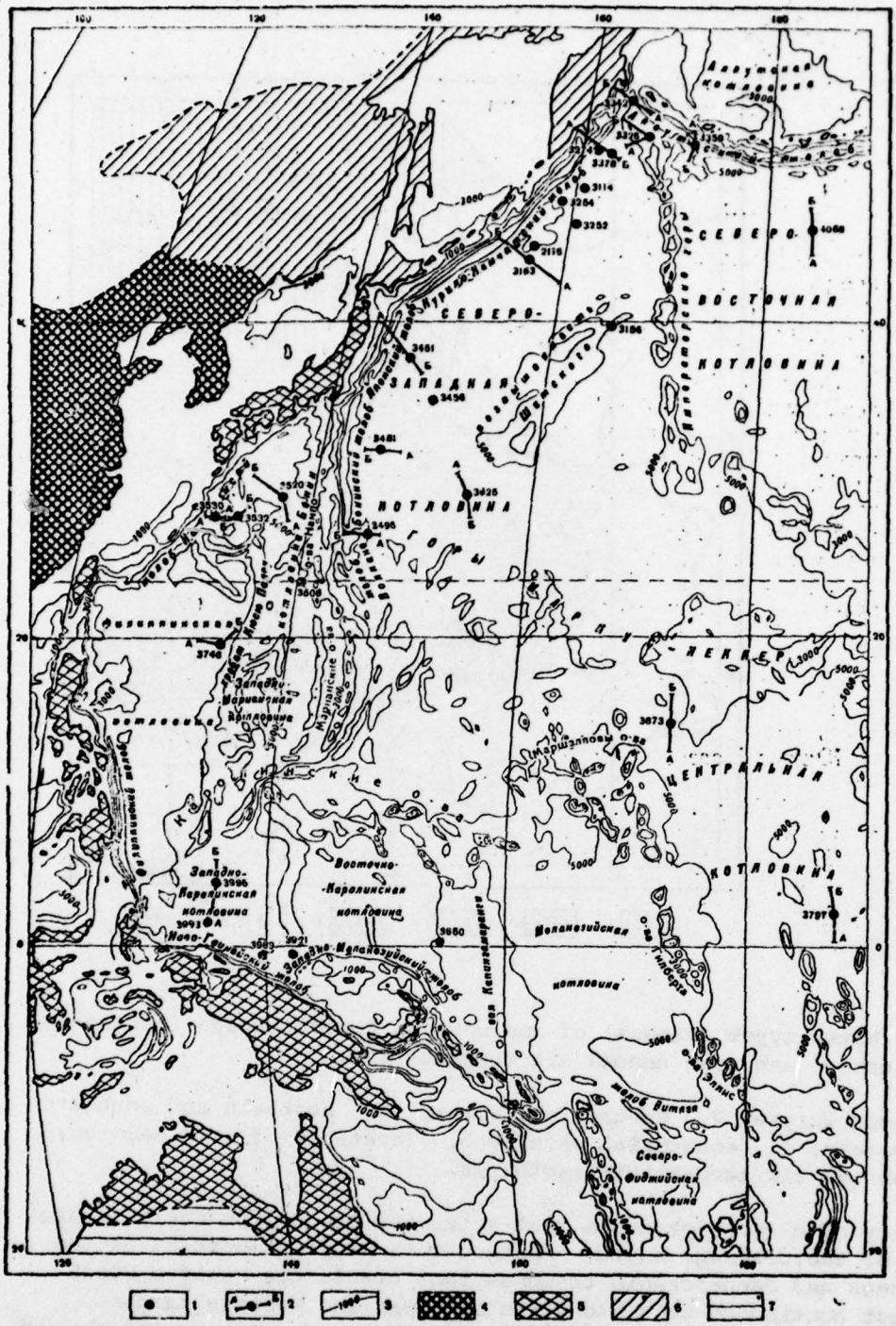

Figure 5. Drainage basin and bottom relief chart of the western Pacific Ocean (from the chart The Bottom Relief of the Pacific Ocean, published by GUGIK, 1963. Scale 1:25,000,000).

1. Locations of analyzed bottom sediment cores; 2. locations of bottom profile sections where cores were taken; 3. isobaths; 4. erosion greater than 240 metric tons/km^2 per year; 5. erosion of 50 to 100 metric tons/km^2 per year; 6. erosion of 10 to 50 metric tons/km^2 per year; 7. arid regions.

undoubtedly influences sedimentation rates and the correlation of terrigenous and biogenic sediment components.

In the open ocean, terrigenous material is distributed mainly by prevailing currents and, to a lesser extent, by tidal currents. As shown by instrument measurements in recent years, the constant (permanent) currents (wind, gradient, etc.) attain velocities of 10 to 25 cm/sec, even at depths of several kilometers in some places [82,160,161]. We will briefly discuss them in relation to the very great influence exerted on sediment deposition in the ocean by the circulation system and the principal characteristics of the water (temperature and salinity). In the central Pacific Ocean, the largest elements of the overall water circulation are the North Tradewind Current, the Equatorial Countercurrent, and the South Tradewind Current (25a, 159).

The North Tradewind Current is located between 9° and 14°N, extending from Central America to the Philippines. This current transports the northern tropical waters that occupy an extensive area between 9° and 20° to 23°N in the western part of the ocean. In the Philippine Islands region a single stream of the North Tradewind current splits into branches. The main branch turns north and forms the beginning of the Kuroshio Current. As it flows past the Japanese Islands, the main branch of the Kuroshio turns east ino the open ocean. The transformed waters of the Kuroshio, known here as the North Pacific Current (Drift) continue to the coast of the United States. Kuroshio waters together with the North Pacific Current form the subtropical waters that occupy a wide belt between 20° to 23°N nnd 35° to 36°N in the western Pacific Ocean. The contact zone of subtropical and tropical waters is called the Subtropical Convergence.

The South Tradewinds Current extends east-west between 4°N and 7°S from the coast of South America to the Solomon Islands and New Guinea. It carries westward the southern tropical waters that occupy the area between 2°N and 26° to 30°S. The North and South Tradewind currents in the region of the Philippine Islands turn gradually to the southeast and the northeast respectively, and form the Equatorial Countercurrent, whose main stream flows eastward between 4° and 9°N. The Equatorial Countercurrent is the nucleus of the equatorial water mass occupying a belt tetween 2° and 9° to 10°N.

Cold abyssal waters rise to the surface in the equatorial region, approximately between 10°N and 8°S, under the influence of the Earth's rotation. An especially large inflow of waters occurs in the equatorial region. The high content of biogenic elements in the abyssal waters stimulates the buoyant devlopment of planktonic organisms in this region.

The cold and relatively low-salinity waters of the Kamchatka and Kurile currents enter the ocean from the Bering and Okhotsk Seas. These waters form the subarctic water mass that is most clearly defined off

Kamchatka and in the Kurile, Komandorskiye, and Blizhniye Islands region. The boundary separating the subarctic and the transformed subtropic waters of the mixing zone has several names: Subarctic Convergence, Second Polar Front, and Kuroshio Front and istthe most important biogeographic boundary in the Pacific Ocean.

The water masses listed above (subarctic, subtropical, northern and southern tropical, and equatorial) have a specific structure and differ in their hydrologic and hydrochemical characteristics (table 7). 41
The main hydrologic boundaries determining the location of different types of waters, not only delineate regions having different physicochemical properties, but are also the most important distribution boundaries of planktonic organisms. Among these organisms, diatomaceous plants and foraminifera are the principal sediment constituents in the western part of the ocean.

In the cold and nutrient-rich subarctic waters, diatomaceous marine plants are the predominant phytoplankton. They comprise 80 ot 90 percent of the total phytoplankton biomass. Two regions are definèd here based on the distribution of biomass and the production and composition of plankton: the neritic region adjoining Kamchatka 42
and the Aleutian, Kurile, and Japanese Islands: and the oceanic region, which occupies the entire water area outside the abyssal trenches.

The neritic zone is characterized by luxuriant development of phytoplankton with a biomass of several grams per m^3 of water. From the quantitative standpoint, such species of diatomaceous plants as Thalassiosira Nordenskioldii, Th. gravida, Buddulphia aurta, and Chaetoceros furcellatus predominate here. Farther from land in the open ocean, the following boreal oceanic species increase in importance: Chaetoceros atlanticus, Coscinodicus marginatus, Thalassiosira longissima, Rhizosolenia hebetata and the biomass decreases gradually to serveral hundred milligrams or less per m^3 [23,67].

Diatomaceous marine plants in the bottom sediments are represented by planktonic species that inhabit mainly the 0 to 100-m water layer. The planktonic nature of most diatomaceous marine plants determines their close ecological connection with the temperature and the hydrochemical properties of the upper water layer. This makes it possible to use many species of marine diatoms, which do not decompose rapidly and which now grow in comparatively narrow temperature ranges, to evaluate past temperature changes. The fact that most shells of dead diatoms are not moved very far horizontally in the open ocean and are buried in sediments in their habitat area is very important in reconstructing paleoclimates [34]. Because of the low solubility of the siliceous skeletons of diatoms, they reach the bottom at any depths and are the main source of amorphous silica accumulation in sediments of the northwest Pacific Ocean. The ebullient development of the diatoms in subarctic waters causes the deposition of siliceous (diatomaceous)

Table 7. Thermohaline characteristics of the water masses of the western Pacific Ocean.*
(Based on representative stations)

Water Masses	Depth Location (m)	T°C	T°C	S	S°/oo
SUBARCTIC WATERS					
Surface**	From 0 to 60-100	+7.5 to 12		32.0-33.2	
Cold Intermediate Layer**	From 60-100 to 200	0.5 to +3.7		33.3	
Warm Intermediate Layer	200-850	3.5		34.1	
Deep Layer	850-3,000	1.7		34.7	
Near-Bottom Layer	3,000 to bottom	1.5		34.74	
SUBTROPICAL WATERS					
Upper Mixed Layer**	0-70	22.2		35.3	
Subsurface Stratified Layer**	70-300	16.0		34.8	
Low Salinity Layer	300-1,000	5.9		34.0	
Deep Layer	1,000-3,500	2-3		34.6	
NORTHERN AND SOUTHERN TROPICAL WATERS					
Upper Mixed Layer	0-75	27.1-27.6		35.0-35.8	
High Salinity Layer	75-300	23-25		35.2-36.1	
Low Salinity Layer	300-800	7.1		34.2	
Deep Layer	800 to 3,000-5,000	2.0		34.7	
EQUATORIAL WATERS					
Low Salinity Sruface Layer	0-50	28.3		34.4	
High and Low Salinity Layers (thin)	50-250	12-28		34.7	
Water Layer with small Thermohaline Gradients	250-4,000	2-12		34.7	

*Data from the Physical Oceanography Section, Institute of Oceanology, USSR Academy of Sciences.

**Summer temperatures and salinities.

silts (oozes) on the bottom in this part of the ocean.

South of the Polar Front within the mixing zone and subtropical waters, the phytoplankton biomass decreases considerably to 50 to 200 mg per m^3 of water, and diatoms still predominate. Such species as Coscinodiscus radiatus, Cos. Zasterophalus, and Pseudoeunotia doliolis attain mass development here. Life is especially sparse in tropical waters, where the plankton biomass is 10 to 50 mg and less per m^3. The proportion of diatoms in tropical plankton decreases and the role of perideneal marine plants, whose organic skeletons are not well preserved in sediments, increases.

Among the zooplankton, planktonic foraminifera are the most important in determining past climatic conditions. Foraminifera form the main calcium carbonate component of pelagic calcareous and terrigenous sediments of the western Pacific Ocean. According to Bradshaw's data, the greatest population density of planktonic foraminifera (greater than 100 spec/m^3) occurs in the subarctic waters off Kamchatka and the Kurile and Aleutian Islands, as well as in equatorial waters [92]. In the mixing zones and subtropical waters, the amount of planktonic foraminifera decreases to 1 to 100 spec/m^3 of water. It should be noted that the areas of greatest foraminiferal population density may not coincide with the regions of their greatest biomass and production, because the valves of these orgainsms are several times as large and thick in tropical and equatorial waters than in the subtropical zone.

The upwelling of cold abyssal waters in the equatorial region and the continuous replenishment of the reserves of nutrients necessary for photosynthesis cause the phytoplankton and zooplankton biomass the flow of biogenic components to the bottom to increase, when compared to tropical regions of the ocean [24,52,91]. 43

Among benthic organisms having mineral skeletons, the principal organisms that form sediments are the colonial corals and mollusks that are distributed mainly in the shelf regions, where shell and spicular sediments are also known to exist. In subtropical, tropical, and equatorial waters, colonial corals are a significant component of sediments not only in shallow coastal waters, but also on the summits of the highest seamounts. Benthic calcareous foraminifera are insignificant in the mass of carbonate material. Deep-sea foraminifera live in conditions of almost constant temperature and salinity and are unable to survive changes of these properties that occur in the upper water layers. The other benthic organisms in the deep ocean have an insignificant biomass (hundredths of a gram per m^2). Polychaetes, which have no skeleton, predominate among these organisms [37]. Their role is reduced here to some transformations of previously deposited material.

Very complex and varied submarine relief greatly influences sediment formation processes [39]. Vertical zoning and intermittent

sediment accumulation are related to relief [11, 14]. The largest geomorphological structures of the floor of the western part of the ocean are island chains, abyssal trenches, oceanic rises and ridges, and the ocean-floor basins (fig.5).

In the north and west, along the Pacific Ocean rim, stretches an almost continuous chain of islands and the abyssal trenches that parallel them. These (features) separate the marginal seas of the Far East, South-East Asia, and Australia from the ocean. Depths in the oceanic treches considerably exceed the mean depths of the ocean floor. The maximum depth in the Aleutian Trench is 7,822 m, in the Kurile-Kmachatka Trench - 10,542 m, in the Japan Trench - 8,412 m, in the Izu Trench - 9,810 m, in the Nansel Trough - 7,507 m, in the Marianas Trench - 11, 024 m, in the Philippine Trench - 10,262 m, in the New Britian Trench - 8,320 m, and in the Bougainville Trench - 9,140 m. All abyssal trenches (troughs) have a sharply defined, elongated form, a V-shaped asymmetric profile, flat level bottom, and steep slopes (ranging from 5° to 7° to 20° to 40°) dissected by ledges and terraces [85]. It was noted above that the abyssal trenches and marginal seas of the Pacific Ocean (Bering, Okhotsk, Japan, Yellow, East China, and South China Seas, seas of the Indonesian Archipelago, and the Solomon Sea) are the regions where most of the terrigenous material removed from the Asiatic continent and the island chains of the western periphery of the ocean is deposited. The sedimentary layer is 1.5 to 2km think in the basins of the Japan, Okhotsk, East China, and South China Seas, whereas on the bed of the Pacific Ocean it averages 300 to 400 m thick, decreasing in many places to 50 to 100 m. In some places, sediments are completely absent [36].

In the region discussed and outside the deep-water trenches, the floor of the Pacific Ocean lies at mean depths of 5,500 to 6,000 m. The seafloor is divided by broad arched rises (called oceanic divides) into a number of basins: Northwest, Northeast, Mariana, etc. (see below). Over large areas the bottom of the basin is an undulating or a hilly plain, but includes highly dissected regions with numerous submarine seamounts and clusters of sea knolls. Zones of tectonic fracturing and submarine ridges of comparatively limited extent occur. 44

The enormous submarine Hawaiian Ridge and its northwestern continuation, the Emperor Seamount Chain, which extends more than 2,500 miles from the Hawaiian Islands to the junction of the Aleutian and Kurile trenches, divides the northern part of the Pacific Ocean into two basins: Northwest and Northeast [18]. The Northwest Basin is one of the largest basins of the western Pacific Ocean, and much of it consists of undulating relief with depths of about 6,000 m. In some parts of the basins, volcanic sea mounts and low hills rise above the plain. In the southeast is an extensive sumarine upland with zones of complex tectonic fracturing, Gentle marginal rises from the edges of the basin along the deep-water ocean trenches [85].

The geomorphology of the Northeast Basin, the largest of the Pacific

Ocean, is extremely heterogeneous. It has enormous areas of quite level bottom (from Alaska to 38°N and from North America to about 165°W) and equally large areas of hilly, finely dissected, "serrated" relief of 100 to 300 m [38]. The largest moutain of the western Pacific Ocean, the Marcus-Necker or Mid-Pacific Ridge, stretches eastwest from the convergence of the Izu-Bonin and Marianas Island chains to the southern island of the Hawaiian Archipelago. This ridge includes many seamounts that merge in a number of places into large moutain masses. The Marcus-Necker Ridge separates the Northwest Basin of the Pacific Ocean from the Mariznas and Central Basins.

West of the Izu-Bonin and Marianas Island chains is the Philippine Basin with depths of 4,500 to 6,500 m. It is bounded on the north by the Japanese Island arc and the Nansei Mountain chain, in the west by the Philippine Islands, and in the south by the Yap and Palau ridges. It has a much greater degree of bottom relief than other basins of the western Pacific. A zone of ridges and clumpy uplands, which stretch north-south from the Palau Islands toward the Borodino Islands, occupies its eastern half and separates the basin from the eastern part. East of the Nansei Chain, extensive sectors of the bottom have a hilly, moutainous relief. Plains regions of simpler structure lie close to the Philippine abyssal trench and east of the meridional zone of ridges.

The next largest structures of the Pacific Ocean floor are the Caroline Ridge and relatively small, meridionally extended Eauripik and Kapingamarangi Ridges. The Caroline Ridge, like other ridges of the western Pacific, contains numerous seamounts, many of which were discovered by the VITYAZ. Some moutains reach the surface as typical coral atolls. South of the Caroline Ridge are the West Caroline, East Caroline, and Melanesian Basins. All three basins have a quite complex relief that is only slightly less dissected than the bottom of the Philippine Basin. Within these basins rise numerous relatively high seamounts and hills. These basins do not exceed 5,500 to 6,000 m in depth and extensive sectors of the bottom are less than 4,500 m deep[85]. 45

The complex bottom structure of the western part of the ocean, not only in island arcs, ocean ridges, and divides, but also in the deep basins, greatly influences the distribution of bottom sediments. It was noted above that the vertical zoning of the sediment accumulation is related to the bottom relief and expresses itself in the regular variation of sediment composition with increased ocean depths, regardless of the distance from dry land. The grain-size composition of the sediments changes first with variations in depth. As a result of increased water movements above the bottom elevations, sediments coarser than those deposited in depressed sectors are deposited on these protrusions. Large variations in relief on the underwater ridges and rises determine the sharp and repeated changes in granulometric composition of the sediments. In regions of dissected relief bottom sediment thickness varies greatly and bedrock (basement rock) is exposed in many places.

Sediment composition varies with water depth. First, this applies to changes in the calcium carbonate content of sediments. In subtropical and tropical regions of the Pacific Ocean and in the depth interval of 4,200 to 4,800 m, foraminiferal silts are replaced by noncalcareous sediments; deepwater red clays, tropical diatom and radiolarian (oozes) in the ocean basins, and terrigenous sediments in the abyssal trenches along the ocean margins. Bottom relief considerably influences the granulometric and mineralogic composition of bottom sediments, also causes significant changes in deposition rates. The average rate of deposition of foraminiferal silts is 5 to 10 times higher than of red clays.

Contemporary volcanic activity significantly influences sediment accumulation along with climate and relief. Intense (volcanic) activity on island chains and, in places, on ocean ridges and rises, results in some admixture of pyroclastic material in all types of sediments in the western Pacific Ocean. The volcanic material influences not only the sedimentation rate, but also the relationship of terrigenous, biogenic, and volcanogenic components in the sediment. The pyroclastic material changed during diagenesis influences the physicochemical properties of the medium (water) and the speed and direction of the diagenetic processes of dilution of the individual substances. The distribution of contemporary sediments in the western Pacific Ocean is shown on charts [11,1],19].

In the western ocean, sediments of the most diverse genetic type are widely distributed: terrigenous, volcanogenic, organogenic (siliceous and calcareous), and polygenic. Within each of these genetic groups, the sediments can be classified by grain-size composition. In addition, numerous outcroppings of hard, mainly volcanic, rocks are found in the regions of sharply dissected relief.

Terrigenous sediments are well developed on the ocean margins, on the shelves and continental slopes, as well as at great depths. They are especially widely distributed in the deep-sea trenches. The grain-size composition of terrigenous sediments is diverse. The pebble-gravel sediments and coarse sands are deposited mainly on the shelves, finer sands and silts(aleurites)mainly on the continental slope, Silty-clays and clayey silts (oozes) are deposited mainly in deep-sea trenches. Volcanogenic sediments are well developed close to the island chains where the sources of contemporary volcanism are located. These sediments are represented by pyroclastic material of various size. 46

Diatom oozes (silts) predominate among organogenic sediments in areas occupied by subarctic waters. These are sediments having a content of amorphous silica (SiO_2) of 10 to 30 percent (classified) as slightly siliceous), and those having a content of amorphous silica more than 30 percent (classified as siliceous sediments). By granulometric composition, these are fine silts, silty-clays, and clayey silts (oozes). The southern boundary of diatom silts coincides

approximately with the Polar Front zone (Subarctic Convergence). Diatom oozes usually are distinguished by an increased content of organic carbon [59]. In equatorial and tropical regions, slightly siliceous radiolarian and diatom (ethmodiscus) silts occur.

Among calcareous sediments of this region, foraminiferal (globigerina) sediments, which cover all bottom elevations (submarine rises, ridges, and mountains) from depths of several hundred meters down to 4 to 4.8 km, are the most widely distributed. At greater depths, as a result of the solution of calcium carbonate in the cold bottom water layers unsatured by $CaCO_3$, calcareous sediments are replaced by noncalcareous sediments (terrigenous silts, siliceous sediments, and deep-water red clays). The foraminiferal sediments are subdivided into slightly calcareous (10 to 30 percent $CaCO_3$) and calcareous ($<$ 30 percent $CaCO_3$). The granulometric composition of the foraminiferal sediments is also varied - from sands to aleuritic-pelitic silts. In the shallow-water areas of the subtropical, tropical, and equatorial ocean, coral reefs and various coral sediments (boulder, pebble, gravel, and, and silt) are widely distributed; along the margins of coral reefs they descend in places to depths of 1,500 to 2,000 m. At the same time, the coralline material is gradually diluted by the shells of planktonic foraminifera. In the northern part of the region, small patches of calcareous shell sediments are widely distributed.

Enormous areas of the ocean bottom, at depths greater than 4,500 to 4,800 m, are covered by polygenic sediments- deep-water red clays. These are the finely dispersed, mainly clayey (less frequently from silty-clayey, noncalcareous and nonsiliceous) silts). High positive values of the oxidation-reduction potential (Eh=450÷550 mv and higher [55]), low organic content, and higher content of many radioactive elements are characteristic of these silts.

Chapter V

THE DISTRIBUTION OF RADIOACTIVE ELEMENTS IN THE SURFACE SEDIMENT LAYER

The radiochemical analyses of 37 surface samples of sediments from the western Pacific Ocean makes it possible to outline the general pattern of U^{238}, Th^{232}, Io, and Ra distribution, as well as of the correlation between them, depending on the lithologic type of sediments and distance from dry land. The grain-size and basic chemical composition, particularly the content of $SiO_{2amorph}$, $CaCO_3$, C_{org}, Fe, Mn, and TiO_2 in the sediments was determined along with the radioelements in all analyzed sediment samples. This permits a quantitative description of the bottom sediment composition and some concept of the content of possible coprecipitators of the radioisotopes. The terrigenous (nonsiliceous and noncarbonate) sediments, slightly siliceous diatom oozes, foraminiferal sands and silts, and deep-sea red clays were studied. The analytic results are given in Appendix I.

Table 8 presents data on the content of radioisotopes in various types of sediments depending on their grain size. The table shows that the concentration of thorium, ionium, and radium in the transition from the sands to silts and to smaller particles (silty-clays and clayey oozes) progressively increases. For example, in terrigenous sediments, the mean content of thorium in silts is twice as large as in sands, and in the silty-clays and clayey-oozes it is about twice as large as in the silts. Ionium presents an even clearer picture. Its content in silty-clays and clayey-oozes is 10 times greater than in the sands, and more than twice as great as in silts. Only the uranium concentration seems almost unrelated to sediment particle size. It is approximately 3.10^{-6} g/g in both sands and clayey-silts. Thus, there is a clear and direct relationship between the degree of of dispersion of sediments and their content of thorium, ionium, and radium.

Of undeniable interest in understanding the process of thorium and ionium incorporation in the bottom is their relationship within the sediments and this relationship is also important to proper use of ionium-thorium methods in dating (sediments). Table 8 shows that the concentration of ionium increases almost ten times in the transition from sands to clayey-oozes, while thorium concentration increases only four-fold. The literature contains many suggestions that both of these isotopes exist in different states in the sea water, but in some mutual relationship that does not change when they enter the bottom sediments. For example, E. Goldberg and M. Koide have noted that thorium has a terrigenous and/or volcanic origin, whereas most

The content of various radioelements in various types of sediments in the western Pacific Ocean.

TABLE 8

Type of sediment based on grain-size	Number of Samples	Th. 10^{-6} g/g		Io. 10^{-6} g/ged.H		U. 10^{-6} g/g		Ra 10^{-6} g/g ed.H		Io/Th *	
		Range	Mean	Range	Mean	Range	Mean	Range	Mean	Range	Mean
				Terrigenous Sediments							
Sands	5	1.0-1.6	1.2	1.0-3.2	2.0	1.0-4.8	3.0	0.6-1.8	1.0	4.2-14.0	11.6
Silts	3	1.0-4.8	2.7	3.0-16.0	9.3	1.8-2.6	2.3	-------	2.4	21.0-25.9	23.3
Silty-clays and clayey oozes	6	2.2-6.6	4.8	10.0-26.5	19.3	1.2-3.6	2.7	6.4-17.0	11.6	18.0-51.4	31.0
				Slightly Siliceous Diatom Oozes							
ilts	3	1.3-1.5	1.4	4.0-7.0	5.0	2.0-6.0	4.0	-------	3.0	18.9-37.8	25.4
ilty-clays and layey-oozes	6	1.4-3.6	2.5	5.0-20.0	14.1	1.5-5.0	34	-------	9.0	12.6-66.5	42.8
				Biogenic Sediments (Calcareous Foraminifera)							
ands	10	-------	1.2	-------	12.0	-------	2.7	-------	11.4	70.0	-----
ine Silty-oozes	12	1.0-1.5	1.25	-------	22.0	-------	---	-------	----	154.0	----
				Polygenic Sediments (Deep-Sea Red Clays)							
ilty-clays and layey-oozes	13	1.4-15.0	6.8	20.0-97.5	40.0	1.8-8.0	4.0	21-72.0	33.3	16.8-170.8	51.7

Here and beyond the relationship of ionium to thorium is expressed as $\frac{\text{number of a dissod/min Io}}{\text{number of a dissod/min Th}}$

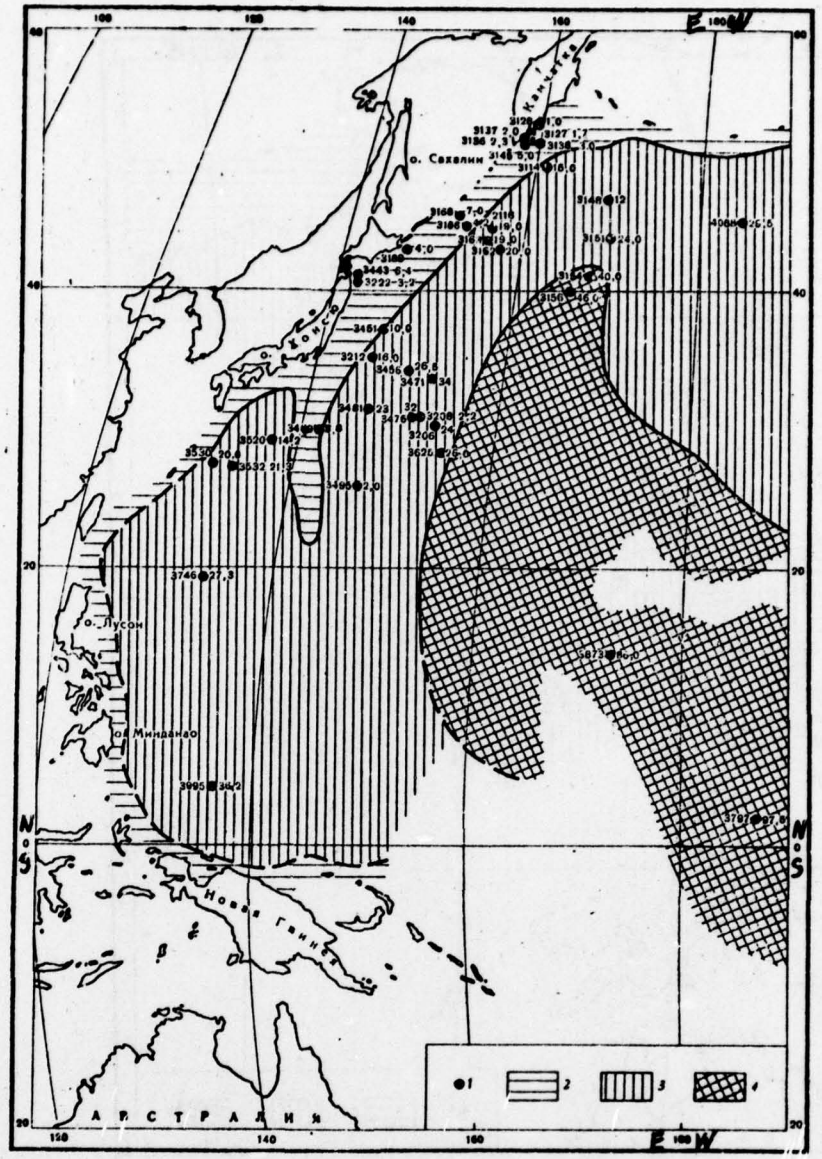

Figure 6. Schematic chart of ionium distribution in the surface sediment layer

1. analyzed sediment samples (numbers denote station numbers and ionium content); 2. less than 10 x 10^{-6}; 3. (10-40) x 10^{-6}. more than 40 x 10^{-6} g/g of U units.

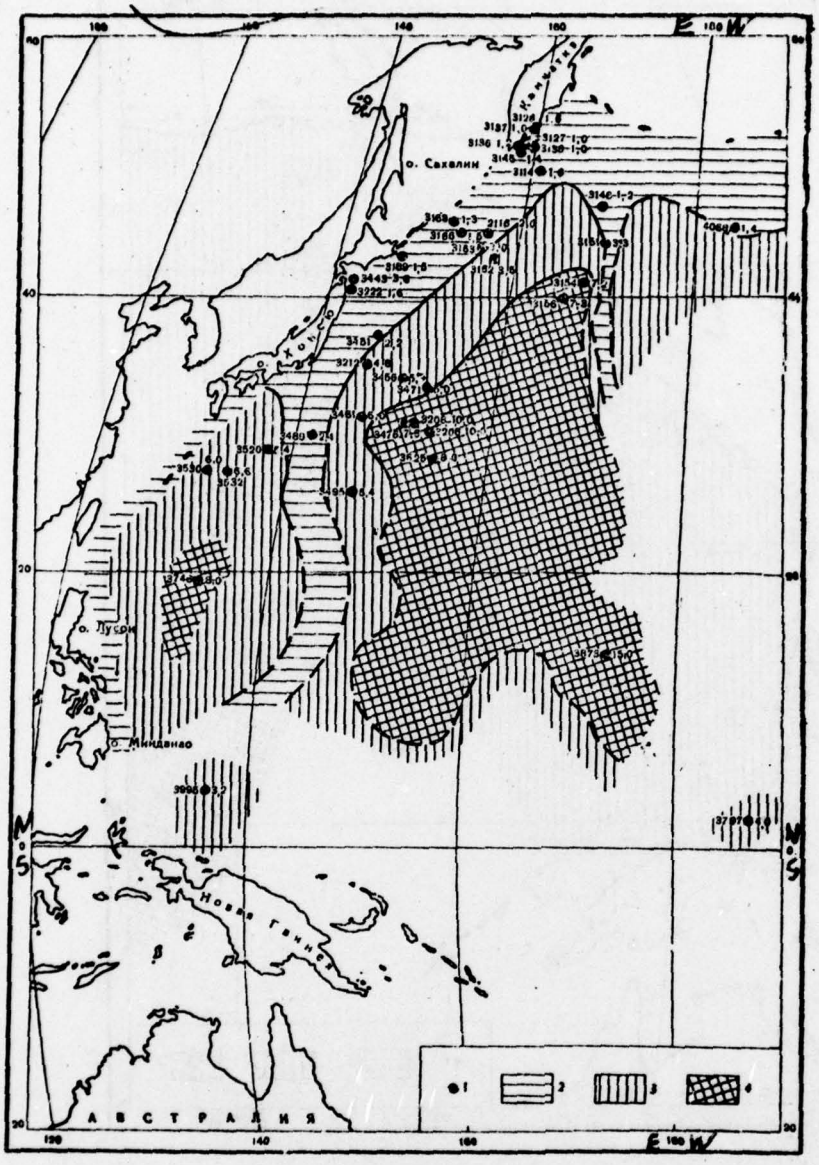

Figure 7. Schematic chart of thorium distribution in the surface sediment layer.

1. analyzed sediment samples (numbers denote station numbers and Th content); 2. less than 3×10^{-6}; 3. ($3-6 \times 10^{-6}$;) 4. more than 6×10^{-6} g/g.

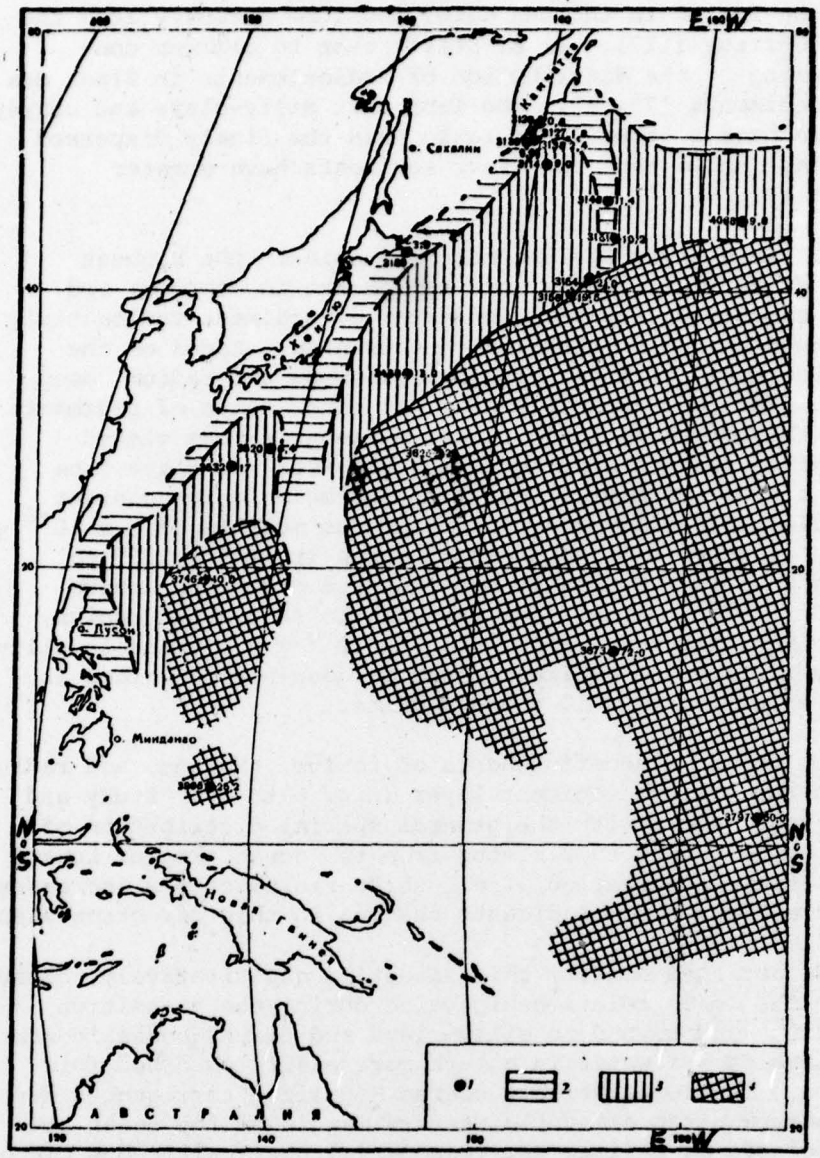

Figure 8. Schematic chart of radium distribution in the surface sediment layer.

1. analyzed sediment samples (numbers denote station numbers and Ra content); 2. less than 10×10^{-6}; 3. $(10\text{-}20) \times 10^{-6}$; 4. more than 20×10^{-6} g/g of U units.

ionium is formed from uranium existing in the sea water, and only 25 percent of the ionium in the sea water can come directly from the continents in detritus [117]. I. E. Starik came to similar conclusions in studing the distribution of radioelements in Black Sea and Antarctic sediments [73,74]. The fact that silty-clays and clayey terrigenous muds have a lower Io/Th ratio than the finely dispersed deep-sea red clays shows that the finer sediments have greater absorption ability.

A study of table 8 permits one more deduction: the highest concentrations of thorium, ionium, and radium are in deep-sea red clays. At the same time, the main indicator of sediment radioactiviy is ionium followed by radium, thorium, and uranium. Based on the content of radioactive elements, especially ionium and radium, deep-sea red clays differ so drastically from all other types of sediments analyzed, that the concentration of these elements can be viewed as the quantitative feature distinguishing deep-sea red clays from other oxidized clayey sediments. In fact, the mean ionium content in clayey and aleuritic-silty-clayey terrigenous muds is 19.3×10^{-6} g/g U units, and in slightly siliceous diatom oozes it is 5×10^{-6} to 14.1×10^{-6} g/g U units, whereas in deep-sea red clays the ionium content is 40.0×10^{-6} U units. The same can be said about radium, whose content changes from 6.4×10^{-6} to 7×10^{-6} g/g U units in silty-clay and clayey terrigenous sediments, and in deep-sea red clays it varies from 21×10^{-6} to 72×10^{-6} g/g U units.

Let us turn to the schematic charts of ionium, thorium, and radium distribution in the surface sediment layer (fig. 6 to 8). Study and comparison of these charts with the general spatial distribution of bottom sediment types shows that moving from the ocean margins toward the open ocean, the concentration of all three radioisotopes increases; the composition of the bottom sediments changes in this direction also.

The data we obtained confirm this situation quantitatively, because the increase in the Io/Th relationship value during the transition from sands to silts and beyond to silty-clays and clayey-oozes indicates that ionium exists in sea water in a much more easily absorbed form than the thorium. The comparatively coarse - grained terrigenous deposits that lie in a narrow strip along the western margin of the ocean are successively replaced by pelitic terrigenous (slightly siliceous diatoms in the north) and then by finely dispersed deep-sea red clays. Therefore, there is a close relationship between the concentration of the radioactive elements in the sediments (Th, Io, Ra), on the one hand, and the types of sediments, their degree of dispersion, and distance from the continent, on the other.

Figure 9 shows the relationship between content of ionium, radium, and thorium in sediments and the content of manganese. The figure shows that, in spite of the great dispersion, there is a direct

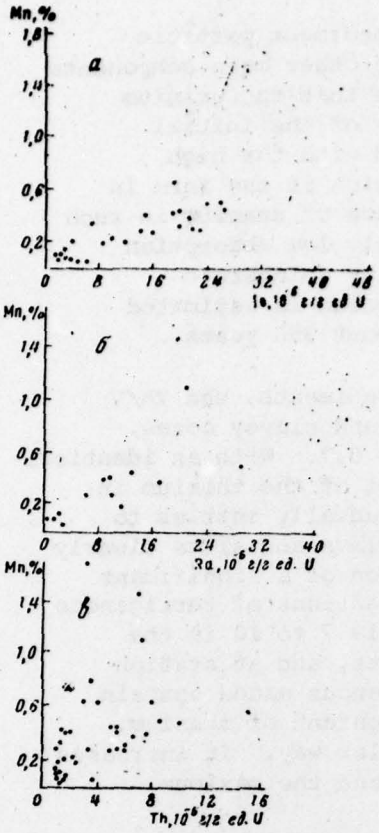

Figure 9. Relationship between the content of (a) ionium and manganese (b), radium and manganese and (c) thorium and manganese in the sediments.

(a) Io, 10^{-6} g/g U units

(b) Ra, 10^{-6} g/g U units

(c) Th, 10^{-6} g/g U units

dependence of ionium and radium content on the quantity of manganese; the relationship is less clear for thorium. The ionium and radium content in several types of finely dispersed deep-sea red clays extracted from parts of the Pacific Ocean farther from dry land (stations 3873, 3797) is considerably larger than one would expect based on the above relationship. No relationship between the content of radioelements and the total (bulk) quantity of Fe and TiO_2 in sediments has been found. Existence of a direct relationship between ionium and radium, on one hand, and manganese on the other, indicates that these radioelements may enter the sediments through coprecipitation with manganese oxides. The other possible entrance of ionium and radium into pelagic silts is coprecipitation by the hydrogenous clayey minerals which, in Arrhenius' and Goldberg's opinions, are formed in the water from dissolved aluminum and silicon [88]. It is also possible that this mechanism results in a high ionium and radium content in the sediments at stations 3873 and 3797.

The behavior of uranium should be discussed separately. The 53

absence of any dependence of uranium content on sediment particle size and the quantity of Mn, Fe, TiO_2, as well as other main components of the mineral composition of sediments indicates that the uranium content depends little on the absorption capacity of the initial components of bottom deposits. This is connected with the high stability of the hexovalent carbonate complex, which is the form in which uranium is found in sea water. The existence of uranium in such a form in the ocean provides it with the relatively low absorption capacity compared to thorium isotopes. As shown by Goldberg's investigations, the half-life of uranium in the ocean is estimated to be 500,000 years, whereas for thorium it is about 350 years.

According to average data for all types of sediments, the Th/U ratio is 1.8 in silty-clays and aleuritic clayey and clayey oozes, decreasing in sandy and silty sediments to 0.3 to 0.7. With an identical uranium content in oozes, this indicates that most of the thorium in fine clays is carried far out to sea, where it gradually settles to the bottom. The magnitude of the Io/U ratio in clays and silts clearly shows a radioactive disequilibrium in the direction of a significant excess of ionium over uranium. If in the silt fractions of terrigenous sediments this ratio is approximately 4, then it is 7 to 10 in the silty-clays and clayey oozes of polygenic sediments, and at station 3797 it even reaches 25. At the same time terrigenous sands contain ionium in smaller quantity than the equilibrium content of uranium. The magnitude of the Ra/U ratio changes in a similar way. It increases from sands to silts and clayey terrigenous silts and the maximum values (about 8) are in deep-sea red clays.

In conclusion one should discuss variations in the Io/Th ratio. Golfberg and Koide noted a relationship between the Io/Th ratio and geographic position [117]. According to their data, pelagic clayey silts (deep-sea red clays) of the eastern Pacific Ocean (between 9° and 42°N) are characterized by a considerably lower Io/Th ratio (40-58) than the deep-sea red clays and pelagic slightly calcareous and calcareous (oozes) of the South Pacific Ocean (143-158). It should be noted that the isotopes were analyzed by washing the radioelements from the sediments, and not by complete decomposition of the sample by fusion.

Our data show that, in the equatorial Pacific Ocean (between 2° and 14°N) and in the northern Pacific (40° to 46 N) deep-sea red clays have a higher (39 to 147 and 40 to 170 respectively) Io/Th ratio and differ quite sharply from the same type of sediments distributed between 19° and 34°N (17 to 26). The reason for this is so far unexplained.

Chapter VI

LITHOLOGY, ABSOLUTE AGE, AND STRATIGRAPHY OF DEEP-SEA SEDIMENTS

1. The Principles of Stratigraphic Classification of Quaternary Deep-Sea Deposits.

The separation of individual layers in deep-sea sediment cores, i.e. determination of their local stratigraphy, can be achieved by both lithologic and micropaleontologic analysis methods. We define lithologic methods of subdividing deep-sea sediments as the sum total of analyses the enable us to separate, in cores, a number of layers differing in grain-size or material composition as well as in textural features. Micropaleontologic types of analysis (diatoms, foraminifera, spore-pollen, radiolaria, spicules, etc) aim to determine the stratigraphy of sediments based on a layer-by-layer study of the content and quantitative distribution of the remains of organisms. Knowing that during the Quaternary period, the systematic composition of the microfauna and microflora changes very little, stratigraphic and paleogeographic reconstructions based on micropaleontologic analysis depend mainly on knowledge of the contemporary ecological conditions (habitat) of the organisms and on comparative evaluation of the effect of possible variations of these conditions in the past. The simultaneous influence of several primary and secondary factors on the ecology of some of these organisms usually introduced conditional elements into stratigraphic and paleogeographic constructions based only on micropaleontologic data.

Several years' work at the USSR Academy of Sciences, Institute of Oceanology, has shown that, based on study of the composition of marine diatoms alone or of the foraminifera in the same cores, one can identify differing numbers of layers, whose boundaries quite often do not coincide. The most rational approach to synthesis of the stratigraphy of Quaternary deep-sea sediments, and reconstruction of Quaternary paleogeographic conditions based on this stratigraphy, is the use of the entire complex of existing methods: lithologic, micropaleontologic, chronological, and the absolute year count.

The criteria for identifying individual layers and horizons within cores are the variation of the grain-size composition of the sediments, the content of amorphous silica (mainly), organic matter, and calcium carbonate (not always), as well as the content of marine diatoms and foraminifera. The boundaries between individual layers were drawn through the median points between the maxima and minima on the material component distribution curve, considering changes in the sediment grain size and in composition of the microflora and microfauna. After defining individual layers and horizons in the cores, the absolute age of the sediments was calculated by the ionium method. In individual cores having slightly changing grain-size and material sediment composition and in unanalyzed cores it was impossible to separate the layers. We present only data on the absolute age of their sediments. 55

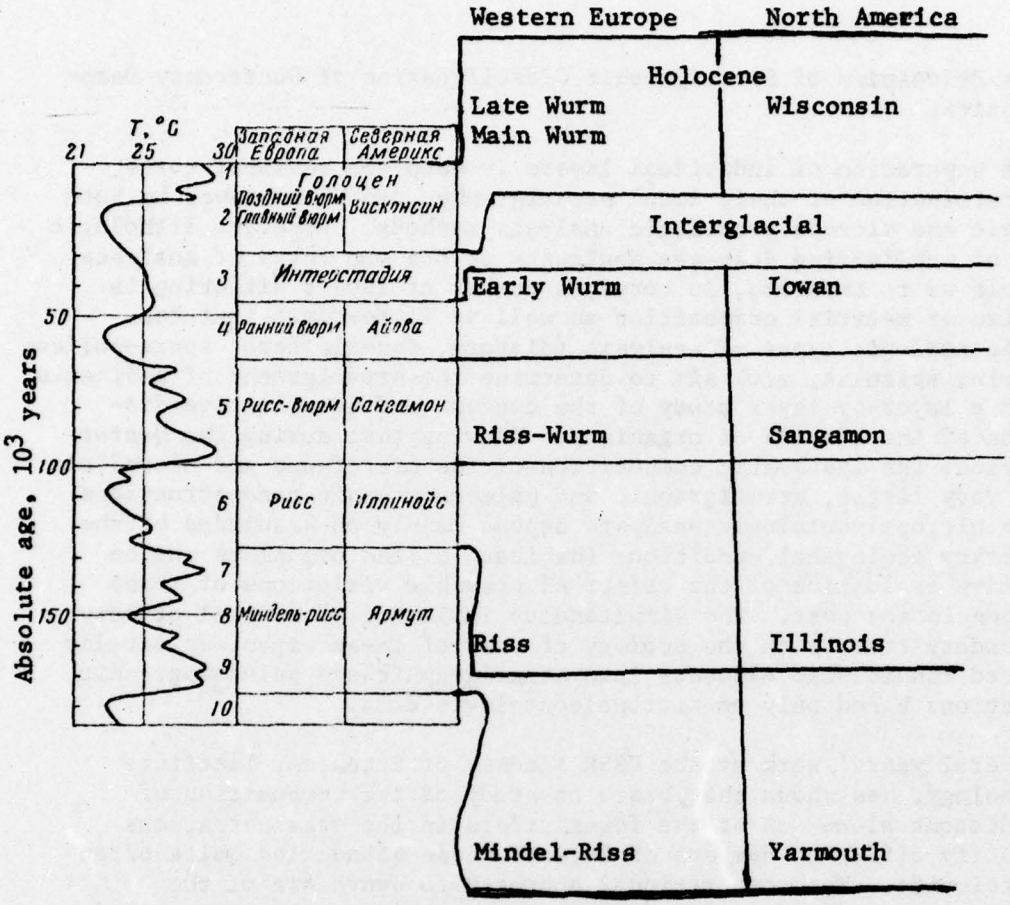

Figure 10. Paleotemperature curve, absolute age of Atlantic Ocean sediments, and correlation with the Quaternary stratigraphy of Western Europe and North America [153].

Establishing surface water temperatures of the ocean during various time intervals was based, first, on the correlation between cold-water (subarctic and northern boreal), temperate warm-water (southern boreal or subtropical), and warm-water (tropical) diatom complexes and, secondly on changes in the material composition of the sediments. In correlating the layers and horizons identified in the western Pacific with glacial and interglacial horizons on the continents of Europe and North America, we depended on the subdivision of the Quaternary period (fig. 10), which, as shown by the latest investigations [102, 153], ties in well with the stratigraphic sequence of Atlantic Ocean sediments. As far as the criteria for the separation of stages and interglacial periods are concerned, it is logical to examine them using the stratigraphy of the longest core taken at station 3163.

The results of the core analyses are presented in the following sequence: (1) cores from the region of subarctic water (stations 3163, 4068, 3378, 3325, 3342, 3359); (2) cores from subtropical and tropical water (stations 3451, 3625, 3495, 3520, 3530, 3481, 3873, 3746); (3) cores from the equatorial Pacific Ocean (stations 3797, 3995, 3993, 3989, 3921, 3650).

2. Core at Station 3163

Location - Northwest Basin of the Pacific Ocean, east of Kunashir Island. Depth - 5,430 m. Length of the core - 1,195 cm. Sampling instrument - hydrostatic tube (corer).

Bottom Relief. Near the station the bottom is a hilly plain (fig.11). Individual hills rise 150 to 200 m above the bottom. Slope gradients range from fraction of a degree to 2°. The core was subjected previously to lithologic, diatom, and foraminiferal analyses to determine the stratigraphy [17, 33, 61, 65].

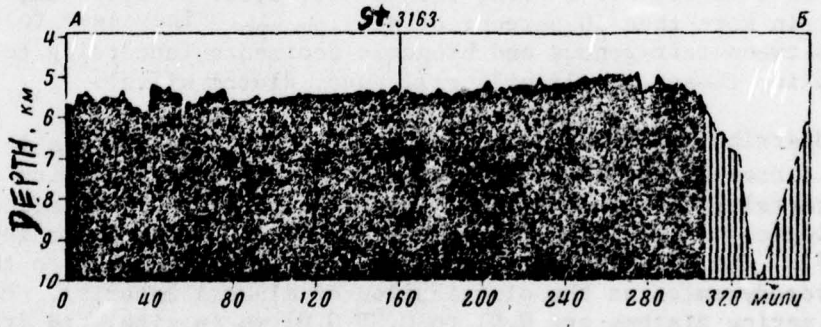

Figure 11. Bottom relief in the region of station 3163 (profile along the line A-B, see fig. 5).

Granulometric Composition. The core consists essentially of noncalcareous clayey-muds (oozes) with numerous layers of clayey silts and fine and coarse, usually thin-bedded silts (fig. 12; Appendix II). The clayey muds (oozes) and silt layers range from several millimeters up to 32 cm thick. The thickest and the coarsest layers of aleuritic sediments are at depths of 33 to 50, 280 to 302, 310 to 323, 385 to 416, 778 to 810, and 996 to 1,020 cm below the surface of the core. In the silty-clayey mud layer, scattered gravel and pebbles and sectors with a considerable mixture of coarse silt and sand grains were found. It seems that the coarser material represents ice-rafted detritus that increased noticeably in quantity and extent during specific epochs and testifies to the increased extent of shore ice in the open ocean and deposition of the solid components of this ice during melting. Part of the pebbles consist of pumice, which can float with the current and be transported for considerable distances by ice.

The Distribution of Amorphous Silica

Amorphous silica is one of the characteristic components of the sediments in the core at station 3163 and marine diatoms are the most important source of the amorphous silica. Radiolaria and the spicules of siliceous sponges are less significant and silicoflagellates are least important [33]. The location of station 3163 in a region where diatomaceous plankton grows ebulliently during the vegetation period (spring-summer) at the present time caused the high content of amorphous silica (approximately 18 percent) in the upper layer (0-20 cm) of the silty-clayey muds.

The quantitative distribution of SiO_2 amorph varies vertically, decreasing in individual layers to 3 to 4 percent and increasing in some layers to 16 percent. This distribution makes it possible to distinguish the following layers enriched with SiO_2 amorph: 0 to 20, 70 to 80, 140 to 220, 250 to 290, 390 to 480, 520 to 580, 840 to 900, 1,040 to 1,130 cm. Muds of similar grain-size composition, but depleted of SiO_2 amorph lie between these layers. At depths of 0 to 20, 150 to 195, 390 to 480, 1,060 to 1,130 cm, the sediments contain more than 10 percent of SiO_2 amorph. They seem to be transitional between terrigenous and biogenic sediments (according to the regular classification these are slightly siliceous, diatom silts). 57

The distribution of SiO_2 amorph in contemporary sediments is the product of a series of complexly intertwined factors: hydrodynamics of the water, interrelationship of biogenic and terrigenous sedimentation rates, and hydrologic and hydrochemical conditions in the upper water layer [9, 15, 19, 49]. The distribution of biogenic silica is subject to the same laws of hydrodynamics as the distribution of mineral material. Most of the valves of marine diatoms are 0.01 to 0.05-0.01 mm in size, and fragments of these valves, which usually comprises more than half of the total quantity of biogenic silica in the sediments, are smaller than 0.01 mm and are buried mainly in the fine silty and clayey (pelitic) muds (oozes). Comparison of the curves of vertical distribution of SiO_2 amorph and of the fine silts and clay fractions of cores shows no connection between abrupt changes in the quantity of SiO_2 amorph and variations in grain-size composition in the clayey to fine silty muds (oozes).

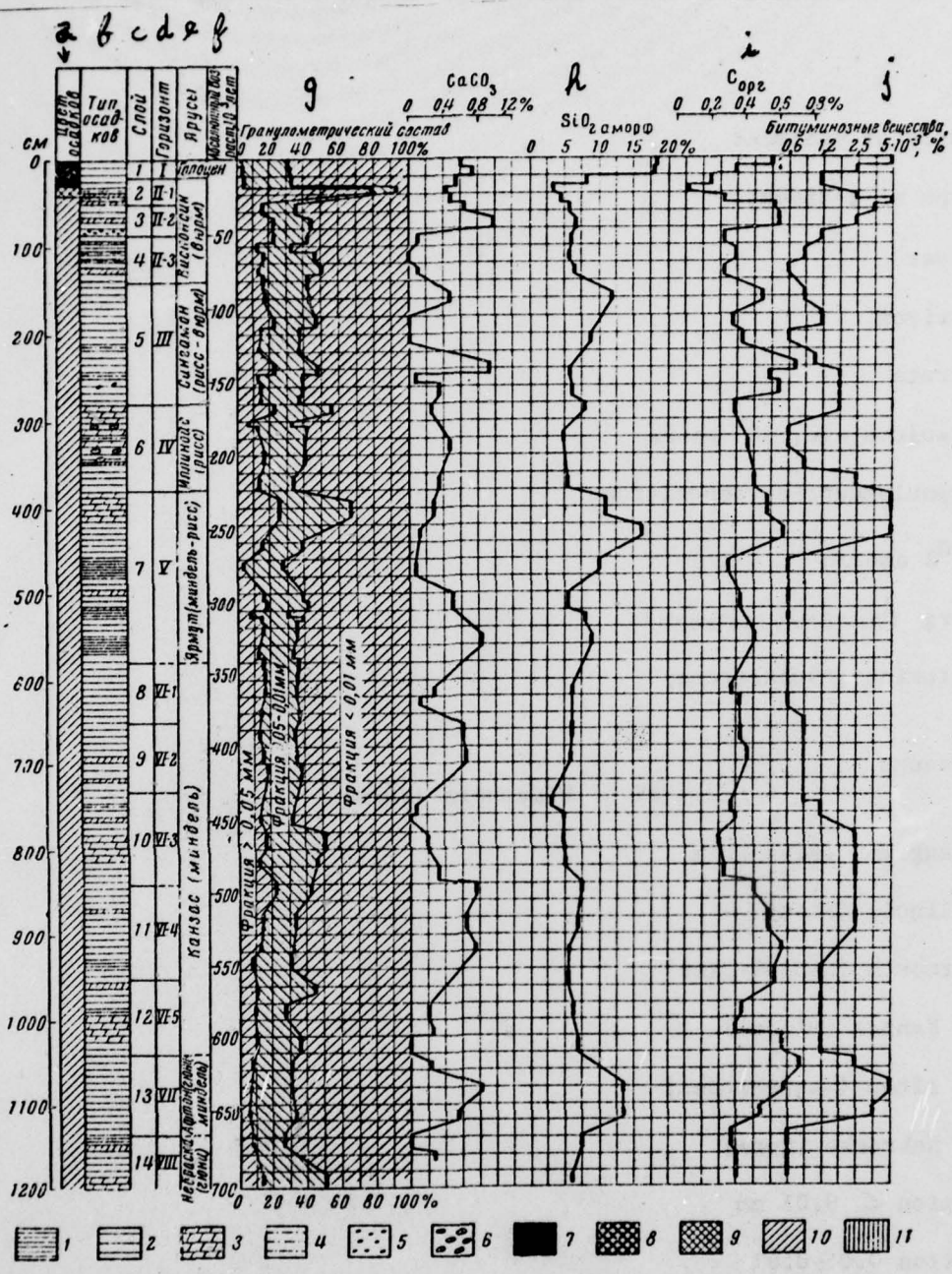

Figure 12. Core at station 3163. 1. clayey muds (oozes) (more than 70% of the fraction < 0.01 mm); 2. silty (aleuritic) clayey muds (50 to 70% of the fraction < 0.01 mm); 3. fine silty (aleuritic) muds (oozes); 4. coarse silts (aleurites); 5. scattered gravel and pebbles; 6. sectors enriched with silts (aleurites); 7. dark brown and brown muds; 8. light brown sediments; 9. brownish-grey mottled grey sediments (the spots are brown); 10. grey and greenish-grey sediments; 11. black sediments. These descriptive markings also apply to other cores.

Descriptive information for figure 12 and following figures.

(a) color of sediment

(b) type of sediments

(c) layer

(d) horizon

(e) Strata

(f) Absolute age, 10^3 years

(g) granulomentric composition

(h) SiO_2 amorph

(i) Corg (organic carbon)

(j) Bituminous substances

1I Holocene

2-4 II Wisconsin (Würm)

5III Sangamon (Riss-Würm)

6IV Illinois (Riss)

7 V Yarmouth (Mindel-Riss)

8-12 VI Kansas (Mindel)

13 VII Afton (Gunz-Mindel)

14 VIII Nebraska (gunz)

z fraction < 0.01 mm

y fraction 0.05-0.01

x fraction > 0.05

In fact, in the fine silt and clay fractions or their sum, the quantity of SiO_2 amorph, varies several fold (fig. 12). At the same time, the layers of coarser-grained sediments always contain considerably less amorphous silica, which supports the validity of the above-described regular relationship between SiO_2 amorph and the sediment grain size. Therefore, the comparatively small changes in grain-size composition that are seen in most of the core sections composed of clayey-fine silty mude, do not cause the abrupt variations in the quantity of SiO_2 amorph in these sediments.

The study of marine diatoms, by A. P. Zhuze, has shown that throughout the entire core, the north-boreal species of diatoms, such as Coscinodiscus marginatus, Thalassiosira excentrica, Thalassiothrix longissima and Rhizosolenia hebetata predominate quantitatively. The quantity and species diversity of the Arctic-boreal (Thalassiosira gravida), south-boreal (Coscinodiscus asteromphalus, Cos. stellaris, Cos. radiatus, Cos. wailessii), and tropical diatoms (Cos. nodulifer, Ethmodiscus rex) either increase or decrease with depth in the core along with the north-boreal species. The vertical variation of the realtionship between these four diatom complexes testifies to the periodic alternation of epochs of higher and lower water temperature in the northwest Pacific Ocean.

The comparison of data on the vertical distribution of the amporphous silica and diatoms in the core shows that layers low in SiO_2 amorph have fewer diatoms and colder water forms of diatoms. It seems that the main cause of the distribution of SiO_2 amorph described above was the decreased biomass and decreased diatom production during the colder intervals, which caused a decrease in the biogenic sedimentation rate.

The Distribution of Organic Matter

The content of organic matter in the core changes in approximately the same way as the content of SiO_2 amorph. Despite the continuous disintegration of organic compounds with depth, no decrease in content of organic matter as a whole, or of the bituminous fraction, is observed here. Individual sediment layers contain even more organic carbon and bitumens than the surface layer. Seven main layers enriched with organic carbon (C_{org}) are identified in the core (0 to 20, 50 to 80, 150 to 170, 220 to 270, 380 to 450, 840 to 960, 1,020 to 1,120 cm). Approximately the same layers contain larger percentages of SiO_2 amorph. Such a characteristic distribution of C org and SiO_2 amorph' as well as the correlation between them, (fig. 13) indicate that fluctuations in ocean-surface water temperatures are reflected in changes in the content of organic-matter along the core. 59

The Distribution of Calcium Carbonate

The entire length of the core contains very little calcareous material (from 0 to 1.09 percent $CaCO_3$), which consists mainly of the remains of shells of planktonic and, to a lesser extent, of benthic calcareous foraminifera. Despite such a low overall content of $CaCO_3$, layers having a relatively high $CaCO_3$ content can be identified in the core (0 to 33, 50 to 80, 150 to 170, 220 to 225, 500 to 590, 650 to 710, 740 to 940, 1,070 to 1,120cm).

Between these layers, the sediments contain little or no $CaCO_3$.

As can be seen from fig. 12, the layers having a higher and a lower content of $CaCO_3$ coincide mainly with layers high and low in SiO_2 amorph and C org. The study by Kh. M. Saidova [66] of the bottom foraminifera[1] in the core to a depth of 605 cm shows that the sediments at the 50 to 77, 224 to 292, 440 to 442, 500 to 518, and 569 to 605-cm levels contain larger quantities of benthic calcareous foraminifera. In almost all cases the increased quantity of benthic calcareous foraminifera is restricted to sediments having a relatively high quantity of $CaCO_3$ and SiO_2 amorph.

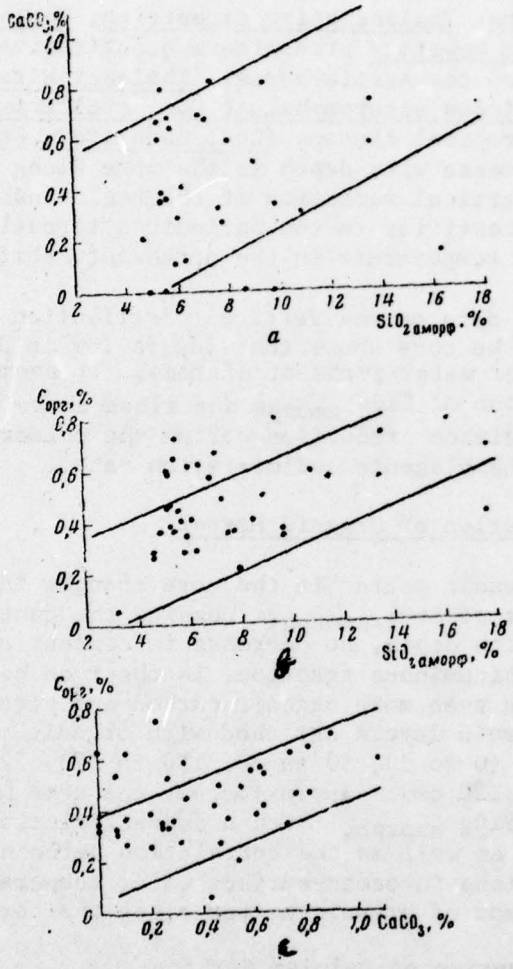

Figure 13. Relationship between the content of amorphous silica (SiO_2 amorph) and calcium carbonate ($CaCO_3$). (a) SiO_2 amorph and C org, $CaCO_3$, (c) C_{org} (c) in the sediments.

[1]The planktonic foraminifera in this core sample have not been studied in detail, but their general distribution has been established. It is the same as that of calcareous benthic foraminifera.

Figure 13 shows a tendency toward a direct relationship between the content of amorphous silica and calcium carbonate in the core and an almost direct relationship between the $CaCO_3$ and $C_{org.}$ Therefore, the sediments with more $CaCO_3$ and benthic calcareous foraminifera were deposited during the period of warming ocean-surface waters. The decrease in the $CaCO_3$ quantity in sediments during the cooling periods could have been caused by the increase in solubility of carbonates due to lower water temperatures [76, 159]. Nevertheless, a whole series of data obtained recently indicated that this was not the only cause of the $CaCO_3$ distribution described above. 60

The shells of planktonic foraminifera, which are 0.1 to 0.2 to 0.5mm in diameter, require several days to settle to a depth of 5,000 m. Like benthic foraminifera, they dissolve mainly on the surface of the bottom [22, 94], where the near-bottom water temperatures are affected very little by the warming and cooling of the ocean-surface water layers [102]. In addition, the increase in the subaerial erosion and submarine deposition of terrigenous material during the glacial epochs reduced the period of contact of calcareous shells with the cold, active, abyssal waters. The increase in salinity by 1 to 2 0/00 during the glacial periods, caused by the lowering of sea level by about 100 m, decreased the solubility of $CaCO_3$ and also counteracted the effect of the increase in sea water activity [133,134].

The almost direct relationship between two biogenic sediment components of differing solubility ($CaCO_3$ and $SiO_{2\ amorph}$) shows that the change in activity of bottom waters was not the critical factor in the vertical distribution pattern of $CaCO_3$ described above. It seems that in the northwest Pacific Ocean, during the warming climatic-trend, conditions favoring the development of marine diatoms were created, production of planktonic and benthic calcareous foraminifera increased, and more $SiO_{2\ amorph}$ organic (carbonate) mater, and biogenic calcareous material were buried in the sediments.

Sedimentary Stratigraphy

The similarities of the vertical distribution of biogenic (amorphous) silica, calcium carbonate, and organic carbon together with data on the variation of the species composition of diatoms makes it possible to identify 14 layers in the core that developed under varied climatic conditions.

The rate of sediment deposition in the core was determined by indirect methods. We conditionally estimate it to be 17 mm/1,000 years. This value was obtained by the ionium method for the core at station 2116 (length 4 m), of the same grain-size and material composition, taken near station 3163 (60 miles north of station 2116 in an area of similar bottom relief [4]). As we will see in chapter VII, the calculated absolute age of the layers of the core at station 3163, based on this rate, coincides well with the absolute age of the corresponding layers of other core samples as determined by direct radiochemical methods. Table 9 gives the thickness of the layers of the core at station 3163, their probable absolute age, and their correlation with the standard stratigraphic sections of Western Europe and North America.

Let us briefly discuss the criteria for determination of the stages and intergalacial periods in the sediments. Layer 1 was undoubtedly formed during the post-glacial period under warning climatic conditions that began approximately 11,000 years ago. We think that layers 2,3, and 4 can be assigned to a single glacial horizon (II); at the same time, layer 3, which was deposited when the ocean-surface water was warming, corresponds, it seems, to the last interglacial period. The latter contention is supported, first by the warm-water appearance of the flora of layer 5, which permits us to assign it to interglacial horizon (III), second, the almost identical ages of the sediments of corresponding stages of the last cooling period of Atlantic Ocean waters [153], and finally, the two-stage character of the last continental glaciation. In his recent works [32, 33], A. P. Zhuze assigns layer 3 in the core at station 3163 and at other stations (3136, 3252, 3274, 3325, 3342, 3359, 3378 and 4066) to the post-glacial climatic optimum (according to A. P. Zhuze this is horizon I, Holocene, layer B), and layer 4 to the late glacial period. The data we obtained, including ionium determinations of the absolute age of this layer, do not confirm similar comparisions in a number of other cores (see below). 61

Layers 8 to 12 in the core at station 3163 are combined into one horizon (VI) based on the low content of SiO_2 amorph in ten sediments and the general cold-water form of the flora. Because the amounts of $CaCO_3$, C_{org}, and bitumens change noticeably in horizon VI, and the diatom composition indicates changes in climate, all of these layers can be assigned to one glacial epoch with only some degree of doubt. It should be noted that the boundary between horizons V and VI also is conditional.

Because the horizons identified in the core reflect climatic fluctuations of the Quaternary period, we attempted to compare these horizons with the glacial and interglacial epochs of North America, Western Europe, and Northeastern USSR. Unfortunately at this time, it is possible to date continental, including lacustrine deposits, only by the radiocarbon method, which is feasible only to 50 to 70 thousand years ago. The stratigraphy of more ancient continental Quaternary deposits, which is based on changes in sediment composition, variations in mammalian fauna and flora, and geomorphologic and archeological data, has not been confirmed by direct age determinations. This makes comparision of continental and marine deposits difficult and the dating of the more ancient stages of Quaternary history less certain. Let us turn to the characteristics of the individual layers and horizons identified in the core at station 3163. 62

Horizon I (0 to 20 cm; Holocene) has a homogeneous grain-size composition of silty-clayey slightly siliceous, diatom muds containing about 18 percent SiO_2 amorph, a high proportion (relative to the underlying layer) of $CaCO_3$ (0.59 to 0.73 percent), C_{org} (0.34 to 0.55 percent), and bitumens (2.5 to 3.7×10^{-3} percent). Oceanic north-boreal diatoms predominate: Coscinodiscus marginatus, Thalassiosira excentrica, Thalassiothrix longissima, Rhizosolenia hebetata, Cos. oculus iridis. Such south-boreal species as Coscinodicus stellaris and Cos. asteromphalus also occur periodically.

Sedimentary stratigraphy of the core at Station 3163

Layer	Horizon	Layer depth from the surface of the bottom (cm)	Thickness (cm)	Absolute Age 10^3 yrs	Stratigraphic Correlation	
					North America	Western Europe
1	I	0-20	20	0-11	HOLOCENE	
2	II	20-50	30	11-30	Wisconsin glacial stage	Principal and late stages of Würm glaciation
3	II	50-86	36	30-50	Inter-glacial stage	Inter-glacial stage
4	II	86-140	54	50-80	Iowan glacial stage	Early Würm glaciation
5	III	140-280	140	80-170	Sangamon interglacial stage	Riss-Würm interglacial stage
6	IV	280-380	100	170-220	Illinoian glaciation	Riss glaciation
7	V	380-580	200	220-340	Yarmouth interglacial period	Mindel-Riss interglacial period
8	VI	580-650	70	340-380	Kansas glaciation?	Mindel glaciation?
9	VI	650-730	80	380-430		
10	VI	730-840	110	430-500		
11	VI	840-950	110	500-560		
12	VI	950-1040	90	560-610		
13	VII	1040-1135	95	610-670	Afton interglacial period?	Gunz-Mindel interglacial period?
14	VIII	1135-1195*	60*	670-700*	Nebraskan glaciation?	Gunz glaciation?

* Horizon was not completely penetrated.

Horizon II (layers 2, 3, 4; Würm glaciation). Layer 2 (20 to 50 cm; Wisconsin glaciation, main and late stages of the Würm glaciation) consists of silty-clayey and fine silty muds (oozes) with interlayers of coarse silts composed of volcanic ash. The layers of ash (for example, 33 to 37 cm) and the high content of volcanic material in the sediments indicate that volcanic activity increased when this layer was formed. Compared to layer 1, the silts contain a smaller percentage of SiO_2 amorph (from 3.25 to 8.06 percent), $CaCO_3$ (0.43 to 0.54 percent), C org (0.06 to 0.27 percent) and bitumens (1.2 to 2.5 X 10^{-3} percent). The diatoms in this layer were identified in the sample only between 20 to 33 cm, and do not vary essentially from the flora of horizon I.

Layer 3 (50 to 86 cm; inter-glacial stage of Würm glaciation) is composed mainly of silty-clayey muds with an interlayer of fine silty mud at a depth of 64 to 69 cm from the surface. At the boundary with layer 4, the sediments contain scattered fine glacial gravel and fragments of pumice-sized gravel. The sediments are characterized by the higher percentage of SiO_2 amorph (5.3 to 6.5 percent), $CaCO_3$ (0.63 to 1.09 percent), C org (0.56 to 0.59 percent), and bitumens (2.5 to 5 X 10^{-3} percent). The diatoms contain considerably more warm-water flora than horizon I and layers 2 and 4. Along with the north-boreal species mentioned above, southern boreal diatoms, Cos. asteromphalus, Cos. stellaris and Cos. radiatus are present in large numbers; the species Cos. angustolineatus which is characteristic at the present time of the plankton of subtropical waters, also appears. The quantity of planktonic and benthic calcareous foraminifera increases among the fauna [66].

Layer 4 (86 to 140 cm; Iowan, glaciation, early stage of the Würm glaciation) is composed of silty-clayey and fine silty muds with numerous interlayers of coarse silts. In this layer, even the finest silts contain an insignificantly small amount of $CaCO_3$ (0 to 0.11 percent) and bitumens (0.6 to 1.2 X 10^{-3} percent) and have quite a low percentage of C org (0.27 to 0.35 percent); the percentage of SiO_2 amorph tends to decrease. Overall, the sediments of this period are coarser and have more volcanic ash and pumice. The flora of this layer resemble cold-water types. The north-boreal species of diatoms, Thalassiosira excentrica, Coscinodiscus marginatus, and Actinocyclus divisus predominate here; Rhizosolenia hebetata, Thalassiothrix longissima, and Coscinodiscus oculus iridis are frequently found. The Artic-boreal neritic species Thalassiosira gravida, as well as sublittoral and fluvial diatoms, appear in noticeable quantities. The subtropical and tropical elements of the flora, which are present in the overlying (II-2) and underlying (III) deposits, are completely lacking.

64

Horizon III (layer 5, 140 to 280 cm; Sangamon, Riss-Würm interglacial period). The sediments of this horizon are silty-clayey muds with interlayers of coarse silt-sized volcanic ash that lie at depths of 212 to 214 and 242 to 244 cm. In the lower part of the layer, at 246 to 255 cm, were semi-rounded andesite-basalt pebbles up to 3 cm in diameter. Their presence in the sediments resulted from accelerated melting of glacial ice during the climatic warming of the interglacial period. A similar occurrence was seen in sediments of the warm stage of the Würm-glaciation (layer 3). The silty-clayey muds located at 145 to 195 cm are rich in skeletal remains of marine diatoms and are classified as slightly siliceous silts (oozes).

The increased volcanic activity of the region during the deposition of horizon IV silts encompassed the lower parts of horizon III. The considerable influx of volcanic material diluted the biogenic silica in the lower part of this layer. However, the increased proportion amorphous silica (5.60 to 11.62 percent) compared to the deposits of horizons II and IV, respectively, above and below, is typical of the sediments of horizon III generally. Individual layers of the silty-clayey muds in horizon III have larger percentages of $CaCO_3$ (up to 0.91 percent), C_{org} (up to 0.69 percent), and bitumens (up to 1.8×10^{-3} percent). The flora in horizon III resemble warm-water diatoms more than those in "glacial horizons (II, layer 2 and 4; IV) and more than those in contemporary sediments and in the warm interstage of the Würm period (II, layer 3). Especially widely represented in the south-boreal species complex: Coscinodicus stellaris, Cos. asteromphalus, Cos. angustolineatus, and Cos. radiatus. Typical topical species, such as Coscinodicus nodulifer, Ethmodiscus rex, Nitzschia marina, Hemidiscus cuneiformis, and Rhizosolenia bergonii appear here and are quite numerous in some layers. Overall, the floral composition testifies to the considerable warming of the surface waters, which (warming) was stronger than during the sediment deposits of the Würm warm stage. According to Kh. M. Saidova's data, the proportion of benthic foraminifera among the Horizon III fauna increases at depths of 224 to 292 cm.

Horizon IV (layer 6, 280 to 380 cm; Illinoian, Riss glaciation) is composed of fine silts and silty-clayey muds with thin interlayers of coarse silts and individual sectors containing high percentages of sand and silt grains. Lesser amounts of $SiO_{2\ amorph}$ (4.61 to 7.85 percent), $CaCO_3$ (0.25 to 0.59 percent), and C_{org} (0.34 to 0.45 percent), coarser grain-sizes (compared to the deposits of horizons III and V), and an abundance of volcanic material characterize the silts of this horizon. The same northern boreal and Arctic-boreal species that typify the flora of horizon II (layers 2 and 4) predominate among the diatoms. The sediments of this period contain the largest quantity of one of the coldest-water neritic species of diatoms in the northwest Pacific Ocean - Thalassiosira gravida. Coscinodiscus oculus-iridis, typical of the cooler water epochs in the northwest Pacific Ocean also appears here [32] and sublittoral marine and redeposited Tertiary diatoms increase.

Horizon V (layer 7, 380 to 580 cm; Yarmouth, Mindel-Riss interglaciation). The sediments of this horizon consist mainly of silty-clayey and clayey muds. The upper part of the layer is coarser grained and is composed mainly of fine silty muds. As in the preceding horizons, which were formed in warmer surface waters (I; II-2; III), horizon V contains a larger percentage of $SiO_{2\ amorph}$ (7.8 to 16.3 percent) than in sediments of the glacial epoch. Individual layers in the horizon have larger quantities of $CaCO_3$, C_{org}, and bitumens. Especially rich in C org and bitumens are the slightly siliceous diatomaceous silts at 380 to 480 cm. According to Kh. M. Saidova's data, the sediments of horizon V, at 440 to 442 and 510 to 518 cm, contain benthic calcareous foraminifera in excessive quantities.

The distribution of biogenic components and changes in the type of

of the diatoms are evidence of two warm climatic stages (380 to 480 and 520 to 580 cm) separated by a cooler stage (480 to 520 cm). The population density of such tropical diatom species as Coscinodiscus nodulifer, Podosira stelligera, Nitzschia marina, Hemidiscus cuneiformis, and Rhizosolenia bergonii increased during the warm stages. At the same time, the warm-water, south-boreal species of Coscinodiscus Wailessii grew luxuriantly. Sediments of the 380 to 480-cm layer were formed under warmer climatic conditions than the silts of the lower part of the layer (520 to 580 cm).

Horizon VI (layers 8, 9, 10, 11, 12; 580 to 1,040 cm; Kansan (?), Mindel (?) glaciations). The sediments consist of silty clayey muds with interlayers of fine silty clayey muds and coarse silts. Compared with interglacial sediments, the percentage of SiO_2 amorph is considerably smaller (2.91 to 7.37 percent), corresponding to the level of the preceding glacial horizon (IV). The distribution of $CaCO_3$, C_{org}, and bitumens vary considerably with depth in the core, which makes it possible to distinguish layers relatively rich in these constituents (650 to 730 and 840 to 950 cm).

The diatom flora generally resemble cold-water suites. There is a mass predominance of Coscinodiscus marginatus; all other Arctic-and north-boreal species prominent in the sediments (Thalassiosira gravida, Porosira glacialis, Biddulphia aurita, Thalassiothrix longissima, Thalassiosira excentrica) are considerably fewer in numbers. This horizon has a noticeable admixture of sublittoral, brackish water and redeposited Tertiary diatoms. The flora in the sediment layers that have a higher content of $CaCO_3$, SiO_2 amorph, and C_{org} as a rule, have a greater resemblance to warm-water flora. For example, at 650 to 700 and 810 to 920 cm, the number of the Arctic-boreal species (Thalassiosira gravida) decreases, and some other species disappear altogether (Porosira glacialis). Ethmodiscus rex and Coscinodiscus wailessii are highly developed. Between these layers, the sediments contain a larger quantity of cold-water species, including Coscinodiscus oculus iridis. Thus, changes in the lithologic composition of diatoms testify to repeated climatic oscillations during the deposition of horizon VI silts.

Horizon VII (layer 13, 1,040 to 1,135 cm; Afton (?), Gunz-Midel (?) interglacial period) is composed of homogeneous silty-clayey, slightly siliceous diatom muds that contain from 9.53 to 13.71 percent amorphous silica, and as a higher percentage of calcium carbonate (0.23 to 0.88 percent), organic carbon (0.49 to 0.73 percent), and bitumens (2.5-5.0 X 10^{-3} percent). North-boreal and south-boreal diatom species attained mass-development; single fragments of tropical species (Ethmodiscus rex and Coscinodiscus angustolineatus) are found. Overall, the diatom complex is like that of horizon I. The climate at that time may have been somewhat warmer than in the present epoch, which is confirmed by the presence of tropical constituents that do not occur in the sediment of horizon I. 65

Horizon VIII (layer 14, 1,135 to 1,195 cm; Nebraskan (?), Gunz (?) glaciations) is composed of clayey, silty-clayey and fine silty muds that contain approximately one-half the SiO_2 amorph (6.28 to 7.61 percent),

$CaCO_3$ (0 to 0.29 percent), C_{org} (0.33 to o.36 percent) of the silts of the horizon VII. North-boreal diatoms (Coscinodiscus marginatus, Thalassiosira excentrica, Rhizosolenia hebetata) and south-boreal species (Coscinodiscus asteromphalus, C. perioratus, Actinoptichus undulatus, etc,) are present simultaneously. The characteristic feature of the flora is significant quantity of diatoms, not peculiar to Quaternary deposits (Coscinodiscus sp., Actinocyclus sp.).

Therefore, based on the data presented above, the following conclusions can be made:

1. Based on lithologic and micropaleontologic study of sediments in the core at station 3163, 14 layers deposited under conditions of either warmer or colder climate were identified. The layers were grouped into 8 stratigraphic horizons and were correlated with the glacial and interglacial deposits of Western Europe and North America.

2. The climatic changes that occurred during the time interval sampled by the core influenced terrigenous as well as biogenic sedimentation. The sediments deposited during the epochs corresponding to the continental glaciation have, in most cases, coarser grains and a considerable admixture of volcanic material. The more cold-water character of the diatoms and the presence of increased quantities of sublittoral and redeposited Tertiary species are characteristic of these sediments. Along with these phenomena, the sediments of the glacial epochs are distinguished by their content of such biogenic components as amorphous silica, calcium carbonate, and organic carbon, which was determined not so much by the great inflow of detrital and volcanic material at that time, as by the lower productivity of the waters of the region under discussion. Sediments that were deposited during the interglacial epochs and glacial interstages are characterized by a finer and more homogeneous grain-sizes and more amorphous silica, carbonates, and organic matter.

3. The distribution of planktonic foraminifera in the core remained unstudied. Nevertheless, it is of undeniable interest that in the last glacial and interglacial stages (layers 3, 5, 7*); the quantity of benthic calcareous foraminifera increased in the sediments. It is possible that epochs of warming climate and rising temperature of the upper water layers, that favor diatom growth were also epochs when the production of planktonic and benthic foraminifera increased, and not only was there more $SiO_{2\ amorph}$ and organic matter, but also more $CaCO_3$ reached the bottom. 66

4. The almost direct relationship between the content of $SiO_{2\ amprph}$, $CaCO_3$, and C_{org} in the core at station 3163 becomes apparent in low concentrations and does not disappear during diagenesis for a period of several hundred thousand years. One might think that the post-sedimentation processes of solution and redistribution of the carbonate, silica, and organic matter could not sediments.

---

*The foraminifera have been studied to a depth of 605 cm, i.e. down to layer 8 inclusively.

5. It seems that the core exposed a large part of the Quaternary sediment series. This is confirmed by the presence in the lowermost part of the core of diatoms that are unknown in the Quaternary flora, according to A. P. Zhuze.

3. Core at Station 4068

Location - Northeast Basin of the Pacific Ocean, 350 miles south of Adak Island (Aleutian Islands). Depth - 5,782 m. Length of core - 332 cm. Collection device - uniflow tube corer.

Bottom relief - Near the station, the bottom is a finely dissected hilly plain (fig. 14) with isolated hills rising 50 to 100 m above the bottom (maximum 200 m) that have slopes of 1° to 4°. The bottom is flat and even in the immediate vicinity of the core station.

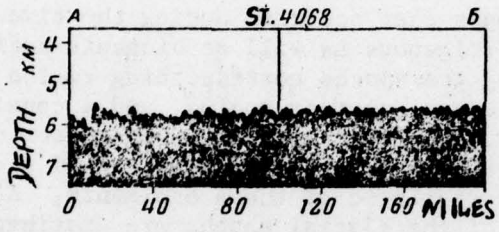

Figure 14. Bottom relief in the region of station 4068 (profile along the line A-B, see fig. 5).

Grain-size Compositon - Almost the entire length of the core, consists of dark brown and brown homogeneous clayey mud (fig. 15). From 71 to 77 percent of the particles are less than 0.01 mm in diameter. Somewhat coarser silty-clayey muds occur at 278 to 310 cm (61.5 percent of the grains are less than 0.01 mm). Particles sizes 0.001 to 0.005 mm predominate, comprising from 32 to 46 percent of the weight of the entire sediment, and more than 50 percent of the fraction is less than 0.01 mm. The most finely dispersed silts (oozes) were in the upper layer of the core (2 to 7 cm); 58 percent of the grains are less 0.001 mm. In the remainder of the core, particles less than 0.001 mm comprise between 13 and 21 percent of the total. The percentage of particles larger than 0.01 mm averages 25 percent and does not vary greatly through the core.

The lack of evidences of sediment redeposition, worm burrows and graded bedding indicates that the entire sequence resulted from the normal process of "particle-by-particle" deposition.

Distribution of Calcium Carbonate, Organic Matter Amorphous Silica, Manganese, and Iron

The sediments contain an insignificantly small percentage of $CaCO_3$, which decreases in the upper 40 cm from 0.45 to 0.03 percent and then varies within a very small range (0.04 to 0.14 percent). The amount of organic carbon, which is 0.33 percent in the upper layer (0 to 2 cm), 68

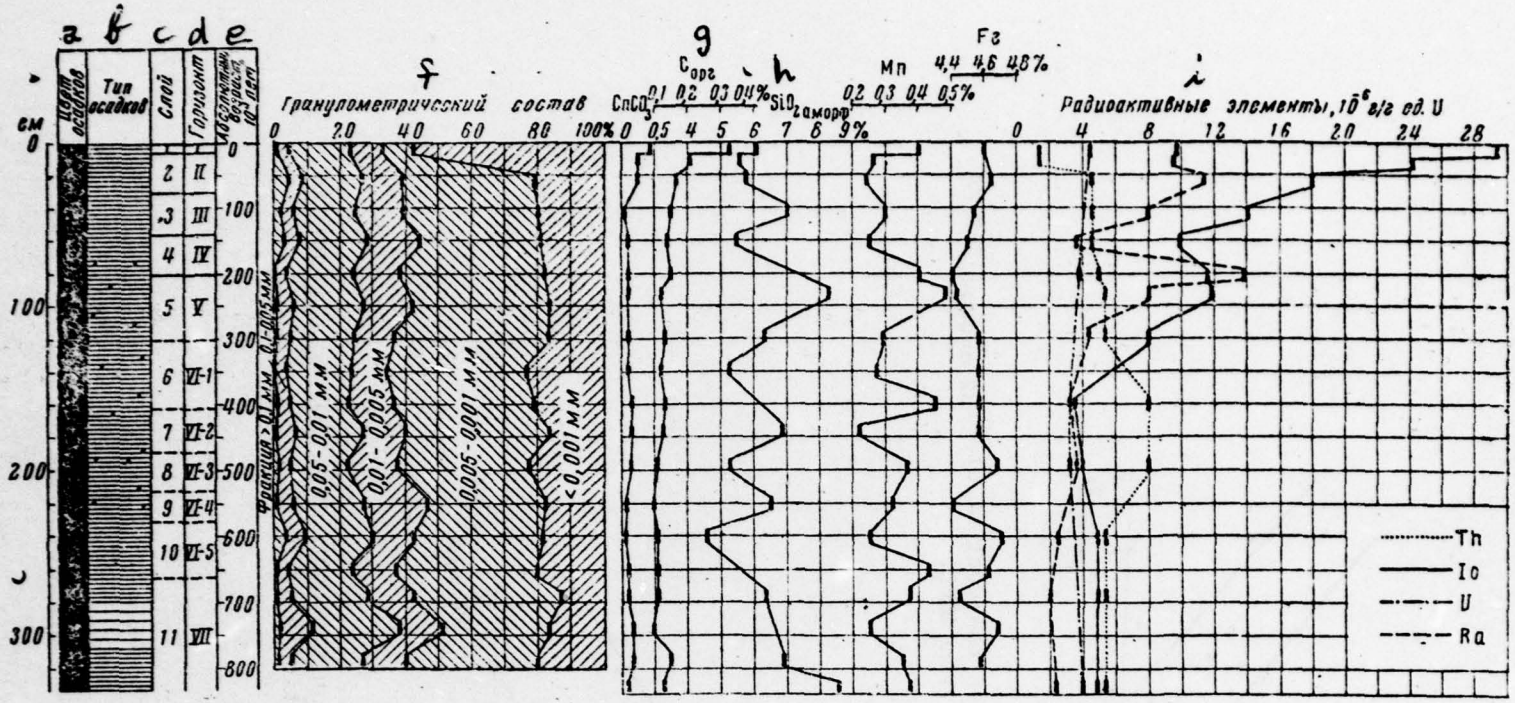

Figure 15. Core sample at station 4068. For conditional markings see figure 12.

a. Color of sediments
b. Type of sediments
c. Layer
d. Horizon
e. Absolute age, 10^3 years
f. granulometric composition
g. Organic carbon
h. SiO_2 amorph
i. Radioactive elements, 10^{-6} g/g of U (uranium) units

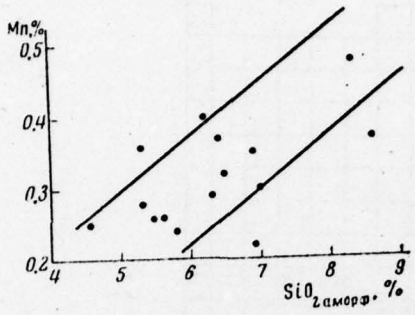

Figure 16. Relationship between the content of SiO_2 amorph and Mn in the core at station 4068.

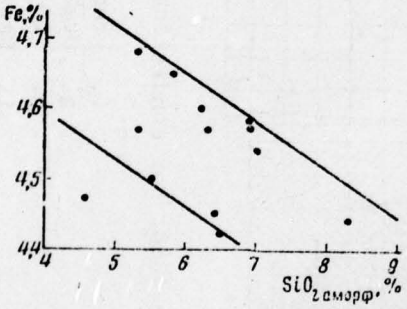

Figure 17. Relationship between the content of SiO_2 amorph and Fe in the core at station 4068.

decreases very rapidly with depth. At 20 to 25 cm, C_{org} already constitutes 0.17 percent, and below this depth it fluctuated between 0.10 and 0.15 percent tending toward a gradual decrease with depth. As in other cores taken in subarctic waters, the sediments from station 4068 contain a noticeable quantity of SiO_2 amorph (from 4.6 to 8.6 percent) varies considerably in the vertical direction. This makes it possible to distinguish in the core six layers having a higher content of SiO_2 amorph (0 to 7, 35 to 55, 80 to 110, 160 to 185, 210 to 226 300 to 332 cm) that are separated by layers low in SiO_2 amorph.

The manganese content varies from 0.48 to 0.22 percent. As a rule, sediments comparatively rich in manganese oxides are darker brown. Manganese distribution in the upper part of the core is similar to that of SiO_2 amorph. There is a nearly direct relationship between the content of Mn and SiO_2 amorph in the sediments, even though the scattering of the different values is considerable (fig. 16). The muds of the core contain from 4.42 to 4.70 percent Fe. Slight variations in the quantity of iron are found only in the lower part of the core. Figure 17 shows an inverse relationship between the amounts of Fe and SiO_2 amorph, although this relationship is not well defined. No relationship has been found between the percentage of Fe and Mn. The data on the content of Fe and Mn have been used in the ionium method of calculating the sedimentation rate.

Composition of Diatoms

Northern boreal (Thalassiosira excentrica, Coscinodiscus marginatus, Rhizosolenia hebetata) and Arctic-boreal (Thalassiosira gravida, Rhizosolenia curvirostris, Actinocystus ochotensis, Porosira glacialis) species predominate among the diatoms. At the same time, some sediment layers contain southern boreal flora in noticeable quantities, for example such species as Actinocyclus curvatulus, Thalassiosira pacifica, Coscinodiccus asteromphalus var. subbuliens, Rhizosolenia styliformis and Dictiocha octonaria. The change in the relationship among these three complexes indicates that the climate of this part of the ocean changed repeatedly during the entire time represented by the core. For example, the sediments of the 0 to 7 and the 40 to 55 cm layers were formed in a warmer climate than the layers directly beneath. Unfortunately, the composition of diatoms has been studied only at a few intervals along the core. Because of the low rate of silt deposition, the intervals between the samples analyzed correspond to time intervals of 40 to 50 thousand years, and it is impossible to reconstruct a continuous record of climatic variations in this part of the ocean.

69

As for as the relationship between the quantity of SiO_2 amorph and the composition of diatoms is concerned, this core apparently does not differ from other cores from the boreal region of the Pacific Ocean in the respect [34]. The increased accumulation of amorphous silica in the sediments occurred here during the epochs of warmer ocean surface waters.

Distribution of Benthic Foraminifera

The benthic foraminifera were studied by Kh. M. Saidova in all samples subjected to grain-size analysis. At depths of 0 to 7, 194 to 223, and 258 to 318 cm, shells of abyssal agglutinative foraminifera were found in the sediments. Foraminifera were found in other analyzed samples. The most significant quantity of abyssal foraminifera were at depths of 0 to 7, 218 to 223, and 318 to 331 cm.

Radioactive Elements and the Sedimentation Rate

Along with the principal components, thorium, uranium, ionium, and radium were found in the sediments. All the data are presented in Appendix III and fig. 15.

The thorium content in the core varies from 1.4×10^{-6} to 8.0×10^{-6} g/g. The upper and lower parts of the core contain noticeably less thorium than the sediments between 140 and 220 cm. The similar thorium distribution indicates as increase in the influx of terrigenous material when the sediments at this level were formed (probably the Midel glacial epoch).

The distribution of radium in the upper part of the core is close to theoretical values. Nevertheless, below the upper maximum, which can coincide with the equilibrium between radium and ionium, agreement with the theoretical curve is interrupted (at about 70 to 80 cm) by a second, even more sharply defined, maximum of radium concentration. At greater depths, the radium content approaches equilibrium values in the uranium - ionium - radium family. The radium content in the upper layer of the sediments (2 to 7 cm), (9.8×10^{-6} g/g units of U) is only twice the equilibrium concentration of uranium (4.5×10^{-6} g/g), and in the lower part of the core the amount of radium, $(2.0\text{-}2.5) \times 10^{-6}$ g/g units of U is less than the equilibrium amount with uranium (4×10^{-6} g/g).

The variation of ionium with depth is especially interesting. In the upper layer of sediments (2 to 7 cm), the concentration of ionium is approximately eight times the equilibrium concentration of uranium. The ionium content decreases smoothly down to 63 cm, increases at approximately 70 to 100 cm, then slowly decreases, and at about 160 cm it approaches the equilibrium concentration with uranium. This permits the assumption that the 160 cm-thick layer was deposited in 400 to 450 thousand years and that the average sedimentation rate is approximately 4 mm per 1,000 years.

Such an age estimate is approximate, because the ionium curve is disrupted at about 70 to 100 cm. It is interesting to note that this layer differs not only in higher ionium content, but also in higher content of radium, manganese, and amorphous silica. It seem that, due to different physicochemical conditions during the period that the sediments in the 70 to 100 cm layer were deposited, more ionium, radium, manganese, and amorphous silica accumulated on the bottom, not only relatively, but absolutely. In fact, the iron content of the sediments of this layer

70

differs little from those above and below. If one ignores the diluting influence of the biogenic components, particularly SiO_2 amorph, then the proportion of iron in the sediments of this layer will be the same as in the upper and middle parts of the core. On the ocean margin where the core was taken, nearly all the iron is terrigenous. Its vertical distribution along with data of the distribution of amorphous silica indicates that the increase in biogenic sedimentation rate was not accompanied by an increase in the delivery of terrigenous material to the bottom. The greater amount of ionium at 70 to 100 cm (which resulted from greater biogenic sedimentation rates) can indicate an increase in the overall quantity of ionium that reached the bottom during this time, as well as its possible genetic connection with biogenic substances. Nevertheless the latter is rather improbable, because the biogenic material, including the silty-clayey and clayey diatom muds, contain even less ionium than the terrigenous silts, not to mention the deep-sea red clays (see chapter V).

The lack of great variation in the grain-size composition of the sediments indicates that the absorptive qualities of their terrigenous components have not changed perceptibly during the deposition of the sediment layer. It is also quite improbable that the greater content of the Io, Ra, Mn, and SiO_2 amorph in the sediments at 70 to 100 cm is caused by the migration of these elements within the silt layer, because of the greater content of all four elements, which are so different in migratory ability. Even manganese, which can be considered the most mobile, exists within the pronounced oxidizing environment retained throughout the entire sedimentary layer (Eh approximately + 500 mv), is in the tetravalent state (+4) and has not entirely migrated. Because of the change in physicochemical conditions during the period when the sediments now at 70 to 100 cm were deposited, more manganese, and the radium and ionium connected with it, was deposited on the bottom. The greater content of SiO_2 in the sediments that resulted from the warmer climate and surface water temperatures, indicates that the physicochemical environment really changed during this time.

In addition to the above data on the sedimentation rate that were obtained by determination of the equilibrium horizon, we also calculated the sediment accumulation rate based on the decay of ionium. This sedimentation rate was also 3.5 to 4 mm per 1,000 years. The similar mean sediment accumulation rates obtained by these two methods indicate the reliability of the determination of the sediment accumulation rate. It can be assumed to average 4 mm per 1,000 years, noral process of ionium deposition on the bottom and the increase in biogenic sedimentation rate took place 200 to 270 thousand years ago (probably during the Mindel-Riss interglacial epoch). The overall age of the core was estimated to be 800 thousand years.

Sedimentary Stratigraphy

The type of distribution of amorphous silica in the core together with data on the diatom composition made it possible to identify seven horizons and 11 layers that were formed under warmer (horizons I, III, V, VII) and colder (horizons II, IV, VI) climatic conditions. The

Table 10

The stratigraphy of the sediments at core station 4068

Layer	Horizon	Depth in Core (cm)	Thickness (cm)	Absolute age (10^{-3}) (yrs)	Stratigraphic Correlation	
					North America	Western Europe
1	I	0-4(7)	4-7	0-11(17)	HOLOCENE	
2	II	4(7)-30	23-26	11(17)-75	Wisconsin and Iowan glacial stages	Würm Glaciation
3	III	30-56	26	75-140	Sangamon interglacial stage	Riss-Würm interglacial stage
4	IV	56-80	24	140-200	Illinoian glaciation	Riss glaciation
5	V	80-120	40	200-300	Yarmouth interglacial stage	Mindel-Riss interglacial stage
6		120-162	42	300-400		
7		162-188	26	400-470		
8	VI	188-212	24	470-530	Kansas glaciation	Mindel glaciation
9		212-230	18	530-570		
10		230-264	34	570-660		
11	VII	264-332*	68	660-830	Afton interglacial stage	Gunz-Mindel interglacial stage

* This horizon was not completely penetrated (by the core).

absolute age of the horizons was derived from the sedimentation rate (table 10). An attempt was made in table 10 to correlate the horizons with contemporary events of the Quaternary period in North America and Western Europe.

Judging from the diatom composition, the surface waters became warmer during the last glaciation. This is confirmed by the appearance, at 20 to 25 cm, of the south boreal flora - Actinocyclus curvatulus and Coscinodiscus asteromphalus, which have also been found in the core in horizons I (Holocene) and VII (interglacial stage). It is possible that this warming corresponds to the deposition of layer 3 at station 3163, as well as at stations 3325, 3342, 3359, and 3378 (see section 4), and correlates with the warm stage of the last glaciation. During formation of the sediments of horizon VI, which we have assigned, conditionally, to the Kansan glaciation, there were two warm stages or even two interglacial epochs (layers 7 and 9), which probably correlate with layers 9 and 11 at station 3163.

4. Core Samples at Stations 3378,3325,3342,3359

Location - Northwest Basin of the Pacific Ocean, east of Kamchatka. Station 3378: depth - 5,460 m, length of core sample - 332 cm; station 3325: depth - 4,016 m, length of core sample - 188 cm; station 3342: depth - 4,588 m, length of core sample - 276 cm. Sampler - uniflow tube corer.

Bottom relief. The core at station 3378 was taken on a hilly plain, approximately 120 miles east of the Kurile-Kamchatka Trench (fig. 18). The core at station 3324 was taken on the bottom of a shallow depression in the central part of the Obruchev underwater plateau (fig. 19). The cores at stations 3342 and 3359 were taken on the outer slope of the Aleutian abyssal trench in an area of complex structure and very dissected bottom (fig. 20, 21).

The core samples were subjected previously to lithological and micropaleontological analysis. The stratigraphic data for the sediments are presented in the literature [13, 29, 34, 61, 66].

Granulometric Composition The Distribution of Amorphous Silica, Organic Matter, and Calcium Carbonate

Although the cores were taken at considerable distances from each other in regions of differing bottom relief, they have a similar and comparatively constant grain-size composition in the vertical direction. The sediment layers are clayey and silty-clayey muds that are repeatedly

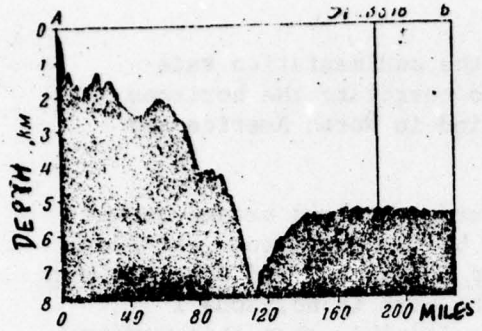

Figure 18. Bottom relief in the area of station 3378 (profile along the line A-B, see fig. 5).

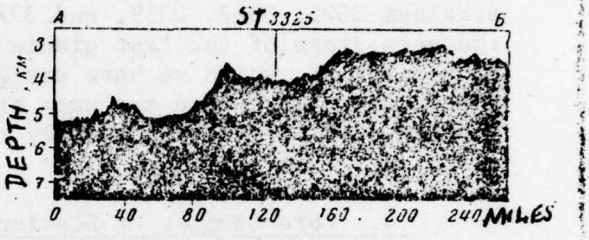

Figure 19. Bottom relief in the area of station 3325 (profile along the line A-B, see fig. 5).

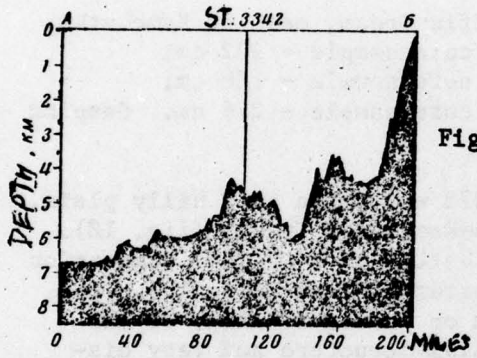

Figure 20. Bottom relief in the area of station 3342 (profile along the line A-B, see fig. 5).

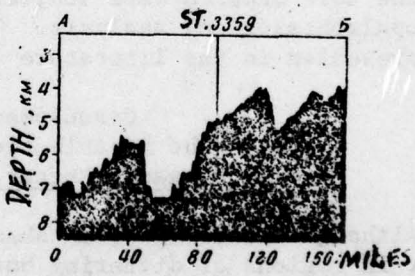

Figure 21. Bottom relief in the area of station 3359 (profile along the line A-B, see fig. 5).

Figure 22. Core at station 3378. For conditional markings see fig. 12.

a - Color of sediments

b - Type of sediments

c - Layer

d - Horizon

e - Grain-size fractions

f - $CaCO_3$

g - C org

h - SiO_2

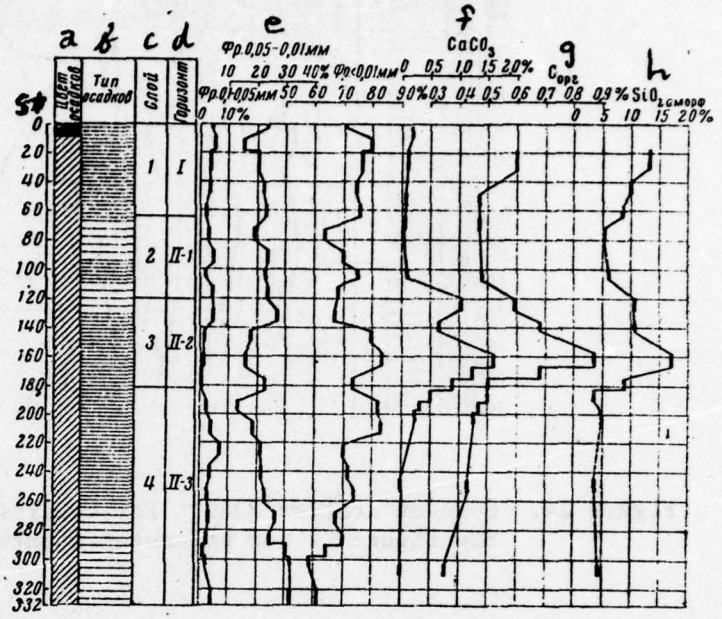

Figure 23. Core at station 3325. For conditional markings see fig. 12. See figure 22 for parameter identifications.

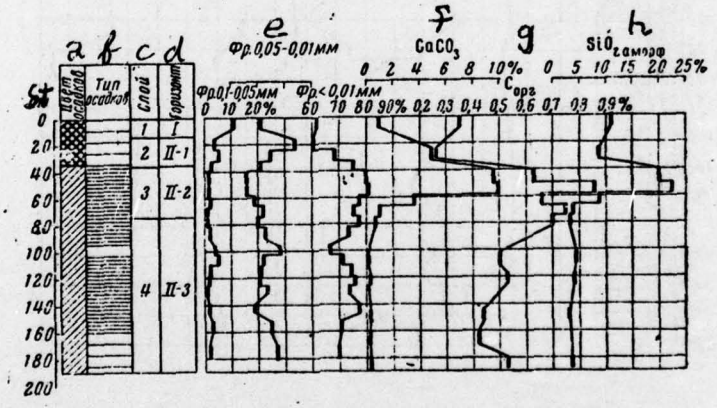

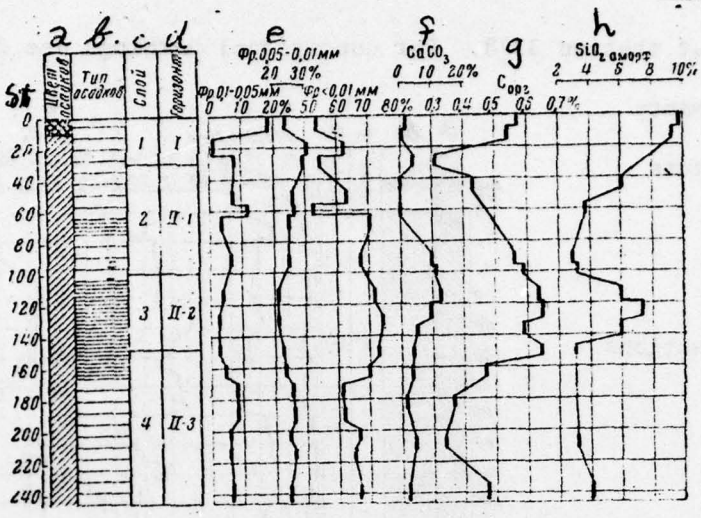

Figure 24. Core at station 3342. For conditional markings see fig. 12. See figure 22 for parameter identifications.

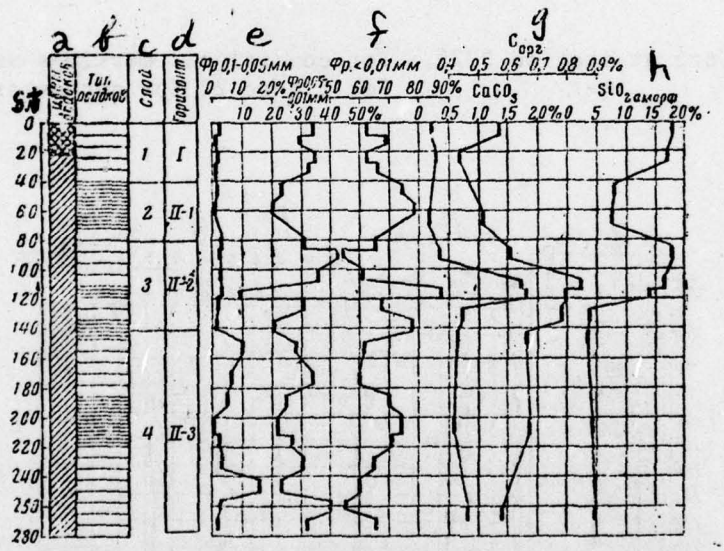

Figure 25. Core at station 3359. For conditional markings see fig. 12. See figure 22 for parameter identifications. 74

interlayered (fig. 22, appendix IV; fig. 23, appendix V; fig. 24, appendix VI; fig. 25, appendix VII). They contain a considerable admixture of volcanic material distributed unevenly through the cores. Several layers have larger amounts of pyroclastic material (40 to 87 and 119 to 276 cm in the core at station 3359) that consist mainly of irregularly shaped grains of volcanic ash of fine silt size.

The oozes of the upper layer, extending down to 32 cm, are tinted by iron and manganese oxides to a brown (station 3378) or light-brown color (stations 3325, 3342, 3359), somewhat deeper they are grey and greyish-green. The oxidized layer is thickest (32 cm) at station 3325. The thickness is determined by the low content of organic matter in the sediments (approximately 0.3 percent C_{org}) and, consequently, the slow reduction rate of the highest oxides of manganese and iron.

The vertical distribution of SiO_2 amorph is identical in all four cores. In the graphic representation of cores, it varies as follows (figs 22-25): From the surface down to some depth, different for each core sample, the content of SiO_2 amorph decreases; then it gradually increases to greater depths to a maximum, then drops sharply; finally, the SiO_2 amorph remains quite low to the bottom of the core.

For example, the sediments of the upper part of the core at station 3359 (fig. 25) contain from 16.8 to 18.2 percent SiO_2 amorph down to 40 cm. Then, down to 80 cm, it comprises 7.5 to 7.6 percent. At 87 to 130 cm, the sediments are again enriched with amorphous silica, which reaches 17.9 percent. In the lower part of the core (130 to 276 cm), the percentage of SiO_2 amorph does not exceed 3.8 to 4.6 percent. Such an amorphous silica distribution defines four layers in the core: 0 to 40 cm layer - silty-clayey slightly siliceous diatom oozes; 40 to 80 cm - mainly clayey sediments lacking silica; 80 to 120 (130) cm - mainly clayey sediments lacking silica; 80 to 120 (130) cm - silty-clayey and clayey slightly siliceous diatom muds; 120 (130)cm to the bottom of the core (276 cm) - silty-clayey (mainly) and clayey sediments lacking silica. The cores at stations 3325 and 3378 have a similar type of SiO_2 amorph distribution. Four layers can also be identified here: Layers 1 and 3 are clayey and silty-clayey slightly siliceous diatom muds, and layers 2 and 4 are clayey and silty-clayey sediments lacking SiO_2 amorph.

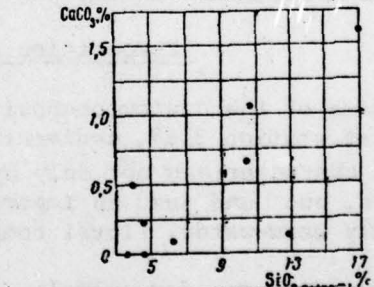

Figure 26. Relationship between the percentage of SiO_2 amorph and $CaCO_3$ in the core at station 3378.

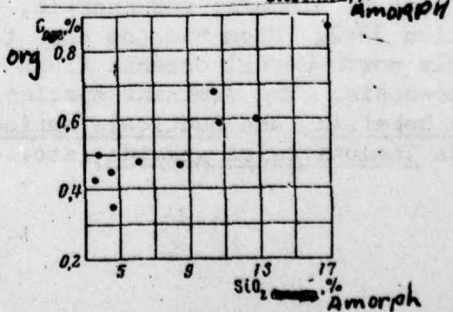

Figure 27. Relationship between the percentage of SiO_2 amorph and C_{org} in the core at station 3378.

The amorphous silica distribution in the core at station 3342 is similar to that described above, nevertheless, as a result of the generally low content of SiO_2 amorph, the silts of the upper layer (1) and the silts from about 100 to 150 cm (layer 3) cannot be called even slightly siliceous, even though they are relatively enriched with SiO_2 amorph. The location of layers enriched or depleted in amorphous silica are compiled in table 11.

Table 11

Depths within cores of layers (in cm) having relatively large (1 and 3) or small (2 and 4) amounts of amorphous silica.

Layer	Stations			
	3378	3325	3342	3359
1	0—65	0—12	0—20 (40?)	0—40
2	65—120	12—35 (40)	20 (40?) — 100	40—70 (80)
3	120—183	35 (40) — 66 (74)	100 — 140 (147)	70 (80) — 120 (130)
4	183—332	66 (74) — 188	140 (147) — 244	120 (130) — 276

Analysis of the relationship between the grain-size composition of the sediments and their SiO_2 amorph content suggests that comparatively small changes in grain-size composition do not greatly influence the SiO_2 amorph distribution. As can be seen from fig. 22 to 25, the vertical distribution of $CaCO_3$ and C org is quite similar to that of SiO_2 amorph. In all cases, one observes the identical layer with a high content of all three components at some depth below the sea (sea) bottom. Above and below this layer lie deposits that either completely lack carbonates or contain much smaller amounts of $CaCO_3$ and C org. Graphs of the relationship of SiO_2 amorph and $CaCO_3$ and SiO_2 amorph and C org (figs. 26,27) show that in spite of the considerable dispersion of values, there is an overall direct or nearly direct realtionship between the content of amorphous silica, carbonates, and organic matter in the sediments.

Composition of Diatoms

Studdes of the diatom composition of sediments have shown that, like the core at station 3168, sediment layers rich in SiO_2 amorph, $CaCO_3$, and C org are characterized not only by a considerably greater number of diatom values, but and just as important, by a different qualitative (relatively warm-water) floral composition.

Let us discuss, for example, the changes in the diatom flora at station 3342. From the top down to 32 cm, in this core, the flora are mainly north-boreal oceanic flora that differ little from the contemporary biocoenosis. The dominant species are Thalassiosira excentrica, Rhizosolenia hebetata, and Denticula marina. Among the neritic species, one often finds Thalassiosira gravida, etc. The considerable quantity of neritic

diatoms is not typical of the upper layer of other sediment cores, which is explained by the proximity of station 3342 to Kamchatka and the Komandorskiye Islands. On the contrary, almost all the cores discussed in this section are characterized by an almost complete lack of sublittoral and redeposited Tertiary diatoms in the surface sediment layer.

Neritic-oceanic species with an admixture of benthic and planktonic forms from the sublittoral zone and individual fresh water diatoms predominate from 32 to 95 cm in the core. The characteristic feature of these deposits is the abundance of redeposited forms within them. Even deeper, between about 95 and 147 cm, the flora consist of masses of warm-water oceanic species, such as Coscinodicus stellaris, Cos. perforatus, Cos. raduis, Cos. asteromphalus var. subbliens and Thalassiosira pacifica. Along with diatoms, a warm-water species of siliceous flagellate aqueous plants, Dictyocha octonaria (which, according to A. P. Zhuze, at the present time develops normally in water temperatures of 18° to 20°C), as well as organic skeletal remains of peridinean marine plants, appear here.

Overall, the sediments in the middle of the cores are characterized by well-preserved valves and the lack of a whole series of the cold-water forms that are widely represented in the deposits above and below. The warm-water diatom complex found here is observed neither among contemporary plankton, nor in the surface sediment layer of the Komandorskiye-Kamchatka region and the Bering and Okhotsk seas. The typical species that comprise this complex normally develop under conditions now existing at the southern boundary of the boreal region (40°N) in surface-water temperatures of 12° to 16 C [34].

At depths of 147 to 244 cm, the small numbers of diatoms are represented by redeposited Quaternary and more ancient marine and fresh water forms that comprise 40 to 50 percent of the diatoms. Warm-water species disappear completely at this depth and Arctic and north-boreal species (Thalassiosira gravida, Th. excentrica, Conscinodiscus curvatulus, Cos. marginatus, Rhizosolenia hebetata) predominate. The entire floral complex 77
is indicative of a noticable climatic cooling during this period. These variations in flora made it possible to divide the sediment layer at station 3342 into four layers. Layers 1 and 3 were formed during periods of warmer climate than existed when the sediemnts of layers 2 and 4 were deposited.

The sediments in the cores at stations 3325, 3359, and 3378 are quite alike in diatom composition and in species variations. There are no convincing data to distinguish layers 1 and 2, therefore the sediments lying above the warm-water layer 3 are either not separated or are separated conditionally (station 3378 [29, 34]). Data on the depth in different cores of layers containing identical and almost identical compositions of diatoms is compiled in table 12.

Table 12

Depth from the sediment surface (in cm) of layers of warm and cold water diatoms.

Layer	Stations			
	3378	3325	3342	3359
1	0-70	0-24	0-32	0-55
2	70-128		32-95	
3	128-191	24-74	95-147	55-142
4	191-332	74-188	147-244	142-276

Comparison of the data in tables 11 and 12 shows that sediment layers defined by their content of amorphous silica and those defined by variations in diatoms almost coincide. The existing differences are related, to a considerable extent, to the insufficient numbers of samples taken for analyses.

Distribution of Benthic Foraminifera

The study the distribution of bottom foraminifera in all samples were the grain-size composition of the sediments was determined [66] has shown that the largest number of benthic calcareous foraminifera occur in layer 3, coinciding with greater proportions of $CaCO_3$, C_{org}, and SiO_2 amorph.

Sedimentary Stratigraphy

Study of the total lithologic and micropaleontologic data confirms that the four sediment layers distinguished in the cores at stations 3378, 3325, 3342, and 3359 have stratigraphic significance and reflect large climatic changes of the Quaternary period. Unfortunately, the attempt to date the sediments by the ionium method at station 3378 and 3325 where the cores were taken comparatively close to dry land was not very successful. It seems that the abundant and chronologically irregular inflow of sedimentary material from dry land led to sharp fluctuations of these hydrogenic components in the sediments and destroyed the relationship between the distribution of the components and water depth. In addition, it was impossible to calculate the absolute age of the sediments of these cores directly. Nevertheless, a whole series of features common to the lithologic and floral composition 78
of the sediments at stations 3378, 3325, 3342, 3359, on the one hand, and to the cores at stations 3162, 3451 etc, on the other, makes it possible to correlate these defined layers, and to date, indirectly in this way, the events fixed within these four core samples, as well as to correlate them with the climatic epochs of North America and Western Europe (table 13).

The typical feature of the two stages of the last glaciation (layers 2 and 4) was the increased content of volcanic material in the sediments. An extremely large quantity of pyroclastic material (volcanic ash) exists in the core at station 3342 located not far from

Table 13

The stratigraphy of the sediments of cores from stations 3378, 3325, 3342, and 3359.

Layer	Horizon	Depth from the sediment surface (cm) (From top of the Core)				Stratigraphic Correlation	
		St 3378	St 3325	St 3342	St 3359	North America	Western Europe
1	II	0-65	0-12	0-32	0-40	Wisconsin glacial stage	Main and Late stages of Wurm glaciation
2		65-120	12-35	32-100	40-80		
3	II	120-190	35-74	100-147	80-140	Interglacial stage	Interglacial stage
4		190-332*	74-188*	147-244*	140-276*	Iowan glacial stage	Early Wurm glaciation

*This layer was not completely penetrated.

the Kronotskiy group of Kamchatka volcanos. Similar evidence of increased volcanic activity throughout the two cold stages of the last glaciation was shown previously in the core at station 3163. Based on the fact that the warm stage of the Würm glaciation began approximately 50,000 years ago, one can calculate the minimum sediment accumulation rate of the cores discussed. These rates approximate: In the core at station 3378 - 4 cm per 1,000 years; at station 3325 - 1.5 to 2 cm per 1,000 years; and at stations 3342 and 3359 - 3 cm per 1,000 years.

5. The Core at Station 3451

Location - Northwest Basin of the Pacific Ocean, east of the Japan abyssal trench. Depth - 5,678 m. Length of core - 267 cm. Sampling instrument - uniflow tube corer.

Bottom relief - Near the station the bottom is a slightly hilly plain. The slopes of the nearest hills are measured in fractions of a degree (0.1° to 0.3°), bottom slopes of 2° to 4° are found in some places. The core at station 3451 was taken on the southeast slope of a low hill rising 130 m above the bottom (fig. 28)

A. P. Zhuze previously analyzed the diatoms in the core [32, 33]. Condensed information on the stratigraphy and absolute age to the sediments is presented in the report by P. L. Bezrukov and E. A. Romankevich [13].

Grain-size Composition

The core is composed mainly of carbonate-free slity-clayey (0 to 25, 97 to 165, 180 to 217 cm) and clayey (25 to 97, 168 to 180 cm) muds of brown (0 to 12 cm) and grey (12 to 267 cm) color (fig. 29, appendix VIII). From 55 to 77 percent of the sediments are pelite particles. The fine and coarse silt fraction comprises, respectively, 17 to 30 and 5 to 14 percent of the sediment weight. Sand-size particles are insignificant (usually 1 to 2 percent). 79

The coarser sediments, silty-clayey and fine silty muds, are located in the core at a depth of 125 to 168 cm. At 133 to 165 and 250 to 267 cm, the sediments contain numerous fine layers (about 1 mm thick or less) enriched with silt-sized volcanic ash.

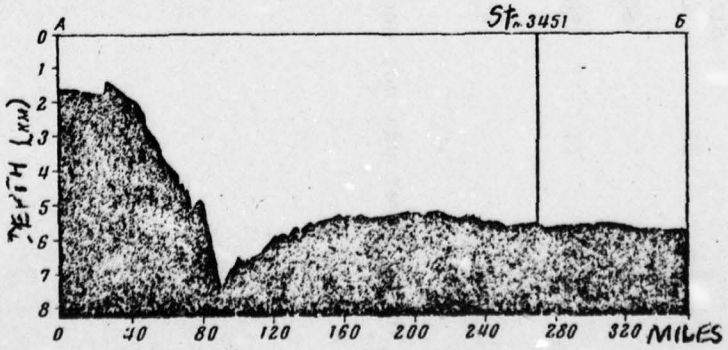

Figure 28. Bottom relief in the area of station 3451 (profile along the line A-B, see fig. 5).

AD-A065 567 NAVAL OCEANOGRAPHIC OFFICE NSTL STATION MS F/G 8/10
STRATIGRAPHY AND ABSOLUTE AGE OF DEEP-SEA SEDIMENTS IN THE WEST--ETC(U)
1979 E A ROMANKEVICH, P L BEZRUKOV
UNCLASSIFIED N00-T-32(532) NL

2 OF 2
AD A065567

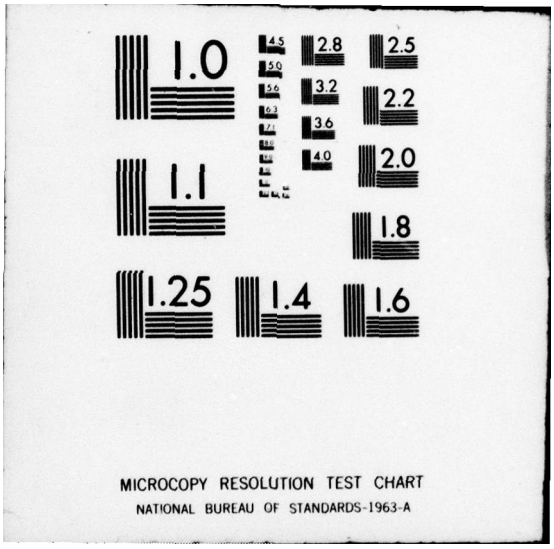
1.0
1.1
1.25
1.4
1.6
1.8
2.0
2.2
2.5
2.8
3.2
3.6
4.0
4.5
5.0
5.6
6.3
MICROCOPY RESOLUTION TEST CHART
NATIONAL BUREAU OF STANDARDS-1963-A

At the same time, the number of sand-sized particles increases, and gravel-sized grains of pumice appear. A layer of fine silt at 165 to 168 cm is composed almost entirely of colorless volcanic glass and contain angular pumice pebbles approximately 3 cm in diameter, as well as some coarse sand-sized grains of pumice.

Distribution of Calcium Carbonate, Organic Matter, Amorphous Silica, and Iron

The sediments contain very little carbonaceous material (0.18 to 0.66 percent). The least amount of $CaCO_3$ occurs in sediments with a large admixture of volcanic material, and these sediments are located at 100 to 180 cm. The content of organic matter varies in the core from 0.94 to 0.38 percent C_{org}. Its vertical distribution through the core permits division of the sediment into five layers: 0 to 30, 30 to 100, 100 to 180, 180 to 240, and 240 to 267 cm. The sediments contain from 3 to 7.2 percent of SiO_2 amorph, dividing the core into five layers: 0 to 20 (26)*, 20 (26) to 60 (66); 60 (66) to 130; 130 to 190 and 190 to 267 cm, among which layers 1, 3, and 5 are rich in amorphous silica and layers 2 and 4 have little SiO_2 amorph.

The total content of iron in the core varies from 4.7 to 3.6 percent The silty-clayey muds at depths of 6 to 30, 105 to 126, and 180 to 267 cm contain higher amounts of iron. The upper oxidized zone in the core is 12 cm thick. In this zone, the sediments are brown and greyish-brown, which indicates the presence of reducing (relative to manganese iron) conditions. The relatively high content of organic matter in the sediments determined the thinness of the oxidized layer and the relatively intense reduction processes that led to the formation of hydrotroilite ($FeS \cdot nH_2O$) at depth of 105 cm. Much of the soluble iron in the reduction zone is in the form of Fe^{**} (ferrous iron) and migrates within the silt layer. The soluble iron is a significant part (about 20 percent) of the total iron and indicates that there is no assurance that the distribution of most of the iron in the core reflects changes in its deposition on the bottom.

Within the core as a whole there is no relationship between the content of SiO_2 amorph and $CaCO_3$, SiO_2 amorph and Fe, and $CaCO_3$ and C_{org}, nevertheless, in spite of some scattering of the values, the

---

*Because sediments in the 20 to 26 cm zone were not analyzed for SiO_2 amorph, the probable boundary of the layer is given in parentheses.

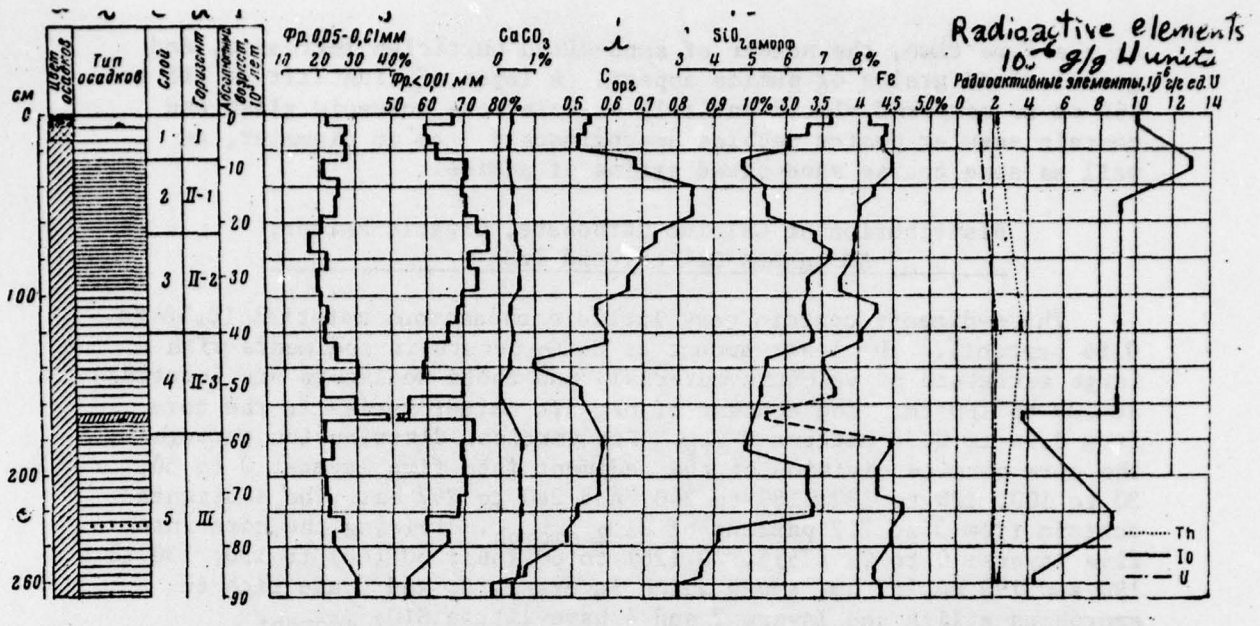

Figure 29. Core sample at station 3451. For conditional markings see fig. 12.

(a, b, c, d, and f are the same as in fig.12)

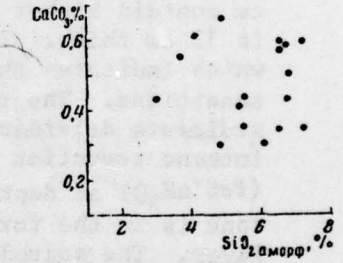

Figure 30. Relationship between the content of SiO_2 amorph and $CaCO_3$ in the sediments of the core at station 3451.

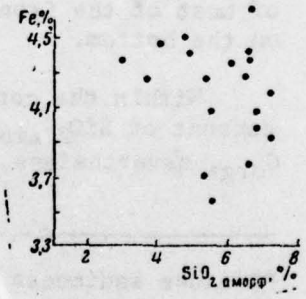

Figure 31. Relationship between the content of SiO_2 amorph and Fe in the sediments of the core at station 3451.

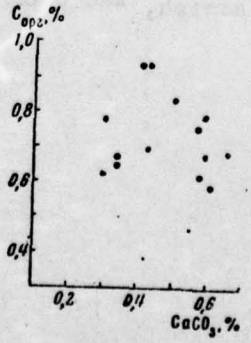

Figure 32. Relationship between the content of $CaCO_3$ and C org in the sediments of the core at station 3451.

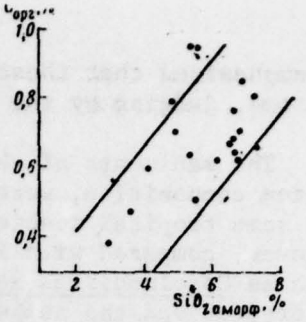

Figure 33. Relationship between the content of SiO_2 amorph and C org in the sediments of the core at station 3451.

direct relationship between the content of SiO_2 amorph and C org can be seen quite clearly (figs. 30-33).

Diatom Composition

The five variations in the composition of marine diatoms in the core testifies to the periodic, sometimes sharp, climatic changes in sedimentation. This enabled A. P. Zhuze to identify five layers in the core at station 3451 [32, 33].

The five layer (0 to 30 cm) is characterized by the predominance of south-boreal diatoms, such as Coscinodiscus asteromphalus, Cos. radiatus, Cos. stellaris, Actinoptychus undulatus f. pacica, and Actinocyclus ehrenbergii, as well as the presence of tropical flora (Planctoniella sol., Cos. nodulifer, Hemidiscus cuneiformis, Cos. africanus). Compared to the underlying layer, the sediemnts at 0 to 30 cm contain fewer cold-water and temperate-cold-water diatoms. Arctic-and north-boreal species of diatoms, such as Coscinodiscus oculus-iridis, Cos. marginatus, Thalassiosira excentrica, etc, predominate in the second layer (30 to 65 cm). The tropical species present in the upper layer are not found here, except for individual specimens of Nitzschia marina. The number of south-boreal diatoms decreases also, and some species, such as Coscinodiscus stellaris and Actinoptychus undulatus f. pacifica, disappear altogether. 82

The sediments of the third layer (56 to 120 cm) are like those of the first in diatom composition. The differences consist of the smaller number of some tropical species (Planctoniella Sol. and Ethmodiscus rex) and in the appearance of the north-boreal species Actinocyclus curvatulus, which is absent in the first layer. It appears that during the deposition of the third layer the climate was cooler than at present.

Tropical flora completely disappear in the fourth layer (120 to 170 cm), the number of boreal species decrease sharply, and north-boreal diatoms increased as compared to the preceding layer. The floral composition indicates a new surface water cooling, which (cooling) was apparently less severe than the one during the formation of the second layer silts. This is confirmed by the absence of such a typical Arctic-boreal species as Coscinodiscus oculus-iridis, the decrease in the number of Arctic-boreal neritic species Thalassiosira gravida and the north-boreal oceanic species Coscinodiscus marginatus. It should

be emphasized that these changes occur while the total quantity of diatoms, judging by the quantity of biogenic silica, is nearly identical.

The sediments of the fifth layer (170 to 230 cm*), based on the diatom composition, were again deposited under warm climatic conditions. The same tropical species as in layers 1 and 3 are present at this depth. However, compared with layers 1 and 3, the number of subtropical species such as Coscinodiscus asteromphalus, Cos. radiatus, and Cos. stellaris is greater and the number of cold-water diatoms somewhat less, which indicates that water temperatures in the northwest Pacific Ocean were higher when the sediments of layers 1 and 3 were laid down. A similar phenomenon was seen earlier in the core at station 3163, which penetrated the fifth layer (see section 2 of this chapter).

Radioactive Elements and the Sedimentation Rate

The core sediments contain 1.2 to 2.2 x 10^{-6} g/g of uranium and 2.2 to 3.6 x 10^{-6} g/g of uranium (U) units of thorium, which are quite low values and usually characterize terrigenous silts with a relatively high rate of inflow of clastic products from the dry land. The content of ionium in the surface sediments (10 x 10^{-6} g/g of U units) is eight times the equilibrium concentration of uranium (1.2 x 10^{-6} g/g). Nevertheless, no consistent decrease of ionium content was seen deeper in the sediments. This may be related both to the changing proportions of terrigenous and biogenic components in the sediments and to the change in absolute quantity of ionium. In this particular case, it seems probable that a change in the rate of biogenic and terrigenous sedimentation took place during the time interval represented by the core. It is interesting that the volcanic ash located at 165 to 168 cm, as well as the silty-clayey muds with numerous inclusions of cinder material, contain a much smaller amount of ionium. This probably results from dilution by rapidly settling pyroclastic material that contains little ionium. The eightfold excess of ionium over uranium and the general slope of the ionium curve make it possible to evaluate the deposition rate of the silts (approximately 30 mm per 1,000 years).

Sedimentary Stratigraphy

The vertical distribution of SiO_2 amorph and, to a lesser degree, of C_{org} and $CaCO_3$ in the core, and the change in species composition of diatoms, reveal five layers that developed under different climatic conditions. Table 14 shows the depth, thickness, and absolute age of these layers, as well as possible correlations with continental deposits of North America and Western Europe.

The layers containing warm-water complexes of marine diatoms (1, 3 and 5) are relatively rich in amorphous silica and have a somewhat larger quantity of biogenic carbonate. Therefore, in the region now occupied by subtropical ocean waters, there is also a direct relationship between temperature variations of the surface water layers and the quantity of amorphous silica in the sediments. This relationship is characteristic of a whole series of cores taken in the northern regions of subtropical water.

* The diatom composition has not been studied below 230 cm.

The formation period of layer 4 (Early Würm) was marked by an increase in volcanic material, which resulted in coarser sediments being deposited during this period. The increase in volcanic material in sediments of the last glacial epoch was noted earlier in the core at station 3163.

The distribution of organic matter in the core at station 3451 is somewhat unusual. Based on analysis of the cores at stations 3163, 3378, 3325, 3342, 3359 and other stations, it was determined that, in the northwest Pacific Ocean, the maximum C_{org} content is confined to sediments enriched with siliceous skeletons of marine diatoms that reached the bottom in larger numbers during the warming climate. In the core discussed, a similar phenomenon is observed during the Riss-Würm interglacial period, but this phenomenon is not characteristic of the warm stage of the Würm period.

6. Core at Station 3625

84

Location - southern part of the Northwest Basin, approximately 720 miles east of the Bonin Islands. Depth - 6,008 m. Length of the core - 369 cm. Sampler - piston frame tube corer.

Bottom relief: Near the station the bottom is a slightly hilly plain. The hills have gradual slopes (up to 1°) and rise a maximum of 100 m above the bottom. Forty-five miles northwest of the station is a sea mount whose summit depth was 1,342 m, with upper slopes of about 10° and lower slopes of about 3°. Approximately 70 miles southeast of the station another seamount rises 1,250 m above the bottom (fig. 34).

Figure 34. Bottom relief in the region of station 3625 (profile along the line A-B, see fig. 5)

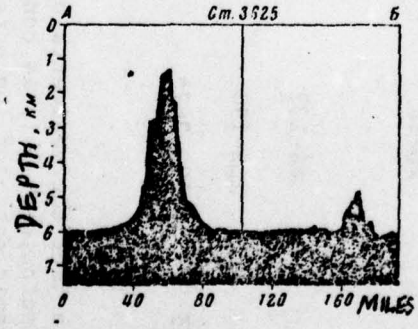

Grain-size Composition and Distribution of Calcium Carbonate, Organic Matter, Amorphous Silica, Iron and Manganese

The core is a homogenous, carbonate-free, brown, deep-sea clayey silt typical of the Northwest Basin. From 76 to 92 percent of the grains are less than 0.01 mm in diameter. The fine silt fraction ranges from 7.4 to 18.2 percent, and coarse silt is less than 1 percent (fig. 35;

Table 14

Stratigraphy of the sediment core at station 3451

Layer	Horizon	Depth in core (cm)	Thickness (cm)	Absolute Age 10^3 yrs	Stratigraphic Correlation North America	Western Europe
1	I	0-26	26	0-9	HOLOCENE	
		26-66	40	9-22	Wisconsin glaciation	Main and Late Wurm glaciation
2						
3	II	66-132	66	22-44	Interglacial stage	Interglacial stage
4		132-190	58	44-65	Iowan glaciation	Early Wurm glaciation
5	III	190-267*	77	65-90	Sangamon interglacial stage	Riss-Wurm interglacial

*It is possible that the sediments of the lower of the part of the horizon were already formed during the penultimate glaciation. This is confirmed by the coarser sediment, the appearance of numerous very thin layers of volcanic ash, and sharp reduction in the number of diatoms.

appendix IX). The calcium carbonate content varies through the core from 0.75 percent to zero, and was least in the 0 to 13, 45 to 80, 140 to 190 cm layers.

The quantity of organic carbon fluctuates within 0.26 to 0.16 percent limits down to 60 cm and the sediments below this depth contain approximately equal quantities of C_{org} (0.15 to 0.10 percent). The SiO_2 amorph content ranges from 1.77 to 0.55 percent through the core. The distribution of SiO_2 in the core makes it possible to identify several layers (0 to 10, 50 to 100, 140 to 190, and 250 to 300 cm) that have relatively large amounts of biogenic silica.

In spite of the great dispersion of values, a tendency to an inverse relationship between the content of SiO_2 amorph and Mn can be seen (fig. 35). Under the pronounced oxidizing conditions that existed during the entire period of deposition represented by the core (Eh is about +500 mv), the manganese and iron have not been significantly redistributed. The vertical variation in their concentration, under slightly varying sedimentation rates, reflects differences in the amount of iron and manganese that settled to the bottom. No relationship has been observed between the content of Fe and SiO_2 amorph and of Fe and Mn.

Figure 35. The relationship between the SiO_2 amorph and Mn content in the core at station 3625.

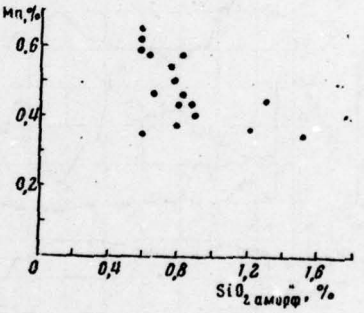

Radioactive Elements and the Sedimentation Rate

The content of uranium in the sediments is 3.8 to 2.8 x 10^{-6} g/g, which is within the usual values for deep-sea deposits, and changes very little with depth. The thorium content, (6-10 x 10^{-6} g/g) is relatively constant through the core. The homogeneous grain-size and material composition of the deep-sea red clays determined the smooth and regular character of ionium and radium concentration with depth. In the upper part of the core, the ionium content is 10 times the equivalent concentration of uranium. The curve of ionium distribution with depth approaches asymptotically the equivalent values of uranium with depth. At 210 to 230 cm, the ionium is already in radioactive equilibrium with uranium, which made it possible to calculate the deposition rate of oozes in the core at station 3625 (6 mm/1,000 yr).

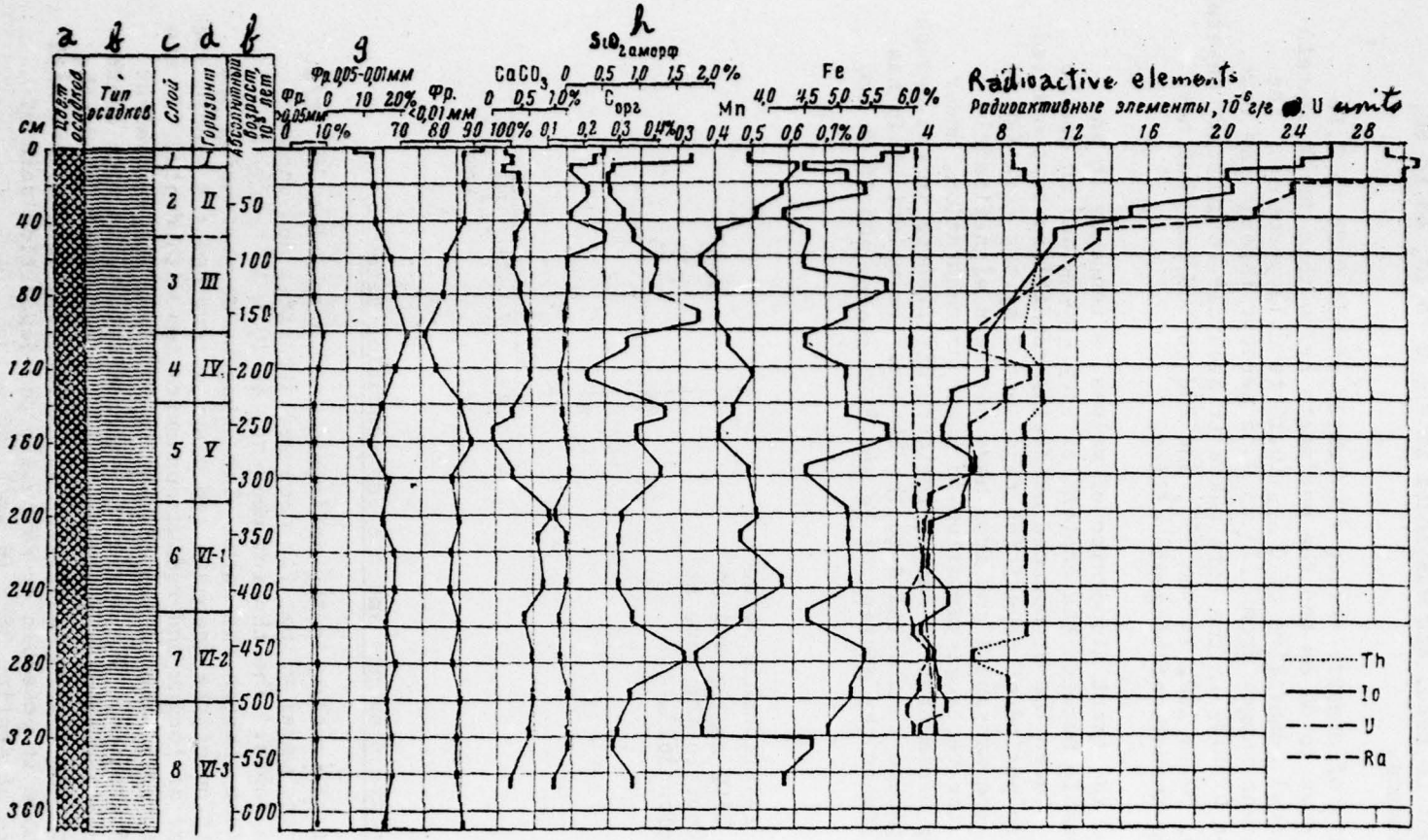

Figure 36. The core sample at station 3625.
For conditional markings see fig. 12

The distribution of radium corresponds to the theory of its behavior in the sediments during uniform deposition with constant arrival of radium at the bottom. As can be seen in fig. 36, the radium concentration increases with depth at first, reaching a maximum at 9 to 12 cm. Farther down, this concentration decreases regularly, being subject at the same time to the exponential law; the half-life period of ionium. It should be emphasized that the distribution curve of radium, as well as ionium, asymptotically approaches the equivalent values of uranium and reaches these values at 200 to 230 cm. Therefore, the curves expressed in units of uranium, ionium, and radium distribution in the sediment column practically merge at 230 cm. This indicates the accuracy of determination of the depth at which radioactive equilibrium occurs in the uranium family, and also of the also of the silt-deposition rate.

Sedimentary Stratigraphy

The vertical variation of SiO_2 amorph through the core made it possible to identify eight separate layers that were formed under warm (layers 1, 3, 5, 7) and cool (layers 2, 4, 6, 8) ocean-surface waters. Table 15 gives the depth, thickness, and absolute age of these layers, and their possible age correlation with glacial and interglacial deposits of North America and Western Europe.

Unfortunately, attempts to determine the composition of marine diatoms and foraminifera were not successful, because they were too few. Most of the samples studied contained no microflora and microfauna. Skeletal remains of the organisms occurred only in layers 3 and 5, which were relatively rich in silica. For example, in layer 3 (60 to 80 cm) numerous poorly preserved radiolaria were found and in layer 5 (140 to 182 cm) large numbers of valves of the tropical marine diatom Ethmodiscus rex were found in addition to the above-mentioned species.

It is impossible not to notice the decrease in $CaCO_3$ content in the silts formed in warm climates (horizons I, III, and V) caused by the greater dilution of $CaCO_3$ during the interglacial epochs. This dilution was caused by a decrease in bottom-water temperature due to a large inflow of glacial meltwater into the subtropical region of the ocean. It should be noted that layer 7 seems to correspond to layer 9 at station 3163 and to layer 7 at station 3625 was also formed under warmer climatic conditions. 87

7. Core Sample at Station 3495

Location - Western end of Marcus-Necker submarine ridge, approximately 220 miles east of the Bonin Islands. Depth - 5,214 m. Length of core - 310 cm. Sampling instrument - uniflow tube corer.

Bottom relief - The core was taken at the foot of a flat-topped seamount at the edge of the uplifted Bonin Island Chain, approximately 25 miles from the summit. The upper slopes of the seamount facing the station have angles of about 10° and the lower slopes are about 5° Southwest of the station, the bottom is a hilly plain with hills 200 m high (fig. 37).

Table 15

Stratigraphy of the sediment core at station 3625

Layer	Horizon	Depth from top of Core (cm)	Thickness	Absolute Age 10^{-3} yrs	Stratigraphic Correlation North America	Western Europe
1	I	0-10	10	0-16	HOLOCENE	
2	II	10-48	38	16-80	Wisconsin and Iowan glaciation	Würm Glaciation
3	III	48-100	52	80-165	Sangamon inter glacial stage	Riss-Würm inter-glacial stage
4	IV	100-138	38	165-230	Illinoian glaciation	Riss glaciation
5	V	138-192	54	230-320	Yarmouth inter-glacial stage	Mindel-Riss inter-glacial stage
6	VI	192-252	60	320-420	Kansan glaciation	Mindel glaciation
7		252-300	48	420-500		
8		300-369*	69	500-580		

*This layer was not completely penetrated.

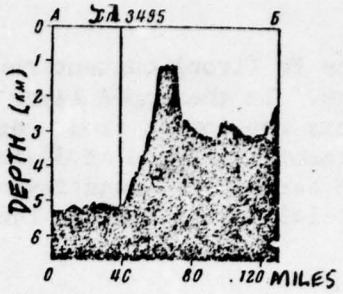

Figure 37. Bottom relief near station 3495 (profile along the line A-B, see fig. 5)

Grain-size Composition

The core is composed of clayey and silty-clayey carbonate-free muds throughout. The silts of the upper part of the core are brown down to approximately 150 cm and light brown below (fig. 38). Coarser silty muds in which 55.5 to 64.4 percent of the grains are less than 0.01 mm are located between 80 and 130 cm, with the coarsest grains at 120 to 130 cm, grading to finer in the upward direction. The texture resembles graded bedding. The silts of the upper layer (0 to 20 cm) of the core contain a considerable admixture of sand particles (7.4 to 11.2 percent). They are characterized by a two-peak histogram with maxima in the pelite (clay-sized grains) and sand fractions. The maximum representing particles larger than 0.1 mm consists of sand and gravel-sized pumice.

Distribution of Calcium Carbonate, Organic Matter, Amorphous Silica, Iron, and Manganese

Throughout the entire length of the core, the sediments contain a very small quantity of $CaCO_3$ (0.50 to 0.09 percent), which varies slightly with depth in the core and increases somewhat in the 0 to 25 cm layer.

Kh. M. Saidova's study of bottom foraminifera has shown that abyssal agglutinated foraminifera predominate throughout the core. The quantity of foraminifera vary considerably through the core and at are numerous at 0 to 20 and 180 to 245 cm. At 110 to 130 cm, bottom calcareous foraminifera, which do not now live at the water depth in which the core was taken, appear in great quantity. The calcareous foraminiferal complex found here is typical of the upper continental slope.

The amount of C_{org} and $CaCO_3$, is highest (0.40 percent) in the surface sediment layer (0 to 15 cm); below that depth it decreases to 0.22 to 0.14 percent. Although the $SiO_{2\ amorph}$ content is small (2 to 6 percent), its vertical distribution make it possible to distinguish three layers in the core enriched with $SiO_{2\ amorph}$ (0 to 5, 20 to 45, 130 to 230 cm). The low $SiO_{2\ amorph}$ content at 5 to 20 cm results from dilution by volcanic material.

The Mn (manganese) content varies vertically from 0.46 to 0.27 percent. The layers with larger amounts of biogenic silica, as a rule, have less manganese. The distribution and the nature of its inverse relationship to $SiO_{2\ amorph}$ do not change when they are recalculated for non-siliceous and carbonate-free material. Figure 39 shows that, despite some dispersion of values in the core, there is an inverse relationship between the content of amorphous silica and manganese that is similar to the core at station 3625.

The Fe (iron) content ranges from 6.02 to 3.01 percent through the core. In the upper layer (0 to 20 cm) and at 130 to 310 cm, the sediments are low in iron. An especially high Fe content (more than 5.5 percent) is found at 34 to 44 and 100 to 110 cm. No relationship is seen between the quantity of Fe and SiO_2 amorph. There is also no clear relationship between the content of SiO_2 amorph, $CaCO_3$, and C org.

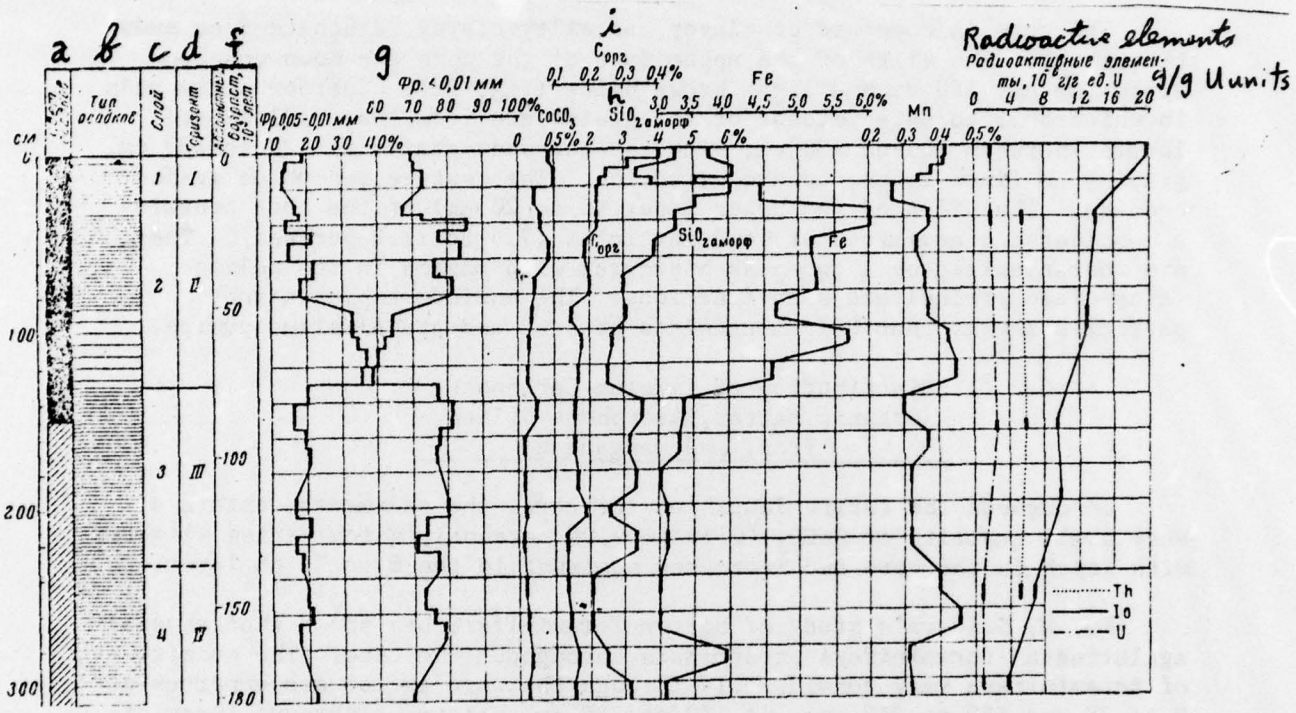

Figure 38. The core at station 3495. For conditional markings see fig. 12.

Composition of Marine Diatoms

A. P. Zhuze's study of the composition of marine diatoms has shown that the following tropical forms predominate throughout the core: Coscinodiscus nodulifer, Nitzschia marina, Hemidiscus cuneiformis, and Ethmodiscus rex. Along with these species, the following south-boreal species appear in considerable numbers and species diversity: Actinocyclus ehrenbergii, Coscinodiscus asteromphalus, Cos. radiatus, etc. In addition to these main groupds of marine plants, individual layers of the sediments contain an admixture of Arctic and Artic boreal diatoms, such as Thalassiosira gravida, Th. excentrica, Thalassiothric longissima, and Actinocyclus ochotensis.

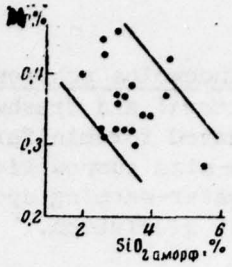

Figure 39. Relationship between SiO_2 amorph and Mn content in the core at station 3495.

Based on changes in the species relationship and quantity of different marine diatom complexes in the core, one can distinguish the following layers: 0 to 20, 20 to 130, 130 to 205, and 205 to 310 cm. The sediments of layers 2 and 4 contain Arctic and north-boreal flora in noticeably large numbers and were formed in surface waters cooler than in the present epoch and in comparison with the time interval of deposition of the muds of layer 3.

Radioactive Elements and the Sedimentation Rate

Data on the distribution of radioelements in the core is presented in figure 38 and appendix X. The thorium content of the surface layer is 5.3 to 5.8 x 10^{-6} g/g U units and the ionium content is 20 x 10^{-6} g/g of U units, which is characteristic of the terrigenous clayey and silty-clayey muds of the Pacific Ocean margins, where the influence of eroded coastal sediments is still quite great. The same thing is indicated by the overall slope of the curve of ionium distribution in the sediments. In the surface sediment layer the concentration of ionium is 10 times the equilibrium concentration of uranium. Farther down the radioactive equilibrium is gradually reestablished, but even at the very bottom of the core the ionium content is still four times the equilibrium concentration of uranium. Although the core at station 3495 did not reach the depth of uranium equilibrium, the mean silt deposition rate was calculated by the ionium method at 17 mm per 1,000 years.

Stratigraphy of the Sediments

Data showing variations in content of amorphous silica, marine diatom species, and abyssal sandy foraminifera divide the core sediments into four layers (horizons). The sediments of horizons II and IV were deposited, judging by the composition of marine diatoms, in a colder climate than the present. These horizons were dated by determinations of the average deposition rate (17 mm per 1,000 years) of the sediments (table 16). This core, shows that the end of the last glacial epoch and the contemporary stage of sedimentation are remarkable for the increase of the biomass of organisms (planktonic organisms with siliceous and calcareous skeletons and benthic species). Certain cold-water marine diatom flora, such as Actinocyclus ochotensis and Thalassiosira excentrica, disappeared during the Holocene. 91

The last glacial period is marked by a considerable decrease in the number of marine diatoms, a drop in the quantity of amorphous silica, and a sharp increase in the flow of detrital iron into the sediments. The quantity of some tropical species of marine diatoms (Coscinodiscus nodulifer, Actinocyclus ellipticus, Chaetoceros coarctatus, Coscinodiscus africanus) decreased noticably. At the same time, north-boreal species

appeared (Actinocyclus ochotensis, Thalassiosira excentrica), the admixture of sublittoral and freshwater forms increased and the number of abyssal agglutinated foraminifera decreased. Data on the variation of the sediment grain-size composition, marine diatoms, and foraminifera do not show a surface-water-warming epoch corresponding to Würm interglacial stage during the last glaciation.

The relatively coarse sediments at 80 to 130 cm, vertical grain-size sorting, and considerable admixture of redeposited marine diatoms are all indicative of sediment redeposition. This material could have been derived from the slopes of the seamount at whose foot the core was taken. In addition, the absolute age of the beginning of the last glaciation and the interglacial epoch (table 16) is somewhat overestimated, because it could not be adjusted for the higher depositional rate of the lower part of the horizon II sediments. Nevertheless, the overall age of the core has been determined correctly, because the average sedimentation rate for the entire layer was used.

The sediments of the last interglacial epoch (horizon III) contain more amorphous silica and very little iron and manganese. The diversity and quantity of tropical marine diatom flora increase and tropical species previously absent in the sediments (Chaetoceros messanensis, Rhizosolenia calcaravis) appear. Horizon III diatoms indicate that the climate was warmer during this period than at present. At 205 to 215 cm from the surface and to the bottom of the core, the diatoms are more of cold-water types. The temporary decrease in SiO_2 amorph in this period, makes it possible to identify horizon IV, whose sediments were deposited during the epoch corresponding to Riss glaciation in Western Eurpoe and Illinoian glaciation in North America. 92

In conclusison, it should be noted that the absolute age of the identified horizons coincides quite well with the age of corresponding horizons in the cores at station 3163, 4068, 3451 and 3625. This indicates that the sedimentation rate increase in horizon II, and the amount of sediment redeposition were small.

8. Core at Station 3520

Location - northern part of the Philippine Trench, approximately 320 miles southeast of Kyushu Island. Depth - 4,223 m. Core length - 377 cm. Sampling instrument - uniflow tube corer.

Bottom relief. The core was taken on the steep southeast slope of a seamount whose summit lies at a depth of about 3,250 m. The bottom is quite sharply dissected near the station (fig. 40).

Table 16

The stratigraphy of sediments of the core of station 3495.

Layer	Horizon	Depth from top of core (cm)	Thickness (cm)	Absolute age (10^3 yr)	Stratigraphic Correlation North America	Western Europe
1	I	0-30	30	0-17	HOLOCENE	
2	II	30-130	100	17-76	Wisconsin and Iowan glacial stage	Würm glaciation
3	III	130-230	100	76-135	Sangamon interglacial period	Riss-Würm interglacial period
4	IV	230-310	80	135-182	Illinois glaciation	Riss glaciation

*This horizon was not completely penetrated.

Figure 40. Bottom relief in the region of station 3520 (profile along line A-B, see fig. 5).

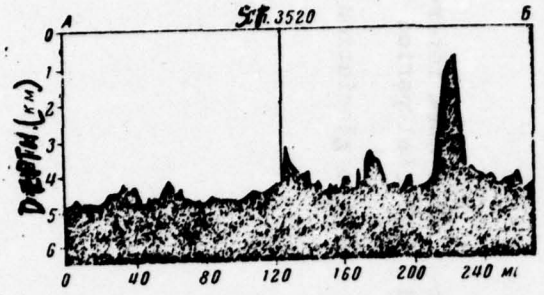

Grain-size and Mineral Composition

The core is composed of clayey and silty-clayey muds with layers of fine silty muds and coarse silts at depths of 12 to 20, 198 to 202 and 307 to 312 cm (fig. 41). The sediments of the upper layer (0 to 17 cm) are brown, changing to grey with a light-brown (20 to 23 cm) and a bluish tint farther down (23 to 307 cm). The silty mud layers are almost black (17 to 20 cm), grey (198 to 202 cm), and light grey (307 to 312 cm). The clayey and silty-muds contain from 55.5 to 82.2 percent of the grain-size fraction less than 0.01 mm. The quantity of fine silt-sized particles varies from 43.5 to 17 percent, and the coarse silt and sand fractions vary form 6.5 to 0.5 percent and from 1.35 to o.16 percent, respectively. The silty sediments[1] at 12 to 20, 198 to 202 and 307 to 312 cm seem to be almost pure, colorless volcanic glass with a very small admixture of ash particles and plagioclase. Ferruginous, limonitized ash particles occur infrequently. At 17 to 20 cm, the silt fraction contains a large admixture of manganese ore.

S. N. Gorbunova analyzed the clayey minerals (fraction below 0.001 mm) in two samples of clayey silts at 50 to 70 and 275 to 300 cm. Intermixed, layered hydromicaceous-montmorillonite and trioctahedral hydromica predominate in the samples and there is an admixture of chlorite and kaolinite. At 50 to 70 cm, the sediments contain a greater quantity of amorphous material. X-ray structural analysis (diffraction) shows that the clayey minerals do not change noticeably with depth.

The Distribution of Amorphous Silica, Calcium Carbonate, Organic Matter, Iron, and Manganese

The content of $SiO_{2\ amorph}$ in the sediments varies from 4.25 to 1.94 percent increasing in the surface layer (0 to 6 cm), and at depths of 55 to 95, 160 to 230, 280 to 310, and deeper than 360 cm. The $CaCO_3$ content varies from 12.9 to 1.4 percent in the vertical direction. The highest content of $CaCO_3$ is at 17 to 50 cm, where the sediments are classified as slightly calcareous foraminiferal oozes.

[1]Fraction with particles 0.1 to 0.05 mm in size was analyzed.

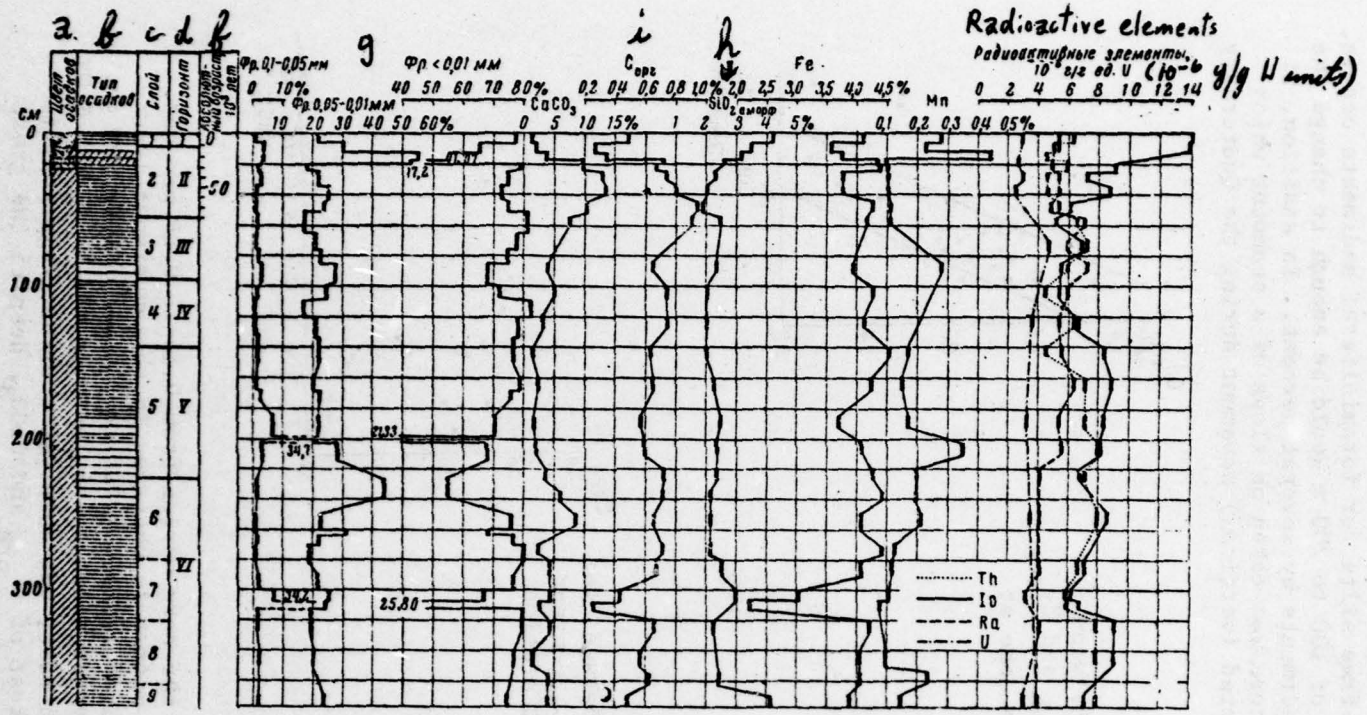

Figure 41. Core at station 3520. For conditional markings see fig. 12.

It is difficult to use the distribution of $CaCO_3$ for stratigraphic purposes, because the core was taken in the depth interval in which substitution of carbonate-free silts for foraminiferal sediments occurs. The change in ocean depth of 100 to 200 m would be enough to change the content of $CaCO_3$ in the sediments by several percent. In addition, it should be noted that the core was taken on slope of a seamount which could have undergone repeated (vertical) movement during the Quaternary period.

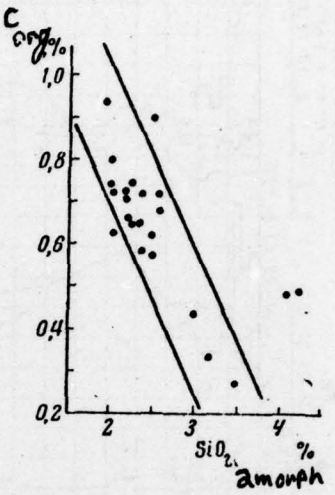

Figure 42. Relationship between the SiO_2 amorph and C_{org} content in the core at station 3520.

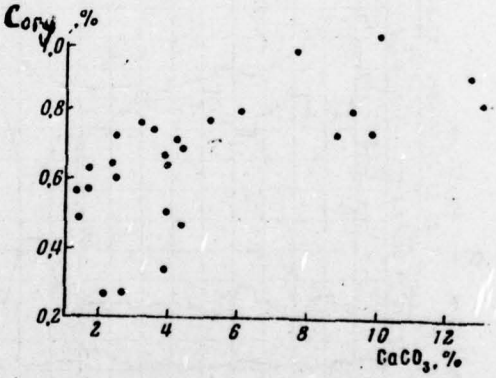

Figure 43. Relationship between the $CaCO_3$ and C_{org} content in the core at station 3520.

The C_{org} content in the core varies from 0.54 to 0.26 percent. Larger amounts of organic matter is observed in the uppermost layer (0 to 6 cm), and at depths of 17 to 60, 220 to 290 and 320 to 360 cm. There is quite a clear inverse relationship between the C_{org} and SiO_2 content (fig. 42). In contrast, one observes a direct relationship (fig. 43) between the content of C_{org} and $CaCO_3$, despite the great scattering of individual values.

The sediments contain from 0.44 to 0.09 percent Mn and from 4.57 to 2.24 percent Fe. The manganese content is especially high in the volcanic ash layer at the boundary between the oxidation and reduction zones. In the present case, the enrichment of sediments with manganese is related mainly to the migration of its mobile lowest valence compounds from the reduction zone. The high concentration of Mn at the boundary between oxidized and reduced sediments frequently occurs in cores from the western Pacific Ocean. At the same time, one must note the increased quantity of Mn in silts having a large percentage of volcanic material. 95

The Composition of Marine Diatoms

The core here differs little in marine diatom composition from the sediments at station 3495. The silts in this core are peculiar in the complete absence of Arctic-boreal flora that occur in small numbers in individual layers at station 3495. The relationship of the population density and quantity of species of the tropical, south- and north-boreal marine diatom complexes also varies here. This makes it possible to distinguish layers formed in warm (0 to 7, 55 to 95, 140 to 226, 280 to 377 cm) or cold (7 to 55, 95 to 140, 226 to 280 cm) surface waters. A relationship between the content of the marine diatoms and amorphous silica is expressed in the increase of warm-water flora during periods of increased deposition of SiO_2 amorph.

Radioactive Elements and the Sedimentation Rate

The thorium, ionium, radium, and uranium composition in core sediments has been determined (fig. 41; appendix XI). The concentration of radioactive isotopes and how they vary with depth are typical of terrigenous sediments. In fig. 41 and appendix XI, it can be seen, first, that the silts contain relatively little thorium (4.6 to 8.0) x 10^{-6} g/g, ionium (14.2 to 7.2) x 10^{-6} g/g U units, and radium (8.4 to 3.2) x 10^{-6} g/g U units, and secondly, that the concentration of ionium in the surface layer is only 5 times that of uranium. Each of these isotopes produces several enrichment and depletion sectors on the graph among the overall lack of a definite pattern of distribution with depth that would be expected based on the radioactive decay laws. Only in the upper part of the core, there is a consistent variation of ionium concentration that made it possible to calculate the silt-deposition rate at depths from 0 to 60-100 cm. This rate was approximately 7mm per 1,000 years. If one assumes that most of the thorium enters the bottom as part of the terrigenous material, then the character of the vertical thorium distribution points to repeated changes in the sedimentation rate of the terrigenous component of the sediments.

Assuming that most of the radium and ionium originates from sea water, one can conclude that the distribution of these elements in the core indicates the variation of the physico-chemical conditions in the water column and the variation of the relationship between the quanities of radioelements descending to the bottom, on one hand, and the terrigenous and biogenic components that dilute the hydrogenic elements, on the other. In this core, there is an almost direct relationship between the thorium and the ionium content (fig. 44) below 60 cm (considerable variations

in the content of radioelements, which variations cannot be explained as the natural decay of these radioelements under conditions of their uniform inflow to the bottom, occur approximately from this depth onward. This indicates that during the change in the physico-chemical conditions of deposition of the hydrogenic component, the sedimentation rate of the terrigenous part of the sediemnts also changes. 96

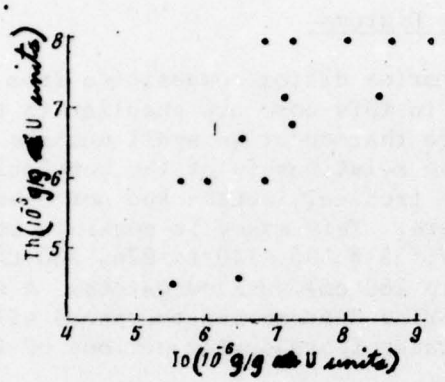

Figure 44. Relationship between the Io and Th content in the core at station 3520.

Sedimentary Stratigraphy

Variations in composition of amorphous silica and the species content of marine diatoms in the core make it possible to divide the sediment column into nine layers (table 17). Only the upper two layers can be dated. Based on the species content of the marine diatoms, the sediments of layers 1, 3, and 5 were deposited when ocean-surface waters were warmer than when layers 2, 4, and 6 were deposited. Data on the absolute age of layers 1 and 2 indicate that their ages correlate with horizons I and II respectively, of the previously described cores at station 3163, 3451 and 4068. Their correlatives on the continents are, respectively, contemporary deposits and those of the last glaciation. Correlation of the older layers with the horizons of other cores is only conditional (table 17). We mentioned above the reasons that force one to use data on the distribution of $CaCO_3$ in the core with great caution for stratigraphic purposes. It should be noted that the increased content of $CaCO_3$ and C_{org} in the sediments corresponds to the last glacial epoch (horizon II). The same thing is seen, but less clearly, in the sediments of horizons IV and VI, as well as in Horizons II, IV, and VI of the core at station 3626.

9. The Core at Station 3532

Location - northern part of the Philippine Basin. Depth - 4,589 m. Core length - 358 cm. Sampling instrument - uniflow tube corer.

Bottom relief. Near the station, within a radius of about 25 to 30 miles, the bottom is a hilly plain. A small sea mountain 350 m above the bottom near the station. The slopes facing the station range up to 3° to 5° (fig. 45).

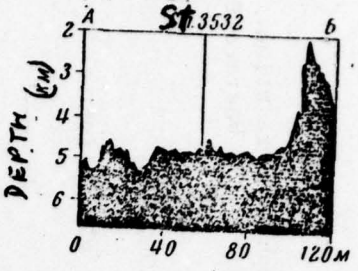

Figure 45. Bottom relief in the region of station 3532 (profile along the line A-B, see fig. 5)

Grain-size Composition and Distribution of Amorphous Silica, Calcium Carbonate, Organic Matter, and Manganese

The core is composed mainly of clayey carbonate-free silts; dark brown (0 to 23 cm), greyish brown (23 to 202 cm), and grey (202 to 358 cm) in color. The color variations show the gradual transition from an oxidizing environment in the upper layers to a reducing environment in the lower parts of the core. At depths of 4 to 10, 59 to 73, 85 to 95, 185 to 202, and 290 to 321 cm, the sediments are somewhat coarser silty-clayey silts. The coarsest sediments, with larger proportions of fine and coarse silt and sand, are located at depths of 59 to 73 and 185 to 202 cm from the top of the core (fig. 46).

The sediments contain from 2.97 to 0.88 percent of $SiO_{2\ amorph}$ and its distribution defines several layers in the core that are relatively high (0 to 10, 23 to 44, 73 to 100, 140 to 220, 330 to 358 cm) and low in $SiO_{2\ amorph}$. The $CaCO_3$ content varies through the core from 1.73 to 0.20 percent. The highest content of calcium carbonate material occurs at 229 to 330 cm (1.18 to 1.73 percent). There is an inverse relationship between the content of $CaCO_3$ and $SiO_{2\ amorph}$ (fig. 47). The sediment layers that are relatively rich in $SiO_{2\ amorph}$ contain a smaller quantity of $CaCO_3$ as was previously noted in several other cores from the subtropical Pacific Ocean (stations 3625, 3520). The C_{org} content ranges from 0.47 to 0.16 percent. The silts of the upper layer of the core and those at 23 to 60 and 210 to 320 cm are distinguished by their greater quantity of C_{org}. Figure 48 shows a direct relationship between the contents of C_{org} and $SiO_{2\ amorph}$. There is no relationship between C_{org} and $CaCO_3$.

The Mn content varies vertically from 1.59 to 0.07 percent. The Mn distribution indicates that redistribution of this element occurred during diagenesis. The higher concentrations of Mn (1.51; 1.59 percent) occur in the dark brown clayey silts in the lower part of the oxidized zone at the bound-ry with the reduction zone. Individual layers in the transitional zone between the reduced and the oxidized sediments also contain an increased percentage of manganese. These layers are distinguished visually by their dark brown color. The intensive migration of the easily mobile compounds of manganous oxide has resulted in a decreased amount of Mn below 120 cm to 0.11 to 0.08 percent.

Table 17

Sedimentary Stratigraphy of the core at station 3520.

Layer	Horizon	Depth from top of core (cm)	Thickness (cm)	Absolute age (10^{-3} yrs)	Stratigraphic Correlation North America	Western Europe
1	I	0-7	7	0-10	HOLOCENE	
2	II	7-55	48	10-80	Last glaciation	
3	III	55-95	40	not dated	---	---
4	IV	95-140	45	not dated	---	---
5	V	140-226	86	not dated	---	---
6		226-280	54	not dated	---	---
7	VI	280-320	40	not dated	---	---
8		320-362	42	not dated	---	---
9		362-377	15*	not dated	---	---

*Layer has not been penetrated completely.

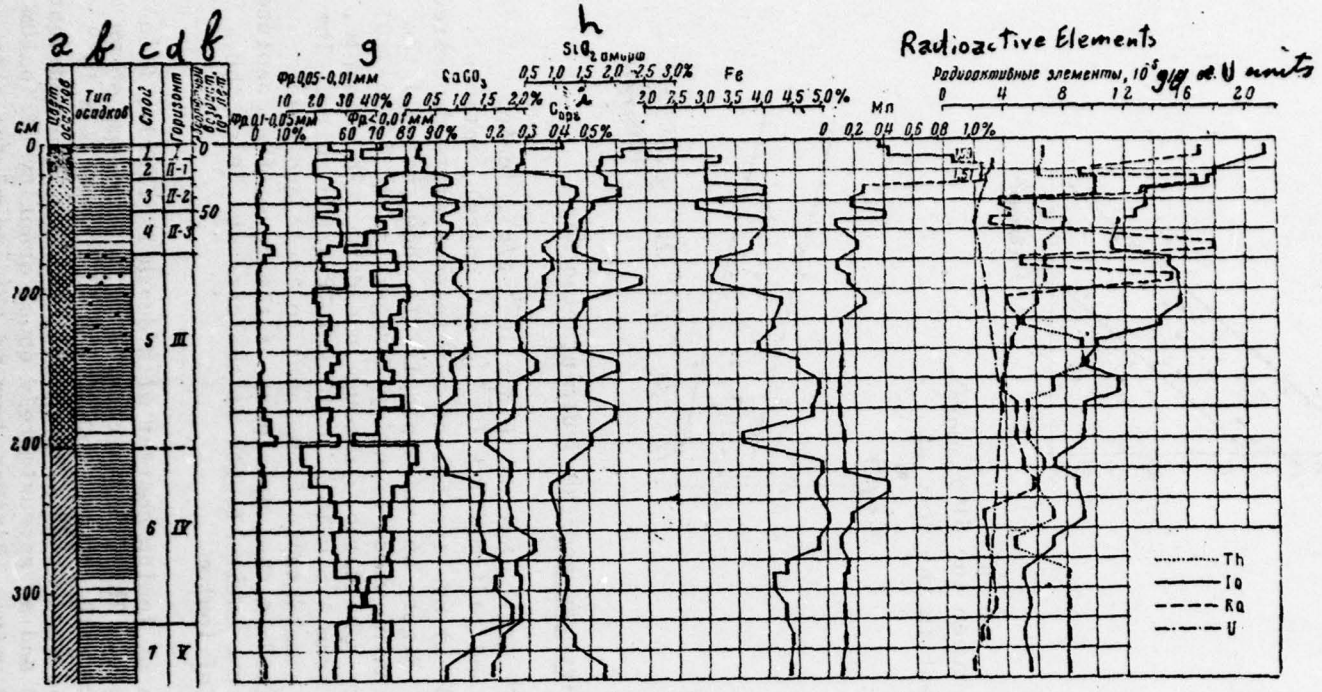

Figure 46. Core at station 3532. For conditional markings see fig. 12.

Figure 47. Relationship between the SiO_2 amorph and $CaCO_3$ content in the core at station 3532.

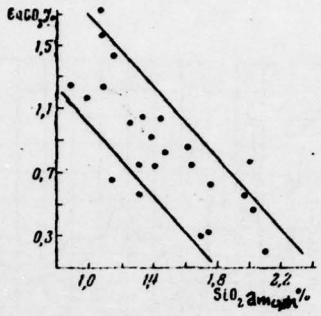

Figure 48. Relationship between the SiO_2 amorph and C_{org} content in the core at station 3532.

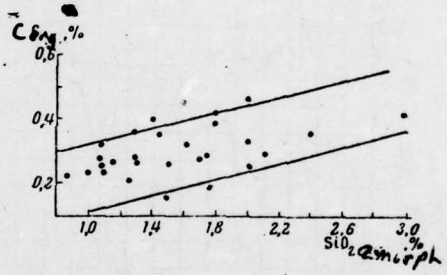

Radioactive Elements and the Sedimentation Rate

The uranium (3.2×10^{-6} g/g), thprium ($6.6_6 \times 10^{-6}$ g/g), ionium (21.3×10^{-6} g/g U units), and radium (17×10^{-6} g/g U units) contents in the upper layer (4 to 10 cm) are typical of terrigenous silts deposited at a relatively high rate. Figure 46 and appendix XII show that all the radioelements (excluding uranium whose quantity changes little [$(3.6\text{-}2.0) \times 10^{-6}$ g/g] with depth) vary considerably through the core. For example, the thorium content varies from 4.5×10^{-6} to 10×10^{-6} g/g U units. The radium content also varies considerable from layer to layer and these variations are sharply defined in the upper part of the core; the absolute quantities of radium along the entire length of the core are below the equilibrium concentrations of ionium.

The graph of variation of ionium content with depth is divided into three clearly defined sectors. The first sector, 0 to 73 (79) cm, shows a regular decrease in ionium with depth (from 21.3×10^{-6} to 11.1×10^{-6} g/g U units). In the second sector, 73 (79) to 125 (135) cm, the sediments contain a relatively higher and an approximately equal quantity of ionium ($(14.2 \text{ to } 15.6) \times 10^{-6}$ g/g U units. Farther down to the end of the core, the ionium content varies but decreases overall. Nevertheless, the equilibrium horizon is not reached, and even at the very bottom of the core

the content of ionium is twice the equilibrium content of uranium.

If the distribution curves for iron and thorium are compared with those for manganese and radium, a definite relationship between these elements can be seen. Many of the sediment layers enriched with iron, for example at 30 to 35, 53 to 57, 140 to 180, and 250 to 255 cm, also contain larger amount of thorium. In the upper part of the core, the Fe and Th curves almost agree. Nevertheless, no relationship exists between the absolute values of the content of these elements in the sediments, which does not negate the possibility that such a relationship exists between Fe and Th. At the present time, unfortunately we lack data on the distribution of these elements in the pelite (clay) fractions of the sediments. In addition, there is no assurance that both elements behave identically under conditions of silt diagenesis in the core. 100

The large amounts of Mn abd Ra that are located at the boundary of the zones of oxidation and reduction probably results from their migration. No relationship has been detected between the distribution of manganese and ionium. This indicates that the above-described type of ionium distribution from the top of the core down to approximately 80 cm is the result of natural radioactive decay of ionium in a constant descent to the bottom. This makes it possible to calculate the silt-deposition rate in the 0 to 80 cm section of the core at approximately 9 mm per 1,000 years. The sediments between 80 to 140 cm possibly were deposited at a higher rate. Nevertheless, it seems impossible to evaluate it, and it is also impossible to calculate the overall age of the sediments exposed by this core.

Sedimentary Stratigraphy

Table 18 presents data on the depth, thickness, and absolute age of the layers defined by the distribution of biogenic silica in the core. By analogy with the above-described cores, whose sediment layers are relatively high in SiO_2 amorph and contain warm-water marine diatom flora, it was assumed[1] that in the given core, the sediments having a high content of SiO_2 amorph (layers 1, 3, 5, and 7) were deposited during climatic periods warmer than those in which the layers directly above and below (layers 2, 4, and 6) were deposited.

During calculation of the silt deposition rate of horizons I and II (layers 1-4), an average sedimentation rate of 9 mm per 1,000 years was adopted. Nevertheless, the character of the ionium distribution made it possible to calculate separately the sediment deposition rate between 0 to 25 and 25 to 78 cm (5 and 20 mm per 1,000 years, respectively). At the same time, it was assumed that the contemporary epoch began 20,000 years ago and the last glaciation began 80,000 years ago. It was impossible to draw the Holocene boundary with precision, because the interval between the upper-layer sediment samples was too large. It seems that this boundary lies somewhere inside the 4 to 10-cm interval, which corresponds to an age of about 10,000 to 12,000 years. 101

During the last glacial epoch, approximately 25 to 50 thousand years ago,

[1]Unfortunately, the composition of marine diatoms in the core was not studied.

Table 18

The stratigraphy of the sediments of the core at station 3532.

Layer	Horizon	Depth from top of core (cm)	Thickness (cm)	Absolute age (10^3 yrs)	Stratigraphic Correlation North America	Western Europe
1	I	0-10	10	0-11	HOLOCENE	
2		10-23	13	11-125	Wisconsin glaciation	Main & Late Würm glaciation
3	II	23-44	21	25-50	Interglacial period	Interglacial peri
4		44-73	29	50-80	Iowan glaciation	Early Würm glaciation
5	III	73-203	130	undated	---	---
6	IV	203-320	117	undated	---	---
7	V	320-358	38*	undated	---	---

*Layer was not completely penetrated.

the ocean-surface waters became warmer, which was reflected in the sediments in the form of a higher content of amorphous silica and organic matter (layer 3). The beginning of the last and the penultimate glaciations, as well as the end of horizon IV (beginning of horizon III) were distinguished by some coarsening of the granulometric composition of the sediments.

10. The Core at Station 3530

Location - northern part of the Philippine Basin, approximately 60 miles east of the Nansei Trough (Ryukyu Trench). Depth - 5,024 m. Length of core - 356 cm. Collection instrument - uniflow tube corer.

Sediment Characteristics and the Distribution of Radioactive Elements

The core is composed of interlayered light brown silty-clayey and clayey terrigenous muds. The grain-size composition of the sediments varies little vertically: the content of the fraction smaller than 0.01 mm varies from 76 to 63.5 percent in the core; the percentage of the fine and coase silt fractions range from 30.6 to 21 8 percent and from 9.6 to 1 percent respectively.

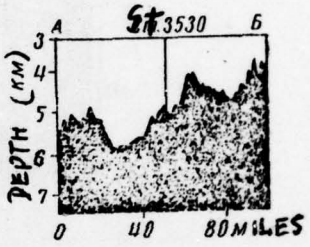

Figure 49. Bottom relief in the region of station 3530 (profile along the line A-B see fig. 5).

The percentage of particles larger than 0.1 mm is insignificant: from 5.1 to 0.6 percent (fig. 50, appendix XIII).

The content of uranium, thorium, and ionium was determined in several samples. The thorium content does not change with depth and is 3×10^{-6} g/g. The concentration of uranium ranges from 2.6 to 1.4×10^{-6} g/g and ionium decreases with depth from 20×10^{-6} down to 6.7×10^{-6} g/g of U units. However, even in the lower parts of the core, ionium does not reach the equilibrium of values of uranium. The low content of thorium and uranium in the core indicates a considerable flow into the bottom of terrigenous materials containing little thorium and uranium and indicates a generally high sediment deposition rate. Based on the ionium distribution, one can estimate the average depositional rate of silts in the core as 13 mm per 1,000 years. The entire core column encompasses a time interval of 270,000 years. A slight coarsening of the sediment at 110 to 210 cm belongs to the period 90 to 160 thousand years ago and is related to a higher proportion of sand and coarse silt. Chronologically, this layer belongs to the period of the last interglacial warming of waters in the western Pacific Ocean. We have not identified stratigraphic horizons in the core because the material and mineralogic composition of the sediments and the microflora and microfaune have not been studied.

Figure 50. The core at station 3530. For conditional markings see fig. 12.

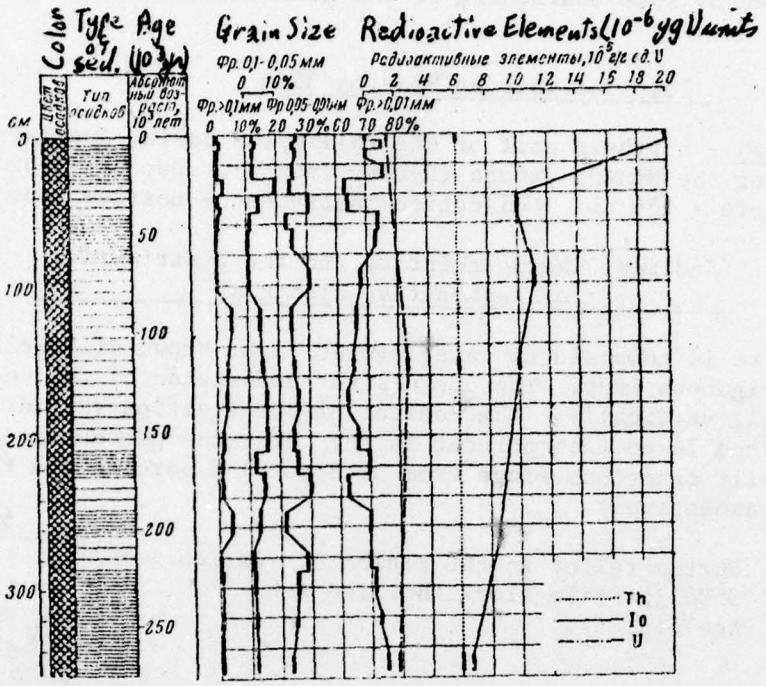

11. The Core at Station 3481

Location - Northwest Basin of the Pacific Ocean, east of the Izu-Bonin abyssal trench. Depth - 6,086 m. Core length - 285 cm. Sampling instrument - uniflow type corer.

Bottom relief. Near the station, the bottom is a rolling plain, sloping down toward the northeast (fig. 51).

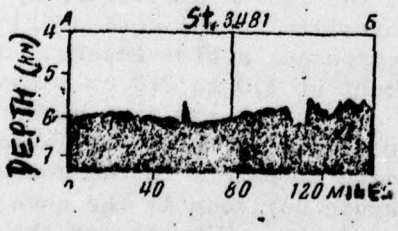

Figure 51. Bottom relief in the region of station 3481 (profile along the line A-B, see fig. 5).

Character of the Sediments and Distribution of Radioactive Elements

The core is composed of silty-clayey muds of brown (0 to 10 cm) and light brown (10 to 285 cm) color with layers, at various depths, of clayey (40 to 51, 148 to 160 cm) and fine silty (9 to 13, 78 to 88, 130 to 135, 184 to 192 cm) muds (fig. 52, appendix XIV). The coarse and fine silt fractions of the core contain a large admixture of ash. The layers of fine silty muds appear as almost pure volcanic ash composed mainly of volcanic glass. Ash particles, plagioclase, hornblende, and mineral grains are present in lesser amounts. At depths of 9 to 13, 38 to 40, and 130 to 135 cm the sediments contain gravel-sized fragments of pumice up to 6 or 7 mm in diameter. The pumice entered the sediments at the end of the glacial and the beginning of the interglacial (postglacial) epochs.

The distribution of uranium, thorium, and ionium were studied. The surface layer of sediments differs little from silts at stations 3530, 3532, and 3520 in content of these radio elements. The content of uranium, thorium, and ionium at station 3481 is 4 x 10^{-6} g/g, 6 x 10^{-6} g/g of U units, respectively. The ionium concentration varies consistently with depth and is least in the fine silt layer at 78 to 88 cm, which seems to reflect the diluting influence of relatively coarse and rapidly settling volcanic and fragmental materials. The regular pattern of variation of the ionium concentration indicates that the mean silt deposition rate in the core is 10 mm per 1,000 years. The foregoing data do not permit subdividing the sediment column into stratigraphic horizons. 103

Figure 52. The core at station 3481. For conditional markings see fig. 12.

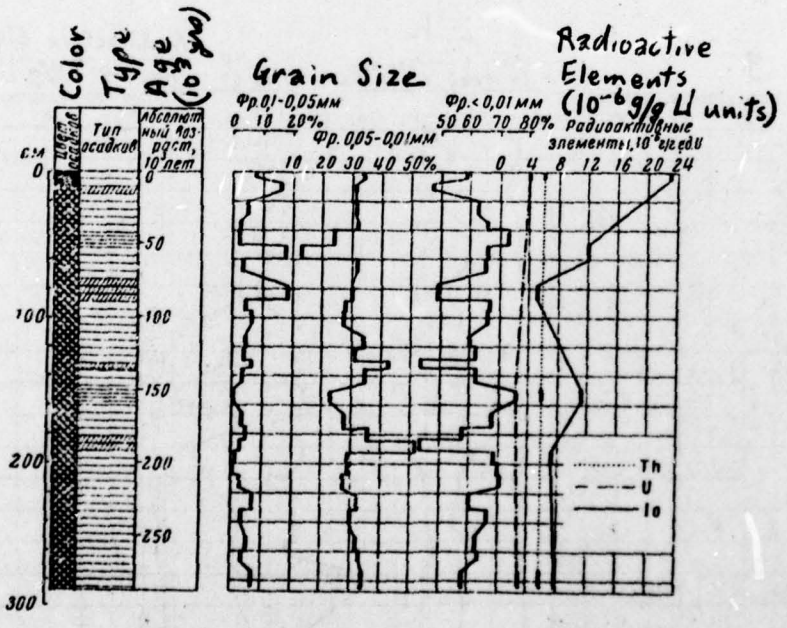

12. The Core at Station 3873

Location - northern part of the Central Basin of the Pacific Ocean, approximately 220 miles northeast of Bikar Atoll (Marshall Islands). Depth - 5,464 m. Core length - 407 cm. Sampling device - piston tube corer.

Bottom relief. The bottom in the region of the station is a plain with isolated gentle swells that rise several tens to 200 m above the bottom and have slope angles of 1° to 2° (fig. 53).

Figure 53. Bottom relief in the region of station 3873 (profile along line A-B, fig. 5).

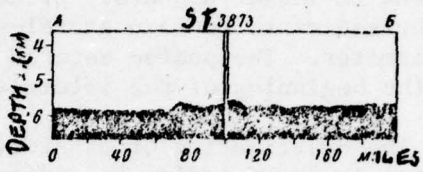

Grain-size Composition and Distribution of Amorphous Silica, Calcium Carbonate, Organic Matter, Iron, and Manganese

The core is composed of homogeneous, finely dispersed, dark-colored, carbonate-free clayey silts along the entire length. Particles from less than 0.001 to 0.005 mm in size comprise on the average about 80 percent of the entire sediment (fig. 54, appendix XV). 105

Figure 54. Core at station 3873. For conditional marking see fig. 12. (a-d, f-j the same as in fig. 12).

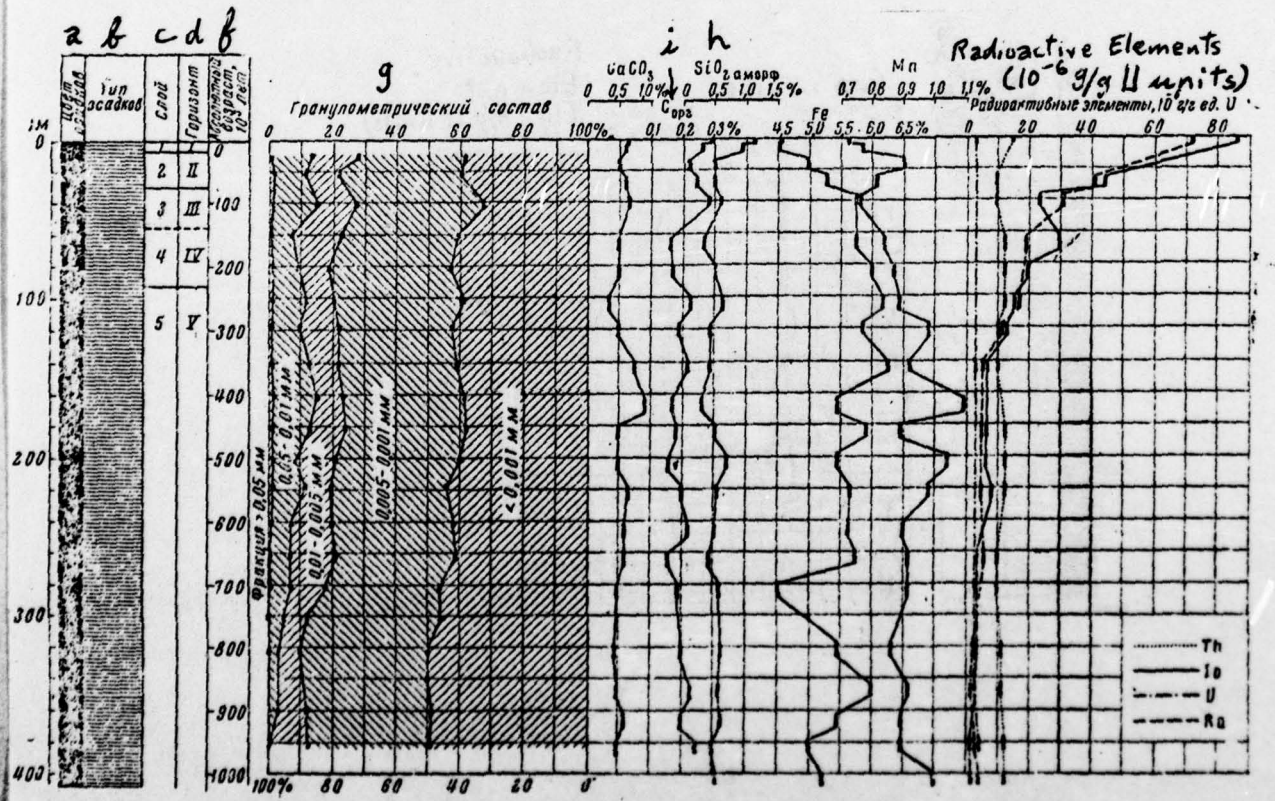

The silts that comprise the core contain, on the average, 10.7 percent of the 0.005 to 0.01 mm fraction. An insignificant content of coarse silt (from traces up to 1.5 percent) and an almost complete absence of sand-sized particles characterize the sediments. At about 220 cm, the proportion of particles less than 0.001 mm increases and the content of coarse silt and sand decreases to zero in the lower parts of the core. Based on visual inspection of the sediments in wet and dry states and their grain-size analysis (single-peak histograms), the silt undoubtedly was deposited during a normal "particle-by-particle" process of sedimentation.

The content of $CaCO_3$ in the core varies from 0.86 to 0.36 percent. The silts have a somewhat higher percentage of $CaCO_3$ than average (0.56 percent), at a depth of 140 to 172 cm (0.75 to 0.89 percent). The sediments contain little organic matter (0.28 to 0.16 percent C_{org}). The highest content of C_{org} was in the surface layer (0 to 6 cm) and at about 30 to 50 cm. No decrease in organic matter with depth has been found. We believe this is related to the great stability of organic matter that is already attained in the upper sediment layer. The content of $SiO_{2\ amorph}$ varies from 1.17 to 0.36 percent through the core. The silts of the upper layer have a somewhat higher percentage of $SiO_{2\ amorph}$ (0.6 cm; 1.17 to 0.95 percent). In the upper part of the core, the distribution curves of amorphous silica, organic matter, and calcium carbonate parallel each other, which probably indicates a direct relationship in the occurrence of these biogenic elements in the bottom. The sediments contain from 4.53 to 6.26 percent Fe and from 0.73 to 1.09 percent Mn.

Radioactive Elements and the Sedimentation Rate

The sediments of the surface layer have a high content of the radioactive elements: Thorium (15×10^{-6} g/g), ionium (86×10^{-6} g/g of U units), and radium (73×10^{-6} g/g of U units). Only the uranium concentration lies within the limits of the usual values for deep-sea sediments (see fig. 54, appendix XV). The content of uranium and thorium barely differ as one probes deeper in the sediment column. For example, the maximum deviation of the thorium content from the mean value (11.4×10^{-6} g/g) does not exceed 20 percent. The content of ionium in the upper layer of the sediments is 24 times the equilibrium concentration of uranium. As shown in fig. 54, the quantity of ionium decreases quite rapidly with depth. At about 50 to 60 cm, the exponential curve of ionium distribution is disturbed. Nevertheless, starting from approximately 80 cm the ionium curve quickly flattens and gradually approaches the value corresponding to the equilibrium value of uranium. The distribution of radium in the sediments is similar to that of ionium. The difference is that at 50 to 80 cm the radium content does not increase. Overall, the distribution of radium in the core is similar to the theoretically computed radium curve.

Based on the observed ionium distribution, the mean deposition rate of the deep-sea red clay in the core is 4 mm per 1,000 years. Assuming that the sediment deposition rate did not change significantly in the past, the maximum on the ionium curve occurred approximately 150 to 200 thousand years ago. The sediments of the lower part of the column could be 1 million years old.

The upper part of this core taken in the tropical region shows, generally, the same changes of material content that were seen much more clearly in cores from the temperate regions of the ocean (station 3163, 3378, 3325, 3342, 4068, 3625, etc). In the upper 80 cm of the core at station 3873 the distribution curves of SiO_2 amorph, C_{org}, and $CaCO_3$ almost parallel each other (see fig. 54).

Five layers can be defined in the upper 100 to 120 cm of the sediments based on the variation of biogenic substabces (mainly amorphous silica, as the most stable biogenic component) in the core. These layers, judging by their age, correspond to like-named horizons of other cores (table 19). The sediments of layers 1, 3, and 5, containing relatively high percentages of amorphous silica, organic carbon, and calcium carbonate (the latter in layers 1 and 3), were formed during the post-glacial (horizon I) and interglacial (horizons III and V) periods. Unforunately, the composition of marine diatoms, which could provide additional information on the stratigraphy of the sediments, were not analyzed.[1] One should note the close coincidence of the absolute age of horizons I, II, III, and IV of the core at station 3873 with the absolute age of the same horizons of the cores at stations 3625, 3495, 3520, and 4068.

13. Core at Station 3746

Location - eastern part of the Philippine Basin. Depth - 5,917 m. Core length - 307 cm. Sampling instrument - piston tube corer.

Bottom relief. The bottom near the station is a finely dissected hilly plain with 200-m hills whose slopes reach 3° (fig. 55).

Figure 55. Bottom relief in the region of station 3746 (profile along the line A-B, see fig. 5).

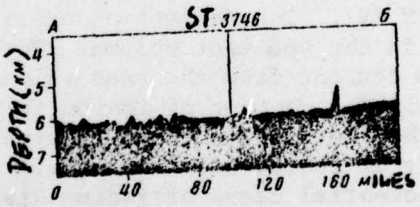

Grain-size Composition
Distribution of Calcium Carbonate, Organic Matter, Iron Manganese, and Amorphous Silica

The core is composed, from top to bottom, of homogeneous carbonate-free, brown clayey silts. Their outward appearance and content of C_{org}, $CaCO_3$, SiO_2 amorph, Fe, and Mn classify these sediments as a typical deep-sea red clay. Particles smaller than 0.01 mm, whose proportion ranges from 79.3 to 85.4 percent, predominate here. The grain-size composition of the silts varies little vertically. The fine silt fraction ranges from 13.8 to 20.0 percent; the coarse silt from 0.2 to 3.2 percent, and there is almost no sand (0.2 to 0.5 percent; fig. 56, appendix XVI).

Table 19

Stratigraphy of sediments of the core at station 3873.

Layer	Horizon	Depth from top of core (cm)	Thickness (cm)	Absolute age (10^3 years)	Stratigraphic Correlation North America	Western Europe
1	I	0-6	6	0-15	HOLOCENE	
2	II	6-30	24	15-75	Last Glaciation	
3	III	30-56	26	75-140	Sangamon Interglacial stage	Riss-Würm Interglacial stage
4	IV	56-92	36	140-230	Illinois glaciation	Riss glaciation
5	V	92-117(?)	--	230-290	Yarmouth Interglacial stage	Mindel-Riss Interglacial stage

The core contains negligible amounts of $CaCO_3$ (0.27 to 0.11 percent), and very little SiO_2 amorph (0.61 to 0.28 percent), and C_{org} (0.31 to 0.07 percent). In the upper 17 to 20 cm the quantity of organic material decreases by almost 2.5 times. Between 20 and 180 cm, the content of C_{org} decreases by half, from 0.13 to 0.07 percent, and even deeper it increases, again reaching 0.13 percent in the lower parts of the column. Such a low content of organic matter and its sharp decrease through the upper centimeters is typical of deep-sea red clays.

Clay Mineral Composition

According to Z. N. Gorbunova, hydromica predominates among the clayey minerals and chlorite, montmorillonite, and kaolinite and present. The content of montmorillonite and kaolinite increase with depth, chlorite and hydromica decrease, and the amount of manganese and iron increases. It is possible that the sediments of the lower part of the core are about 1 million years old and were deposited at the end of the Tertiary period in a warm climate.

Radioactive Elements and the Sedimentation Rate

The uranium, thorium, and ionium contents were determined (fig. 56, appendix XVI). The uranium content varies very little through the core (from 3.0×10^{-6} to 4.3×10^{-6} g/g), thorium content is quite high (6 to 11) $\times 10^{-6}$ g/g, and the ionium distribution is close to the theoretically calculated value and shows no significant deviatopns from the asymptotic law. The slope of the radium distribution curve agrees with that of the ionium curve. Nevertheless, the absolute radium content is considerably higher in the upper part of the core and the lower part contains a lower number of equilibrium values. Despite the quite regular ionium distribution, it is difficult to find the equilibrium horizon. The ionium content approaches the equilibrium value with uranium at 70 to 100 cm; below the concentration of ionium increases and again approaches equilibrium values at about 230 and 280 cm. This complicates calculations by the equilibrium-horizon method. Based on the mean sedimentation rate calculated on ionium (3 to 3.3 mm per 1,000 years), one can assume that the entire core sample covers 1 million years. 109

Sedimentary Stratigraphy

The vertical distribution of SiO_2 amorph, C_{org}, $CaCO_3$, Fe, and Mn do not show stratigraphic horizons in the core. Sediments at 5 to 10, 29 to 33, and 83 to 87 cm have a relatively higher SiO_2 amorph content and, judging by their absolute age, were deposited during periods of warmer climate (fig. 56).

14. Core at station 3797

Location - Central Basin of the Pacific Ocean, approximately 280 miles north of Canton (Phoenix) Island. Depth - 5,328 m. Core length - 316 m. Sampler - uniflow tube corer.

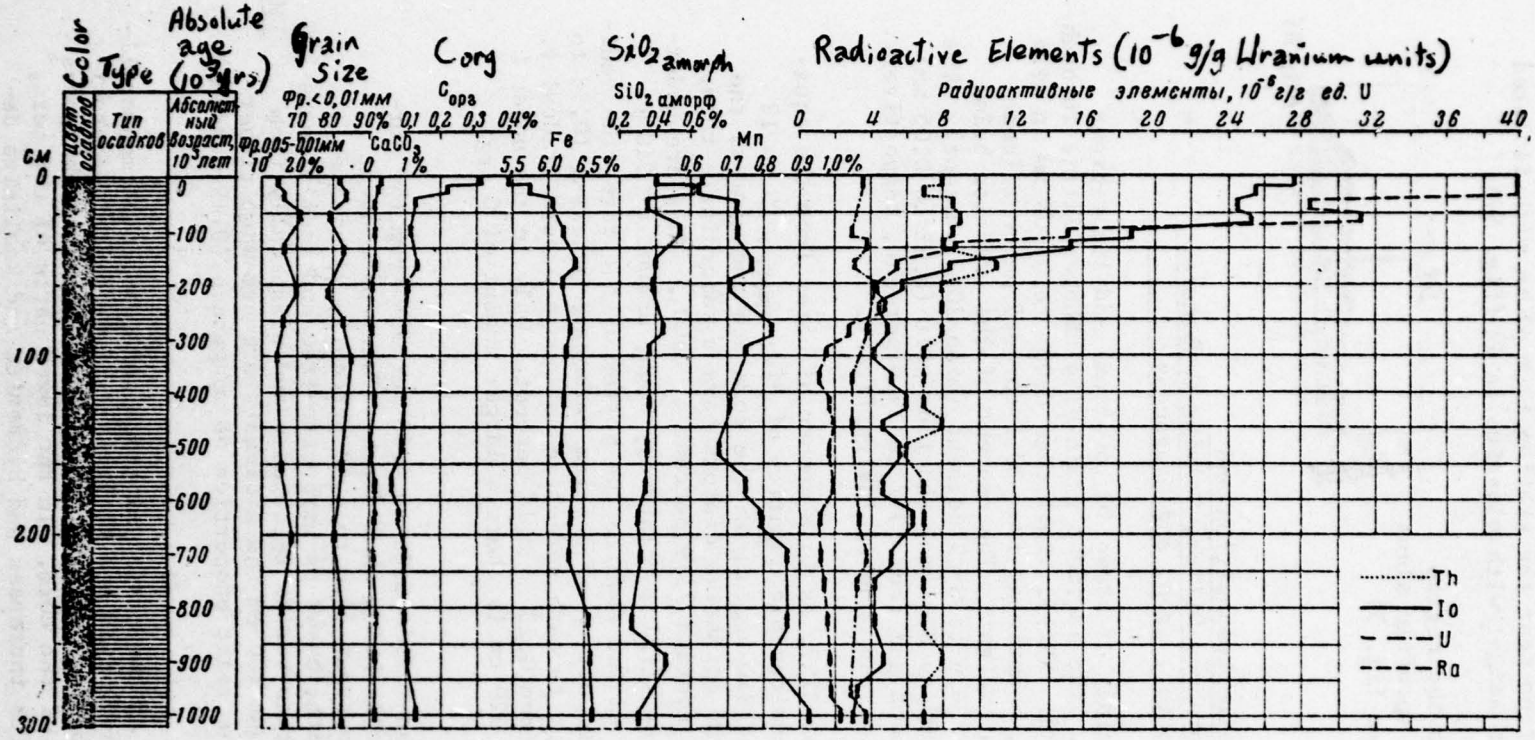

Figure 56. The core at Station 3746. For conditional markings see fig. 12.

Bottom relief. The bottom near the station is a plain with isolated gradual rises, 50 to 300 m in height, with slopes up to 1° (fig. 57).

Figure 57. Bottom relief in the region of station 3797 (profile along the line A-B, see fig. 5)

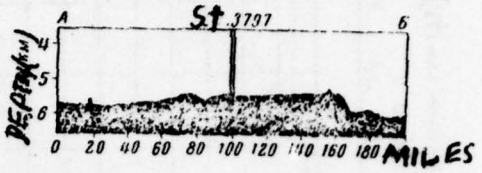

Grain-size Composition and Distribution of Amorphous Silica, Calcium Carbonate, Organic Matter, Iron, and Manganese

The core is composed mainly of brown (0 to 45 cm) and light-brown (45 to 316 cm) clayey silts. The sediment grain-size changes little throughout the core (fig. 58, appendix XVII). Particles 0.001 to 0.005 mm in size predominate among the silts, comprising from 20.5 to 43.5 percent (mean 34.5 percent) of the sediment weight. The content of the fraction below 0.001 mm is quite high, from 24.9 to 35.9 percent (mean 28.2 percent). The quantity of coarse sand (0.005 to 0.01 mm) and fine silt (0.01 to 0.05 mm) varies from 7.7 to 26.4 percent and from 10.2 to 19.9 percent, respectively. The content of the coarse silt and sand is insignificant.

The sediments of station 3797, as in a number of cores from the equatorial Pacific, contain a considerable quantity of SiO_2 amorph (5 to 12 percent). The main source of SiO_2 amorph in the core are radiolaria; the tropical and subtropical forms of marine diatoms have a subordinate role. At 2 to 10 cm, the sediments contain 23.6 percent of $CaCO_3$. They are underlain by silts having less, but still a relatively high, amount of $CaCO_3$ (about 6 percent). Below 22 cm and down to the bottom of the core, the sediments contain a negligible proportion of calcium carbonate material (0.38 to 0.18 percent). The transition to carbonate-free sediments occurs gradually. The content of C_{org} ranges from 0.23 to 0.14 percent. Only in the upper layer (2-17 cm) and at 90 to 120 cm is there a larger amount of C_{org} (0.38 to 0.36 percent).

The content of Fe increases from 3.06 to 4.68 percent from the surface to 86 cm, and varies little below that depth. The iron content through the core is almost constant (4.0 to 4.68 percent), with some tendency to increase with depth, based on carbonate-free and nonsiliceous sediments. The Mn concentration varies repeatedly and drastically from 0.19 to 1.38 percent. At about 100 cm the sediments are somewhat richer in organic matter and have the least proportion of manganese (0.19 percent) of the entire core. 110

Z. N. Gorbunova's study of the clayey minerals has shown that monmorillonite predominates and that hydromica and kaolinite are present in approximately equal but lesser quantities. A high content of amorphous substances characterizes the upper part of the core. In the lower parts of the core, the quantity of montmorillonite increases and hydromica and kaolinite decrease correspondingly.

Radioactive Elements and the Sedimentation Rate

The finely dispersed clayey silts of the upper part of the core, including the slightly calcareous foraminiferal sediments, are characterized by a high content of ionium and thorium, with the concentration of uranium not exceeding the usual values in deep-sea deposits. Figure 58 shows that the uranium content is almost invariable with depth and is 2.7 to 3.2×10^{-6} g/g. The quantity of thorium in the upper part of the core is quite low (3 to 4) $\times 10^{-6}$ g/g. At 127 to 162 cm, it is approximately 4 times as much and remains high- (16 to 12) $\times 10^{-6}$ g/g. The high thorium content is also peculiar to the 60 to 90 cm layer (6 to 12) $\times 10^{-6}$ g/g. The layers with high (60 to 90 and 140 to 316 cm) and low (97 to 127 cm) content of Fe are also high and low in thorium. This relationship between iron and thorium and the type of distribution in the core indicates the terrigenous origin of thorium.

The curve of ionium distribution in the 0 to 40 cm layer is like the theoretical one. The noticeable decrease in ionium and radium concentration at 5 to 10 cm results from dilution by the biogenic carbonate found here in large quantities. It is not clear why the sharp increase in ionium and radium in the 40 to 90 cm section of the core is not accompanied by any changes in granulometric and material composition of the sediments.

In the upper part of the core, the radium content is 17 times and the ionium is 30 times greater than the equilibrium concentration of uranium. Such a disturbance of the radioactive equilibrium in the uranium series, usually observed in deep-sea red clays, makes it possible to compute the age by the ionium method. The average deposition rate of silts in the upper part of the core is 3 mm per 1,000 years and the entire core can represent approximately 1 million years.

Sedimentary Stratigraphy

The grain-size and material data of this core are insufficient to divide the sediment column into stratigraphic horizons. A.P. Zhuze has studied the marine diatoms in 20 samples spaced at 10 to 20-cm intervals along the core. Based on the variation in numbers and size of the tropical marine diatoms that predominate here, A. P. Zhuze identified four layers in the core that were deposited in warm (I-0 to 42 cm; III-130 to 220 cm) or cold (II-42 to 130 cm; IV-220 to 316 cm) waters. He believes that horizon I was formed during the post-glacial period, horizons II and IV - during the last and the penultimate glacial epochs, respectively, and horizon III - during the interglacial period preceding the Wurm (Wisconsin) glaciation. 112
However, the absolute age data do not confirm such a comparison. The ago of the horizons must be considerably older. According to A. P. Zhuze, beginning at a depth of 260 cm one finds a silicoflagellate marine species of plant (Mesozena elliptica) in mass quantities (up to 7.5 million shells per gram of sediment). These are characteristic of Tertiary sediments and are not found in Quaternary deposits. The absolute ago of these sediments, in which large numbers of Mesozena elliptica appear, cannot be less than 800 to 900 thousand years old according to the ionium method of dating. This indicates that the core at station 3797 exposed the entire sequence of Quaternary sediments as well as the upper parts of Tertiary deposits.

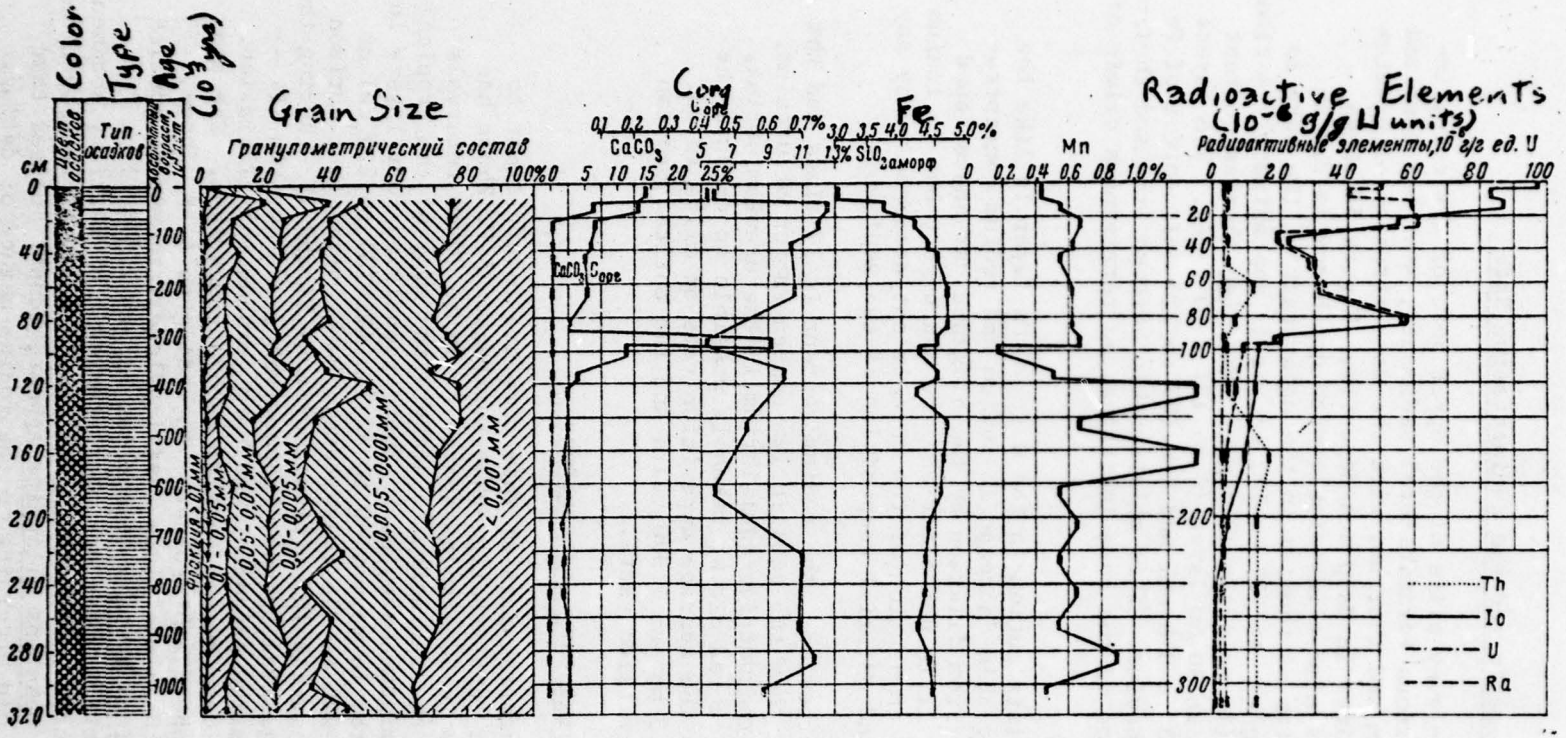

Figure 58. The core at station 3797. For conditional markings see fig. 12.

15. Core at Station 3995

Location - central part of the East Caroline Basin. Depth - 4,854 m. Core length - 301 cm. Sampling instrument - uniflow tube corer.

Bottom relief. Near the station, the bottom is a hilly plain with numerous hills up to 400 m high, with slope gradients that range from fractions of a degree up to 10. The core was taken from a small depression between hills having slope angles of up to 1.7° (fig. 59).

Figure 59. Bottom relief in the region of station 3995 (profile along line A-B, see fig. 5).

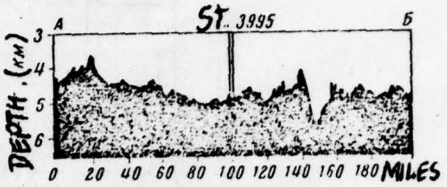

Grain-size and Material Composition

The core is composed of homogeneous clayey silts containing 47.6 to 33.1 percent (mean 40 .6 percent) of 0.001 to 0.005 mm grains and 34.5 to 11. 8 percent (mean 20.2 percent) of grains less than 0.001 mm (fig. 60, appendix XVIII). The silts contain approximately equal percentages of coarse pelites (24.7 to 11.8 percent, average 18.8 percent) and fine silt (25.0 to 10.2 percent, average 17.1 percent). Small amounts of coarse silt (9.9 to 0.3 percent, mean 3.0 percent) and the nearly complete absence of sand particles characterizes the entire core.

A triple alternation of brown (0 to 24, 142 to 195, and 250 to 301 cm) and grey (24 to 142 and 195 to 250 cm) silts is seen in the core. The brown and light brown silts contain little C_{org} and bituminous substances and are enriched with manganese (almost wholly in the form of divalent manganese). The grey sediments contain a large amount of organic matter (up to 1.01 percent C_{org}) and have very little bulk manganese and none of its highest valence compounds. There are three layers (0 to 36, 128 to 190 and 238 to 301 cm) with low and two layers (36 to 128 and 190 to 238 cm) with high contents of organic matter.

The content of $CaCO_3$, which is derived mainly from the shells of planktonic foraminifera, changes from 0.07 to 14.6 percent through the core. The regular variation of $CaCO_3$ defines three layers that are low (0 to 45, 110 to 170 and 240 to 301 cm) and two layers that are high (45 to 110 and 170 to 240 cm) in carbonate material. The muds at about 47 to 88 (94) cm are slightly calcareous foraminiferal sediments (10 to 30 percent of $CaCO_3$). The sediments contain from 4.31 to 5.73 percent iron. The upper part of the core, down to about 115 cm, contains less iron (4.31 to 5.11 percent, average 4.7 percent) than the lower part (5.03 to 5.74 percent, average 5.4 percent).

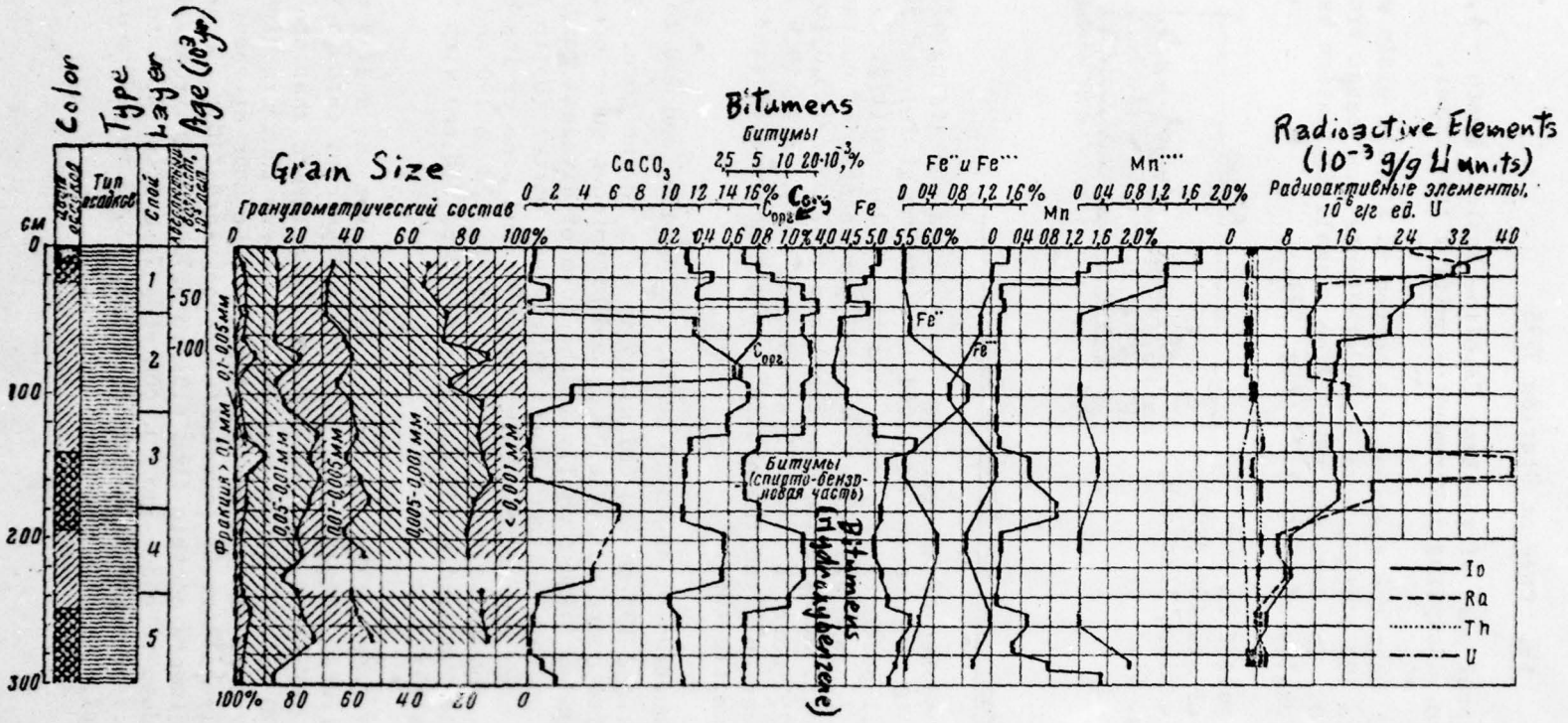

Figure 60. The core at station 3995. For conditional markings, see fig. 12.

The content of uranium, thorium, ionium, and radium was determined and the data are presented in figure 60 and appendix XVII. The surface sediment layer has a comparatively low thorium content (3.2×10^{-6} g/g) and a rather high content of radium (25.2×10^{-6} g/g of U units) and ionium (36.2×10^{-6} g/g of U units), which are close to the values found in deep-sea red clays. The concentration of uranium is within the usual limits for deep-sea sediments and does not vary greatly in the vertical direction (2 to $3.2) \times 10^{-6}$ g/g. The distribution of thorium within the core is similar to the distribution of iron described above. The upper part of the core contains 26×10^{-6} to 3.2×10^{-6} g/g of thorium and the lower part contains 3.4 to $4.8 \cdot 10^{-6}$ g/g of thorium. Figure 61 shows that overall there is a direct relationship between the iron and thorium content in the sediments, despite the dispersion of values.

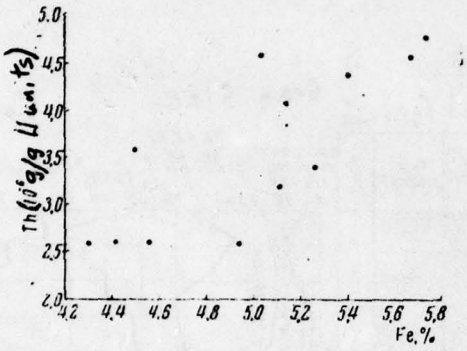

Figure 61. Relationship between the Fe and Th content in the core at station 3995.

The amount of ionium in the surface layer of the sediments is 12 times the equilibrium concentration of uranium and decreases rapidly from the surface down to about 80 cm, becomes approximately constant down to 173 to 197 cm, then decreases regularly. The radium distribution curve is very complex. It is worthy of note that oxidized sediments at 130 to 190 cm (which are low in organic matter and high in manganese) contain a sharply increased quantity of radium. The concentration at 0 to 90 cm is considerably lower and between 90 to 180 cm is considerably higher than the equilibrium concentration of ionium. The ionium and the radium curves practically converge in the deepest part of the core.

Unlike the silts of station 3797 and 4068, where the layer of the equilibrium state in the uranium family is clearly defined, ionium and radium approach equilibrium with uranium only in the lowest parts of the core. This is indicative of a higher sedimentation rate at station 3995. Based on ionium decay, the sedimentation rate can be calculated only for the 0 to 80 cm section of the core. It is approximately 7 mm per 1,000 years. It is impossible to determine the sedimentation rate of silts in the rest of the column.

16. Sedimentary Stratigraphy of the Equatorial Zone

The distribution of calcium carbonate, organic matter, bitumens, and manganese in the core at station 3995 (section 15) permits identification of five sediment layers of different lithologic composition, 0 to 45, 45 to 110 (130), 110 (130) to 180, 180 to 240, and 240 to 301 cm. At present it is difficult to determine whether these layers are correlative with corresponding stratigraphic horizons of sediments of the northwest Pacific Ocean. The absolute age of sediments in the equatorial Pacific Ocean was determined in one only core at station 3995, and only the upper 80 cm of the sediments could be dated. The distribution of the radium family elements in the 80 to 180-cm section of the core at station 3995 seems to indicate an increased sedimentation rate (under the uniform deposition of ionium). The change in 115
the sedimentation rate creates some doubt of the validity of age calculations for this core, therefore, the question of correlating the five above-mentioned horizons with the epochs of warming and cooling of high latitude waters remains open.

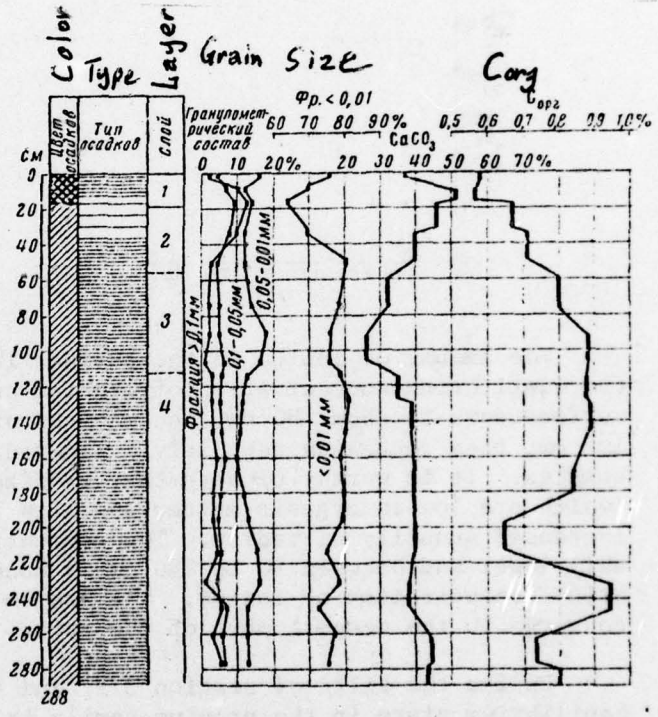

Figure 62. The core at station 3921. For conditional markings see fig. 12.

At the same time it should be noted, that in a whole series of other core samples (stations 3921, 3989, 3993, 3650; see fig. 1, appendix XIX-XXII) taken at and near the equator (2°N - 1°S), the sediments of surface layer 1 (from 0 to 8 to 10 cm) contain less biogenic carbonate material and organic matter (the latter calculated from carbonate-free sediments) than the silts of the underlying layer 2. Deeper within these cores, which are approximately 3 m long, is one more layer with a higher content of $CaCO_3$. For example, the $CaCO_3$ content in the upper layer of the core at station 3921 taken at depth of 2,868 m, is 37 percent, and at 10 cm it

reaches 51 percent; farther down, the $CaCO_3$ gradually decreases to 26 percent (at 105 cm) and in the lower part of the core it gradually increases again to 45 percent (fig. 62). In other cores (stations 3993, 3989, and 3650) the distribution of calcium carbonate is similar to its distribution at stations 3995 and 3921 (fig. 63-65).

Figure 63. The core at station 3993.
For conditional markings see fig. 12.

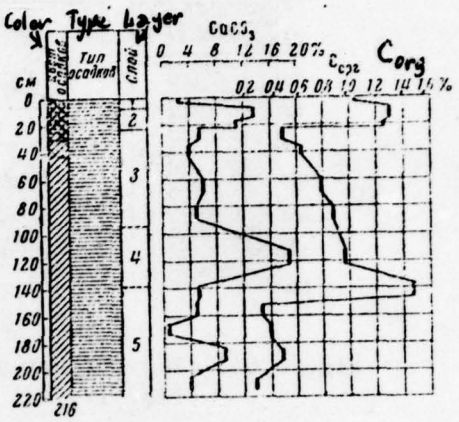

Contemporary sediments of the equatorial zone of the west Pacific Ocean are characterized by smaller amounts of $CaCO_3$, whereas the sediments of the preceding epoch, which quite probably corresponds to the epoch of cooler surface waters north of the equatorial zone, are distinguished by a higher content of $CaCO_3$ and organic matter (not always of the latter). The data confirm the existing theory that, in the equatorial Pacific Ocean, the sediments having a large content of $CaCO_3$ were deposited during periods of cold surface waters caused by intensified vertical circulation and increased upwelling of cold abyssal waters to the surface in the equatorial region [91]. 117

The above-mentioned feature of water circulation in the equatorial region, seen most clearly in the eastern Pacific, is reflected in the stratigraphy of cores from the equatorial western Pacific Ocean. The arrival of a considerable mass of cold waters rich in biogenic elements during the "glacial" epochs compensated for the depletion in the nutrients occurring through photosynthesis, and created favorable conditions for the growth and reproduction of organisms, including those with calcareous and siliceous skeletons. This was recorded in the bottom sediments of the equatorial Pacific Ocean in the form of higher $CaCO_3$ and C_{org} contents in "glacial" sediments, as well as in the increased thickness of the bottom sediments.

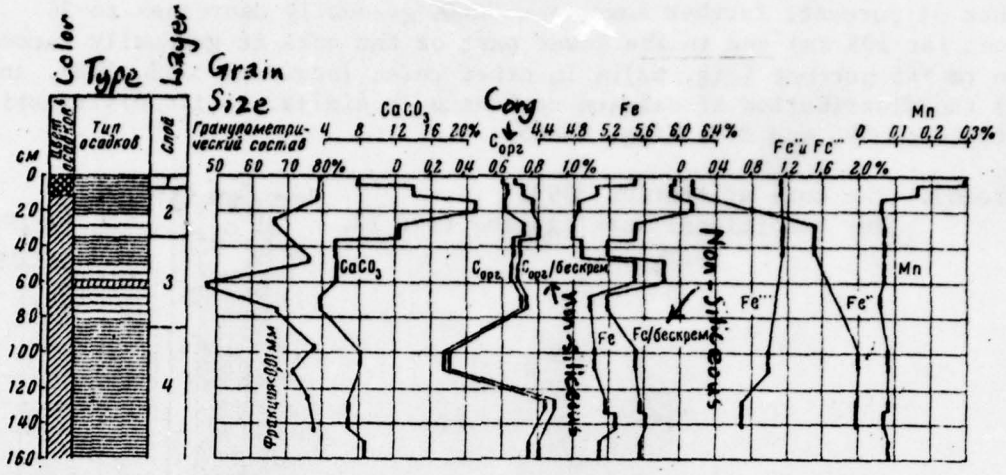

Figure 64. The core at station 3989. For conditional markings see fig. 12.

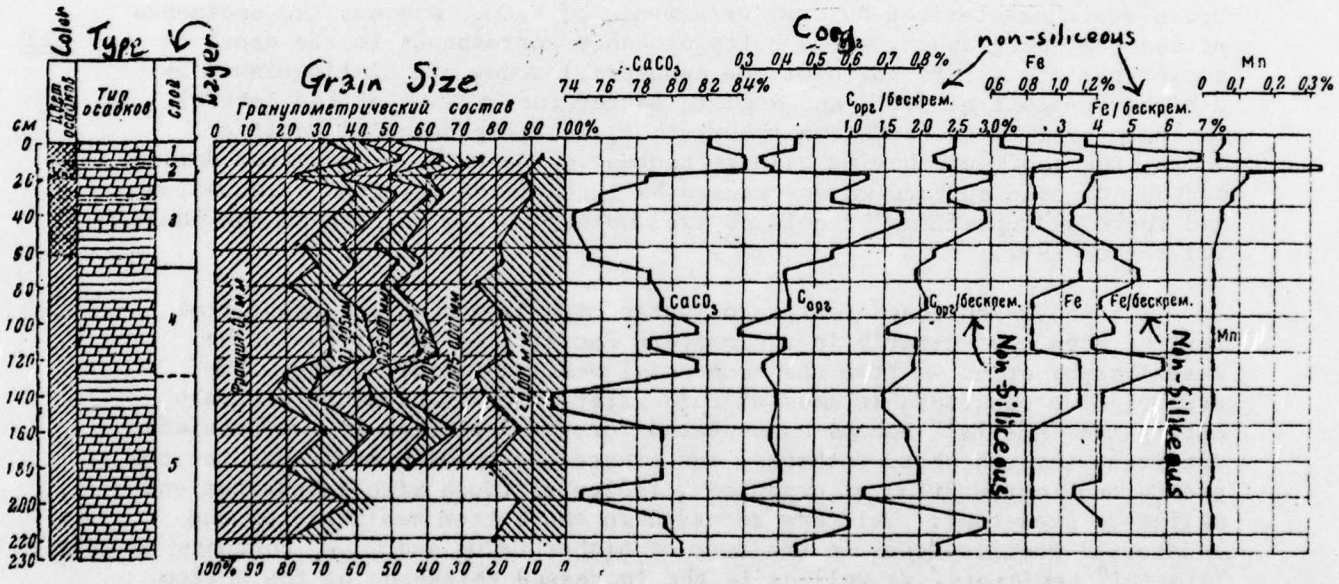

Figure 65. The core at station 3650. For conditional markings see fig. 12.

Chapter VII

118

The History of Deepwater Sedimentation of the Quaternary Period in the Western Pacific

Several single-age stratigraphic horizons that formed in colder and warmer climatic periods were identified through lithologic and micropaleontologic analyses bottom sediment cores from the western Pacific Ocean. These horizons were observed from the Aleutian to Komandorskiye Islands in the north to the Marshall Islands in the south, i.e. over a distance of several thousands of kilometers.

Based on the consistent distribution patterns of U^{238}, Th^{232}, Th^{230}, and Ra in the fourteen cores,[1] the sediment deposition rates, and the absolute age of the layers were calculated. An important result of this study was to confirm, through absolute-age calculation methods, the conclusion that in the temperate and tropical Pacific Ocean warm and cold climatic periods occurred at the same time (table 20). This deduction was first made from an identical and periodic variation, in different core samples, of the lithologic composition of the bottom sediments and the species composition of the marine diatoms. Certain differences in the absolute age of analogous horizons in the individual cores are related, first to the impossibility of drawing boundaries between the horizons with the required precision (with low sedimentation rates this leads to certain, sometimes significant, variations in the absolute age of the horizons) and secondly, to the assumptions made in dating the sediments by the ionium method (see chapter II).

In the longest core samples (stations 3163 and 4068), the Quaternary deposits are subdivided, respectively, into 14 and 11 layers which we combined into eight and seven stratigraphic horizons, respectively. Horizon I corresponds to the Holocene and an age of about 12 thousand years; horizons III, V and VII formed under warmer climatic conditions are correlated, respectively, with the Riss-Würm (Sangomon), Mindel-Riss (Yarmouth) and Gunz-Mindel (Aftonian) inter-glacial periods of Western Europe and North America. The interglacial deposits are divided and overlain by sediments of horizons II, IV, and VIII which are correlated, respectively, with the Würm (Wisconsin and Iowan stages), Riss (Illinoian), Mindel (Kansan), and Gunz (Nebraskan) glaciations. It should be emphasized, that the correlation of Horizons VI, VII, and VIII with earlier Quaternary glacial advances and interglacial stages in quite conditional.

Data on the absolute age of the glacial and interglacial epochs in the western Pacific Ocean are summarized and the limits of estimates of 119
the absolute age of the sediments in the different cores are presented in table 21, which shows that the last continental glaciation began an average of about 75 thousand years ago and ended 11 to 12 thousand years ago. This glaciation had two stages; within the limits of the region discussed these stages are shown most clearly in the northwestern part of the ocean. The climatic cooling at the beginning of the Würm period (approximately 50 to 75 thousand years ago, horizon II, stage 3) and at its end (11 to 30 thousand years ago; horizon II, stage 1) was separated by a

[1]The coordinates of the stations are given in appendix XXIII.

Table 20

Comparison of the thickness and absolute age of stratigraphic horizons in the cores from the temperate and tropical regions of the Pacific Ocean (thickness in cm, absolute age in thousands of years).

Horizon-Layer	STRATIGRAPHIC CORRELATION North America	Western Europe	Sub-3163 Thickness (cm)	Absolute Age (10^3 yrs)
I	HOLOCENE	HOLOCENE	20	0-11
II-1	Wisconsin	Main and Late stage of Würm glaciation	30	11-30
II-2	Interglacial Stage		36	30-50
II-3	Iowan Glaciation	Early Würm	54	50-80
III	Sangamon interglacial stage	Riss-Würm interglacial stage	140	80-170
IV	Illinois glaciation	Riss glaciation	100	170-220
V	Yarmouth interglacial stage	Mindel-Riss interglacial stage	200	200-340
VI-1			70	340-380
VI-2	Kansas glaciation	Mindel glaciation	80	380-430
VI-3			110	430-500
VI-4			110	500-560
VI-5			90	560-610
VII	Afton interglacial stage	Gunz-Mindel interglacial Stage	95	610-670
VIII	Nebraskan glaciation	Gunz glaciation	60*	670-700*

* Hoizon (layer was not completely penetrated
** Thickness of the entire horizon II (II-1, II-2, II-3)
*** Absolute age of the entire horizon II (II-1, II-2, II-3)

TEMPERATE ZONE									
Arctic Water						Sub-Tropical Water			
3378	3325	3342	3359	4068		3451		3625	
Thickness (cm)					Absolute age (10^3yrs)	Thickness (cm)	Absolute age (10^3yrs)	Thickness (cm)	Absolute age (10^3yrs)
65	12	32	40	4-7	0-11(17)	26	0-9	10	0-16
55	23	68	40			40	9-22		
70	39	47	60	23-26**	11(17)-75***	66	22-44	38**	16-80***
142*	114*	97*	136*			58	44-65		
				26	75-140	77*	65-90*	52	80-165
				24	110-200			38	165-230
				40	200-300			54	230-320
				42	300-400			60	320-420
				26	400-470			48	420-500
				24	470-530			69*	500-580*
				18	530-570				
				34	570-660				
				68*	660-830				

TROPICAL ZONE

Tropical Water

Thickness	Absolute Age (10^3 yrs)	Thickness (cm)	Absolute Age (10^3 yrs)	Thickness (cm)	Absolute Age (10^3 yrs)	Thickness (cm)	Absolute Age (10^3 yrs)
30	0-17	7	0-10	10	0-11	6	0-15
				13	11-25		
100	*** 17-76	** 48	*** 10-80	21	25-50	** 24	*** 15-75
				29	50-80		
100	76-135	40	not dated	130	not dated	26	75-140
80*	135-182	45	ditto	117	ditto	36	140-230
		86	ditto	* 38	ditto	25	230-300
		151*					

period (horizon II, stage 2) during which the climatic conditions, based on the composition of the marine diatoms, were the same as or warmer than at present, but cooler than those that existed during the preceding interglacial epochs (horizons III and V).

In reference to the different points of view with regard to the correlation of the stratigraphic horizons identified in the northwest Pacific Ocean with the glacial and interglacial deposits on the continents, one should say the following. In several of her latest papers [32, 22], A. P. Zhuze recognized, in Holocene[1] sediments in the cores from the northwest Pacific, a layer of the so-called climatic optimum (layer IB) which corresponds to layer 2 of horizon II in the cited paper. A.P. Zhuze assigned sediments, that she had previously viewed as interglacial (horizon III; [29, 124], to this layer. The basis for the review of such a correlation was as follows: 1. the presence of deposits formed during the Holocene under conditions of short-term (2,000 to 4,000 years) warming of the climate in Western Europe; 2. the absence or weak presence, in a series of cores from the northwest Pacific (station 3325,3359,3378,3163, 3252, etc), of the sediment layer with more cold-water diatoms directly below the contemporary deposits.

The following should be noted. First, as was shown by the isotopic determinations of paleotemperatures in the Atlantic, the ocean surface-water temperature during the glacial epochs differed from the temperature of the interglacial epochs by 2° to 4°C (maximum of 5° to 6°C), however, during the climatic optimum in the Holocene, the ocean-water temperature increased only by 1°C. Such a small increase in the temperature seems to have had an little influence on the marine diatom composition.

Secondly, determination, by the ionium method, of the sediment deposition rate at stations 3451, 3156, 3520, 3495, and 3163, in which the composition of marine diatoms was studied by A. P. Zhuze, has shown that the thickness of the "climatic optimum" layer recognized by A. P. Zhuze in measured in tens of centimeters. This is in conflict with the short duration of the "climatic optimum" in Western Europe (2 to 4 thousand years). During this period, in the part of the ocean where taken, the maximum accumulation of sediments on the bottom ranged from fractions of 1 cm to 9 cm. The direct determination of the age of this layer in several cores results in an age of 25 to 50 thousand years, i.e. corresponding in time to the warm stage of the last glaciation.

All these factors forced us to the conclusion that the "climatic optimum" layer recognized by A. P. Zhuze was really formed during a warm epoch within the last glaciation. According to the data of American researchers, in the Atlantic Ocean, the warm stage of the last glaciation stands out as clearly as in the Pacific Ocean and has the same absolute age 30 to 50 thousand years (table 22).

---

[1] Holocene, as A. P. Zhuze understands it, includes horizons I, II, III, and part of horizon IV, according to our classification.

Table 21

The absolute age of sediments of the glacial and interglacial epochs of the western Pacific Ocean.

Horizon (layer)	Number of stages	STRATIGRAPHIC CORRELATION Western Europe	North America	Number of cores penetrating the layer	Range of variation of the age of the beginning of the period (horizon) (10^3 yrs)	End and beginning of the period (horizon) (10^3 yrs)	Mean duration of period (10^3 yrs)
I	1	HOLOCENE		8	9-17	0-12	12
II	3	Main and Late Würm glaciation	Wisconsin Glaciation	8	22-30	12-26	14
		Interglacial	Period	8	44-50	26-48	22
		Early Würm glaciation	Iowan glaciation		65-80	48-75	27
III	1	Riss-Würm interglacial stage	Sangamon interglacial stage	5	135-170	75-150	75
IV	1	Riss-glaciation	Illinois glaciation	4	200-230	150-220	70
V	1	Mindel-Riss interglacial stage "	Yarmouth interglacial stage	4	300-340	220-315	95
VI	5	Mindel glaciation	Kansan glaciation	2	610-660	315-635	--
VII	1	Gunz-Mindel interglacial stage	Afton interglacial stage	1	-------	610-670	--
VIII	1	Gunz glaciation	Nebraskan glaciation	1	-------	670	--

Table 22

Comparison of the absolute age of glacial and interglacial deposits in the Pacific and Atlantic Oceans.

STRATIGRAPHIC CORRELATION		ABSOLUTE AGE (based on mean data in 10^3 yrs)	
Western Europe	North America	Pacific Ocean	Atlantic Ocean*
HOLOCENE		0-12	0-11
Main and Late stages of Würm glaciation	Wisconsin glaciation	12-26	11-30
Interglacial Stage		26-48	30-50
Early Würm	Iowan glaciation	48-75 (48-61)	50-65
Riss-Würm interglacial stage	Sangamon interglacial stage	75-150 (61-94	65-100
Riss glaciation	Illinois glaciation	150-220 (94-110)	100-130
Mindell-Riss interglacial stage	Yarmouth interglacial stage	220-315 (110-166)	130-175

*Based on protactinium-ionium method of dating [153].

The sediments of the Riss-Würm (Sangamon) interglacial stage (horizon III) are 75 to 150 thousand years old, the Riss (Illinoian) glaciation (horizon IV) sediments are 150 to 220 thousand years old, the Mindel-Riss (Yarmouth) interglacial stage (horizon I) is 220 to 315 thousand years old. Consequently, the epochs of cool and warm waters lasted approximately the same length of time in the north Pacific (64 to 75 thousand years), which indicates the period of climate variation with the full cycle lasting about 130 to 150 thousand years.

Table 22 correlates the absolute age of the glacial and interglacial epochs of the Pacific (from our data) and of the Atlantic (from the data of American researchers). The recalculated ages of the sediments, that we obtained by the ionium methods are shown in parenthesis. They were recalculated by comparing age determinations of the same samples from the Atlantic Ocean by both the ionium and protactinium-ionium methods [153]. We adopted the following recalculation coefficients: 0 to 50 thousand years 1; 50 to 70 thousand years - 1.2; 100 to 150 thousand years - 1.6; more than 220 thousand years - 1.9.

Several conclusions appear from a study of the table. First, both warm and cool water epochs occurred simultaneously in the Pacific and the Atlantic Oceans during the Late Quaternary Period. Specifically, the warm stage of the last glacial epoch occurred simultaneously in both oceans and had approximately the same duration. Second, the age-determination results obtained by the ionium and the protactinium-ionium methods coincide well for the last 50 to 75 thousand years and diverge considerably for more ancient deposits. Third, if the adopted coefficients of transition from the ionium to the protactinium-ionium methods are based on a considerably larger quantity of data, the identical age of the events in the western and eastern hemispheres will be confirmed for the older stages of Quaternary history. 121

Repeated variations of climate and water temperature are reflected in the terrigenous and biogenic sedimentation in the Pacific Ocean. The sediments deposited during the interglacial epochs and the last interglacial period in the temperate region of the Pacific Ocean are usually characterized by a finer and more homogeneous grain-size composition, higher content of SiO_2 amorph, a complex of warm-water marine diatoms, and (often, but not always) a high content of $CaCO_3$ and organic matter. In the northern region in subarctic waters, slightly siliceous diatom silts were deposited during the warmest stage. Diatom silts were most widely distributed, during the Mindel-Riss interglacial stage of the Pleistocene, when even in waters of the Kuroshio and Oyashio (currents) mixing zone, sediments having a relatively high content of biogenic silicia (derived from marine diatoms) were deposited.

In this part of the ocean, the periods of warm climate and, correspondingly, of surface-water temperature increase, which created more favorable conditions for the survival of marine diatoms, were also periods when planktonic foraminifera increased, and not only more SiO_2 amorph and organic matter, but also more $CaCO_3$ reached the bottom. An analogous increase in $CaCO_3$ content during the periods of warmer climate is typical (of sediments) 122

in the temperate, tropical, and equatorial regions of the Atlantic and Arctic Oceans. However, in the tropical Pacific Ocean, interglacial deposits relatively rich in the skeletal remains of marine diatoms do not contain larger amounts of $CaCO_3$. On the contrary, here is a tendency toward an increase in $CaCO_3$ during periods of cooler climate. One may assume that this is related to the lower temperature of bottom water layers along the periphery of the tropical ocean during interglacial epochs, caused by glacial melt waters. At the same time, the rate of dissolution of calcareous foraminifera on the bottom increased as a result of the increase in activity of the cold bottom waters.

Sediments deposited during the glacial epochs in the temperate and tropical Pacific Ocean are coarser grained in several cases, especially in cores taken along the periphery of the Northwest Basin. Ice rafted material appears in sediments belonging to the boundary of the glacial and interglacial epochs, which testifies to the increased entrance of shore ice into the ocean. Ash layers are confined to sediments of the glacial epochs and indicate the intensified volcanic activity at this time. The volcanoes of Kamchatka and the Kuriles probably were more active during the last glaciation. This is confirmed in the horizon II deposits in cores 123 at stations 3359, 3163, and 3451 by the increase in ash layers and inclusions as well as by the overall increase in the content of pyroclastic material in the sediments.

The decrease in $SiO_{2\ amorph}$ content, as well as (but not always) of $CaCO_3$ and C_{org} is characteristic of the sediments of the glacial epochs in the North Pacific Ocean. This probly was caused by the decreased productivity of ocean waters. The decreased productivity during the glacial epochs in the temperate zone was related to the increased duration of the ice cover and the shorter vegetation period of marine diatoms, and in more southern (tropical) regions it was connected with a sharply defined shortage of biogenic nutrient elements in the surface waters. As a result, conditions were less favorable for the existence of marine diatoms during the glacial epochs, a smaller number of their siliceous skeletal remains descended to the bottom. This phenomenon was marked in the North Pacific Ocean by the complete disappearance of the slightly siliceous diatom silt (ooze) deposition zone that is so typical of the contemporary and interglacial stages of the Quaternary history of the ocean.

Not only did the quantity of marine diatoms change during the glacial epochs, but the realtionship of Arctic, northern, south-boreal, and tropical floral complexes in the sediments also changed to an increase in the cold-water flora distributed in higher latitudes. At the same time as one moves farther south, across the boundaries of subarctic waters and of the Kuroshio and Oyashio intermixing zone to the equatorial Pacific Ocean, the differences between the species content of marine diatoms of the glacial and interglacial epochs become less pronounced. At the same time, the sediments are less clearly stratified. This is because the difference between temperatures of the glacial and nonglacial climates decreased toward the equator [25].

Special sedimentation conditions were created in the equatorial Pacific Ocean, where, under the influence of the Earth's rotational forces, cold waters rich in biogenic elements rise toward the surface. They continuously compensate for the depletion of the biogenic substances necessary for photosynthesis and facilitate the increased productivity of the equatorial zone. The equator and the regions immediately to the north and south (1^{o} to 2^{o} of latitude), where the largest water masses are involved, have especially favorable conditions. The upwelling of water was more intensive during the glacial epochs, during which more favorable conditions developed for plankton growth, including the sediment-forming group that predominates here - calcareous foraminifera. 124

The sediment cores taken in the western ocean in the equatorial region (stations 3921, 3993, 3650, etc) contain the chronology of changes in productivity of the equatorial region. Unlike the more northern regions, the deep-sea sediments of layers 1 and 3 are characterized here by less $CaCO_3$ and C_{org} than in the underlying sediments of layers 2 and 4, which correspond in time to the high latitude glacial epochs. An analogous picture of the alternation of layers rich and poor in biogenic components ($CaCO_3$, $SiO_{2\ amorph}$, P) can be seen, according to Arrhenius, in the eastern equatorial Pacific Ocean [87, 89-91].

The close relationship between hydrologic, biological, and geologic processes in the ocean that is so characteristic of the contemporary stage of development, also existed during older stages of the Quaternary. The climatic and vertical zoning of sedimentation continued throughout the Quaternary. The periodic climatic changes led to displacement of the main climatic sedimentation zones. During the glacial epochs, the temperate climatic zone was shifted southward and, in the Komandorskiy-Kamchatka region, approached Arctic conditions. This was the main cause of the decrease in SiO_2 amorph in the sediments and the complete disappearance of diatom silts during this period. It should be noted that, if in the Komandorskiye-Komchatka region the content of SiO_2 amorph in the sediments was 2.5 to 5 times lower during the glacial period than during the interglacial periods, then this difference was even less (1.2 to 2 times lower) in the area of the Kuroshio and Oyashio intermixing zone and in the northern subtropical region. Unfortunately, the absence of isotope measurements of the paleotemperatures prevents a dependable evaluation of the displacement values of the climatic zones and identification of the latitudes that were occupied by these zones during the different stages of the Quaternary.

Let us turn again to the question of sediment deposition rate and the thickness of individual sediment layers in the northwest Pacific. Table 23, where the data were summarized, and figures 66 and 67 show that sedimentation rates, as well as the sediment thicknesses were also simultaneously undergoing great changes. In the Northwest Basin of the Pacific Ocean, sedimentation rates (at least during the last 80 to 300 thousand years) were higher than in the other basins of this part of the ocean. Especially high sedimentation rates and sediment thicknesses occur along the margin of this basin, in the west and in the northwest (17-30-40 mm per 1,000 years), and on the outer slope of the Aleutian abyssal trench (30 mm per

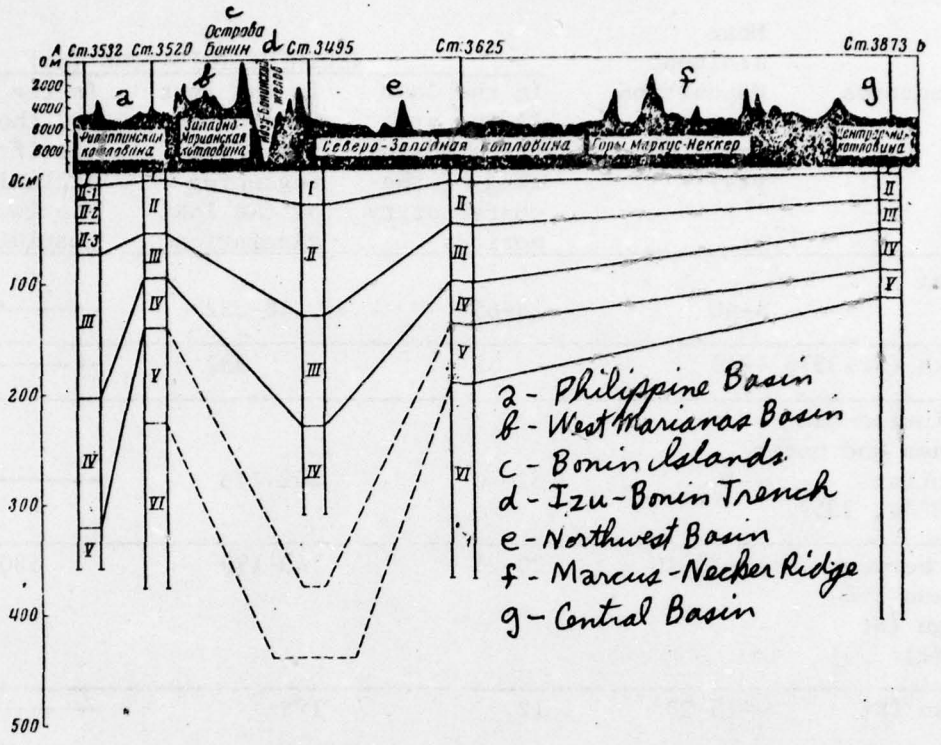

Figure 66. Comparison of the thickness of horizons of identical age in the western Pacific Ocean (section along line A-B, see fig.1)

I - Holocene; II-1 - Wisconsin glaciation (main and late stages of Würm glaciation), II-2 - the Würm intergalcial stage, II-3 - Iowan glacial stage, III - Sangamon (Riss-Würm) interglacial period, IV - Illinoian (Riss) glaciation, V - Yarmouth (Mindel-Riss) intergiacial period, VI - Kansan (mindel) glaciation.

1,000 years). According to the sedimentation rate, this part of the basin is closer to geosynclines than it is to platforms.

Relatively low rates, as well as smaller sediment thicknesses or submarine elevations in the Northwest Basin are notable. For example, on the Obruchev submarine rise (station 3325) the sedimentation rate is approximately one-half that on the bottom directly adjoining the elevation 126
on the west and the north. The sedimentation rate and sediment thickness are even less in the region of the Shatskiy Rise (4 mm per 1,000 years). The sedimentation rates and, correspondingly, the sediment thickness decrease, not only on underwater elevations, but also as one moves farther into the central (southern) part of the Northwest Basin.

Table 23

Large Relief Features	Mean sediment deposition rate (mm/1,000 yrs)	SEDIMENT THICKNESS (cm) In the last 11,000 yrs (from beginning of the contemporary period.	In the last 80 thousand yrs (from beginning of the last glaciation	In the last 300 thousand yrs (from the beginning of the last interglacial stage
Northwest Basin: As a whole	4-40	4-65	48-332	----------
Near Kamchatka (St.3378	--40	65	332	----------
Junction of Kurile-Kamchatka Trenches and outer slope of Aleutian Trench (St. 3342, 3359)	--30	32-40	242-276	----------
Ocean margin between the Kuriles and the Hawaiian Ridge (St 3163,3451,3481)	17-30-10	20-26	140-190	580
Obruchev Rise (St 3325)	--15-20	12	188	----------
Southern part of basin (St. 3625)	6	10	48	192
Shatsky Rise (St. 3156)	4	--	----	----------
Western end of Marcus-Necker Mountain system (Ridge) (St. 3495)	17	30	130	----------
Bonin Basin (St. 3506)	10	--	---	----------
Philippine Basin: Northern part (St. 3520, 3532, 3520)	13-9-7	7-10	55-73	226
Central part (St. 3746)	3	----	-----	----------
West Caroline Basin (St.3995)	7	----	-----	----------
Northeast Basin (St. 4068)	4	--6	26	120
Central Basin (St. 3797, 3873)	3-4	6	30	117

Sedimentation rates and sediment thickness in the northwest Pacific Ocean.

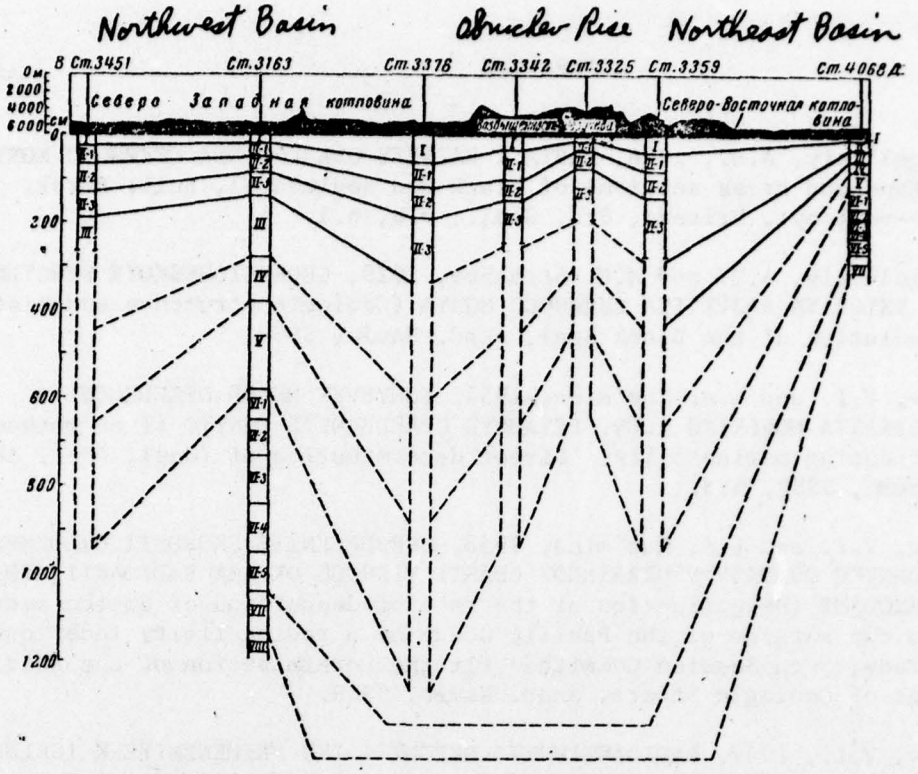

Figure 67. Comparison of thickness of horizons of identical age in the western Pacific (section along line CDE, see fig. 1).

Conditional markings I - VI see fig. 66; VII - Afton (Gunz-Mindel) interglacial stage; VIII - Nebraska (Gunz) glaciation.

The sedimentation rate is relatively high in the North Philippine Basin (7 to 13 mm per 1,000 years; stations 3530, 3532, and 3520) and in the Bonin Basin (10 mm per 1,000 years; station 3506); whereas in the central Philippine Basin it is very low (3 mm per 1,000 years; station 3746). A comparatively high rate of sedimentation (17 mm per 1,000 years) is also seen at station 3495 at the foot of the mountain in the Marcus-Necker Seamount system. Here, and in the core at station 3359, thin layers of redeposited sediments have been deposited in the last glacial epoch. The Northeast and Central Basins of the Pacific Ocean, at least where these cores were taken (stations 4068, 3797, and 3873), are characterized by very low and approximately equal deposition rates and sediment thickness deposited during the last 300 thousand years.

In conclusion, one should note that the intergrated study of bottom sediment cores from the western Pacific made it possible for the first time, to establish their stratigraphy, not only by methods of relative geochronology, but also of absolute geochronology. Further studies of these and other cores will make it possible to define more accurately many problems yet unclear and to reveal the paleogeography of the Pacific Ocean in greater detail than is possible at present.

1. Arkhangel'skiy, A.D., 1928, KARTA I RAZREZY OSADKOV DNA CHERNOGO MORYA (Maps and cross sections of Black Sea sediments), Bull. Morsk. Ob-va Ispyt. Prirody, Otd. Geol., v.b, n.1.

2. Arkhangel'skiy, A.D. and N.M. Strakhov, 1929, GEOLOGICHESKOYE STROYENIYE I ISTORIYA RAZVITIYA CHERNOGO MORYA (Geologic structure and historical evolution of the Black Sea), Akad. Nauk, SSSR.

3. Baranov, V.I. and L.A. Kuz'mina, 1954, IONYEVYY METOD OPREDELENIYA VOZRASTA MORSKIKH ILOV. PRYAMYE OPREDELNIYE IONIYO (I on method of dating marine silts. Direct determination of ions), Dokl. Akad. Nauk, SSSR, n.3.

4. Baranov, V.I. and L.A. Kuz'mina, 1958, OPREDELENIYE SKOROSTI OTLOZHENIYA DONNYKH OSADKOV V OKRAINNOY CHASTI TIKHOGO OKEANA RADIOAKTIVNYMI METODAMI (Determination of the rate of deposition of bottom sediments in the margins of the Pacific Ocean by a radioactivity technique), Trudy, 5-th Session Committee fir the Determination of the Absolute Age of Geologic Strata, Akad. Nauk, SSSR.

5. Baranov, V.I., 1947, RADIOAKTIVNYYE METODY I IKH PRIMENENIYE K ISSLEDOVANIYU POCH' (Radioactive methods of Studying the Grass-Chemical Composition of Soils, v. IV,n.2, Akad. Nauk, SSSR.

6. Baranov, V.I. and L.A. Kuz'mina, 1960, RADIOKHIMICHESKIY ANALIZ GLUBOKOVODNYKH MORSKIKH OTLOZHENIY V SVYAZI S OPREDELENIYEM SKOROSTI OSADKONAKOPLENIYA (Radiochemical analysis of deepwater marine sediments in relation to the determination of the rate of sedimentation), Trudy, 6th Session, Committee for the Determination of the Absolute Age of Geologic Strata, Akad. Nauk, SSSR.

7. Baranov, V.I. and L.A. Kuz'mina, 1958, SKOROST' OTLOZHENIYA ILOV INDIYSKOGO OKEANA (Rate of deposition of Indian Ocean silts), Geokhimiya, n.2.

8. Baranov, V.I. and L.A. Kuz'mina, 1957, SODERZHANIYE RADIOAKTIVNYKH ELEMENTOV V DONNYKH OTLOZHENIYAKH TIKHOGO OKEANA V RAYONYE YAPONSKIKH OSTROVOV (Content of radioactive elements in Pacific Ocean bottom sediments near the Japanese Islands), Geokhimiya, N.1.

9. Bezrukov, P.L., 1955, DONNYYE OTLOZHENIYA KURILO-KAMCHATSKOY VPADINY (Bottom sediments of the Kurile-Kamchatka trench), Trudy, Inst. Okeanol., Akad. Nauk, SSSR, v. 12.

10. Bezrukov, P.L., 1960, DONNYYE OTLOZHENIYA OKHOTSKOGO MORYA (Bottom sediments of the Okhotsk Sea), Trudy, Inst. Okeanol., Akad. Nauk, SSSR, v.32.

11. Bezrukov, P.L., A.P. Lisitsyn, V.P. Petelin and N.S. Skornyakova, 1961,

KARTA DONNYKH OSADKOV MIROVOGO OKEANA, in SOVREMYENNNYKH OSADKI MORYEY I OKEANOV (Bottom sediment chart of the World Ocean, in contemporary sediments of the seas and oceans), publ. Akad. Nauk , SSSR.

12. Bezrukov, P.L. and A.P. Lisitsyn, 1960, KLASSIFIKATSIYA OSADKOV SOVREMYENNYKH MORSKIKH VODOYEMOV (Classification of sediments of contemporary marine water bodies), Trudy, Inst. Okeanol., Akad. Nauk , SSSR, v.32.

13. Bezrukov, P.L. and E.A. Romankevich, 1960, K STRATIGRAFII I LITOLOGII DONNYKH OTLOZHENIY SEVERO-ZAPADNOY CHASTI TIKHOGO OKEANA (Stratigraphy and lithology of bottom sediments of the northwest Pacific Ocean), Dokl., Akad. Nauk , SSSR, v.130, n.2.

14. Bezrukov, P.L., 1962, O NERAVNOMERNOSTI RASPREDELENIYA GLUBOKOVODNYKH OKEANICHESKIKH OSADKOV (Irregular distribution of deepwater oceanic sediments), Okeanology, v.2, n.1.

15. Bezrukov, P.L., 1955, O RASPROSTRANENII I SKOROSTI NAKOPLENIYA V OKHOTSKOM MORYE KREMNISTIKH OSADKOV (Occurrence and rate of accumulation of Okhotsk Sea siliceous sediments), Doklady, Akad. Nauk , SSSR, v. 103, n.3.

16. Bezrukov, P.L., and A.P. Lisitsyn, 1957, OSADKO OBRAZOVANIYE V DAL'NYEVOSTOCHNYKH MORYAKH V CHETVERTICHNOYE VREMYA (Sedimentation in the Far Eastern seas in Quaternary times), Trudy, Com. for the Study of the Quaternary Period, v.13.

17. Bezrukov, P.L., 1960, OSADKOOBRAZOVANIYE V SEVERO-ZAPADNOY CHASTI TIKHOGO OKEANA (Sedimentation in the northwest Pacific Ocean), Internat. Geol. Congress, 21st Session, Problem 10, Doklady, Soviet Geology publ. Akad. Nauk , SSSR.

18. Bezrukov, P.L. and G.B. Udintsev, 1955, O SEVERNOM OKONCHANII PODVODNOGO GAVAYSKOGO KHREBTA (Northern end of the submarine Hawaiian Ridge), Dokl., Akad. Nauk , SSSR, v.103, n.6.

19. Bezrukov, P.L., A.P. Lisitsyn, E.A. Romankevich and N.S. Skornyokova, 1961, SOVREMENNOYE OSADKOOBRAZOVANIYE V SEVERO CHASTI TIKHOGO OKEANA (Contemporary sedimentation in the North Pacific Ocean) in contemporary sediments of the seas and oceans, publ. Akad, Nauk , SSSR.

20. Belov, N.A. and N.N. Lapina, 1962, DONNYYE OTLOZHENIYA SEVERNOY CHASTI GRENLANDSKOGO MORYA (Bottom sediments of the northern Greenland Sea), Nauchn.-Tekhn. Bull., n.2-3 (20-21), Murmansk Polar Inst. Com. Fish. and Oceanogr..

21. Belov, N.A. and N.N. Lapina, 1958, NOVYYE DANNYYE O STRATIFIKATSII DONNYKH OTLOZHENIY ARTICHESKOGO BASSEYNA SEVERNOGO LEDOVITOGO OKEANA (New data on the layering of bottom sediments of the Arctic Basin of the Arctic (Northern Icy) Ocean), Dokl., Akad. Nauk , SSSR, v.122, n.1.

22. Belyayeva, N.V., 1962, RASPREDELENIYE PLANKTONNYKH FORAMINIFER V VODAKH I OSADKAKH INDIYSKOGO OKEANA (Distribution of planktonic foraminifera in the water and sediments of the Indian Ocean), Dissertation M.

23. Bogarov, V.G., 1958, PRODUKSTIYA PLANKTONA I KHARACTERISTIKA BIOGEOGRAFICHESKIKH OBLASTEY OKEANA (Plankton production in typical biogeographic regions of the ocean), Dokl., Akad. Nauk , SSSR, v.118, n.5.

24. Bogorov, V.G. and M.E. Vinogradov, 1960, RASPREDELENIYE BIOMASSY ZOOPLANKTONA V TSENTRAL'NOY CHASTI TIKHOGO OKEANA (Distribution of zooplankton biomass in the central Pacific Ocean), Trudy, Bses. Gidrobiol. O-va, n.10.

25. Bryks (Brooks), K., 1952, KLIMATY PROSHLOGO (Climates of the Past), IL.

25a. Burkov, V.A., 1963, TSIRKULYATSIYA VOD V SEVERNOY CHASTI TIKHOGO OKEANA (Water circulation in the North Pacific Ocean), Okeanology, v.3, n.5.

26. Vernadskiy, V.I., 1934, OCHERKI GEOKHIMII (Outline of chemistry), publ. ONTI NKPP SSSR, Federal Scientific-Technical Mining-Geology-Petroleum, pub. M.-L.-Grozny-Novosibirsk.

27. Vinogradov, A.P., 1944, GEOKHIMIYA RASSEYANNYKH ELEMENTOV MORSKOY VODY (Geochemical dispersion of elements in seawater), Advances in Chemistry, v. 13, n.1.

28. Zhaikov, A.P., 1961, STSINTILLYATSIONNYY METOD SCHETA C^{14} I PRIMENENIYE RADIOUGLYERODNOGO METODA K IZUCHENIYU PROTSESSOV SOVREMENNOGO OSADKOOBRAZOVANIYA (Scintillation method for recording Carbon-14 and use of radioactivity methods to study contemporary sedimentation processes), Dissertation, Fond. Radiev. Inst. Akad. Nauk , SSSR.

29. Zhuze, A.P., 1959, DIATOMOVYYE V DONNYKH OTLOZHENIYAKH SEVEROZAPADNOY CHASTI TIKHOGO OKEANA (Diatoms in the bottom sediments of the northwest Pacific Ocean), Dokl. Akad, Nauk , SSSR, v.125, n.4.

30. Zhuze, A.P. and E.V. Koreneva, 1959, DIATOMOVYY I SPOROVO-PYLTSYEVOY ANALIZ DONNYKH OTLOZHENIY DAL'NYEVOSTOCHNYKH MORYEY (Diatom and pollen-spare analysis of bottom sediments of the Far Eastern seas), pub. 221 Akad. Nauk , SSSR, Geograf. series, n.2.

31. Zhuze, A.P., 1954, SOPOSTAVLENIYE REZUL'TATOV DIATOMOVOGO ANALIZA OTLOZHENIY OKHOTSKOGO I BERINGOVA MORYEY (Comparative results of diatom analysis of sediments of the Okhotsk and Bering seas), Dokl., Akad. Nauk , SSSR, v.98, n.1.

32. Zhuze, A.P., 1961, STRATIGRAFIYA DONNYKH OTLOZHENIY NA SEVERO-ZAPADYE TIKHOGO OKEANA (Stratigraphy of bottom sediments in the northwest Pacific Ocean), Trudy, Inst. Geol., Akad. Nauk , Estonian SSR, n.VIII.

33. Zhuze, A.P., 1961, STRATIGRAFIYA OSADKOV I PALEOGEOGRAFICHESKIYE USLOVIYA OSADKONAKOPLENIYA V SEVERO-ZAPADNOY CHASTI TIKHOGO OKEANA. PO DANNYM DIATOMOVOGO ANALIZA (Sedimentary stratigraphy and paleogeographic conditions of sediment deposition in the northwest Pacific Ocean. Data from diatom analysis), XIX Geographic Congress, Stockholm.

34. Zhuze A.P., 1962, STRATIGRAFICHESKIYE I PALEOGEOGRAFICHESKIYE ISSLEDOVANIYA V SEVERO-ZAPADNOY CHASTI TIKHOGO OKEANA (Stratigraphic and paleogeographic research in the northwest Pacific Ocean), publ. Akad. Nauk, SSSR.

35. Zalmanzon, E.S., 1957, OPREDELENIYA FORM NEKOTORYKH ELEMENTOV I ANALIZ KOLLOIDNOY FRAKTSII GLIN (Distribution form of some elements and analysis of the colloidal fraction of clays), in Methods of Studying Sedimentary Rocks, v.II, Government Geology publ., 64.

36. Zverev, S.M., V.M. Korylin and G.B. Udintsev, 1961, MOSHCHNOST' DONNYKH OTLOZHENIY V OKEANYE (Thickness of bottom sediments in the ocean), in Contemporary Sediments of the Oceans and Seas, publ. Akad. Nauk, SSSR.

37. Zenkevich, L.A., N.G. Barsanova and G.M. Belyayev, 1960, KOLICHESTVENNOYE RASPREDELENIYE DONNOY FAUNY V ABISSALI MIROVOGO OKEANA (Quantitative distribution of bottom fauna in the abysses of the World Ocean), Dokl., Akad. Nauk, SSSR, v.130, n.1.

38. Zenkevich, L.A., 1961, NOVYYE DANNYYE O REL'YEFYE DNA SEVEROVOSTOCHNOY CHASTI TIKHOGO OKEANA (New information on the bottom relief of the northeast Pacific Ocean), Trudy, Inst. Okeanol., Akad. Nauk, SSSR, v.45.

39. ------1963, Karta "REL'YEF DNA TIKHOGO OKEAN" (Bottom relief of the Pacific Ocean), 1:25,000,000, publ. Glau. Upr. Geod. i Kartogr., Ministry of Geology and Conservation of Mineral Resources, SSSR, M.

40. Korenyeva, Ye. V., 1961, ISSLEDOVANIYE METODOM SPOROVO-PYL'TSYEVOGO ANALIZA DVUKH KOLONOK MORSKIKH OTLOZHENIY IZ YAPONSKOGO MORYA (Study of two marine sediment cores from the Japan Sea by the spore-pollen analysis method), Okeanlogiya, v.1, n.4.

41. Korenyeva, Ye. V., 1957, SPOROVO-PYL'TSYEVOY ANALIZ DONNYKH OTLOZHENIY OKHOTSKOGO MORYA (Spare-pollen analysis of bottom sediments of the sea of Okhotsk), Trudy, Inst. Okeanol., Akad. Nauk, SSSR, v.22.

42. Koshi, F.F., 1956, GEOKHIMICHESKIY BALANS V GIDROSFERYE (Geochemical equilibrium in the hydrosphere), Nuclear Geology, IL.

43. Kuznetsov, V.I., 1944, TSVETNAYA REAKTSIYA NA TORIY (Color reactions in thorium), J. General Chemistry, n.9-10.

44. Kuznetsov, Yu. V., 1958, IZUCHENIYE RASPREDELENIYA RADIOELEMENTOV V MORSKIKH OSADKAKH (Study of the distribution of radioactive elements in marine sediments), Dissertation L.

45. Kuz'mina, L.A., 1958, OPREDELENIYE URANA, TORIYA I IONIYA V MORSKIKH ILOV (Distribution of uranium, thorium and ionium in marine silts), Analytic Chemistry, n.1.

46. Kurbatov, L.M., 1937, O RADIOAKTIVNOSTI ZHELEZO-MARGANTSYEVYKH POROD I OPREDELENIYE SKOROSTI IKH OBRAZOVANIYA RADIOAKTIVNYM METODOM (Radioactivity of ferro-manganese rocks and determination of their rate of formation by a radioactive method), Trudy, XVII Session, International Geologic Congress, v.IV, M. GONTI.

47. Lapina, N.N. and N.A. Belov, 1961, OSOBENNOSTI PROTSESSA OSADKOOBRAZOVANIYA V SEVERNOM LEDOVITOM OKEANYE (Special sedimentation processes in the Arctic Ocean), in Contemporary Sediments of the Seas and Oceans, publ. Akad. Nauk , SSSR.

48. Leonova, L.I., 1956, LYUMINESTSENTNYY METOD OPREDELENIYA MALYKH KOLICHESTV URANA V IZVERZHENNYKH PORODAKH (Luminescent method of detecting small amounts of uranium in igneous rocks), Geochemistry, n.8.

49. Lisitsyn, A.P., 1955, RASPREDELENIYE AUTIGENNOGO KREMNEZEMA V DONNYKH OTLOZHENIYAKH ZAPADNOY CHASTI BERINGOVA MORYA (Distribution of authigenic silica in bottom sediments of the western Bering Sea), Dokl., Akad. Nauk , SSSR, v.103, n.3.

50. Malinin, S.I., 1951, K METODIKYE VODNOGO MEKHANICHESKOGO ANALIZA SOVREMEN - NYKH OSADKOV (Aqueous method for mechanical analysis of contemporary sediments), Trudy, Inst. Okeanol., Akad. Nauk , SSSR, n.5.

51. Petelin, V.P., 1961, NOVYY METOD VODNOGO MEKHANICHESKOGO ANALIZA MORSKIKH OSADKOV (New method for aqueous mechanical analysis of marine sediments), Okeanologiya, v.1, n.1.

52. Petelin, V.P. and I.A. Aleksina, 1961, O VYBORYE METODA VODNOGO MEKHANI-CHESKOGO ANALIZA MORSKIKH DONNYKH OSADKOV (Selection of an aqueous method for mechanical analysis of marine bottom sediments), Okeanologiya, v.1, n.4.

53. Pettersen, G., 1956, RADIOAKTIVNOST' I VOSRAST OKEANICHESKOGO DNA (Radio-activity and age of the ocean bottom), in Nuclear Geology, IL.

54. Ponomaryev, A.I., 1951, METODY KHIMICHESKOGO ANALIZA MINERALOV I GORNYKH POROD (Chemical analysis methods of minerals and rocks), publ. Akad. Nauk , SSSR.

55. Romankevich, E.A. and N.V. Petrov, 1961, OKISLITEL'NO-VOSSTANOVITEL'NYY POTENTSIAL I pH OSADKOV SEVERO-VOSTOCHNOY CHASTI TIKHOGO OKEANA (Oxidation-reduction potential and pH of sediments of the northeast Pacific Ocean), Trudy Inst. Okeanol., Akad. Nauk , SSSR, n.45.

56. Romankevich, E.A., 1958, ORGANICHESKOYE VESHCHESTVO V DONNYKH OTLOZHENIYAKH SEVERO-ZAPADNOY CHASTI TIKHOGO OKEANA VOSTOKU OT KAMCHATKI (Organic content in bottom sediments of the northwest Pacific Ocean-east of Kamchatka), Dissertation, M.

57. Romankevich, E.A., 1960, ORGANICHESKOYE VESHCHESTVO V DONNYKH OTLOZHENIYAKH TIKHOGO OKEANA K VOSTOKU OT KAMCHATKI (Organic content of Pacific Ocean sediments west of Kamchatka), Trudy Oceanog. Commiss., Akad. Nauk , SSSR, in Marine Chemistry, publ. Akad. Nauk , SSSR.

58. Romankevich, E.A., 1957, ORGANICHESKOYE VESHCHESTVO V KOLONAKH DONNYKH OTLOZHENIY SEVERO-ZAPADNOY CHASTI TIKHOGO OKEANA K VOSTOKU OT KAMCHATKI (Organic content of bottom sediment cores from the northwest Pacific Ocean east of Kamchatka), Dokl., Akad. Nauk , SSSR, v.116, n.3.

59. Romankevich, E.A., 1962, ORGANICHESKDYE VESHCHESTVO V POVERKH-NOSTNOM SLOYE OSADKOV ZAPADNOY CHASTI TIKHOGO OKEANA (Organic content of the surface sediment layer of wester Pacific Ocean), in Oceanographic Investigations, n.5 (series IGY) pub. Akad. Nauk , SSSR.

60. Romankevich, E. A., 1959, O SOSTAVYE I RASPREDELENII RASTITEL'NYKH PIGMENTOV V OTLOZHENIYAKH SEVERO-ZAPADNOY CHASTI TIKHOGO OKEANA K VOSTOKU OT KAMCHATKI (Composition and distribution of plant pigments in sediments of the northeast Pacific Ocean east of Kamchatka), Dokl., Akad. Nauk , SSSR, v. 124, n.6.

61. Romankevich, E.A., 1963, CHETVERTICHNYYE GLUBOKOVODNYYE OTLOZHENIYA SEVERO-ZAPADNOY CHASTI TIKHOGO OKEANA I IKH ZNACHENIYE DLYA PALEOGEOGRAFII (Deepwater Quaternary sediments of the northwest Pacific Ocean and their significance to paleography), publ. Akad. Nauk , SSSR, Geogr. Series, n.5.

62. Savvin, S.B., 1959, ARSENAZO III (Arsenic III), Dokl., Akad. Nauk , SSSR, v.127.

63. Saidova, Kh. M., 1957, RASPREDELENIYE FORAMINIFER V TOLSHCHYE OSADKOV OKHOTSKOGO MORYA (Distribution of foraminifera in the sediment layer of the Okhotsk Sea), Dokl., Akad. Nauk , SSSR, v.114, n.6.

64. Saidova, Kh. M., 1959, RASPREDELENIYE FORAMINIFER V DONNYKH OTLOZHENIYAKH I PALEOGRAFIYA SEVERO-ZAPADNOY CHASTI TIKHOGO OKEANA (Distribution of forminifera in the bottom sediments and the paleogeography of the northwest Pacific Ocean), Dokl., Akad. Nauk , SSSR, v.129, n.6.

65. Saidova, Kh. M., 1960, STRATIGRAFIYA OSADKOV I PALEOGEOGRAFIYA SEVERO-ZAPADNOY CHASTI TIKHOGO OKEANA I DAL'NEVOSTOCHNYKH MORYI Y SSSR PO DONNYM FORAMINIFERAM (Sedimentary stratigraphy and paleogrography of the northwest Pacific Ocea nad the far eastern seas of the USSR based on bottom foraminifera), in the book-International Geologic Congress, 21 st Session, (Problem X), Dokl., Soviet Geology, publ. Akad. Nauk , SSSR.

66. Saidova, Kh. M., 1961, EKOLOGIYA FORAMINIFER I PALEOGEOGRAFIYA DAL' NYEVOSTOCHNYKH MORYEY I SEVERO-ZAPADNOY CHASTI TIKHOGO OKEANA (Ecology of the foraminifera and paleogeography of the far eastern seas and the northwest Pacific Ocean), publ. Akad. Nauk, SSSR.

67. Semina, G.I., 1955, SOSTAV I RASPREDELENIYE FITOPLANKTONA V SEVERO-ZAPADNOY CHASTI TIKHOGO OKEANA VESNOY I OSEN'YU 1955 G. (Composition and distribution of phytoplankton in the northwest Pacific Ocean in spring and fall, 1955), Dokl., Akad. Nauk, SSSR, v.110, n.3.

68. Sechkina, T.V., 1959, DIATOMOVYYE V DLINNOY KOLONKYE DONNYKH OTLOZHENIY IZ YAPONSKOGO MORYA (Diatoms throughout a bottom sediment core from the Sea of Japan), Dokl., Akad. Nauk, SSSR, v.126, n.1.

69. Starik, E. Ye., Kuznetsov, Yu. V., Grashchenko, S. M. and M.S. Frenklikh, 1958, K VOPROSU OB IONIYEVOM METODYE OPREDELENIYA VOZRASTA MORSKIKH OSADKOV (Problem of the ionium method of determining the age of marine sediments), Geochemistry, n.1.

70. Starik, I. Ye., A.S. Starik, G.C. Plotkina and L.V. Talitskaya, 1955, METODIKA OPREDELENIYA IONIYA (Methods of determining ionium), Bull., Akad. Nauk, SSSR, Commission for Determining the Absolute Age of Geologic Formations, n.1.

71. Starik, I. Ye. and O.S. Melikova, 1941, OB OPREDELENII IONIYA PO RADIYU (Determination of ionium through radium), Dokl., Akad. Nauk, SSSR, v,31, n.9.

72. Stark, I. Ye., A.P. Lisitsyn and Yu. V. Kuznetsov, 1963, O MEKHANIZMA UDALENIYA RADIYA 12 MORSKOY VODY 1 YEGO NAKOPLENIYA V DONNYKH OSADKAKH MORYEY 1 OKEANOV (The process of removal of radium from seawater and its accumulation in the bottom sediments of the seas and oceans), Antarktika, n.2.

73. Starik, I. Ye., Yu. V. Kuznetsov and V.K. Legin, 1959, O FORMAKH NAKHOZHDENIYA URANA I TORIYA V DONNYKH OTLOZHENIYAKH ANTARKTIKI (The form of occurrence of uranium and thorium in Antarctic bottom sediments), Radiochemistry, v.1., n.3.

74. Starik, I. Ye., Yu. V. Kuznetsov, D.S. Nikolayev, V.K. Legin, K.F. Lazarev, S.M. Grashchenko and L.B. Kolyadin, 1959, RASPREDELENIYE RADIOELEMENTOV V OSADKAKH CHERNOGO MORYA (Distribution of radio elements in Black Sea sediments), Dokl., Akad. Nauk, SSSR, v.129, n.5.

75. Starik, I.Ye., A.P. Lisitsyn and Yu.V. Kuznetsov, 1959, TEMPY SEDIMENTATSII V YUZHNOY CHASTI INDIYSKOGO OKEAN (Sedimentation rates in the southern Indian Ocean), in Intern. Oceanog. Congr., preprint, New York.

76. Strakhov, N.M., 1951, IZVESTKOVO-DOLOMITOVYYE FATSII SOVREMENNYKH I DREVNIKH VODOYEMOV-OPYT SRAVNITEL'NO-LITOLOGICHESKOGO ISSLEDOVANIVA (Calcareous

dolomitic facies of Recent and ancient water bodies an experiment in comparative lithologic research), Trudy, Geol. Inst., Akad. Nauk , SSSR, Geol, Series, n.45, issue 124.

77. Strakhov, N.M., N.G. Brodskaya, L.M. Knyazyeva, A.N. Razzhivina, M.A. Rateyev, D. G. Sapozhnikov and Ye. S. Shishova, 1954, OBRAZOVANIYE OSADKOV V SOVREMENNYKH VODOYEMAKH (Sediment formation in contemporary water bodies), publ. Akad. Nauk , SSSR.

78. Strakhov, N.M, 1960, OSNOVY TEORII LITOGENEZA (Fundamental theories of lithogenesis), v.I, publ. Akad. Nauk , SSSR.

79. Strakhov, N.M., 1956, TIPY OSADOCHNYKH PROTSESSOV I FORMATSII OSADOCHNYKH POROD (Types of sedimentation processes and the formation of sedimentary rocks), publ. Akad. Nauk , SSSR, Geol. Series, n.5.

80. Strakhov, N.M., 1956, (n.8 in series of same title as ref. 79).

81. Strakhov, N.M., 1962, ETAPY RAZVITIYA VNESHNIKH GEOSFER I OSADOCHNOGO PORODOBRAZOVANIYA I ISTORII ZEMLI (Evolution of the crust of the geosphere and sedimentary rock formation and history of the Earth), publ. Akad. Nauk , SSSR, Geol. Series, n.12.

82. Sysoyev, N.N., 1959, O TECHENIYAKH V OKEANE (Oceanic currents), Dokl. Akad. Nauk , SSSR, v.125, n.5.

83. Sysoyeva, N.N., 1956, RATSIONAL'NAYA KONSTRUKTSIYA GRUNTOVOY UDARNOY TRUBKI (Efficient construction of an impact soil corer), Trudy, Inst. Okean., Akad. Nauk , SSSR, v.19.

84. Udintsev, G.B., A.P. Lisitsyn, V.F. Kanayev, N.L. Zenkevich and F.I. Ganpantserov, 1956, KONSTRUKTSIYA PORSHNEVOY TRUBKI C AVTOMATICHESKOY STABILIZATSIYEY PORSHNYA (Construction of a piston corer with an automatically stabilized piston), Trudy, Inst. Okean., Akad. Nauk , SSSR, n.19.

85. Udintsev, G.B., 1960, O REL'YEFYE DNA ZAPADNOY CHASTI TIKHOGO OKEANA (Bottom relief of the western Pacific Ocean), in Oceanologic Researches, n.2 (IGY Results series), publ. Akad. Nauk , SSSR.

86. Arrhenius, G., G. Kjellberg and W. Libby, 1951, Age determination of Pacific chalk ooze by radiocarbon and titanium content, Tellus, n.4.

87. Arrhenius, G., 1959, Climatic records on the ocean floor, Scripps Inst. Ocean., Contrib., 811-819.

88. Arrhenius, G. and E. Goldberg, 1955, Distribution of radioactivity in pelagic clays, Tellus, v.7, n.2, 226-231.

89. Arrhenius, G., M. Bramlette and E. Picciotto, 1957, Localization of radioactive and stable heavy nuclides in ocean sediments, Nature, v.180, 85-86.

90. Arrhenius, G., 1959, Sedimentation on the ocean floor, Scripps Inst. Ocean. Contrib.

91. Arrhenius, G., 1952, Sediment cores from the East Pacific, Swed. Deep-Sea Exp. Rept, v.5, fasc.1.

92. Bradshaw, I.S., 1959, Ecology of living planktonic foraminifera in the North and equatorial Pacific Ocean, Cushman Found. Contrib., v.10, pt.2, 25-64.

93. Bramlette, M. and W. Bradley, 1940, Geology and biology of North Atlantic deep-sea cores between Newfoundland and Ireland, Pt. Lithology and geologic interpretation, US Geol. Surv. Prof. Paper, N-196A.

94. Bramlette, N., V. Pelagic sediments, in Oceanography Wash., 345-366.

95. Broecker, W., K. Turekian and B. Heezen, 1958, The relation of deep-sea sedimentation rates to variations in climate, Am. Jr. Sci., v.256, 503-517.

96. Brotzen, F. and A. Dinesen, 1959, on the stratigraphy of some bottom sections from the Central Pacific, Rept. Swed. Deep-Sea Exp. 1947-48, v.X, fasc.3.

97. Correns, C., 1937, Sediments des äquatorialen Atlantischen Ozeans, Wiss. Ergebn. Deutsch Atlan. Exp. METEOR, 1925-27, Bd.3,298.

98. Cushman, I., 1941, A study of the foraminifera contained in cores from the Bartlett Deep , Am. J. Sci. 239, 128-147.

99. Cushman, I. and L. Henbest, 1940, Geology and biology of North Atlantic deep-sea cores between Newfoundland and Ireland, pt. 2-Foraminifera USGS Prof. Paper 196-A, 35-56.

100. Emiliani, C. and T. Mayeda, 1961, Carbonate and oxygen isotope analysis of core 241 A., J. Geol., v.69, n.6.

101. Emiliani, C., 1958, Paleotemperature analysis of core 280 and Pleistocene correlations, J. Geol., v.66, 264-275.

102. Emiliani, C., 1955, Pleistocene temperatures, J. Geol., v.63, n.6.

103. Emiliani, C., 1955, Pleistocene temperature variations in the Mediterranean, Quaternaria, v.2, 87-98.

104. Emiliani, C., 1957, Temperature and age analysis of deep-sea cores, Science, v.125, n.3244.

105. Emiliani, C., J. Wiseman and R. Yaikovsky, 1959, The relationship between paleotemperatures and carbonate content in a deep-sea core: a discussion, J. Geol., v.67, n.5.

106. Ericson, D., M. Ewing, G. Wollin and B. Heezen, 1961, Atlantic deep-sea sediment cores, Bull., Geol. Soc. Am., v.72, n.2.

107. Ericson, D. and G. Wollin, 1956, Correlation of six cores from the equatorial Atlantic and the Caribbean, Deep-Sea Research, n.2.

108. Ericson, D., W. Broecker, J. Kulp and G. Wollin, 1956, Late Pleistocene climates and deep-sea sediments, Science, v.124,385-389.

109. Ericson, D. and G. Wollin, 1956, Micropaleontological and isotopic determinations of Pleistocene climates, micropales., v.2, n.3.

110. Ericson, D., M. Ewing and G. Wollin, 1963, Pliocene-Pleistocene boundary in deep-sea sediments, Science, n.3556.

111. Ericson, D, M. Ewing, B. Heezen and G. Wollin, 1955, Sediment deposition in the deep Atlantic, Geol. Soc. Am., Spec. Paper n.62, 205-220.

112. Ericson, D., 1953, Sediments of the Atlantic Ocean, Col. Univ., Lamont Geol. Observ., Tech. Rept.-Submarine Geology, n.1, 34.

113. Evans, R., A. Kip and E. Moberg, 1938, The radium and radon content of Pacific Ocean water, life and sediments, Am. J. Sci, v. 36, 241-259.

114. Flint, R., 1957, Glacial and Pleistocene geology, John Wiley, N.Y.

115. Foyn, I., B. Karlik, H. Petterson and E. Rona, 1939, The radioactivity of seawater, Nature, v.143, n.3616.

116. Goldberg, E., 1961, Chemical and mineralogical aspects of deep-sea sediments, in Physics and cehmistry of the earth, v.4, Pergamon Press.

117. Goldberg, E. and M. Koide, 1962, Geochronological studies of deep-sea sediments by the ionium/thorium method, Geochim. et Cosmochim, Acta, v.26, 417-450.

118. Goldberg, E. and M. Koide, 1958, Ionium-thorium chronology in deep-sea sediments of the Pacific, Science, v.128, n.3330.

119. Goldberg, E. and E. Picciotti, 1955, Thorium determination in manganese nodules, Science, v. 121, n. 3147, 613.

120. Hamilton, E., 1957, Planktonic foraminifera from an equatorial Pacific core, Microplaeo., v.3., n.1., 69-73.

121. Hough, J., 1953, Pleistocene climatic record in a Pacific Ocean core sample, J. Geol., v.61, n.3.

122. Isaac, N. and E. Picciotti, Ionium determination in deep-sea sediments, Nature, v. 171, 742-743.

123. Joly, J., 1908, The radioactivity of seawater, Philos. Mag., v.15, 385-393.

124. Louse, A., 1960, Les diatomés des depôts de fond de la partie nord-ouest de l'Ocean Pacifique (Diatoms in the bottom deposits of the northwest Pacific), Deep-Sea Research, v.6, 187-192.

125. Koczy, F., E. Picciotti, L. Poulaert and S. Wilgain, 1957, Mesures des isotopes du thorium dans l'eau de mer (Measurements of thorium isotopes in sea water), Geochim.et Cosmochim Acta, v.2, 103-129.

126. Koczy, F., 1958, The natural radium in the ocean as a tracer, 2nd Internat. Conf. Peaceful Uses of Atomic Energy, A/conf. 15/p/2410, USA.

127. Koczy, F., 1949, Thorium in sea water and marine sediments, Geol. foren i Stockholm forhandl., I, 238.

128. Kroll, V., 1954, On age determination in deep-sea sediments, Deep-Sea Res., v.1.

129. Kroll, V., 1955, The distribution of radium in deep-sea cores, Swedish Deep-Sea Exp. 1947-48, Rept. v.10, Spec. Invest. n.1.

130. Kroll, V., 1953, Vertical distribution of radium in deep-sea sediments, Nature, v. 171.

131. Kullenberg, B., 1947, The piston core sampler, Svenska Hydr-Biol. Komm. skr., tr. ser. Hydr., v.1, n.2, 1-46.

132. Kurbatov, L., 1935, Radioactivity of ferro-manganese formations in seas and lakes of the USSR, Nature, v.136, 871.

133. Libby, W., E. Anderson and J. Arnold, 1949, Age determination by radiocarbon content, Science, v.109, 227.

134. Libby, W., 1955, Radiocarbon dating, Univ. Chicago Press.

135. Miyake, I. and Y. Sugimura, 1961, Ionium-thorium chronology of deep-sea sediments of the western North Pacific Ocean, 10th Pacific Sci. Cong., Abstracts, p.379.

136. Niino, H. and K. Emery, 1961, Sediments of the shallow portions of the East China Sea and South China Sea, Bull., Geol. Soc. Am., v.72, n.5.

137. Olausson, E., 1961, Remarks on some Cenozoic core sequences from the Central Pacific, Goteborgs Kungl. Vet. och Vitterhets-Samhal. Handl. Sjalte Föl., ser. B, v.8, n.10.

138. Ovey, C., 1950, On the interpretation of climatic variations as revealed by a study of samples from one equatorial Atlantic deep-sea core, Roy. Meteor. Soc. Cent. Proc., 211-215.

139. Peters, B., 1955, Radioactive beryllium in the atomosphere and on the earth, Proc., Indian Acad. Sci., v.41, 67-71.

140. Petterson, H., 1937, Das verhaltnis thorium zu uran in den gesteinen und im meer, Sitzber. Akad. Wiln, n.400 a.

141. Pettersson, H., 1953, Radium and the deep sea, Am. Scientist, v. 41, 245-255.

142. Pettersson, H., 1951, Radium and deep-sea chronology, Nature, v. 167, 942.

143. Philippi, E., 1910, Die grundproben der Deutschen Sudpolar Expedition 1901-1903, Deutsch Su dpolar Exp., Bd. 2, H.1, Berlin.

144. Phleger, F., 1948, Foraminifera of a submarine core from the Caribbean Sea, Goteborgs Kungl . Vet. och, Vitterhets-Samhalle, Handl. sjatte Fol., ser. B, v.5, n.14.

145. Phleger, F., F. Parker and J. Peirson, 1953, North Atlantic foraminifera, Rept., Swed. Deep-Sea Exp. 1947-48, v.7, 122.

146. Picciotto, E., 1961, Geochemistry of radio active elements in the ocean and the chronology of deep-sea sediments, in Oceanography, Wash., 367-390.

147. Picciotto, E. and S. Wilgain, 1954, Thorium determination in deep-sea sediments, Nature, v. 173, 632.

148. Piggott, C. and W. Urry, 1942, Radioactivity of ocean sediments. IX. The radium content of sediments of the Cayman Trough, Am. J. Sci. v. 240, I-12.

149. Piggott, C. and Urry, W., 1912, Time relations in ocean sediments, Bull., Geol. Soc. Am., v. 53, 1187-1210.

150. Revelle, R., M. Bramlette, G. Arrhenius and E. Goldberg, 1955, Pelagic sediments of the Pacific, Geol. Soc. Am., Spec. Paper 240, 1-12.

151. Riedel, W., M. Bramlette and F. Parker, 1963, Pliocene-Pleistocene boundary in deep-sea sediments, Science, v. 140, n.3572.

152. Rona, E. and W. Urry, 1952, Radioactivity of ocean sediments, VIII. Radium and uranium content of ocean and river waters, Am. J. Sci., v.250, 241-262.

153. Rosholt, J., C. Emiliani, J. Geiss, F. Koczy and P. Wangersky, 1961, Absolute dating of deep-sea cores by the Pa^{231} / Th^{230} method, J. Geol., v.69, n.2.

154. Rubin, M. and H. Suess, 1955, U.S. Geological Survey radiocarbon dates, II, Science, v. 121, 481-488.

155. Rubin, M. and H. Suess, 1956, U.S. Geological Survey radiocarbon dates, III, Science, v. 123, 442-448.

156. Schott W., 1935, Die foraminiferen in dem aequatoriolen teil des Atlantischen Ozeans, Wiss. Ergebn. Deutsch Atlant. Exp. METEOR, 1925-27, bd. 3, teil 3, p. 43-134.

157. Schott, W., 1952, On the sequence of deposits in the equatorial Atlantic Ocean, Goteborgs Kungl. Vet-Och, Vitterhets-Samhal handl., Sjatte Föl., ser. 3, bd.6, n.2, 15.

158. Schott, W., 1954, Über stratigraphische untersuchungsmethoden in rezenten tiefseesedimenten, Heideberg Beitr. Mineral und Petrol., v.4.

159. Sverdrup, H., M. Johnson and R. Fleming, 1942, The oceans-their physics, chemistry and general biology, N.Y.

160. Swallow, I., 1957, Some further deep current measurements using neutrally buoyant floats, Deep-Sea Research, v.4, n.2.

161. Swallow, M., 1961, Deep currents in the open ocean, Oceanus, v.7, n.3.

162. Urry, W. and C. Piggot, 1941, Apparatus for determination of small quantities of radium, Am. J. Sci., v. 239, 633.

163. Urry, W., 1941, Am J. Sci., v. 239, n.3.

164. Urry, W. and C. Piggot, 1942, Radioactivity of ocean sediments, V. Concentrations of the radio-elemts and their significance in red clay, Am. J. Sci., v. 240, n.1, 93-103.

165. Urry, W., 1949, Radioactivity of ocean sediments, VI. Concentration of the radio-elements in marine sediments of the southern hemisphere, Am. J. Sci., v.247, 257-275.

166. Urry, W., 1948, Radioactivity of ocean sediments, VII, J. Marine Research, v.7, 618-640.

167. Urry, W., 1942, The radio-elements in non-equilibrium systems, Am. J. Sci., v. 240,426-436.

168. Volchor, H. and J. Kulp, 1957, The ionium method of age determination, Geochim. et Cosmochim. Acta, v.2, n.4.

169. Wiseman, J. 1958, Secondary oscillations in an equatorial Atlantic deep-sea core, Nature, v.182, n.4648.

170. Wiseman, J., 1954, The setermination and significance of past temperature changes in the upper layer of the equatorial Atlantic Ocean, Proc. Royal Soc. A, v. 222, 296-323.

171. Wiseman, J., 1959, The relation between paleotemperature and carbonate in equatorial Atlantic pilot core, J. Geol., v. 67, 685-690.

APPENDIXES

KEY TO SEDIMENT TYPES

B - Brown
C - Coarse
Ca - Calcaeeous
Cl - Clay
D - Dark
Di - Diatomaceous
E - Fine
Fo - Forminiferal
Gn - Green
Gy - Gray
L - Light
M - Mud
Me - Medium
S - Sand
Si - Silt
Sil - Siliceous
Sl - Slightly

APPENDIX I

Characteristics of the Surface Sediment Layer of the Western Pacific Ocean and the Radio-Isotope Content of the Sediments

Station	Sediment Type	Granulometric Composition (%)						Air-Dried Sediment (%)						Air-Dried Sediment (10^{-6} g/g U units)				
		>0.1 мм	0.1–0.05 мм	0.05–0.01 мм	0.01–0.005 мм	0.005–0.001 мм	<0.001 мм	Mn	Fe	TiO_2	$CaCO_3$	SiO_2 аморф	$C_{орг}$	U	Th	Io	Ra	Io/Th
		Terrigenous Sediments Терригенные осадки																
		Non-Carbonate and Non-Siliceous Sediments * Бескарбонатные и бескремнистые осадки (<10% $CaCO_3$) (< 10 % SiO_2 аморф)																
3127	FS, DGy	—	—	—	—	—	—	0,10	4,69	0,76	0,16	—	0,51	2,7	1,0	1,7	1,8	12,0
3128	MS, DGy	—	—	—	—	—	—	—	—	—	—	—	—	3,5	1,6	1,0	0,6	4,2
3136	"	—	—	—	—	—	—	0,11	5,49	0,69	0,18	1,41	0,38	3,0	1,2	2,3	0,6	14,0
3137	FS, DGy	—	—	—	—	—	—	0,08	5,96	—	0,25	—	0,71	4,8	1,0	2,0	—	14,0
3222	MS, Gn, Gy	64,3	8,42	6,16	21,06 *	—	—	0,08	6,09	0,66	0,00	4,38	0,66	1,0	1,6	3,2	—	14,0
3138	CSi, Gn/Gy	—	—	—	—	—	—	0,14	8,84	1,22	0,36	—	0,72	2,6	1,0	3,0	2,4	21,0
3212	FSiM, B	5,83	28,61	25,42	9,31	18,75	12,08	0,26	4,16	0,62	0,26	6,49	0,65	2,6	4,8	16,0	—	23,1
3189	FSiM, GyB	41,33	8,67	22,83	27,17 *	—	—	0,19	4,16	0,63	0,25	—	0,31	1,8	2,4	8,8	—	25,9
3151	SiClM, DGy	17,7	10,53	14,7	51,3 *	—	—	0,27	4,15	0,69	0,0	7,31	0,35	3,6	3,3	24,0	10,2	51,4
3451	SiClM, B	1,86	9,07	21,86	67,21 *	—	—	—	4,17	—	0,11	7,23	0,65	1,2	2,2	10,0	—	31,5
3456	ClM, LB	0,51	1,28	20,26	77,95 *	—	—	0,42	4,19	0,65	0,63	0,22	0,37	3,6	5,4	26,5	13,0	35,0
3520	ClM, B	0,24	0,73	21,05	77,08 *	—	—	0,28	4,12	—	1,41	4,25	0,49	3,0	5,4	14,2	6,4	18,0
3530	SiClM, LB	1,13	2,26	26,84	69,74 *	—	—	0,31	4,22	—	0,20	2,34	0,39	1,4	6,0	20,0	—	23,1
3532	SiClM, DB	1,30	1,30	32,18	65,23 *	—	—	0,43	2,00	—	0,20	3,00	0,29	3,2	6,6	21,3	17,0	22,4
		Slightly Siliceous Diatom Muds (ooze) Слабокремнистые диатомовые илы																
3166	MSiSlSil DiM, B	21,76	24,59	19,76	12,24	18,12	3,53	0,19	4,30	0,54	0,00	12,20	0,36	2,0	1,5	4,2	—	19,6
3168	"	6,06	30,82	32,22	9,13	17,03	4,74	0,29	3,94,	0,53	0,22	14,25	0,44	—	1,3	7,0	—	37,8
2116	SiCl, SlSil DiM, LB	0,5	3,2	34,5	61,8 *	—	—	0,35	6,04	0,57	0,31	16,46	0,09	3,3	2,0	19,0	—	66,5
3114	"	2,5	6,9	19,2	71,4 *	—	—	0,37	—	—	—	10,18	—	4,8	1,6	15,0	9,0	65,8
3145	SiCl, Sl SilDiM GnGy	4,9	9,7	21,2	64,3 *	—	—	0,04	3,63	0,57	0,20	16,88	1,23	2,6	1,4	5,0	—	28,0
3162	Cl, SlSil DiM, DB	1,87	8,13	32,29	12,08	38,96	6,67	0,58	2,97	0,40	10,91	17,07	0,10	5,0	3,5	20,0	—	39,9
3163	SiCl, SlSil DiM, B	1,04	10,75	30,45	16,42	31,94	9,40	0,53	3,05	—	0,56	17,85	0,55	—	3,0	19,0	—	44,1
3443	SiCl, SlSil DiM, GyGn	0,86	4,73	24,95	60,46 *	—	—	0,04	3,00	0,52	1,04	12,93	2,39	1,5	3,6	6,4	—	12,6

* See key on preceding page.

APPENDIX I (con)

Station	Sediment Type	Granulometric Composition (%)						Air-Dried Sediment (%)						Air-Dried Sediment (10^{-6} g/g Hunts)				
		>0,1 мм	0,1—0,05 мм	0,05—0,01 мм	0,01—0,005 мм	0,005—0,001 мм	<0,001 мм	Mn	Fe	TiO_2	$CaCO_3$	SiO_2 аморф.	$C_{орг}$	U	Th	Io	Ra	Io/Th
							Биогенные осадки											
3148	S,Ca Fo, LB **	57,2	16,8	3,0	23,0 *	—	—	0,07	1,20	0,16	66,07	—	0,34	2,7	1,2	12,0	11,4	70,0
3208	FSu M,Ca Fo, L Gy	10,4	24,3	17,2	48,1 *	—	—	0,06	1,04	0,12	78,97	1,06	0,52	—	1,0	22,0	—	154,0
3189	FSu M,Si, Di, Gn Gy	10,67	13,17	28,17	11,33	24,50	12,16	0,04	2,21	0,40	2,00	34,44	1,33	6,0	1,5	4,0	3,0	18,9
	Polygenic Sediments (Deepwater Red Clays, Slightly Siliceous and Slightly Calcareous Deepwater Oozes).																	
3154	Cl M, DGy **	7,3	3,9	16,3	72,5 *	—	—	0,99	3,83	0,52	0,11	9,93	0,48	6,6	7,2	40,0	2,1	38,5
3156	"	0,5	1,4	16,2	81,9 *	—	—	1,28	3,86	0,58	0,34	12,39	0,39	8,0	7,0	45,0	19,5	45,0
3206	"	2,5	1,0	19,0	77,5 *	—	—	0,47	4,11	0,61	0,55	4,02	0,40	5,2	10,0	24,0	—	16,8
3471	"	0,29	2,01	27,44	11,78	37,50	20,98	0,43	4,09	0,63	0,41	6,41	0,67	3,8	5,0	34,0	—	47,6
3476	"	0,42	3,16	7,16	89,26 *	—	—	0,38	3,60	0,54	0,54	4,01	0,31	3,2	7,6	32,0	—	29,4
3481	Si Cl M, B	0,21	7,29	33,96	58,54 *	—	—	0,29	3,88	0,56	0,11	—	0,37	2,4	6,0	23,0	—	26,6
3495	"	5,00	3,05	26,29	64,76 *	—	—	0,42	4,89	0,74	0,38	3,17	0,40	1,8	5,4	20,0	—	25,9
3625	Cl M, B	Необн.	0,81	12,16	87,03 *	—	—	0,49	5,88	0,76	0,36	1,68	0,16	3,2	8,6	26,0	29,0	21,0
3716	"	0,54	3,24	13,78	82,44 *	—	—	0,63	5,40	0,77	0,27	1,82	0,31	3,6	8,0	27,3	40,0	23,8
3797	"	2,16	1,62	13,51	82,70 *	—	—	0,44	3,06	—	23,58	5,8	0,38	3,0	4,0	97,5	50,0	170,8
3873	Cl M, DB	—	—	—	—	—	—	0,73	4,57	—	0,64	1,17	0,20	3,6	15,0	86,0	72,0	39,9
3995	Cl M, B	0,32	0,32	13,55	85,81 *	—	—	1,77	5,12	—	0,63	—	0,33	3,0	3,2	36,2	25,2	79,1
4068	Cl M, DB	1,28	2,91	18,84	9,88	8,84	58,25	0,40	4,60	—	0,45	0,2	0,33	4,5	1,4	29,5	9,8	147,0

* Fracture less than 0.01 mm.

** See key on first page of appendixes

APPENDIX II

Characteristics of the Sediment Core at Station 3163

Depth from surface layer to bottom of core (cm)	Sediment Type		Granulometric Composition (%)				Air-Dried Sediment (%)			
			>0.1 мм	0.1—0.05 мм	0.05—0.01 мм	<0.01 мм	$CaCO_3$	C_{org}	битумы* (хлороформная часть)	$SiO_{аморф}$
0—10	Алевритово-глинистый ил	Silty Clayey Mud	0,4	1,5	28,5	69,6	0,59	0,55	0,0050	17,85
10—20	То же	" " "	0,3	3,2	28,1	68,4	0,73	0,34	0,0025	17,82
20—33	» »	" " "	1,3	2,7	28,0	68,0	0,54	0,20	0,0012	8,08
33—37	Крупный алеврит	Coarse Silt	38,60	40,20	14,80	6,4	0,43	0,06	—	3,25
44—50	Мелкоалевритовый ил*	Fine Silty Mud	—	—	—	—	0,47	0,27	0,0025	4,70
50—57	Алевритово-глинистый ил	Silty Clayey Mud	9,0	6,7	20,2	64,1	0,63	0,56	0,0050	5,27
57—64									0,0037	
64—69	Мелкоалевритовый ил*	Fine Silty Mud	—	—	—	—	—	—	—	—
69—79	Алевритово-глинистый ил	Silty Clayey Mud	12,3	9,8	22,1	55,8	1,09	0,59	0,0025	6,50
79—83	То же*	" " "	—	—	—	—	—	—	—	—
86—96	» »	" " "	12,4	9,5	20,2	57,9	0,11	0,27	0,0012	5,93
96—106	» »	" " "	5,4	7,5	20,2	66,9	—	—	—	—
114—125	» »	" " "	7,2	9,3	29,3	54,2	0,00	0,35	0,0009	5,48
125—131	Мелкоалевритовый ил	Fine Silty Mud	10,1	4,2	36,2	49,5	0,11	0,27	0,0006	6,35
133—150	Алевритово-глинистый ил	Silty Clayey Mud	8,0	8,0	26,1	57,9	—	—	—	—
155—164	То же	" " "	9,6	8,1	25,2	57,1	0,47	0,50	0,0012	11,62
181—193	» »	" " "	12,4	9,1	25,1	53,4	0,00	0,33	0,0012	9,75
193—201	» »	" " "	7,3	7,3	22,4	63,0	—	—	—	—
200—210	Алевритово-глинистый ил*	Silty Clayey Mud	—	—	—	—	0,00	0,38	0,0006	8,61
217—220	То же	" " "	6,9	6,1	23,3	63,7	—	—	—	—
224—238	» »	" " "	12,1	8,0	25,6	54,3	—	—	0,0012	—
238—246	» »	" " "	12,4	10,4	25,3	51,9	0,91	0,69	—	5,60
246—255	» »	" " "	5,6	6,5	25,8	62,1	0,07	0,54	0,0018	—
257—270	» »	" " "	8,7	5,0	24,2	62,1	0,34	0,59	0,0018	6,08
274—280	» »	" " "	9,0	4,8	22,6	63,6	—	—	—	—
280—290	Мелкоалевритовый ил	Fine Silty Mud	14,8	7,8	32,8	44,6	0,25	0,34	0,0018	7,85
302—305	Алевритово-глинистый ил	Silty Clayey Mud	3,0	4,2	25,2	67,6	—	—	—	—
305—308	То же	" " "	5,4	6,4	29,4	58,8	—	—	—	—
312—323	Крупный алеврит*	Coarse Silt	—	—	—	—	—	—	0,0006	4,61
327—335	Мелкоалевритовый ил*	Fine Silty Mud	—	—	—	—	0,45	0,42	0,0012	—
335—350	Алевритово-глинистый ил	Silty Clayey Mud	9,2	7,2	22,4	61,2	—	—	—	—
350—360	То же*	" " "	—	—	—	—	—	—	0,0012	—
364—380	» »	" " "	6,2	7,0	20,0	66,8	0,34	0,45	0,0025	5,42
392—410	Мелкоалевритовый ил	Fine Silty Mud	9,0	16,4	41,4	33,2	0,27	0,53	0,0050	10,85
410—416	То же*	" " "	—	—	—	—	—	—	—	—
424—433	Алевритово-глинистый ил*	Silty Clayey Mud	—	—	—	—	0,11	0,63	0,0050	16,31
440—450	То же	" " "	7,2	6,8	23,6	62,4	—	—	—	—
465—479	Глинистый ил	Clayey Mud	1,0	3,2	22,8	73,0	0,07	0,31	0,0006	9,79
500—510	Алевритово-глинистый ил	Silty Clayey Mud	8,1	8,1	21,3	62,5	0,50	0,37	0,0006	5,41
510—518	Тоже	" " "	11,8	6,1	23,1	59,0				
518—528	» »	" " "	4,0	4,4	21,4	71,2	—	—	—	—
528—532	» »	" " "	7,3	6,3	23,1	63,3	—	—	0,0006	7,82

* Bitumen (trichloromethane portion) • Based on visual and microscopic examination.

APPENDIX II (con)

Depth from Surface Layer to Bottom of Core (cm)	Sediment Type		Granulometric Composition (%)				Air-Dried Sediment (%)			
			>0,1 мм	0,1—0,05 мм	0,05—0,01 мм	<0,01 мм	$CaCO_3$	$C_{орг}$	битумы (хлороформенная вытяжка)	SiO_2 аморф
532—550	Алевритово-глинистый ил	Silty Clayey Mud	7,6	6,4	20,6	65,4	—	—	—	—
550—560	То же*		—	—	—	—	0,82	0,46	—	8,99
569—576	» »		5,8	5,6	20,6	68,0	—	—	—	—
576—590	» »		8,6	6,0	20,5	64,5	—	—	—	—
590—605	» »		10,4	5,3	18,8	65,5	—	—	—	—
610—620	» »		9,2	6,4	18,0	66,4	0,27	0,33	—	5,98
620—632	» »		—	—	—	—	0,11	0,37	0,0006	—
639—645	» »		6,2	6,8	22,8	64,2	—	—	—	—
653—660	» »						0,61	0,38	0,0009	5,83
660—671	» »		6,6	5,4	21,2	66,8	—	—	—	—
687—700	» »		7,2	7,4	19,4	66,0	0,64	0,42	—	5,73
700—710	» »		6,4	10,6	19,8	63,2	—	—	—	—
742—747	Крупный алеврит*	Coarse Silt	—	—	—	—	—	—	0,0009	2,91
747—760	Алевритово-глинистый ил*	Silty Clayey Mud	—	—	—	—	0,07	0,33	0,0012	—
760—763	То же*		—	—	—	—	0,00	0,35	0,0012	4,95
763—770	» »		6,2	6,2	19,6	68,0	—	—	—	—
783—800	Мелкоалевритовый ил	Fine Silty Mud	6,8	8,8	35,2	49,2	0,20	0,26	0,0025	4,68
810—820	Алевритово-глинистый ил	Silty Clayey Mud	5,0	6,8	34,0	54,2	—	—	0,0025	4,92
820—835	То же*		—	—	—	—	0,32	0,28	0,0025	—
840—850	» »		17,2	5,0	20,2	57,6	0,77	0,46	—	7,37
875—893	» »		9,0	4,8	18,8	67,6	0,64	0,54	0,0025	6,92
913—918	» »		5,4	7,0	19,0	68,6	0,75	0,62	—	5,52
925—940	Глинистый ил	Clayey Mud	2,6	5,8	21,2	70,4	—	—	—	—
940—960	Алевритово-глинистый ил*	Silty Clayey Mud	—	—	—	—	—	0,57	0,0012	5,34
960—970	То же	" " "	4,2	6,2	34,6	55,0	—	—	—	—
970—978	Алевритово-глинистый ил	Silty Clayey Mud	—	—	—	—	—	—	0,0012	—
983—996	Глинистый ил	Clayey Mud	4,2	5,2	18,8	71,8	0,20	0,39	0,0012	6,25
1010—1115	То же*	" "	—	—	—	—	0,25	0,35	—	—
1021—1041	Алевритово-глинистый ил	Silty Clayey Mud	4,0	6,0	25,6	64,4	0,00	0,63	0,0012	7,15
1050—1060	То же		4,0	3,6	22,8	69,6	0,23	0,73	0,0025	9,53
1079—1084	» »		2,0	4,4	24,0	69,6	0,82	0,64	0,0050	13,71
1110—1115	» »		2,0	3,8	26,6	67,6	0,55	0,49	0,0037	13,61
1135—1150	Глинистый ил	Clayey Mud	4,4	3,8	18,8	73,0	0,00	0,33	0,0006	7,61
1155—1185	Алевритово-глинистый ил*	Silty Clayey Mud	—	—	—	—	0,29	0,36	0,0006	—
1185—1195	Мелкоалевритовый ил	Fine Silty Mud	4,0	9,2	37,0	49,8	—	—	—	6,28

APPENDIX III

Characteristics of the Sediment Core at Station 4068

Depth from Surface of Core to Bottom of Core	Sediment Type	Granulometric Composition (%)						Air-Dried Sediment (%)					Air-Dried Sediment (% 10^{-6} g/g Units)				Non-Siliceous & Non-Carbonate Sediments (%)	
		>0.1 мм	0.1–0.05 мм	0.05–0.01 мм	0.01–0.005 мм	0.005–0.001 мм	<0.001 мм	$CaCO_3$	$C_{орг}$	$SiO_{2аморф}$	Fe	Mn	Th	Io	Ra	U	Fe	Mn
491 2–7	Глинистый ил	1,28	2,91	18,84	9,88	8,84	58,25	0,45	0,33	6,2	4,60	0,40	1,4	29,5	9,8	4,5	4,92	0,43
7–14	» »	—	—	—	—	—	—	0,23; 0,29	0,21	5,6	—	0,26	1,4	24,2	9,6	—	—	0,27
20–25	» »	4,27	3,82	18,43	12,92	39,66	20,90	0,25	0,17	5,8	4,65	0,24	4,6	16,0	11,4	—	4,95	0,25
40–45	» »	1,59	3,41	19,02	15,37	40,85	19,77	0,03; 0,02	0,15	7,0	4,54	0,30	4,6	14,0	8,0	—	4,88	0,32
58–63	» »	2,76	4,68	20,53	15,96	37,13	18,94	0,09	0,14	5,5	4,50	0,26	4,6	10,0	3,7	—	4,76	0,27
78–83	» »	0,65	3,11	20,26	13,38	44,55	18,05	0,11	0,15	—	4,42	0,40	5,0	11,6	13,8	3,8	—	—
90–95	» »	—	—	—	—	—	—	0,09	0,12	8,3	4,44	0,48	5,4	11,8	8,1	—	4,84	0,52
98–103	» »	1,00	4,86	21,29	15,00	41,28	16,57	—	—	—	—	—	—	—	—	—	—	—
116–121	» »	1,23	3,70	19,26	12,47	45,93	17,41	0,10	0,13	6,3	4,57	0,29	5,4	8,1	4,4	—	4,88	0,31
136–141	» »	1,21	3,08	19,23	11,09	41,98	23,41	0,08	0,12	5,3	4,57	0,28	—	—	—	—	4,83	0,30
156–161	» »	1,42	3,63	17,69	13,85	42,42	20,99	0,14; 0,11	0,13	—	4,57	0,45	8,0	3,6	3,4	—	—	—
174–179	» »	0,92	5,98	20,57	18,87	42,89	16,67	0,14	0,13	6,9	4,57	0,22	—	—	—	—	4,91	0,24
194–199	» »	1,91	3,71	17,53	14,72	39,44	22,69	0,12	0,11	5,3	4,68	0,36	8,0	4,0	3,7	3,3	4,91	0,38
218–223	» »	1,76	4,94	21,53	18,59	35,65	17,53	0,06	0,10	6,5	4,42	0,32	—	—	—	—	4,72	0,34
238–243	» »	4,21	5,47	20,95	12,42	38,42	18,53	0,04	0,11	4,6	4,70	0,25	5,4	4,9	2,5	—	4,92	0,26
258–263	» »	0,85	3,66	19,88	13,17	42,56	19,88	0,09	0,11	—	4,63	0,43	—	—	—	—	—	—
273–278	» »	1,25	4,87	23,12	14,13	43,63	13,00	0,09	0,11	6,4	4,45	0,37	5,4	4,9	2,0	—	4,76	0,40
293–298	Алевритово-глинистый ил	2,38	9,70	26,43	13,17	31,88	16,44	0,18	0,10	—	4,68	0,25	—	—	—	—	—	—
313–318	Глинистый ил	1,25	4,25	21,37	13,75	39,00	20,38	0,18	0,15	6,9	4,58	0,35	—	—	—	—	4,92	0,38
328–332	» »	—	—	—	—	—	—	0,11	0,13	8,6	—	0,37	5,4	4,9	2,4	4,0	—	0,30

Clayey Mud
Silty Clayey Mud
Clayey Mud
"
"

APPENDIX IV

Characteristics of the Sediments of the Core at Station 3378

Depth Below Surface of Core (cm)	Sediment Type		Granulometric Composition (%)				Air-Dried Sediment (%)				Eh, mv	pH
			>0.1 мм	0.1—0.05 мм	0.05—0.01 мм	<0.01 мм	$CaCO_3$	$C_{орг}$	SiO_2 аморф	битумы (хлороформенная часть)		
0—2	Глинистый ил	Clayey Mud	2,18	4,32	23,00	70,50	—	—	—	—	—	—
2—10	» »		—	—	—	—	0,18	—	—	0,0012	—480	7,5
10—18	» »		0,69	5,17	15,17	78,97	—	—	—	—	—	—
18—32	» »		0,28	3,10	20,10	75,78	0,11	0,60	12,84	0,0025	—	—
40—48	» »		0,26	3,20	22,40	74,14	—	—	9,82	—	—	—
48—56	» »		—	—	—	—	0,04	0,47	—	0,0025	—	—
56—64	» »		0,25	2,25	22,50	75,00	—	—	8,38	—	—	—
64—72	» »		—	—	—	—	0,04	0,47	—	0,0037	—	—
72—80	Алевритово-глинистый ил	Silty Clayey Mud	15,06	2,71	18,76	63,47	—	—	5,05	—	—	—
88—95	То же	" " "	2,44	4,63	23,41	69,52	—	—	—	—	—	—
100—106	Глинистый ил	Clayey Mud	0,24	2,19	23,17	74,40	0,09	0,48	6,16	0,0025	—	—
112—120	Алевритово-глинистый ил	Silty Clayey Mud	3,41	4,63	23,66	68,30	—	—	—	—	—	—
120—128	То же		—	—	—	—	1,05	0,59	10,66	0,0025	—92	7,0
128—136	» »		0,85	5,11	27,23	66,81	—	—	—	—	—	—
136—142	» »		—	—	—	—	0,64	0,68	10,38	0,005	—	—
142—150	Глинистый ил	Clayey Mud	0,84	2,25	17,74	79,17	—	—	—	—	—	—
158—167	То же		0,35	1,40	15,81	82,81	1,59	0,87	17,01	0,01	—	—
167—175	» »		—	—	—	—	1,24	0,68	—	—	—	—
175—183	» »		2,53	1,26	22,95	73,26	0,91	0,50	8,85	0,03	—136	7,4
183—191	» »		—	—	—	—	0,52	0,50	3,86	—	—142	7,7
191—198	» »		0,91	2,73	14,24	82,12	0,32	0,47	—	0,015	—	—
198—206	» »		—	—	—	—	0,23	0,45	4,51	0,0025	—	—
206—214	» »		3,93	4,35	19,02	72,70	—	—	—	0,0025	—	—
221—229	Алевритово-глинистый ил	Silty Clayey Mud	1,10	7,34	21,65	69,91	—	—	—	—	—	—
237—245	Глинистый ил	Clayey Mud	2,32	3,58	21,89	72,21	—	—	—	—	—	—
245—253	То же		—	—	—	—	0,0	0,43	3,60	0,0012	—	—
253—261	» »		1,20	3,00	23,20	73,60	—	—	—	—	—	—
268—275	Алевритово-глинистый ил	Silty Clayey Mud	1,84	3,67	26,94	67,55	—	—	—	—	—	—
283—290	Глинистый ил	Clayey Mud	1,24	3,30	25,15	70,31	—	—	—	—	—	—
290—298	Алевритово-глинистый ил	Silty Clayey Mud	2,47	2,06	31,13	64,34	—	—	—	—	—	—
298—304	То же		6,26	2,42	32,73	58,59	—	—	—	0,0006	—	—
304—310	» »		—	—	—	—	0,0	0,35	4,58	0,0006	—73	7,9
310—320	» »		—	—	—	—	—	—	—	0,0006	—	—
320—332	» »		2,20	4,00	32,60	61,20	—	—	—	—	—	—

APPENDIX V

Characteristics of the Sediment of the Core at Station 3325

Depth Below Surface of Core (cm)	Sediment Type	Granulometric Composition (%)				Air-Dried Sediment (%)				Eh, mv	pH
		>0.1 мм	0.1—0.05 мм	0.05—0.01 мм	<0.01 мм	$CaCO_3$	C_{org}	SiO_2 аморф.	Сапропелевая часть (хлороформ-экстракт)		
0—8	Алевритово-глинистый ил (Silty Clayey Mud)	1,46	11,04	25,83	61,67	0,95	0,35	10,92	0,0006	—	—
9—16	То же	—	—	—	—	—	—	—	0,0006	+555	7,2
16—24	» »	1,63	3,90	33,82	60,65	—	—	—	—	—	—
24—32	» »	0,77	5,57	25,19	68,47	5,05	0,26	8,75	0,0006	—	—
32—40	Глинистый ил (Clayey Mud)	0,90	2,70	20,89	75,51	—	—	—	0,0025	—	—
40—50	» »	1,94	1,94	15,81	80,31	9,89	0,63	20,16	0,01	—	—
50—58	» »	2,22	2,00	15,33	80,44	9,87	0,86	22,48	0,015	—	—
58—66	» »	1,05	2,32	18,74	77,89	3,55	0,66	8,42	0,02	+386	7,6
66—74	» »	0,85	1,52	22,03	75,60	1,02	0,75	3,85	0,02	+331	7,9
74—82	» »	0,85	1,69	19,83	77,63	0,75	0,70	3,54	0,01	—	—
82—90	» »	1,19	2,22	22,90	73,69	—	—	—	0,0075	—	—
96—102	Алевритово-глинистый ил (Silty Clayey Mud)	1,15	3,93	28,20	66,72	—	—	—	—	—	—
102—110	Глинистый ил (Clayey Mud)	0,83	5,33	22,33	71,50	0,29	0,50	4,45	0,0025	+140	—
110—118	» »	1,48	2,41	20,92	75,19	—	—	—	—	—	—
118—125	» »	1,16	1,94	20,77	76,13	0,32	0,53	4,04	0,0025	—	—
125—132	» »	0,80	1,60	23,80	73,80	—	—	—	—	—	—
140—145	» »	1,04	2,08	18,96	77,92	—	—	—	—	—	—
145—152	» »	—	—	—	—	0,36	0,44	3,16	0,0035	—	—
152—160	» »	1,40	2,80	25,20	70,60	—	—	—	—	—	—
160—170	» »	—	—	—	—	0,29	0,42	—	0,0035	+21	6,7
170—180	Алевритово-глинистый ил (Silty Clayey Mud)	1,19	1,69	27,29	69,83	—	—	—	—	—	—
180—188	То же (" " ")	—	—	—	—	0,36	0,53	3,66	0,0025	−14	6,8

APPENDIX VI

Characteristics of the Sediments in Core at Station 3342

Depth Below Surface of Core (cm)	Sediment Type		Granulometric Composition (%)				Air-Dried Sediment (%)				mv	
			>0,1 мм	0,1—0,05 мм	0,05—0,01 мм	<0,01 мм	$CaCO_3$	$C_{орг}$	SiO_2 аморф	Битумы (хлороформенная часть)	Eh, мв	pH
0—9	Алевритово-глинистый ил	Silty Clayey Mud	3,01	19,3	24,09	53,55	0,16	0,57	9,70	—	—	—
9—16	То же		—	—	—	—	0,07	0,54	9,27	0,0025	+144	7,1
16—25	» »		5,71	1,67	30,48	62,14	—	—	—	—	—	—
25—32	» »		7,06	8,24	29,41	55,29	0,39	0,31	—	0,0025	—	—
32—40	» »		—	—	—	—	—	—	—	—	—	—
40—47	» »		—	—	—	—	0,0	0,43	6,11	0,0031	—	—
47—56	» »		2,86	7,43	26,67	63,04	—	—	—	—	—	—
56—63	» »		8,39	12,10	26,77	52,74	—	—	3.71	0,0037	—	—
63—72	Глинистый ил	Clayey Mud	0,81	3,90	24,88	70,41	—	—	—	—	—	—
72—80	» »		—	—	—	—	—	—	—	—	—	—
80—88	» »		—	—	—	—	—	—	—	0,0037	—	—
88—95	Алевритово-глинистый ил	Silty Clayey Mud	0,96	6,58	24,93	67,53	0,98	0,56	2,90	0,005	—	—
95—101	То же		—	—	—	—	1,12	0,59	3,20	0,005	—	—
101—110	» »		—	—	—	—	—	—	—	0,01	−33	7,3
110—118	Глинистый ил	Clayey Mud	2,09	4,17	21,57	72,17	1,25	0,64	6,05	0,01	—	—
118—128	» »		—	—	—	—	0,95	0,65	7,40	0,02	—	—
128—132	» »		1,21	2,93	21,55	74,31	—	—	—	—	—	—
132—140	» »		—	—	—	—	0,52	0,59	6,05	0,06	+434	7,2
140—147	» »		—	—	—	—	—	—	—	—	+390	7,5
147—152	» »		1,25	2,96	22,78	73,01	0,38	0,65	2,96	0,03	—	—
152—158	» »		—	—	—	—	—	—	—	0,02	—	—
158—165	» »		1,13	5,16	23,55	70,16	0,36	0,47	—	0,01	—	—
165—170	» »		—	—	—	—	—	—	—	0,005	—	—
170—178	Алевритово-глинистый ил	Silty Clayey Mud	4,39	8,64	25,45	61,52	—	—	—	0,005	—	—
178—185	То же		—	—	—	—	0,14	0,37	—	0,005	—	—
185—194	» »		3,36	8,48	25,92	62,24	—	—	—	—	—	—
200—205	» »		2,20	6,30	24,72	66,78	—	—	—	—	—	—
205—211	» »		—	—	—	—	0,38	0,34	3,20	0,005	+95	7,3
211—217	» »		2,75	6,24	25,97	65,04	—	—	—	—	—	—
217—234	» »		—	—	—	—	—	—	—	0,005	—	—
234—244	» »		2,81	6,41	24,37	66,41	0,20	0,48	4,1	0,005	+128	7,2

APPENDIX VII

Characteristics of the Sediment Core at Station 3359

Depth Below Surface of Core (cm)	Sediment Type	Granulometric Composition (%)				Air-Dried Sediment (%)				mv	pH
		>0.1 мм	0.1—0.05 мм	0.05—0.01 мм	< 0.01 мм	$CaCO_3$	$C_{орг}$	SiO_2 аморф	битумы (хлороформенная часть)	Eh. мв	
0—10	Алевритово-глинистый ил (Silty Clayey Mud)	0,31	2,81	34,37	62,51	0,23	0,57	18,16	0,0021	+490	7,2
10—15	То же	Следы	1,13	29,58	69,29	—	—	—	0,0018	—	—
21—28	» »	»	2,29	35,08	62,62	0,27	0,44	16,80	0,0031	—	—
28—35	» »	»	1,39	32,79	65,81	—	—	—	—	—	—
43—50	Глинистый ил (Clayey Mud)	0,19	1,70	23,58	74,53	—	—	8,05	0,0025	—	—
55—62	» »	0,21	1,05	20,42	78,31	—	—	—	—	—	—
62—70	» »	—	—	—	—	0,18	0,51	7,57	0,0037	+119	7,0
79—87	Алевритово-глинистый ил (Silty Clayey Mud)	0,24	3,02	31,16	65,58	—	—	—	—	—	—
87—93	То же	0,27	2,70	42,70	54,30	0,36	0,61	17,89	0,005	—	—
100—108	» »	0,25	2,68	35,85	61,22	—	—	—	—	—	—
108—114	» »	—	—	—	—	1,73	0,85	16,72	0,005	—	—
114—119	Глинистый ил (Clayey Mud)	0,81	3,03	8,89	87,27	1,82	0,80	13,85	0,010	—	—
119—127	Алевритово-глинистый ил (Silty Clayey Mud)	0,53	1,58	30,88	67,01	—	—	—	0,018	—	—
127—135	То же	—	—	—	—	0,18	0,79	3,91	0,020	—68	7,1
135—142	Глинистый ил (Clayey Mud)	0,67	1,34	20,84	77,15	—	—	—	0,015	—	—
142—150	То же	—	—	—	—	0,14	0,67	3,76	0,010	—	—
150—156	Алевритово-глинистый ил (Silty Clayey Mud)	0,57	9,81	27,92	61,70	—	—	—	0,0075	—	—
156—162	То же	—	—	—	—	—	—	—	0,0075	—	—
170—178	» »	0,40	6,00	33,40	60,20	—	—	—	0,0075	—	—
185—192	Глинистый ил (Clayey Mud)	0,60	4,44	24,65	70,31	—	—	—	0,0075	—	—
200—212	» »	4,15	0,57	21,51	73,77	0,11	0,67	4,42	0,005	—84	7,0
212—219	» »	0,79	1,98	26,34	70,89	—	—	—	—	—	—
219—227	» »	—	—	—	—	—	—	—	0,005	—	—
227—235	Алевритово-глинистый ил (Silty Clayey Mud)	2,38	2,38	30,46	64,77	—	—	—	—	—	—
235—242	То же	—	—	—	—	—	—	—	0,005	—	—
242—250	» »	1,03	15,67	23,30	60,00	—	—	—	—	—	—
250—257	» »	—	—	—	—	—	—	—	0,0037	—	—
257—262	» »	1,89	2,53	40,21	55,37	—	—	—	—	—	—
262—269	» »	—	—	—	—	0,32	0,59	4,62	0,0025	—209	7,6
269—276	» »	0,82	1,44	31,96	65,78	—	—	—	0,0025	—219	7,6

APPENDIX VIII

Characteristics of the Sediment Core at Station 3451

Depth Below Surface of Core (cm)	Sediment Type		Granulometric Composition (%)					Air-Dried Sediment (%)				Air-Dried Sediment 10^{-6} g/g Uranium			Non-Siliceous & Non-Carbonate Content (%)
			>0.1 мм	0.1—0.05 мм	0.05—0.01 мм	<0.01 мм		$CaCO_3$	Copr.	SiO_2 аморф	Fe	Th	Io	U	Fe
0—5	Алевритово-глинистый ил	Silty-Clayey Mud	1,86	9,07	21,86	67,21	0—6	0,34	0,65	7,23	4,17	2,2	10,0	1,2	4,52
5—12	То же		2,28	11,22	27,15	59,35	0—12	—	0,64	6,60	4,40	—	—	—	4,73
12—16	» »		1,36	11,46	26,40	60,78	12—20	0,30	0,62	6,12	4,34	—	—	—	4,64
16—25	» »		1,19	9,11	26,93	62,77	25—30	0,30	0,78	4,79	4,50	—	13,0	—	4,74
25—35	Глинистый ил	Clayey Mud	1,15	5,75	21,84	71,26	40—45	0,41	0,94	5,41	4,26	—	—	—	4,52
35—45	» »		0,82	3,79	25,68	69,71	50—56	0,43	0,94	5,47	4,07	—	9,1	—	4,32
45—56	» »		0,66	3,52	24,61	71,21	65—70	0,50	0,84	6,81	3,97	—	—	—	4,28
56—65	» »		0,62	4,17	21,25	73,96	75—80	0,59	0,80	7,23	3,91	—	—	—	4,24
65—75	» »		0,67	5,05	17,36	76,92	90—95	0,57	0,76	6,58	3,77	—	—	—	4,06
75—85	» »		0,78	5,30	22,16	71,76	105—110	0,34	0,67	6,53	4,26	—	—	—	4,57
85—97	» »		1,49	5,11	19,57	73,83	114—120	—	—	—	—	3,6	9,1	2,2	—
97—105	Алевритово-глинистый ил	Silty Clayey Mud	2,57	7,33	20,59	69,51	120—125	0,43	0,70	6,76	4,06	—	—	—	4,37
105—114	То же		2,02	6,46	22,63	68,89	135—140	0,35	0,50	5,48	3,56	—	—	—	3,78
114—125	» »		2,96	8,87	21,74	66,43	150—155	—	0,63	5,31	3,70	—	—	—	3,94
125—135	» »		3,17	11,17	24,66	60,10	155—165	—	—	—	—	—	9,1	—	—
135—145	» »		1,73	8,48	30,65	59,14	160—168	0,16	0,41	—	2,73	—	3,8	—	—
145—155	» »		1,15	7,78	20,97	70,00	180—185	0,66	0,69	4,91	4,44	—	—	—	4,70
155—165	» »		1,63	13,17	30,24	54,96	195—210	0,59	0,68	6,60	4,36	—	—	—	4,70
165—168	Мелковалевритовый ил	Fine Silty Mud	3,25	14,28	39,61	42,86	215—222	0,58	0,62	6,66	4,66	—	—	—	5,02
168—180	Глинистый ил	Clayey Mud	0,42	5,11	21,49	72,98	222—230	—	—	—	—	—	8,8	—	—
180—190	Алевритово-глинистый ил	Silty Clayey Mud	1,03	4,74	24,33	69,60	230—236	0,61	0,59	4,14	4,47	—	—	—	4,69
190—200	То же		0,83	8,54	20,84	69,79	250—256	0,55	0,47	3,66	4,26	—	—	—	4,44
200—210	» »		0,71	7,43	21,77	70,09	256—260	—	—	—	—	2,4	4,4	2,0	—
210—222	» »		0,11	9,26	22,78	66,85	260—267	0,43	0,38	2,97	4,36	—	—	—	4,51
222—230	» »		2,00	11,27	26,73	60,00									
230—237	» »		1,53	8,08	24,04	66,35									
256—267	» »		1,31	14,43	29,51	54,75									

APPENDIX IX

Characteristics of the Sediment Core at Station 3625

Depth Below Surface of Core (cm)	Granulometric Composition (%)				Air-Dried Sediment (%)					Air-Dried Sediment 10^{-6} g/g U units			
	>0.1 мм	0.1–0.05 мм	0.05–0.01 мм	<0.01 мм	$CaCO_3$	$C_{орг}$	$SiO_{2\,аморф}$	Fe	Mn	Th	Io	U	Ra
0—3	0,24	0,48	7,38	91,90	—	—	—	—	—	—	—	—	—
3—5	Нет	0,81	12,16	87,03	0,36	0,26	—	5,88	—	8,6 *	26 *	3,2 *	29,0 *
5—9	—	—	—	—	0,29	0,23	1,68	5,54	0,49	—	—	—	—
9—13	—	—	—	—	0,13	0,16	0,58	4,47	0,62	8,6	24,4	—	30,8
14—20	—	—	—	—	0,34	—	0,55	5,08	—	9,2	20,2	—	30,0
20—22	Нет	0,47	12,24	87,29	—	—	—	—	—	—	—	—	—
22—27	—	—	—	—	0,36	0,21	0,57	5,31	0,58	10,0	20,5	—	23,7
35—40	—	—	—	—	0,43	0,16	0,75	4,21	0,54	10,0	15,0	—	21,7
40—42	Нет	0,24	12,86	86,90	—	—	—	—	—	—	—	—	—
47—52	—	—	—	—	0,30	0,25	0,87	4,52	0,43	10,0	10,8	—	13,2
60—62	Нет	0,89	17,11	82,00	—	—	—	—	—	—	—	—	—
62—67	—	—	—	—	0,27	0,15	1,21	4,46	0,36	—	—	—	—
75—80	—	—	—	—	0,36	0,15	1,12	5,57	0,40	—	—	—	—
80—82	Нет	1,15	17,70	81,15	—	—	—	—	—	—	—	—	—
90—95	—	—	—	—	0,43	0,14	1,77	5,02	0,40	—	—	—	—
102—104	Нет	3,16	21,05	75,79	—	—	—	—	—	—	—	—	—
104—110	—	—	—	—	0,48	0,14	0,79	4,45	0,43	9,0	7,0	2,8	6,0
120—122	Нет	2,28	18,23	79,49	—	—	—	—	—	—	—	—	—
122—127	—	—	—	—	0,48	0,13	0,24	5,01	0,49	10,0	7,0	—	9,3
134—140	—	—	—	—	—	—	—	—	—	10,0	5,0	—	8,0
140—142	Нет	0,27	14,13	85,60	—	—	—	—	—	—	—	—	—
142—147	—	—	—	—	0,27	0,13	1,30	5,01	0,44	—	—	—	—
152—160	—	—	—	—	Необн.	0,14	0,89	5,57	0,40	9,0	4,5	—	6,0
160—162	Нет	0,24	11,43	88,33	—	—	—	—	—	—	—	—	—
170—176	—	—	—	—	—	—	—	—	—	9,0	6,0	—	6,1
176—180	—	—	—	—	0,25	0,15	1,22	4,45	0,48	—	—	—	—
180—182	Нет	0,24	16,19	83,57	—	—	—	—	—	—	—	—	—
190—196	—	—	—	—	—	—	—	—	—	9,0	5,7	3,0	3,7
198—203	—	—	—	—	0,75	0,11	0,71	5,00	0,50	—	—	—	—
203—205	Нет	0,42	14,32	85,26	—	—	—	—	—	—	—	—	—
205—211	—	—	—	—	—	—	—	—	—	9,0	3,7	—	3,4
210—215	—	—	—	—	0,57	0,14	0,65	5,01	0,46	—	—	—	—
220—222	Нет	0,44	16,89	82,67	—	—	—	—	—	—	—	—	—
222—230	—	—	—	—	—	—	—	—	—	9,0	3,5	—	3,4
235—240	—	—	—	—	0,66	0,14	0,62	5,02	0,57	—	—	—	—
240—242	Нет	0,47	17,41	82,12	—	—	—	—	—	—	—	—	—
242—250	—	—	—	—	—	—	—	—	—	9,0	4,7	—	2,6
253—258	—	—	—	—	0,41	0,12	0,82	4,46	0,46	—	—	—	—
258—260	Нет	0,24	15,18	84,58	—	—	—	—	—	—	—	—	—
260—266	—	—	—	—	—	—	—	—	—	9,0	3,3	—	2,8
275—280	—	—	—	—	0,52	0,12	1,51	5,29	0,34	6,0	3,9	—	3,5
280—282	Нет	0,56	16,94	82,50	—	—	—	—	—	—	—	—	—
290—296	—	—	—	—	—	—	—	—	—	8,0	4,2	—	3,1
295—300	—	—	—	—	0,50	0,14	0,79	5,03	0,37	—	—	—	—
300—302	Нет	0,28	15,28	84,44	—	—	—	—	—	—	—	—	—
302—308	—	—	—	—	—	—	—	—	—	8,0	4,6	—	2,5
314—320	—	—	—	—	0,45	0,14	0,60	4,73	0,35	8,0	3,1	3,8	2,9
320—322	Нет	0,25	16,00	83,75	—	—	—	—	—	—	—	—	—
322—327	—	—	—	—	0,50	0,14	0,59	4,48	0,65	—	—	—	—
340—342	Нет	0,24	16,59	83,17	—	—	—	—	—	—	—	—	—
342—347	—	—	—	—	0,20	0,10	0,82	5,01	0,57	—	—	—	—
367—369	Нет	0,23	14,48	85,29	—	—	—	—	—	—	—	—	—

* 3-7 cm from the top

APPENDIX X

Characteristics of the Sediment Core at Station 3495

Depth Below Surface of Core (cm)	Sediment Type		Granulometric Composition (%)				Depth From Surface of Core (cm)	Air-Dried Sediment (%)					Air-Dried Sediment 10^{-6} g/g Units		
			>0.1 мм	0.1—0.05 мм	0.05—0.01 мм	<0.01 мм		$CaCO_3$	$C_{орг}$	$SiO_{2аморф}$	Fe	Mn	Th	Io	U
0—5	Алевритово-глинистый ил	Silty Clayey Mud	7,44	3,95	19,07	69,54	0—5	0,44	0,40	4,49	3,70	0,42	—	20,0	2,0
5—10	Глинистый ил	Clayey Mud	11,25	4,79	13,75	70,21	5—10	—	0,31	—	—	0,42	—	—	—
10—20	» »		8,60	4,80	13,60	73,00	10—15	0,50	0,25	3,36	4,06	0,38	—	—	—
30—34	Алевритово-глинистый ил	Silty Clayey Mud	5,32	10,02	16,97	67,69	15—20	0,50	0,23	3,80	3,51	0,34	—	—	—
34—37	Глинистый ил		2,56	6,74	17,91	72,79	20—30	0,29	0,22	5,00	—	—	—	—	—
37—44	То же	Clayey Mud	0,22	0,44	13,72	85,62	35—45	0,32	0,22	4,39	6,02	0,37	—	—	—
44—50	» »		0,23	0,46	21,81	77,50	37—44	—	—	—	—	—	5,4	14,0	1,8
50—60	» »		0,20	0,98	15,10	83,72	50—60	0,43	0,19	3,89	5,18	0,34	—	—	—
60—70	» »		0,27	1,07	22,25	76,41	70—80	0,23	0,20	3,02	5,24	0,36	—	—	—
70—80	» »		Следы	0,51	17,95	81,54	89—95	0,18	0,15	3,07	4,68	0,37	—	—	—
90—103	Алевритово-глинистый ил	Silty Clayey Mud	0,38	1,72	33,52	64,38	103—111	0,16	0,18—0,17	2,66	5,68	0,43	—	—	—
103—110	То же		0,59	2,55	34,51	62,35	120—130	0,14	0,17	2,56	4,63	0,45	—	—	—
110—120	» »		0,57	2,47	37,00	59,96	141—150	0,25	0,16	3,55	3,35	0,30	—	—	—
120—130	» »		2,02	3,64	38,79	55,55	160—170	0,10	0,16	3,18	3,29	0,37	5,8	9,6	2,5
130—140	Глинистый ил	Clayey Mud	0,47	1,87	20,09	77,57	180—190	0,16	0,17	3,34	3,03	0,32	—	—	—
140—155	То же		0,64	1,49	16,59	81,28	200—205	0,13	0,19	2,65	3,13	0,32	—	10,0	—
155—165	» »		0,69	1,61	19,95	77,75	215—225	0,09	0,14	3,35	3,13	0,32	—	—	—
165—175	» »		0,71	1,43	20,95	76,91	240—249	0,11	0,14	2,04	3,01	0,40	—	—	—
195—205	» »		0,60	1,80	17,20	80,40	249—257	—	—	—	—	—	5,3	7,0	1,0
205—215	» »		2,00	2,60	21,20	74,20	260—270	0,14	0,15	2,09	3,01	0,46	—	—	—
215—224	» »		6,74	4,63	17,26	71,37	283—290	0,18	0,17	2,55	3,96	0,31	—	—	—
235—245	» »		0,59	2,38	19,40	77,63	300—310	0,14	0,16	2,01	3,12	0,32	—	4,0	1,0
245—257	» »		1,03	4,83	20,69	73,45									
257—265	» »		0,58	1,75	21,36	76,31									
265—275	» »		0,39	1,75	18,83	79,03									
307—310	Алевритово-глинистый ил	Silty Clayey Mud	4,00	5,50	21,67	68,83									

170 A

APPENDIX XI Characteristics of the Sediment Core at Station 3520

Depth Below Surface of Core (cm)	Sediment Type	Granulometric Composition (%)				Depth From Surface of Core (cm)	Air-Dried Sediment (%)					Air Dried Sediment 10^{-6} g/g Units				Non-carbonate and Non-Siliceous Portion					
		>0.1 мм	0.1–0.05 мм	0.05–0.01 мм	<0.01 мм		$CaCO_3$	$C_{орг}$	SiO_2 аморф	Fe	Mn	Th	Io	Ra	U	% Fe	% Mn	10^{-6} g/g Units Th	Io	Ra	U
0–5	Глинистый ил	Clayey Mud																			
5–12	Алевритово-глинистый ил	Silty Clayey Mud																			
12–17	Мелкоалевритовый ил	Fine Silty Mud																			
17–20	То же	" " "																			
20–23	Глинистый ил	Clayey Mud																			
23–34	То же																				
34–43	» »																				
43–51	» »																				
57–65	» »																				
65–76	» »																				
76–87	» »																				
87–98	Алевритово-глинистый ил	Silty Clayey Mud																			
98–110	Глинистый ил	Clayey Mud																			
110–122	То же																				
122–133	» »																				
133–150	» »																				
160–168	» »																				
168–174	» »																				
185–198	» »																				
198–202	Крупный алеврит	Coarse Silt																			
202–214	Алевритово-глинистый ил	Silty Clayey Mud																			
214–226	Глинистый ил	Clayey Mud																			
226–238	Алевритово-глинистый ил	Silty Clayey Mud																			
238–252	Глинистый ил	Clayey Mud																			
252–260	» »	" "																			
260–263	Алевритово-глинистый ил	Silty Clayey Mud																			
263–272	Глинистый ил	Clayey Mud																			
272–281	» »	" "																			
290–300	» »	" "																			
300–307	Алевритово-глинистый ил	Silty Clayey Mud																			
307–312	Крупный алеврит	Coarse Silt																			
312–327	Глинистый ил	Clayey Mud																			
336–352	» »	" "																			
367–377	» »	" "																			

0–5	Глинистый ил	0,24	0,73	21,95	77,08	0–6	1,41	0,49	4,25	4,10	0,28	5,4	14,2	6,4	3,0	4,37	0,30	5,7	15,0	6,8	3,2
5–12	Алевритово-глинистый ил	0,38	3,81	30,10	65,71	6–12	2,16	0,27	3,49	3,53	0,23	5,4	14,0	5,1	—	3,74	0,24	5,7	14,8	5,4	—
12–17	Мелкоалевритовый ил	0,40	3,63	54,90	41,07	12–17	3,89	0,34	3,20	3,73	0,09	4,6	7,2	8,0	—	4,01	0,10	4,9	7,7	8,6	—
17–20	То же	7,27	22,75	52,76	17,22	17–20	9,33	0,72	2,60	4,33	0,44	6,0	7,7	8,4	2,7	4,92	0,50	6,8	8,7	9,5	3,1
20–23	Глинистый ил	0,37	2,20	18,35	79,08	20–23	9,82	0,67	—	4,37	0,10	6,0	9,2	4,9	—	4,98	0,11	6,8	10,5	5,6	—
23–34	То же	0,55	2,90	22,00	74,55	25–30	12,94	0,74	2,27	3,77	0,10	4,6	7,3	5,4	3,0	4,44	0,12	5,4	8,6	6,4	3,5
34–43	» »	1,09	1,09	25,27	72,55	35–40	12,56	0,80	2,01	3,75	0,10	4,6	8,8	4,8	2,5	4,39	0,12	5,4	10,3	5,6	2,9
43–51	» »	0,53	0,87	23,86	74,74	45–51	10,30	0,94	1,94	4,22	0,11	5,4	6,2	5,0	—	4,81	0,12	6,1	7,1	5,7	—
57–65	» »	0,20	1,20	17,40	81,20	55–60	7,57	0,90	2,48	4,18	0,11	6,6	5,2	7,0	—	4,64	0,12	7,3	5,8	7,8	—
65–76	» »	0,18	0,74	21,30	77,78	65–76	—	—	—	—	—	7,2	7,1	6,0	4,8	—	—	—	—	—	—
76–87	» »	0,31	2,03	22,82	74,84																
87–98	Алевритово-глинистый ил	0,86	2,76	28,28	68,10	85–90	3,96	0,65	2,33	3,95	0,28	6,0	5,6	7,3	—	4,21	0,30	6,4	6,0	7,8	—
98–110	Глинистый ил	1,07	1,59	25,13	72,21	100–107	5,23	0,73	2,07	4,29	—	4,5	5,5	6,0	—	4,50	—	4,8	5,9	6,5	—
110–122	То же	0,17	0,68	16,95	82,20																
122–133	» »	0,18	0,71	20,88	78,23	120–127	3,21	0,74	2,05	4,13	—	6,6	6,5	5,4	3,6	4,35	—	7,0	6,9	5,7	3,8
133–150	» »	0,18	1,23	21,93	76,66	140–145	1,66	0,63	2,06	4,57	0,17	4,6	8,4	5,6	—	4,74	0,18	4,8	8,7	5,8	—
160–168	» »	0,17	1,02	19,83	78,98	160–167	2,38	0,65	2,32	4,26	0,15	7,2	8,9	6,4	—	4,46	0,16	7,5	10,4	6,7	—
168–174	» »	0,18	2,18	21,82	75,82																
185–198	» »	1,33	6,50	21,50	70,67	185–192	1,73	0,57	2,48	3,71	0,17	7,2	8,4	5,4	3,3	3,87	0,18	7,5	8,7	5,6	3,4
198–202	Крупный алеврит	22,55	34,67	21,45	21,33																
202–214	Алевритово-глинистый ил	0,30	2,66	28,57	68,27	202–210	2,52	0,59	2,42	4,10	0,35	8,0	8,0	5,6	—	4,31	0,37	8,4	8,4	5,9	—
214–226	Глинистый ил	0,28	2,95	24,33	72,44																
226–238	Алевритово-глинистый ил	0,16	0,81	43,55	55,48	220–227	3,64	0,72	2,43	4,28	0,20	8,0	6,8	4,1	—	4,55	0,21	8,5	7,2	4,4	—
238–252	Глинистый ил	0,71	5,03	20,32	73,94	235–240	6,05	0,72	2,23	4,42	0,20	—	—	—	—	4,81	0,22	—	—	—	—
252–260	» »	0,18	0,87	22,78	76,17	250–256	8,78	0,66	2,21	4,08	0,21	8,0	8,6	4,1	3,6	4,58	0,23	9,0	9,7	4,6	4,0
260–263	Алевритово-глинистый ил	0,22	0,86	31,32	67,60	270–275	2,46	0,71	2,22	4,42	0,13	—	—	—	—	4,64	0,14	—	—	—	—
263–272	Глинистый ил	0,18	0,86	21,72	77,24	278–282	4,25	0,68	2,57	4,12	0,12	6,8	7,2	4,1	—	4,42	0,13	7,3	7,7	4,4	—
272–281	» »	0,18	0,54	19,10	80,18																
290–300	» »	0,19	1,35	21,54	76,92																
300–307	Алевритово-глинистый ил	0,51	6,64	25,25	67,23	300–307	4,44	0,44	3,05	3,04	0,11	6,0	6,0	3,3	—	3,28	0,12	6,5	6,5	3,6	—
307–312	Крупный алеврит	15,80	34,20	24,20	25,80	307–312	2,68	0,26	—	2,24	0,08	6,0	6,8	—	—	2,36	0,09	6,3	7,2	—	—
312–327	Глинистый ил	0,17	0,87	19,13	79,83	320–327	4,43	0,66	2,24	4,23	—	8,0	9,2	4,2	—	4,52	—	8,6	9,9	4,5	—
336–352	» »	1,35	1,68	19,83	77,14	340–350	1,41	0,57	—	4,04	0,10	8,0	9,2	—	—	4,08	0,10	8,3	9,6	—	—
367–377	» »	0,38	1,13	23,40	75,09	355–362	3,97	0,62	2,47	4,08	0,24	—	—	—	—	4,36	0,26	—	—	—	—
						370–377	4,05	0,48	4,17	3,91	0,15	8,0	7,2	3,2	4,0	4,26	0,16	8,7	7,8	3,5	4,3

APPENDIX XII

Characteristics of the Sediment Core at Station 3532

Depth Below Surface of Core (cm)	Sediment Type	Granulometric Composition (%)			
		>0,1 мм	0,1—0,05 мм	0,05—0,01 мм	<0,01 мм
0—4	Глинистый ил — Clayey Mud	1,78	2,29	24,43	71,50
4—10	Алевритово-глинистый ил — Silty Clayey Mud	1,30	1,30	32,18	65,23
10—20	Глинистый ил — Clayey Mud	0,38	0,38	19,24	80,00
23—27	» »	0,33	1,82	24,79	73,06
27—35	» »	0,40	1,20	27,40	71,00
35—39	» »	0,18	0,36	20,18	79,28
39—44	» »	0,33	0,49	26,88	72,30
44—48	» »	0,32	0,32	20,65	78,71
48—52	» »	0,41	1,93	27,45	70,21
52—59	» »	0,53	3,19	23,54	72,74
59—68	Алевритово-глинистый ил — Silty Clayey Mud	1,94	2,69	28,51	66,86
68—73	То же — " " "	11,22	5,47	24,03	59,28
73—79	Глинистый ил — Clayey Mud	0,37	2,39	21,28	75,96
79—85	» » — " "	0,37	1,10	22,02	76,51
85—95	Алевритово-глинистый ил — Silty Clayey Mud	Следы	0,81	30,24	68,95
96—106	Глинистый ил — Clayey Mud	0,19	0,38	18,87	80,56
106—115	» »	0,57	0,38	21,13	77,92
115—125	» »	0,36	0,36	24,68	74,60
125—135	» »	Следы	0,27	23,33	76,40
135—140	» »	0,20	0,40	24,60	74,80
140—147	» »	0,15	0,78	27,29	71,78
147—153	» »	0,84	2,10	24,84	72,42
153—161	» »	0,31	0,95	22,99	75,75
161—170	» »	0,58	1,31	27,01	71,10
170—177	» »	1,11	0,93	19,81	78,15
177—185	» »	2,09	2,26	24,69	70,96
185—195	Алевритово-глинистый ил — Silty Clayey Mud	2,20	3,80	24,20	69,80
195—202	То же — " " "	4,58	5,76	27,29	62,37
202—215	Глинистый ил — Clayey Mud	0,73	1,27	14,55	83,45
215—222	» »	0,33	1,65	17,52	80,50
222—229	» »	0,54	2,14	17,50	79,82
229—240	» »	Следы	0,34	24,62	75,04
240—250	» »	»	0,33	25,45	74,22
250—260	» »	»	Следы	27,77	72,23
260—266	» »	»	0,16	25,37	74,47
268—274	» »	»	Следы	25,27	74,74
274—280	» »	»	0,18	26,19	73,63
280—290	» »	»	0,17	25,98	73,85
290—300	Алевритово-глинистый ил — Silty Clayey Mud	»	0,17	33,10	66,73
300—310	То же — " " "	»	0,16	34,84	65,00
310—321	» »	0,17	0,85	29,66	69,32
321—330	Глинистый ил — Clayey Mud	Следы	0,20	25,80	74,00
330—337	» »	»	0,40	25,80	73,80
346—358	» » — " " "	0,20	0,40	24,80	73,60

* 310-315 cm

APPENDIX XII (con)

Depth below Surface of Core (cm)	Air-Dried Sediment (%)					Air-Dried Sediment 10^{-6} g/g Limits			
	$CaCO_3$	C_{opr}	$SiO_{2amorph}$	Fe	Mn	Th	Io	Ra	U
0—4	0,22	0,42	2,97	—	0,37	—	—	—	—
4—10	0,20	0,29	2,10	2,00	0,43	6,6	21,3	17,0	3,2
10—15	0,32	0,29	1,74	3,24	0,86	—	—	—	—
15—20	0,30	0,27	1,70	3,01	1,59	—	—	—	—
20—25	—	—	—	—	—	6,3	18,0	9,0	—
23—27	0,75	0,42	1,80	3,01	1,51	—	—	—	—
25—30	—	—	—	—	—	10,0	17,6	16,8	2,7
30—35	0,45	0,47	2,03	4,02	0,26	—	—	—	—
33—37	—	—	—	—	—	10,0	13,3	13.1	—
40—45	0;86	0,45	1,61	2,85	0,18	6,0	13.4	3,6	—
50—53	0,61	0,43	—	—	0,40	6,6	12,7	4,3	—
53—57	0,75	0,43	1,41	4,00	0,07	8,0	11,6	3,0	2,0
68—73	0,57	0,36	1,31	3,78	0,21	6,6	11,1	18,0	—
79—85	0,91	0,39	1,80	3,17	0,08	6,6	14,9	5,0	—
90—95	0,80	0,36	2,40	3,12	0,15	6,6	15,5	15,0	—
106—110	1,05	0,35	1,45	4,22	0,25	6,0	15,6	4,0	2,7
120—125	1,00	0,27	1,31	4,12	0,09	5,0	14,2	4,8	—
135—140	1,06	0,28	1,34	3,86	0,10	9,0	10,0	4,3	—
147—153	0,75	0,33	2,00	4,54	0,09	9,0	9,0	3,9	—
161—170	0,82	0,26	1,47	4,84	0,08	7,0	11,3	3,6	—
177—185	0,55	0,25	1,96	4,74	0,08	5,4	9,1	4,6	3,6
195—202	0,48	0,16	1,54	3,62	0,11	5,4	9,0	4,6	—
215—220	0,66	0,24	1,14	4,90	0,11	6,4	7,1	5,0	—
229—235	1,25	0,23	0,88	4,79	0,41	6,0	8,7	5,8	—
250—255	1,18	0,24	0,98	5,01	0,16	7,0	9,0	2,4	—
268—274	1,24	0,32	1,08	4,85	0,10	4,5	7,0	2,6	—
280—290	1,57	0,26	1,08	4,32	0,14	—	—	—	—
290—300	1,43	0,27	1,15	4,11	0,11	8,0	5,0	2,9	—
310—321	1,73	0,27	1,07	4,30	0,11	8,0*	5,4*	3,1*	—
330—337	1,02	0,21	1,26	4,41	0,11	8,0	5,1	2,2	2,6
350—358	0,61	0,18	1,16	4,35	0,09	8,0	5,5	1,7	—

APPENDIX XIII Characteics of the Sediment Core at Station 3530

" XIV " " " " " " " " " 3481

Depth Below Surface of Core (cm)	Sediment Type	Granulometric Composition (%)				Air-Dried Sediment 10^{-6} g/g Units		
		>0.1 мм	0.1—0.05 мм	0.05—0.01 мм	<0.01 мм	Th	¹⁰	U
Station 3530								
0—5	Алевритово-глинистый ил — Silty Clayey Mud	1,13	2,26	26,84	69,74	6,0	20,0	1,4
5—10	Глинистый ил — Clayey Mud	1,41	2,64	20,46	75,49	—	—	—
10—16	» » — " "	0,77	1,99	26,69	70,55	—	—	—
21—30	» » — " "	0,89	2,24	20,80	76,07	—	—	—
30—40	Алевритово-глинистый ил — Silty Clayey Mud	2,54	9,58	24,37	63,51	—	—	—
40—52	То же — " " "	1,28	4,28	30,57	63,87	—	10,0	—
52—64	Глинистый ил — Clayey Mud	0,94	1,57	23,31	74,18	—	—	—
64—75	» » — " "	0,72	1,00	25,43	72,85	—	—	—
90—103	Алевритово-глинистый ил — Silty Clayey Mud	0,63	0,79	30,48	68,10	—	11,0	—
115—130	То же	5,07	3,77	24,49	66,66	—	—	—
150—157	» »	3,86	5,14	25,43	65,57	6,0	10,0	2,6
170—183	» »	3,46	6,32	26,77	63,45	—	—	—
195—210	» »	2,35	6,08	25,00	66,57	—	—	—
210—225	Глинистый ил — Clayey Mud	1,50	2,26	25,86	70,38	—	—	—
225—240	Алевритово-глинистый ил — Silty Clayey Mud	1,61	5,37	29,70	63,32	—	—	—
250—264	Глинистый ил — Clayey Mud	5,12	2,88	21,76	70,24	—	—	—
264—270	Алевритово-глинистый ил — Silty Clayey Mud	—	—	—	—	—	8,5	—
276—289	То же — " " "	0,60	1,04	28,80	69,76	—	—	—
289—305	Глинистый ил — Clayey Mud	0,92	1,68	25,65	71,75	—	—	—
318—325	» » — " "	0,74	1,33	25,04	72,89	—	—	—
345—356	» » — " "	0,60	1,35	23,76	74,29	6,0	6,7	1,8
Station 3481								
0—5	Алевритово-глинистый ил — Silty Clayey Mud	0,21	7,29	33,96	58,54	6,0	23,0	4,0
9—13	Мелкоалевритовый ил — Fine Silty Mud	5,42	16,11	31,63	46,84	—	—	—
20—30	Алевритово-глинистый ил — Silty Clayey Mud	0,69	5,69	31,55	62,07	—	—	—
35—40	То же — " " "	0,16	2,17	31,94	65,72	—	—	—
40—51	Глинистый ил — Clayey Mud	1,16	2,08	24,30	72,46	—	—	—
51—60	Алевритово-глинистый ил — Silty Clayey Mud	3,46	17,62	13,10	65,82	—	12,0	—
60—69	То же — " " "	0,62	2,92	31,69	64,77	—	—	—
78—88	Мелкоалевритовый ил — Fine Silty Mud	2,99	18,11	30,09	48,81	—	4,7	—
88—96	Алевритово-глинистый ил — Silty Clayey Mud	0,93	3,85	28,46	66,76	—	—	—
96—105	То же — " " "	0,76	5,65	27,17	66,42	—	—	—
113—121	» » — " " "	0,94	4,41	34,02	60,63	—	—	—
121—130	» » — " " "	1,80	3,94	31,31	62,95	—	—	—
130—135	Мелкоалевритовый ил — Fine Silty Mud	7,69	6,27	42,49	43,55	—	—	—
135—145	Алевритово-глинистый ил — Silty Clayey Mud	0,29	3,30	34,68	61,73	—	—	—
150—157	Глинистый ил — Clayey Mud	0,65	—	23,77	75,57	5,8	11,0	2,1
166—175	Алевритово-глинистый ил — Silty Clayey Mud	1,05	3,65	27,65	67,65	—	—	—
175—184	То же — " " "	2,98	4,48	35,66	57,76	—	—	—
184—192	Мелкоалевритовый ил — Fine Silty Mud	2,12	2,73	52,12	43,03	—	—	—
192—200	Алевритово-глинистый ил — Silty Clayey Mud	1,81	1,08	29,00	68,11	—	7,0	—
200—208	То же	0,35	0,86	29,31	69,48	—	—	—
208—217	» »	0,31	2,48	27,44	69,77	—	—	—
221—232	» »	0,65	7,14	32,21	60,00	—	—	—
232—240	» »	0,92	3,05	29,77	66,26	—	—	—
250—260	» »	0,19	5,37	31,85	62,59	—	—	—
260—266	» »	0,32	3,78	32,91	62,99	—	—	—
274—285	» »	0,65	7,10	34,19	58,06	5,6	7,6	2,5

APPENDIX XV

Characteristics of the Sediment Core at Station 3873

Depth Below Surface of Core (cm)	Granulometric Composition (%)						Depth Below Surface of Core (cm)	Air-Dried Sediment (%)					Air-Dried Sediment 10^{-6} g/g Units			
	> .1 мм	0.1—0.05 мм	0,05—0.01 мм	0,01—0,005 мм	0,005—0,001 мм	<0,001 мм		$CaCO_3$	$C_{орг}$	$SiO_{2аморф}$	Fe	Mn	Th	Io	Ra	U
10—12	0,16	0,48	12,08	14,98	33,17	39,13	0—2	0,64	0,28	1,17	4,57	0,73	15,0	86,0	72,0	3,6
20—22	0,15	0,94	10,01	10,17	38,98	39,75	2—6	0,61	0,26	0,95	4,53	0,77	—	—	—	—
40—42	Следы	0,99	13,76	12,11	39,80	33,33	12—20	0,50	0,22	0,50	5,02	0,90	—	—	—	—
59—61	0,14	0,42	6,76	15,35	36,20	41,13	24—30	0,61	0,24	0,46	5,29	0,81	10,0	44,0	41,5	—
80—82	0,13	0,79	8,42	9,61	37,76	43,29	36—40	0,63	0,28	0,48	5,75	0,76	10,0	23,5	30,4	—
100—102	0,13	0,82	11,10	8,49	40,14	39,32	62—70	0,48	0,16	0,36	5,76	0,84	12,0	29,2	19,3	—
117—119	0,14	0,83	9,03	11,94	34,44	43,62	80—86	0,52	0,17	0,52	5,99	0,87	12,0	20,0	19,5	—
140—142	0,13	1,05	12,24	9,08	36,58	40,92	100—108	0,36	0,23	0,63	6,17	0,89	12,0	15,5	16,3	—
160—162	0,14	1,54	13,74	8,28	37,45	38,85	117—123	0,52	0,19	0,45	5,85	0,98	10,0	12,6	10,3	—
180—182	0,13	1,14	11,77	11,14	37,97	37,85	140—146	0,75	0,22	0,44	6,26	0,92	10,0	6,4	5,9	3,2
199—202	0,13	1,39	6,96	12,15	39,37	40,00	162—172	0,89	0,17	0,30	5,47	1,09	—	—	—	—
220—222	0,15	1,07	10,38	7,48	36,34	44,58	180—188	0,52	0,18	0,52	5,91	0,89	12,0	6,1	4,7	—
240—242	0,13	0,65	6,75	12,86	37,92	41,69	199—207	0,52	0,16	0,70	5,47	1,04	12,0	6,0	—	—
260—262	0,15	0,46	6,66	14,24	37,62	40,87	218—226	0,63	0,20	0,54	5,68	0,98	12,0	7,9	4,7	—
280—282	0,14	0,56	6,80	10,28	35,97	46,25	242—250	0,61	0,22	0,52	5,63	0,90	—	—	—	—
300—302	Следы	0,26	4,08	7,37	42,11	46,18	260—268	0,59	0,16	0,43	5,75	0,92	10,0	3,6	5,7	—
322—326	»	0,13	3,21	7,06	39,92	49,68	280—288	0,50	0,19	0,61	4,53	0,92	10,0	3,8	—	—
360—362	»	0,17	2,56	8,38	40,00	48,89	318—326	0,45	0,20	0,63	5,47	0,87	11,0	3,8	2,1	2,8
379—382	»	Сле м	0,48	12,34	38,29	48,89	344—351	0,48	0,23	0,58	6,00	0,92	11,0	3,2	1,8	2,6
							362—370	0,59	0,20	0,62	5,47	0,90	—	—	—	—
							379—385	0,50	0,25	0,50	5,02	0,90	12,0	0,8	2,6	3,2
							400—407	—	—	0,56	5,19	1,01	12,0	1,1	3,5	—

APPENDIX XVI

Characteristics of the Sediment Core at Station 3746

Depth Below Surface of Core (cm)	Granulometric Composition (%)				Air-Dried Sediment (%)					Air-Dried Sediment 10^{-6} g/g U units			
	>0.1 mm	0.1—0.05 mm	0.05—0.01 mm	<0.01 mm	$CaCO_3$	$C_{орг}$	$SiO_{2\,аморф}$	Fe	Mn	Th	Io	Ra	U
0—5	0,54	3,24	13,78	82,44	0,27	0,31	0,41	5,46	0,63	8,0	27,5	40	3,6
5—10	—	—	—	—	0,25	0,22	0,61	5,73	0,62	7,0	25,4	40	—
10—13	0,24	0,71	15,48	83,57	—	—	—	—	—	—	—	—	—
13—17	—	—	—	—	0,16	0,13	0,35	6,05	0,73	8,6	24,4	28,4	—
21—25	0,23	0,46	20,00	79,31	—	—	—	—	—	9,0	25,2	31,2	—
29—33	—	—	—	—	0,16	0,12	0,54	6,21	0,73	8,6	18,5	15,0	3,0
36—40	—	—	—	—	—	—	—	—	—	8,0	15,1	8,7	3,8
40—43	0,22	0,22	16,22	83,34	—	—	—	—	—	—	—	—	—
47—51	—	—	—	—	0,18	0,13	0,41	6,33	0,77	11,0	8,4	5,5	3,1
59—63	—	—	—	—	0,13	0,11	0,39	6,20	0,71	8,0	5,8	4,3	4,3
63—66	0,25	1,23	18,76	79,76	—	—	—	—	—	—	—	—	—
70—74	—	—	—	—	—	—	—	—	—	8,0	4,5	4,6	—
80—83	0,24	0,71	15,71	83,34	—	—	—	—	—	—	—	—	—
83—87	—	—	—	—	0,13	0,10	0,44	6,28	0,82	8,0	4,9	2,8	3,8
96—100	—	—	—	—	0,13	0,10	0,37	6,24	0,75	7,0	4,2	1,5	—
100—103	0,24	0,47	13,88	85,41	—	—	—	—	—	—	—	—	—
110—114	—	—	—	—	—	—	—	—	—	7,0	5,1	1,2	3,0
123—128	—	—	—	—	0,18	0,10	0,36	6,20	0,71	7,0	6,0	1,7	—
136—140	—	—	—	—	—	—	—	—	—	8,0	4,7	1,9	3,0
148—156	—	—	—	—	0,11	0,09	0,35	6,17	0,68	6,0	5,6	1,7	—
161—164	0,24	0,24	15,71	83,81	—	—	—	—	—	—	—	—	—
168—176	—	—	—	—	0,18	0,07	0,35	6,36	0,75	7,0	4,7	1,9	—
186—194	—	—	—	—	0,18	0,09	0,31	6,32	0,79	7,0	6,4	1,2	3,4
200—203	0,23	0,46	18,60	80,71	—	—	—	—	—	—	—	—	—
208—214	—	—	—	—	0,18	0,10	0,32	6,30	0,86	7,0	5,2	1,3	3,8
223—230	—	—	—	—	—	—	—	—	—	7,0	4,3	1,5	3,3
240—243	0,24	0,24	16,14	83,38	—	—	—	—	—	—	—	—	—
243—250	—	—	—	—	0,20	0,10	0,28	6,54	0,86	7,0	4,3	1,7	—
265—270	—	—	—	—	0,18	0,11	0,46	6,57	0,82	8,0	4,8	1,8	—
283—289	—	—	—	—	—	—	—	—	—	7,0	2,9	1,9	3,0
297—303	—	—	—	—	0,16	0,13	0,31	6,58	0,92	7,0	3,1	2,4	3,8
204—307	0,24	0,48	16,43	82,85	—	—	—	—	—	—	—	—	—

APPENDIX XVII

Characteristics of the Sediment Core at Station 3797

Depth Below Surface of Core (cm)	Sediment Type	Granulometric Composition (%)						Air-Dried Sediment (%)				Air-Dried Sediment 10^{-6} g/g Units			
		Гранулометрический состав, %						Воздушно-сухой осадок, %				Воздушно-сухой осадок, 10^{-6} г/г ед. U			
		>0.1 мм	0.1—0.05 мм	0.05—0.01 мм	0.01—0.005 мм	0.005—0.001 мм	<0.001 мм	$CaCO_3$	$C_{орг}$	Fe	Mn	Th	Io	U	Ra
0—2	Глинистый ил — Clayey Mud	2,16	1,62	13,51	82,70*	—	—	—	—	—	—	4,0**	97,5**	3.0	50,5**
2—10	" " — " "	—	—	—	—	—	—	23,58	0,38	3,06	0,44	3,0***	83,5***	—	40,5***
10—12	Алевритово-глинистый ил — Silty Clayey Mud	1,26	17,38	19,40	10,33	26,70	24,93	—	—	—	—	—	—	—	—
12—17	" " " — " " "	—	—	—	—	—	—	6,32	0,36	3,72	0,56	4,0	87,2	—	59,5
20—22	Глинистый ил — Clayey Mud	0,32	9,21	15,24	14,28	35,87	25,08	—	—	—	—	—	—	—	—
22—27	" "	—	—	—	—	—	—	0,38	0,23	4,19	0,68	3,0	55,5	—	61,5
33—35	" "	0,56	8,61	14,44	14,72	35,56	26,11	—	—	—	—	4,0	22,1	—	18,5
35—40	" "	—	—	—	—	—	—	0,38	0,22	4,39	0,63	—	—	—	—
40—42	" "	0,30	10,68	13,06	11,87	35,61	28,48	—	—	—	—	—	—	—	—
42—47	" "	—	—	—	—	—	—	0,25	0,20	4,56	0,55	—	—	—	—
47—52	" "	—	—	—	—	—	—	—	—	—	—	4,0	29,8	—	28,2
60—62	" "	0,68	6,35	14,06	14,74	37,19	26,98	—	—	—	—	—	—	—	—
62—67	" "	—	—	—	—	—	—	0,23	0,21	4,68	0,63	12,0	31,5	2,8	33,0
80—82	" "	0,47	6,82	14,35	16,47	32,24	29,65	—	—	—	—	—	—	—	—
82—86	" "	—	—	—	—	—	—	0,27	0,16	4,68	0,63	6,0	56,5	—	57,5
90—92	" "	0,32	8,25	14,29	8,25	43,17	25,72	—	—	—	—	—	—	—	—
92—97	" "	—	—	—	—	—	—	0,36	0,76	4,56	0,68	3,0	19,5	—	18,3
97—100	" "	—	—	—	—	—	—	0,18	0,33	4,30	0,19	4,0	12,7	—	8,4
100—102	" "	1,35	7,14	12,24	13,96	43,20	22,11	—	—	—	—	—	—	—	—
110—112	" "	0,25	7,40	19,90	10,20	31,38	30,87	—	—	—	—	—	—	—	—

* For the fraction smaller than 0.01 mm
** At depths of 0-5 cm
*** At depths of 5-10 cm

APPENDIX XVII (con)

Depth Below Surface of Core (cm)	Sediment Type	Granulometric Composition (%)						Air-Dried Sediment (%)				Air-Dried Sediment 10^{-6} g/g Limits			
		Гранулометрический состав, %						Воздушно-сухой осадок, %				Воздушно-сухой осадок, 10^{-6} г/г ед. U			
		>0,1 мм	0,1—0,05 мм	0,05—0,01 мм	0,01—0,005 мм	0,005—0,001 мм	<0,001 мм	$CaCO_3$	Copr	Fe	Mn	Th	Io	U	Ra
112—117	Глинистый ил / Clayey Mud	—	—	—	—	—	—	0,20	0,18	4,54	0,52	—	—	—	—
120—122	» »	0,28	8,15	16,03	26,36	26,90	22,28	—	—	—	—	—	—	—	—
122—127	» »	—	—	—	—	—	—	0,23	0,15	4,28	1,38	4,0	11,7	—	6,3
140—142	» »	0,93	3,73	10,25	19,57	43,48	22,04	—	—	—	—	—	—	—	—
142—147	» »	—	—	—	—	—	—	0,27	0,15	4,68	0,67	—	—	—	—
160—162	» »	0,82	4,35	11,14	15,49	39,67	28,53	—	—	—	—	—	—	—	—
162—168	» »	—	—	—	—	—	—	0,25	0,14	4,63	1,38	16,0	9,2	2,7	2,9
180—182	» »	0,89	8,04	12,80	7,74	39,58	30,95	—	—	—	—	—	—	—	—
182—187	» »	—	—	—	—	—	—	0,25	0,15	4,59	0,55	—	—	—	—
200—202	» »	1,48	6,23	12,17	15,44	32,34	32,34	—	—	—	—	—	—	—	—
202—207	» »	—	—	—	—	—	—	0,20	0,13	4,46	0,66	12,0	3,0	—	2,1
220—222	» »	1,03	6,14	13,04	22,51	28,64	28,64	—	—	—	—	—	—	—	—
222—228	» »	—	—	—	—	—	—	0,27	0,14	4,42	0,54	—	—	—	—
240—242	» »	1,28	6,14	12,02	11,76	40,92	27,88	—	—	—	—	—	—	—	—
242—248	» »	—	—	—	—	—	—	0,23	0,14	4,42	0,66	12,0	0,6	—	0,9
260—262	» »	0,99	7,90	14,07	16,05	33,09	27,90	—	—	—	—	—	—	—	—
262—267	» »	—	—	—	—	—	—	0,18	0,15	4,31	0,56	—	—	—	—
280—282	» »	1,25	8,75	16,00	11,25	30,25	32,50	—	—	—	—	—	—	—	—
282—287	» »	—	—	—	—	—	—	0,32	0,16	4,45	0,90	—	—	—	—
300—302	» »	0,53	6,38	15,69	10,64	30,85	35,91	—	—	—	—	—	—	—	—
302—306	» »	—	—	—	—	—	—	0,23	0,16	4,50	0,48	—	—	—	—
310—314	» »	—	—	—	—	—	—	—	—	—	—	12,0	0,6	3,2	0,9
314—316	» »	0,27	7,10	15,30	21,86	20,49	34,98	—	—	—	—	—	—	—	—

APPENDIX XVIII

Characteristics of the Sediment Core at Station 3995

Depth Below Surface of Core (cm)	Granulometric Composition (%) — Гранулометрический состав, %						Глубина от поверхности дна, см	Air-Dried Sediment (%) — Воздушно-сухой осадок, %					Air-Dried Sediment 10^{-6} g/g Units — Воздушно-сухой осадок, 10^{-6} г/г сл. U			
	<0.1 мм	0.1—0.05 мм	0.05—0.01 мм	0.01—0.005 мм	0.005—0.001 мм	<0.001 мм		$CaCO_3$	$C_{орг}$	битуминозные вещества	$Fe_{вал}$	Mn	Th	Io	U	Ra
0—4	0,32	0,32	13,55	85,81*			0—12	0,63	0,33	0,0037	5,11	1,77	3,2	36,2	3,0	25,2
							12—18	0,48	0,34	0,0050	4,94	1,35	2,6	31,0	—	33,0
12—14	Следы	3,34	11,50	19,29	33,02	32,85	18—24	0,39	0,49	0,0075	4,84	1,16	—	—	—	—
							26—36	1,68	0,40	0,0150	4,56	0,14	2,6	25,1	—	12,3
24—26	0,28	3,87	10,77	17,46	33,09	34,53	36—45	0,30	1,01	0,0200	4,88	0,17	—	—	—	—
45—47	2,27	1,82	10,23	17,27	41,59	26,82	47—60	11,6	0,82	0,0150	4,42	0,13	2,6	22,2	2,7	11,0
60—62	0,43	2,62	10,92	24,67	33,41	27,95	65—76	—	—	0,0170	—	—	2,6	15,0	2,8	11,7
76—78	0,49	6,44	15,18	18,65	46,37	12,87	80—88	14,62	0,65	0,0170	4,31	0,11	2,6	14,5	—	11,0
92—94	0,20	0,59	13,02	21,30	38,66	26,23	94—105	3,16	0,74	0,0150	4,49	0,09	3,6	14,0	3,2	16,3
105—108	Следы	1,61	15,12	22,99	44,96	15,32	115—128	0,20	0,60	0,0150	5,03	0,07	—	—	—	—
128—130	0,15	3,48	24,24	13,94	41,67	16,52	130—138	0,18	0,34	0,0050	5,73	0,10	4,8	14,2	—	19,1
142—144	0,25	9,93	15,14	12,90	47,64	14,40	144—157	0,18	0,31	0,0037	5,26	0,53	3,4	14,8	2,0	39,7
157—160	0,15	3,70	25,04	14,07	45,19	11,85	160—173	—	—	0,0037	—	—	4,6	15,3	—	20,0
173—176	0,14	3,71	21,71	20,29	35,86	18,29	176—187	6,39	0,29	0,0050	5,11	0,87	—	—	—	—
195—197	0,16	1,56	19,53	16,25	42,81	19,69	197—210	0,43	0,58	0,0150	5,03	0,14	4,6	8,7	—	7,2
210—212	Следы	2,01	20,64	21,48	36,24	19,63	220—226	4,95	0,56	0,0150	5,14	0,13	4,1	8,5	—	8,5
226—228	0,22	1,11	14,67	84,0*	—	—	238—245	0,70	0,20	0,0100	5,26	0,08	—	—	—	—
236—238	Следы	1,95	19,22	18,73	44,63	15,47	252—260	0,29	0,26	0,0037	5,66	0,45	4,6	5,3	—	4,0
250—252	0,14	4,73	17,57	19,05	42,97	15,54	268—271	—	—	0,0037	—	—	—	—	—	—
268—271	Следы	2,91	23,85	20,03	39,75	13,46	271—278	0,07	0,26	—	5,45	0,31	—	—	—	—
292—301	0,29	1,17	21,77	76,77*	—	—	285—288	0,95	0,27	0,0037	5,40	0,76	4,6	3,7	3,2	4,9
							295—301	1,97	0,29	0,0037	5,28	1,49	—	—	—	—

* Fraction less than 0.01 mm

APPENDIX XIX

Characteristics of the Sediment Core at S. Station 3921

Depth Below Surface of Core (cm)	Sediment Type	Granulometric Composition (%)				Depth Below Core Surface (cm)	Air-Dried Sediment (%)				Non-Carbonate Portion (%)		
		>0.1 мм	0.1—0.05 мм	0.05—0.01 мм	<0.01 мм		$CaCO_3$	C_{opr}	Fe	Mn	C_{opr}	Fe	Mn
0—2	Глинистый ил — Clayey Mud	2,53	4,60	16,55	76,32	0—4	36,84	0,58	3,62	0.17	0.91	5.73	0,27
9—11	» » — " "	10,41	6,94	12,45	70,20	11—16	51,60	0,57	—	0.13	1.18	—	0,27
16—18	Алевритово-глинистый ил — Silty Clayey Mud	12,88	9,42	13,84	63,86	18—33	45,83	0,67	3,32	0.40	1.24	6.12	0,74
33—35	То же — " " "	9,68	8,63	12,21	69,48	35—50	39,82	0,71	3,56	0.04	1.18	5.91	0,07
50—52	Глинистый ил — Clayey Mud	3,08	4,40	12,09	80,43	60—76	32,1	0,80	3.85	0.05	1.33	5.67	0.07
74—76	» »	2,35	4,94	13,88	78,83	92—106	26,0	0,88	4,18	0.05	1.32	5.64	0.07
90—92	» »	1,98	4,94	17,04	76,04	115—128	34,91	0,88	3,58	0.04	1.35	5.50	0.06
106—108	» »	1,33	6,22	16,67	75,78	130—145	38,78	0,89	3,50	0.04	1.45	5,71	0.06
113—115	» »	2,56	5,35	12,56	79,53	169—180	39,28	0,84	3,35	0.06	1.38	5.51	0,10
128—130	» »	2,47	4,94	11,46	81,13	197—213	39,66	0,65	3,70	0.06	1.07	6,13	0,10
145—147	» »	2,99	5,52	10,80	80,69	232—245	38,82	0,95	3,51	0.06	1.55	5.73	0,10
160—162	» »	4,14	6,44	10,34	79,08	262—276	45,28	0,74	3,37	0,06	1.35	6.15	0,11
180—182	» »	3,30	4,84	11,87	80,0	278—288	43,6	0,80	3,31	0,08	1.42	5.86	0,14
195—197	» »	3,08	4,40	13,18	79,34								
213—215	» »	4,52	4,76	15,71	75,01								
230—232	» »	1,26	4,21	15,79	78,74								
245—247	» »	7,36	6,21	13,10	73,33								
260—262	» »	5,93	3,30	13,19	77,58								
276—278	» »	5,98	5,28	13,33	75,41								

APPENDIX XX

Characteristics of the Sediment Core at S. Station 3993

Depth within Core (cm)	Air-Dried Sediment (%)				Depth Within Core (cm)	Air-Dried Sediment (%)			
	$CaCO_3$	C_{opr}	Fe	Mn		$CaCO_3$	C_{opr}	Fe	Mn
0—4	11,64	1,04	4,48	0,34	113—123	19,03	0,97	4,43	0,20
8—16	13,66	1,30	4,45	0,84	123—125	—	—	—	—
16—18	—	—	—	—	139—147	5,37	1,48	5,02	0,21
18—23	11,19	0,26	4,47	2,00	147—149	—	—	—	—
23—31	5,59	0,50	4,73	0,16	152—160	5,16	0,35	5,28	0,22
34—36	—	—	—	—	164—166	—	—	—	—
36—42	4,00	0,64	5,60	0,06	166—174	1,30	0,40	5.44	0.15
55—57	—	—	—	—	182—185	—	—	—	—
60—70	6,12	0,79	4,74	0,09	185—193	8,9	0,49	4,72	0,14
70—72	—	—	—	—	202—205	—	—	—	—
80—90	5,18	0,38	5,02	0,11	206—214	3,96	0,30	5,29	0,16
90—92	—	—	—	—	214—216	—	—	—	—
109—111	—	—	—	—					

* Surface sediment layer (0-4 cm) had the following grain-size composition: fractions; 0.1 mm - 0.23%, 0.1-0.05 mm - 0.47%, 0.05 - 0.01 mm - 9.53%, less than 0.01 mm - 89.76%.

APPENDIX XXI

Characteristics of the Sediment Core at Station 3989

Depth Below Surface of Core (cm)	Sediment Type	Granulometric Composition (%)			
		>0.1 мм	0.1—0.05 мм	0.05—0.01 мм	<0.01 мм
0—2	Глинистый ил — Clayey Mud	Не обн.	1,56	19,55	78,89
11—13	» » — " "	0,21	3,37	17,89	78,53
25—27	Алевритово-глинистый ил — Silty Clayey Mud	1,03	9,14	23,62	66,21
46—48	Глинистый ил — Clayey Mud	0,19	2,31	21,15	76,35
60—62	Мелкоалевритовый ил — Fine Silty Mud	0,16	15,61	37,39	46,83
75—77	Алевритово-глинистый ил — Silty Clayey Mud	0,22	2,79	30,11	66,88
96—98	Глинистый ил — Clayey Mud	0,91	1,82	19,64	77,63
110—112	» » — " "	0,36	3,61	24,14	71,89
125—127	» » — " "	0,19	3,48	20,18	76,15
143—145	» » — " "	0,39	2,77	19,21	77,63

Depth Below Surface of Core (cm)	Air-Dried Sediment (%)					Non-Carbonate Portion (%)	
	$CaCO_3$	$C_{орг}$	битумы (хлороформенная часть)	$Fe_{общ}$	$Mn_{орг}$	$C_{орг}$	$Fe_{общ}$
2—5	7,89	0,60	0,0025	5,47	0,29	0,68	5,93
5—11	14,12	0,62	0,0025	5,07	0,16	0.72	5.90
13—20	20,97	0,61	0,0012	4,86	0,06	0.77	6,14
20—25	17,17	0,65	0,0018	—	—	—	—
27—35	12,54	0,72	0,0075	4,81	0,07	0,82	5,50
35—46	5,25	0,66	0,01	4,91	0,07	0,70	5,18
48—60	5,32	0,65	0,0037	5,52	0,07	0,69	5,83
68—75	3,75	0,71	0,0037	4,99	0,06	0,74	5,18
80—90	—	—	0,0037	—	—	—	—
98—110	8,01	0,28	0,0025	5,06	0,08	0,30	5,50
118—125	9,10	0,94	0,0037	—	—	—	—
127—133	7,18	0,84	0,0037	5,17	0,08	0,90	5,56
133—143	6,25	0,12	0,0037	5,27	0,07	0,13	5,62
150—160	8,53	0,75	0,0037	5,09	0,08	0,82	5,56

APPENDIX XXII

Characteristics of the Sediment Core at Station 3650

Depth Below Surface of Core (cm)	Sediment Type	Granulometric Composition (%) Гранулометрический состав, %						Air-Dried Sediments (%) Воздушно-сухой осадок, %				Non-Carbonate Sediments (%) Бескарбонатный осадок, %		
		>0.1 мм	0.1—0.05 мм	0.05—0.01 мм	0.01—0.005 мм	0.005—0.001 мм	<0.001 мм	$CaCO_3$	$C_{орг}$	Fe	Mn	$C_{орг}$	Fe	Mn
0—2	Мелкоалевритовый ил Fine Silty Mud	32,55	9,64	10,42		47,39		—	—	—	—	—	—	—
2—7	» » " " "	—	—	—	—	—	—	82,21	0,49	0,66	0,06	2,75	3,71	0,34
10—12	Крупный алеврит Coarse Silt	40,84	12,06	11,78	11,21	17,29	6,82	—	—	—	—	—	—	—
12—15	» »	—	—	—	—	—	—	84,14	0,35	1,11	0,04	2,21	6,99	0,25
18—20	Мелкоалевритовый ил Fine Silty Mud	—	—	—	—	—	—	84,14	0,38	0,84	0,33	2,40	5,30	2,08
20—22	» » " " "	23,54	12,27	13,19	5,82	32,82	12,36	—	—	—	—	—	—	—
22—25	» »	—	—	—	—	—	—	78,46	0,65	0,83	0,12	3,02	3,85	0,56
30—32	Крупный алеврит Coarse Silt	40,0	11,62	9,34	3,52	24,95	10,57	—	—	—	—	—	—	—
32—37	» »	—	—	—	—	—	—	76,87	0,55	0,85	0,08	2,38	3,67	0,34
40—42	Мелкоалевритовый ил Fine Silty Mud	—	—	—	—	—	—	—	—	—	—	—	—	—
42—50	» » " " "	—	—	—	—	—	—	74,37	0,75	0,84	0,05	2,93	3,28	0,20
58—60	Алевритово-глинистый ил Silty Clayey Mud	25,42	11,12	9,73	7,75	26,62	19,36	—	—	—	—	—	—	—
64—68	Мелкоалевритовый ил Fine Silty Mud	—	—	—	—	—	—	75,28	0,55	1,12	0,03	2,22	4,53	0,12
68—70	» »	28,86	11,24	12,19	6,29	22,67	18,75	—	—	—	—	—	—	—
75—80	Алевритово-глинистый ил Silty Clayey Mud	—	—	—	—	—	—	78,69	0,42	1,11	0,03	1,97	5,20	0,14
80—82	» » »	21,87	11,87	14,30	3,55	22,80	25,61	—	—	—	—	—	—	—
90—96	Мелкоалевритовый ил — Fine Silty Mud	—	—	—	—	—	—	79,37	0,43	0,84	0,03	2,08	4,07	0,14
96—98	» »	32,10	10,38	13,52	4,00	20,67	19,33	—	—	—	—	—	—	—
106—109	» »	—	—	—	—	—	—	81,42	0,29	0,84	0,03	1,56	4,52	0,16
112—118	» »	—	—	—	—	—	—	78,69	0,42	0,81	0,03	1,97	3,91	0,14
118—120	» »	32,74	12,26	12,83	5,47	20,28	16,42	—	—	—	—	—	—	—
125—130	Алевритово-глинистый ил Silty Clayey Mud	—	—	—	—	—	—	81,42	0,36	1,11	0,03	1,93	5,97	0,16
130—132	» » »	19,81	9,26	13,52	7,59	24,07	25,74	—	—	—	—	—	—	—
140—142	» » »	15,93	10,92	17,41	8,05	24,17	23,52	—	—	—	—	—	—	—
142—150	» » »	—	—	—	—	—	—	73,23	0,40	1,11	0,03	1,50	4,14	0,11
160—162	» » »	31,27	12,55	16,09	7,82	18,27	14,00	—	—	—	—	—	—	—
162—168	» » »	—	—	—	—	—	—	79,37	0,38	0,84	0,02	1,84	4,07	0,10
180—182	» » »	21,10	12,38	16,88	5,05	23,12	21,47	—	—	—	—	—	—	—
182—190	» » »	—	—	—	—	—	—	79,37	0,41	0,84	0,03	1,98	4,07	0,15
195—200	» » »	—	—	—	—	—	—	74,82	0,30	0,84	0,02	1,19	3,31	0,08
200—202	» » »	37,45	12,64	14,82	13,73	18,18	13,73	—	—	—	—	—	—	—
211—215	» » »	—	—	—	—	—	—	79,60	0,60	0,84	0,03	2,94	4,12	0,15
220—222	» » »	20,46	11,34	17,60	7,87	21,02	21,11	—	—	—	—	—	—	—
225-230	» » »	—	—	—	—	—	—	80.28	0.45	—	0.03	2.28	—	0.15

APPENDIX XXIII

Depths and Coordinates (Lat.-Long.) of Stations

Station No.	Water Depth (m)	Coordinates		Station No.	Water Depth (m)	Coordinates	
		Lat.	Long.			Lat.	Long.
3116	5220	44°43'1 N	156°49'0 E	3274	5417	51°04'0 N	162°13'3 E
3114	5571	48 43 2	160 55 9	3443	1427	41 01 6	142 26 7
3127	122	52 08 4	158 29 2	3451	5678	37 27 1	146 54 8
3128	76	52 57	159 22	3456	6056	34 51 0	149 46 0
3136	627	51 32 7	158 35 6	3471	6076	34 03 8	152 26 9
3137	1647	51 29 5	158 42 8	3476	5578	31 25 6	150 47 8
3138	2497	51 24 8	158 54 1	3481	6086	31 31 0	145 42 2
3145	4925	50 58 9	159 56 0	3489	4596	30 06 3	141 51 7
3148	3050	46 52 0	169 22 8	3495	5154	26 16 0	145 47 3
3151	5110	44 09 4	170 07 0	3520	4223	28 53 3	137 21 1
3154	5630	41 02 0	167 22 2	3530	5024	27 30 3	131 31 6
3156	5510	39 57 0	165 07 8	3532	4589	27 31 8	133 46 1
3162	5560	43 15 3	157 48 2	3625	6008	28 48 6	154 02 0
3163	5430	43 45 7	156 34 9	3650	2365	0 02 1	154 41 8
3166	5020	44 42 9	153 49 0	3746	5971	19 18 9	134 12 4
3168	6180	45 41 7	152 36 7	3797	5328	2 01 5	172 32 5 W
3189	1750	43 15 9	146 54 1	3873	5464	14 16 2	173 11 7 E
3206	5920	30 48 8	153 02 0	3921	2868	0 55 2 S	142 30 5
3208	2760	31 32 2	151 14 4	3989	3920	0 48 0	139 24 0
3212	5830	35 41 7	145 39 0	3993	4243	1 53 5 N	135 13 8
3222	1455	40 47 7	142 58 7	3995	4854	3 59 0	135 33 8
3252	5420	45 58 0	160 30 1	4068	5782	45 50 8	175 46 6 W
3254	5040	47 35 0	158 34 4				